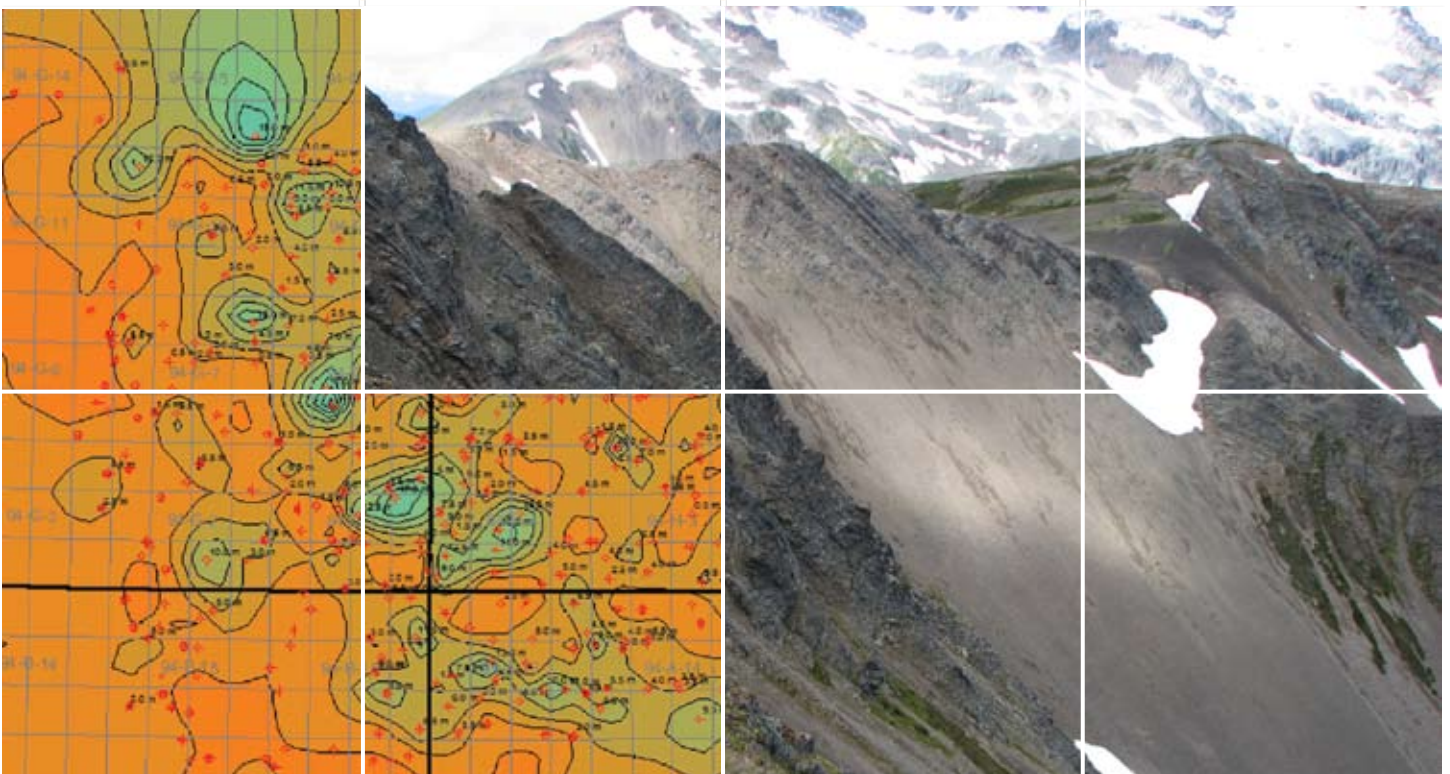


# Oil And Gas Geoscience Reports 2008

**BC Ministry of Energy, Mines and Petroleum Resources**



**Oil and Gas Division  
Resource Development and Geoscience Branch**



© British Columbia Ministry of Energy, Mines and Petroleum Resources  
Oil and Gas Division  
Resource Development and Geoscience Branch  
Victoria, British Columbia, May 2008

Please use the following citation format when quoting or reproducing parts of this document:

Ferri, F., Nixon, G.T. and Reyes, J. (2008): Organic Geochemistry of Late Triassic to Early Jurassic Sedimentary Rocks in Northern Vancouver Island; Geoscience Reports 2008, BC Ministry of Energy, Mines and Petroleum Resources, pages

Colour digital copies of this publication in Adobe Acrobat PDF format are available, free of charge, from the BC Ministry of Energy, Mines and Petroleum Resources website at:

<http://www.em.gov.bc.ca/subwebs/oilandgas/pub/reports.htm>

**Front cover images:**

*Left side:* Halfway Formation porosity (contour interval 2 m) for areas north of the Peace River block. Green represents thick porosity. Orange and brown represent low totals. Porosity cut-off is 10%.

*Right side:* Looking north along Ashman Ridge. The contact between the Spatsizi Formation and Bowser Lake Group can be seen at the right side of the photo, near the top of the large snow field.

**Back cover images:**

*Left side:* Intertidal zone in the Union Bay area, northern Vancouver Island.

*Bottom left of centre:* Oil drilling rig in Chilliwack, BC, ca. 1906. Photo courtesy of BC Archives collections; call number G-07686.

*Right side:* Boreal plains, Fort St. John region.

## FOREWORD

Geoscience Reports is published by the Resource Development and Geoscience Branch of the Oil and Gas Division, British Columbia Ministry of Energy, Mines and Petroleum Resources. Like its predecessor, Summary of Activities, Geoscience Reports is an annual publication highlighting petroleum-related geological activities carried out by staff of the Resource Development and Geoscience Branch.

Articles in this volume cover a wide range of topics, including: 1) CO<sub>2</sub> sequestration; 2) geology and geophysics within the Nechako Basin; 3) organic-rich siltstones along northern Vancouver Island; 4) coal and coal bed gas; 5) studies in northeast BC, including Triassic porosity trends and well disposal; 6) the history of oil and gas exploration in BC and 7) water sampling guidelines.

This year's volume has benefited from an editorial review by Justine Pearson and the excellent services of Tetrad Communications.

Vic Levson  
Executive Director  
Resource Development and Geoscience Branch

# TABLE OF CONTENTS

## GEOSCIENCE REPORTS 2008

PRELIMINARY INTERPRETATION OF THE SOUTHERN NECHAKO BASIN FROM POTENTIAL FIELD DATA .....	1
<i>by Melvyn E. Best</i>	
SYNOPSIS OF THE REPORT "RECOMMENDED SAMPLING, ANALYSIS, AND REPORTING PROTOCOLS FOR BASELINE GROUNDWATER SAMPLING IN ADVANCE OF COALBED GAS DEVELOPMENT IN THE TELKWA COALFIELD, BRITISH COLUMBIA" .....	9
<i>by Susan Chaytor and Rachel Shaw</i>	
ORGANIC GEOCHEMISTRY OF LATE TRIASSIC TO EARLY JURASSIC SEDIMENTARY ROCKS IN NORTHERN VANCOUVER ISLAND .....	13
<i>by Filippo Ferri, Graham T. Nixon and Julito Reyes</i>	
CARBON CAPTURE AND STORAGE IN BRITISH COLUMBIA .....	25
<i>by Alf Hartling</i>	
NORTHEASTERN BRITISH COLUMBIA DISPOSAL WELL STUDIES .....	33
<i>by Ed Janicki</i>	
PETROLEUM EXPLORATION HISTORY OF NORTHEASTERN BRITISH COLUMBIA .....	41
<i>by Ed Janicki</i>	
TRIASSIC POROSITY TRENDS IN NORTHEASTERN BRITISH COLUMBIA .....	59
<i>by Ed Janicki</i>	
NECHAKO PROJECT UPDATE .....	67
<i>by Janet Riddell and Filippo Ferri</i>	
DIFFUSIVITY AND DIFFUSION COEFFICIENTS OF ANTHRACITE .....	79
<i>by Barry Ryan and Karin Mannhardt</i>	
PRELIMINARY ANALYSES OF COAL REFUSE MATERIAL FROM VANCOUVER ISLAND .....	99
<i>by Barry Ryan</i>	
A FIRST LOOK AT THE ELECTRICAL RESISTIVITY STRUCTURE IN THE NECHAKO BASIN FROM MAGNETOTELLURIC STUDIES WEST OF NAZKO, B.C. (NTS 092 N, O; 093 B, C, F, G) .....	119
<i>by J. Spratt and J. Craven</i>	

# PRELIMINARY INTERPRETATION OF THE SOUTHERN NECHAKO BASIN FROM POTENTIAL FIELD DATA

Melvyn E. Best<sup>1</sup>

Best, Melvyn E., (2008), Preliminary Interpretation of the Southern Nechako Basin from Potential Field Data in Geoscience Reports 2008, *BC Ministry of Energy, Mines and Petroleum Resources*, pages 1-7.

<sup>1</sup>Bemex Consulting International , 3701 Wild Berry Bend, Victoria, B.C V9C 4M7; 250-657-4225; Best@islandnet.com

## INTRODUCTION

The Nechako Basin is one of the interior basins within British Columbia (Figure 1). Most of the basin is covered with glacial overburden of variable thickness, and in the southern Nechako Basin basalt flows cover a significant portion of the surface (Riddell 2006). The report focuses on the southern portion of the basin for two reasons: firstly, sediments are known to exist in the southern portion of the basin, implying at least the possibility of oil and gas accumulations, and secondly, a regional gravity survey was carried out by Canadian Hunter Exploration Limited in the southern Nechako Basin.

In the early 1980s Canadian Hunter carried out an exploration program consisting of 2D seismic reflection and gravity surveys (Best 2004). The quality of the original seismic data was generally poor due to the basalt cover, thus making subsurface mapping difficult. The gravity survey located a number of Bouguer gravity lows within the survey area that could be sediment-filled basins. Several wells were drilled based on the combined survey results, but no commercial accumulations of hydrocarbons were found. However, sediments were encountered in a couple of wells, as well as oil staining and gas kicks. Since that time, no exploration activity has taken place within the basin.

This report discusses the steps involved in processing the Canadian Hunter gravity data and the Geological Survey of Canada (GSC) aeromagnetic data for the southern Nechako Basin (Figure 1). A discussion is presented of how the gravity data set was manipulated to produce a digital grid. The aeromagnetic data were provided by the GSC as a 200 m by 200 m digital grid. This report explains how subsidiary maps, such as derivative and shaded relief maps, were obtained from the digital grids.

One of the objectives of this report is to provide access to the maps and images generated during this project. The maps and images available are listed in Appendices A and

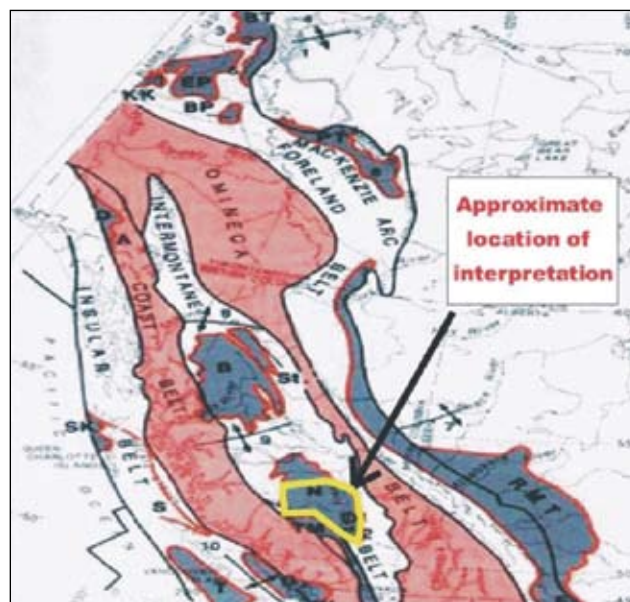


**Figure 1: The grey shaded area with the letter N is the outline of the Nechako Basin. The yellow outline represents the approximate location of the gravity data in the southern Nechako Basin.**

B of this report; they can be downloaded from the Interior Basins website of the BC Ministry of Energy, Mines and Petroleum Resources at the following web address; [http://www.em.gov.bc.ca/subwebs/oilandgas/petroleum\\_geology/cog/interior.htm](http://www.em.gov.bc.ca/subwebs/oilandgas/petroleum_geology/cog/interior.htm). In addition, a preliminary interpretation of the data based on magnetic lineaments is provided. This interpretation is not detailed but has been provided to give the reader an initial overview of the main features observed within the data sets.

## POTENTIAL FIELD DATA

The gravity data collected by Canadian Hunter were available as a hand-contoured Bouguer gravity map. The original field data do exist but are confidential. To allow

further processing of the gravity data, the contour map was digitized along each contour to provide a digital database. The digitizing was carried out by Focus Corporation of Victoria. These data were then entered into Geosoft Oasis Montaj (Version 6.4.1, 2007), and a 200 m by 200m grid of the Bouguer gravity data was generated using the minimum curvature gridding option. The location of the gravity survey lines are shown on Petroleum Geology Map 2006-1 (map 1 of 3 in Riddell 2006). The average spacing between lines is 10 km, so a 200 m grid is a smoothed version of the data. Fortunately the gravity data are quite smooth so that changes in the magnitude of the Bouguer gravity with position are generally small. The colour image in Figure 2 of this gridded data was compared with the original Bouguer gravity contour map and found to represent the original data accurately. Very few gravity survey lines are located near the edges of the Bouguer gravity map (Riddell 2006). Care should therefore be exercised when interpreting features near the edges of the Bouguer gravity map and the images derived from it.

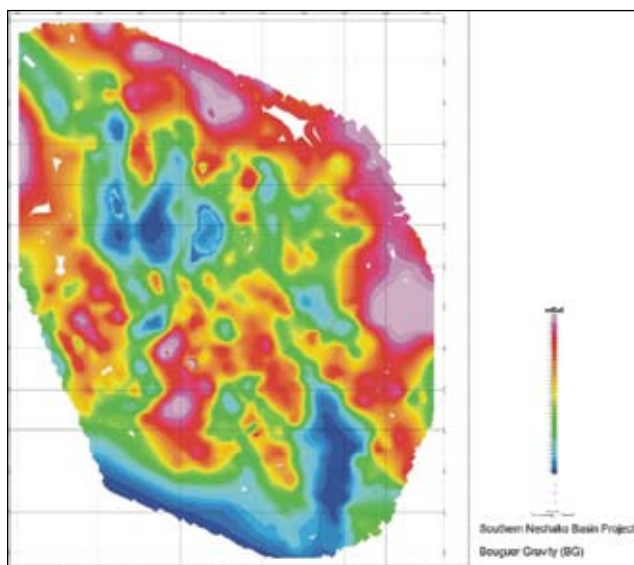


**Figure 2: Bouguer gravity map generated from the digitized contour data.**

The aeromagnetic data were obtained from the GSC as 200 m by 200 m total magnetic field intensity (TMI) gridded data. All data corrections, including levelling, were carried out before the grid was created. The gridded data were entered into Geosoft Oasis Montaj to generate the colour image in Figure 3. The magnetic survey covers a larger area than the gravity survey, which is outlined by the black polygon on the figure.

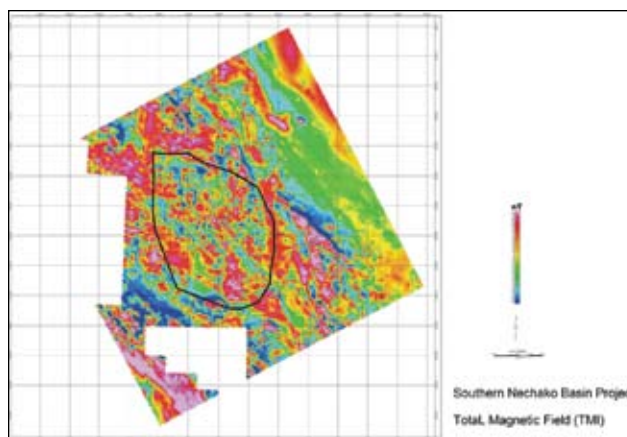


**Figure 3: Total magnetic field intensity (TMI) map.**

## DERIVED GRIDDED MAPS

The gravity and magnetic grids were subsequently used to generate a number of derivative and shaded relief grids and maps with the Geosoft software. A list of the Geosoft maps and grids and the images generated from them is provided in Appendix A; these are available at the Interior Basins website of the BC Ministry of Energy, Mines and Petroleum Resources (the web address is provided in Appendix A)

Geosoft maps have a title, a scale, and UTM and/or latitude and longitude coordinates. Geosoft grids do not have these features. Geosoft map and grid files can only be read using Geosoft software; however, there is free software available from the Geosoft website (<http://www.geosoft.com>) to display these files. In addition, .jpg images of most of the Geosoft maps were generated within Geosoft for those who prefer bitmap images.

### *Gravity products*

Only first derivative grids and maps (first horizontal derivative in the x and y directions, [i.e., N-S and E-W], the first vertical derivative, and the analytic derivative) were computed because the gravity data is smooth and the spacing between survey lines large. Shaded relief maps with the sun in the northeast were also computed for several of these maps.

### *Magnetic products*

First derivative grids and maps (first vertical derivative, analytic derivative, x and y, [i.e., N-S and E-W], and horizontal derivatives) were computed. In addition, the second vertical derivative was computed since the TMI has significant spatial variation. Shaded relief maps with the sun in the northeast (and a few with the sun in the northwest) were computed for some of the derivative maps

## Derivative maps

The vertical and horizontal derivatives, which are basically the rate of change of the magnetic or gravity field, can be computed from the gridded data. The x and y horizontal derivatives can be computed numerically from the gridded data by taking the difference between successive grid values and dividing by the grid spacing. The vertical derivative can be computed by applying a frequency domain operator derived from potential field theory to the frequency domain magnetic field data and then using the inverse Fourier transform to compute the corresponding spatial domain vertical derivative.

Computing the derivative of the magnetic or gravity field is equivalent to applying a filter operation to the magnetic or gravity data. Derivative operators are somewhat similar to high pass filters since they emphasize shorter wavelength (shallower) magnetic or gravity sources.

**Horizontal derivative maps** The horizontal derivative has a peak value over the edge of the magnetic or gravity source body. It has a peak at the steepest slope, which is basically the maximum rate of change of the magnetic or gravity field. Horizontal derivatives can be computed in the x and y directions as well as any arbitrary direction.

**Vertical derivative maps** The first vertical derivative usually locates the edge of a magnetic or gravity source body. Sometimes the second vertical derivative is computed, although there is usually more noise and any effects of improper levelling of aeromagnetic data will stand out strongly.

**Analytic signal maps** The analytic signal, or total gradient, is the square root of the sum of the squares of the x and y horizontal gradients and the z (vertical) gradient. The maxima (ridges and peaks) of the computed analytic signal locate the edges and corners of magnetic and gravity source bodies (for example, basement fault block boundaries, basement lithology contacts, fault/shear zones, igneous and salt diapirs, etc.). Analytic signal maxima for magnetic data have the property that they occur directly over faults and contacts, regardless of structural dip and independent of the direction of induced and/or remanent magnetism.

## Shaded relief maps

Artificial shading of coloured maps and images can be used to enhance linear features. This technique was originally designed to enhance satellite images but is now applied routinely to geophysical data. An artificial (mathematical) illumination source is beamed at the image from a specific location (for example, from the northwest at an angle of 45° from the horizontal) and the projected shadow is calculated for each pixel. If there are strong northeast-trending features in the image, they will be emphasized by

their shadow. Different illumination angles and azimuths will cause the eye to focus on different linear features.

## PRELIMINARY INTERPRETATION

The lineament interpretation is based on the magnetic data, particularly the second vertical derivative map (Figure 4). Figure 5 shows the lineament interpretation overlying the second vertical derivative map. The location of the gravity survey is also outlined on Figure 5. The main lineament trends are approximately NNW-SSE, NW-SE, and NE-SW, although other lineament directions can be seen on the map. The NNW-SSE trend is roughly parallel to the Fraser fault, and the NW-SE trend is roughly parallel to the Yalakom fault.

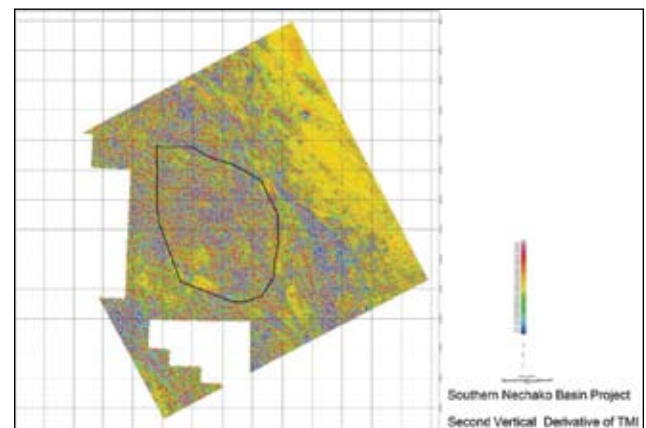


**Figure 4: Second vertical derivative of the TMI map. The location of the gravity survey is outlined on the map for reference.**

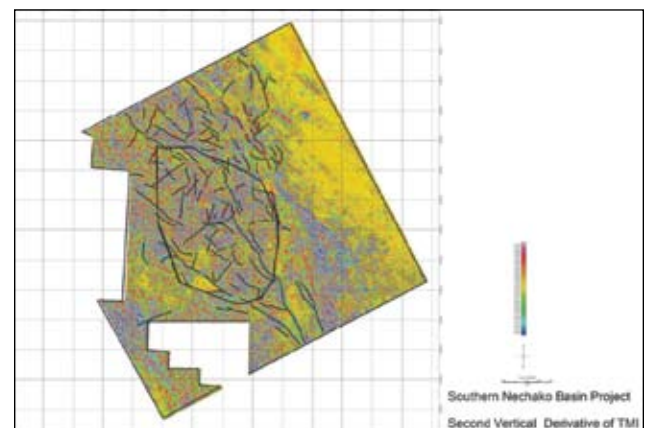


**Figure 5: Second vertical derivative of the TMI map with lineament interpretation overlain on it.**

Figure 6 shows the locations of the lineaments and the outline of the gravity survey. There are interesting features associated with several of these lineaments. For example, lineament B follows the mapped contact between Hazelton Group rocks and granites of Late Cretaceous age. Lineament A also follows a mapped contact. Lineament C appears to follow a contact, although there is significant Quaternary cover in the area, making it difficult to compare to known geology. Lineament D is coincident with a mapped fault (the mapped fault is the section of the lineament next to the letter D in figure 6). Lineament D is part of the Fraser fault system, and lineament G and its extensions to the northwest are associated with the Yalakom fault system.



**Figure 6: Lineament interpretation with interesting features labelled.**

Lineaments F and K separate a gravity low to the north from a gravity high to the south. In addition, there appears to be a change in geology, although Quaternary cover makes it difficult to be certain (Riddell 2006). The southern section of lineament H and lineament J bracket Taylor Creek sediments exposed along the Nazko River valley. The two NNE-SSW lineaments associated with lineament E are coincident with mapped faults. These two lineaments are also associated with known seismic activity (Best and Lakings 2008).

Figure 7 is the Bouguer gravity map with the lineaments overlain on it. Figure 8 is the Bouguer gravity map with polygons of the geology as well as the lineaments. The Hazelton Group rocks in the north (Riddell 2006) are associated with high gravity values. Indeed the two fingers of high gravity (labelled A on Figure 7) are associated with

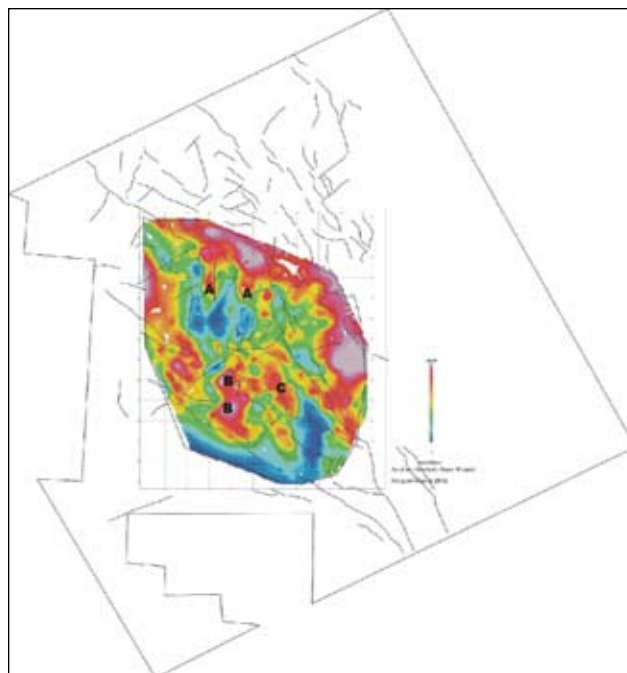


**Figure 7: Bouguer gravity map with lineaments overlain on it.**

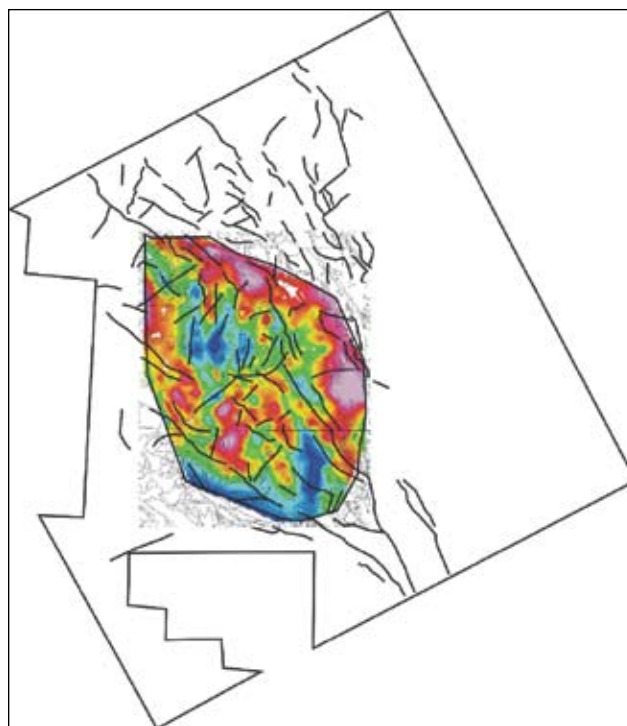


**Figure 8: Bouguer gravity map with geology polygons and lineaments.**

mapped outcrops of Hazelton Group rocks. Similarly the large gravity high in the south (labelled B on Figure 7) appears to be associated with Triassic diorites and tonalites. The rocks associated with the gravity high labelled C are not identifiable because of Quaternary and basalt cover. The gravity lows appear to be associated with Paleogene

Endako Group rocks and Early Cretaceous granodiorites (Riddell 2006).

Figure 9 is the total magnetic intensity map with polygons of geology as well as lineaments. The outline of the gravity survey is also shown on this figure. The Hazelton Group rocks in the northern part of the gravity survey (labelled A in the figure) are associated with lower values of the magnetic field. The large magnetic feature in the south-central area of the gravity survey (labelled B in the Figure) is associated with Spences Bridge Group rocks. There are many more subtle features, sometimes associated with lineaments and sometimes not, which should be followed up in future studies.

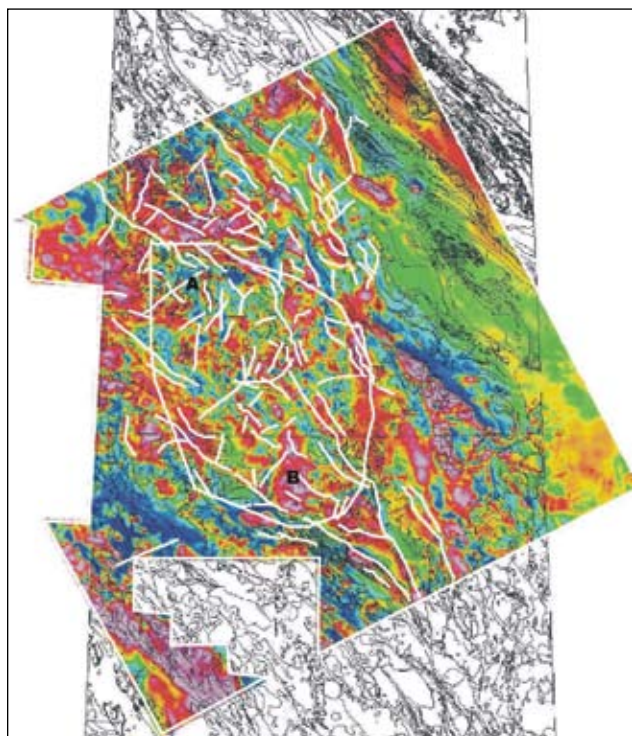


Figure 9: TMI map with geology polygons and lineaments.

## CONCLUSIONS

The derivative and shaded relief maps generated from the gravity and magnetic data in the southern Nechako Basin have provided a preliminary interpretation of the potential field data. Many lineaments derived from the second vertical derivative of the TMI were found to correlate with known geology and helped define boundaries within the survey area. A qualitative relationship can be observed between known geology and the gravity and magnetic data, even though no detailed modelling was carried out. Further modelling of the combined data set would be a useful exercise to help quantify the geology in areas of Quaternary and basalt cover.

Appendix B lists some additional CorelDraw (.cdr) files of the lineament map overlaying the second vertical derivative map and other derivative gravity and magnetic maps, as well as the TMI and Bouguer gravity maps. These are also available at the Interior Basins website of the BC Ministry of Energy, Mines and Petroleum Resources.

## REFERENCES

- Best, M.E. (2004): Qualitative interpretation of potential field profiles, southern Nechako Basin; Summary of Activities 2004, *BC Ministry of Energy and Mines*, pages 73 to 78.
- Best, M.E., and Lakings, J. (2008): Results from a reconnaissance microearthquake survey in the Nechako Basin of British Columbia, October 12 – December 17, 2006; Petroleum Geology Open File 2007-12, *BC Ministry of Energy, Mines and Petroleum Resources*.
- Riddell, J.M. (compiler) (2006): Geology of the southern Nechako Basin NTS 92N, 92O, 93B, 93C, 93F, 93G; *BC Ministry of Energy, Mines and Petroleum Resources*, Petroleum Geology Map 2006-1, 1:400 000 scale, 3 sheets.

## APPENDIX A

### List Of Maps, Grids, And Images

These are available at the Interior Basins website of the BC Ministry of Energy, Mines and Petroleum Resources  
[http://www.em.gov.bc.ca/subwebs/oilandgas/petroleum\\_geology/cog/interior.htm](http://www.em.gov.bc.ca/subwebs/oilandgas/petroleum_geology/cog/interior.htm)

#### Gravity Geosoft Grids

grid type	file name
Analytic derivative	grav_analytic.grd
Hor gradient (N-S direction)	grav_hor_grad_0.grd
Hor gradient (E-W direction)	grad_hor_grad_90.grd
First vertical derivative	grav_vd1.grd
Bouguer gravity	grav_grid.grd

#### Gravity Geosoft Maps

map type	file name
Analytic derivative	grav_analytic.map
Hor gradient (E-W direction)	grav_hor_grad_90.grd.map
First vertical derivative	grav_vd1.grd.map
Bouguer gravity	grav_grid.grd.map
Bouguer gravity (shad NW)	grav_grid.grd_shad315.map
Bouguer gravity (shad NE)	grav_grid.grd_shad45.map

#### Gravity images

image type	file name
Bouguer gravity	grav.grd.jpg
First vertical derivative	grav_vd1.jpg
First vert der (shad NE)	grav_vd1_shad45.jpg
Analytic derivative	grav_analytic.jpg
Hor gradient (N-S)	grav_hor_der_0.jpg
Hor gradient (E-W)	grav_hor_der_90.jpg
Bouguer gravity (shad NW)	grav_shad315.jpg
Bouguer gravity (shad NE)	grav_shad45.jpg

#### Magnetic Geosoft Grids

grid type	file name
Analytic derivative	mag_analytic.grd
Hor gradient (N-S direction)	mag_hor_grad_0.grd
Hor gradient (E-W direction)	mag_hor_grad_90.grd
TMI (shad NE)	mag_shad_45.grd
First vertical derivative	mag_vd1.grd
Second vertical derivative	mag_vd2.grd
Total magnetic intensity (TMI)	magnetics_200m.grd

#### Magnetic Geosoft Maps

map type	file name
analytic derivative	mag_analytic.grd.map
analytic derivative (shad NW)	mag_analytic_shad315.map
analytic derivative (shad NE)	mag_analytic_shad45.map
analytic derivative (shad NE and masked to gravity map)	mag_analytic_shad45_mask.map
magnetic hor gradient (N-S)	mag_hor_grad_0.grd.map
magnetic hor gradient (N-S and masked to gravity map)	mag_hor_grad_0_mask.grd.map
magnetic hor gradient (E-W)	mag_hor_grad_90.grd.map
magnetic hor gradient (E-W and masked to gravity map)	mag_hor_grad_90_mask.grd.map
First vertical der (shad NW)	mag_vd1_shad315.map
First vertical der (shad NE)	mag_vd1_shad45.map
First vertical der (shad NE and masked to gravity map)	mag_vd1_shad45_mask.map
Second vertical der	mag_vd2.grd.map
Second vertical der (masked to gravity map)	mag_vd2_mask.map
Second vertical der (shad NW)	mag_vd2_shad315.map
Second vertical der (shad NE)	mag_vd2_shad45.map
Second vertical der (shad NE and masked to gravity map)	mag_vd2_shad45_mask.map
TMI and masked to gravity map	magnetics_200m.grd_mask.map
TMI with mask outline of gravity map	magnetics_200m.grd_mask_outline.map
TMI (shad NE)	magnetics_200m.grd_shad45.map
Total magnetic intensity (200 m grid) (TMI)	magnetics_200m.grd.map

#### Magnetic images

image type	file name
TMI (200 m grid)	mag_200m_grd.jpg
TMI (200 m grid and outline of gravity mask)	mag_200m_grd_mask_outline.jpg
Analytic derivative	mag_analytic.jpg
Analytic der (shad NW)	mag_analytic_shad315.jpg
Analytic der (shad NE)	mag_analytic_shad45.jpg
Analytic der (with mask of gravity map)	mag_analytic_shad45_mask.jpg
Hor der (N-S)	mag_hor_der_0.jpg
Hor der (E-W)	mag_hor_der_90.jpg
First vertical derivative	mag_vd1.jpg
First vertical der (shad NW)	mag_vd1_shad315.jpg
First vertical der (shad NE)	mag_vd1_shad45.jpg
Second vertical derivative	mag_vd2.jpg
Second vert der (shad NE)	mag_vd2_shad45.jpg
TMI with mask of gravity map	magnetics_200m.grd_mask.jpg

## APPENDIX B

### *List Of Coreldraw (CDR) Files Of Lineaments Overlaying Maps*

These are available at the Interior basins website of the BC Ministry of Energy, Mines and Petroleum Resources  
[http://www.em.gov.bc.ca/subwebs/oilandgas/petroleum\\_geology/cog/interior.htm](http://www.em.gov.bc.ca/subwebs/oilandgas/petroleum_geology/cog/interior.htm)

#### **Gravity files**

<b>map type</b>	<b>file name</b>
First vertical derivative map	grav_1vd_lineaments.cdr
Analytic derivative map	grav_analytic_lineaments.cdr
Bouguer gravity map	grav_grid_lineaments.cdr
Bouguer gravity map with geology polygons	grav_geology_lineaments.cdr

#### **Magnetic files**

<b>map type</b>	<b>file name</b>
Second vertical derivative map	mag_v2d_lineaments.cdr
First vertical derivative map	mag_1vd_lineaments.cdr
Analytic derivative map	mag_analytic_lineaments.cdr
Horizontal derivative (N-S) map	mag_hor_der_0_lineaments.cdr
Horizontal derivative (E-W) map	mag_hor_der_90_lineaments.cdr
TMI map	mag_200m_grid_lineamants.cdr
TMI map with geology polygons	mag_geology



# SYNOPSIS OF THE REPORT “RECOMMENDED SAMPLING, ANALYSIS, AND REPORTING PROTOCOLS FOR BASELINE GROUNDWATER SAMPLING IN ADVANCE OF COALBED GAS DEVELOPMENT IN THE TELKWA COALFIELD, BRITISH COLUMBIA”

*Susan Chaytor<sup>1</sup> and Rachel Shaw<sup>2</sup>*

---

## ABSTRACT

*This synopsis provides a summary of the key points from the report, “Recommended sampling, analysis, and reporting protocols for baseline groundwater sampling in advance of coalbed gas development in the Telkwa Coalfield, British Columbia” (the Protocols Report) by Dr. Tony Gorody of Universal Geoscience Consulting, Inc.*

*The advent of baseline groundwater sampling, analysis, and monitoring in the oil and gas industry in advance of drilling new wells is a relatively new concept; however, the protocols recommended in the Protocols Report have been gradually developed and successfully tested for 15 years. These include protocols for field sampling, sample analysis, data documentation, and quality control/quality assurance procedures. By using the consistent procedures outlined in the Protocols Report, the quality of groundwater data collected may be improved, and this can help stakeholders reliably evaluate whether groundwater in a producing basin is being adversely affected by oil and gas operations.*

Chaytor, S. and Shaw, R., (2008), Synopsis of the report “Recommended Sampling, Analysis, and Reporting Protocols for Baseline Groundwater Sampling in Advance of Coalbed Gas Development in the Telkwa Coalfield, British Columbia;” in Geoscience Reports 2008, *BC Ministry of Energy, Mines and Petroleum Resources*, pages 9-11.

<sup>1</sup>Resource Development and Geoscience Branch, BC Ministry of Energy, Mines and Petroleum Resources; 250-953-3800; Susan.Chaytor@gov.bc.ca

<sup>2</sup> Resource Development and Geoscience Branch, BC Ministry of Energy, Mines and Petroleum Resources; 250-387-1667; Rachel.Shaw@gov.bc.ca

**Key Words:** Groundwater sampling, coalbed gas, coalbed methane, sampling procedures, stable isotopes.

---

## INTRODUCTION

The report, “Recommended sampling, analysis, and reporting protocols for baseline groundwater sampling in advance of coalbed gas development in the Telkwa Coalfield, British Columbia” (the Protocols Report) was prepared for the Ministry of Energy, Mines and Petroleum Resources (the Ministry) by Dr. Tony Gorody of Universal Geoscience Consulting, Inc. This synopsis was written to provide a summary of the key points; interested parties are encouraged to contact the Ministry for a copy of the full-length report.

The objective of the Protocols Report is to recommend standardized baseline groundwater sampling, analysis, and reporting protocols in advance of coalbed gas (CBG) development in the Telkwa Coalfield tenure area. As applied in the report, baseline sampling is intended to provide the foundations for additional groundwater monitoring during future CBG exploration and development activities. Such monitoring would provide a valuable screening tool for

evaluating whether CBG activities are affecting groundwater either tapped by domestic wells or issuing from springs.

The approach proposed in the Protocols Report is to sample and test for the most direct, abundant, and obvious signs of groundwater contaminants potentially related to CBG development; this would require analyzing and comparing data derived from sampling groundwater in coalbed gas reservoirs as well as springs and sources designated for domestic use. Sample selection criteria are not addressed in the Protocols Report.

Recommendations presented in the report address the two major environmental concerns related to the potential impact of CBG development on potable groundwater resources. These are 1) contamination of aquifers with migrated hydrocarbon gas and 2) declining aquifer yield resulting from drawdown associated with CBG water production. Consistent baseline sampling and analysis protocols will make it possible to reliably assess potential impacts to

the groundwater environment. Although emphasis in the Protocols Report is placed on sampling cased and completed water wells, similarly rigorous protocols would apply to the sampling of open wells, springs, and surface water resources.

Recommendations presented in the Protocols Report include the following:

- Standard field sampling protocols to ensure consistent analytical results;
- Standard analyses to evaluate the origin of naturally occurring gas in water resources;
- Standard data maintenance and recording practices and;
- Selected quality assurance and control considerations that allow the information collected to withstand public and scientific scrutiny.

To keep the Protocols Report reasonably brief, established conventional surface water and groundwater sampling protocols are not repeated.

## DISCUSSION: FIELD SAMPLING

Field sampling protocols recommended in the Protocols Report focus on the collection and documentation of information resulting from many sources, including interviews of water users; observations of surroundings, water sources, hydrologic setting, and mechanical well components; and a hazard assessment of the site, including confined space protocols if necessary. Techniques for decontamination of sampling equipment, recording static water levels, and purging wells are detailed, as are recommendations on which samples should be filtered in the field.

Detailed rationale and sample-collection procedures are presented for

- alkalinity;
- free and dissolved hydrocarbon gas concentration measurements;
- stable isotopic and chromatographic analysis of free and dissolved gas;
- volatile organic compounds;
- Biologic Activity Reaction Test (BART™) screening; and
- tests for dissolved sulfide.

Procedures are given for conditions of both effervescent and non-effervescent water.

## DISCUSSION: SAMPLE ANALYSIS

The Protocols Report specifies the following analytical procedures:

- *Routine analyses for dissolved inorganic constituents and physical properties (including general water quality parameters, major ions, halides, trace metals, and nutrients)*: Repeated sampling and analysis of the major ions can be used to establish the presence of multiple aquifers, to observe differences in aquifer mixing rates that influence dissolved gas concentrations, to document seasonal changes in precipitation rates, recharge rates, and discharge rates, and to document the influence of irrigation.
- *Measurement of dissolved atmospheric and hydrocarbon gases in the C<sub>1</sub>-C<sub>4</sub> range*: Measuring gas component ratios at either a contaminant or pollutant site can also help establish the role that hydrocarbon-oxidizing bacteria play in altering the original source-gas composition. Repeated, temporal analysis of dissolved gas composition at a contaminant or pollutant site will reveal the rate at which the source gas is consumed.
- *Measurement of volatile organic compounds (VOCs), including total extractable petroleum hydrocarbons*: Measurement of volatile organic compounds can help differentiate a naturally occurring gas-pollutant source from a refined-product pollutant source.
- *Biological Activity Reaction Test (BART™)*: This protocol suggests measuring for specific bacteria that are the most common indicators of potential bacteria-related water well problems.
- *Stable isotopes of the gas (if either thermogenic gas components are detected or dissolved methane concentrations exceed 2 mg/L)*: Stable carbon and deuterium isotopes of methane provide an independent means to determine the origin of gases and are conventionally used to differentiate between biogenic and thermogenic methane sources. Both chromatographic composition and isotope ratios are used to differentiate naturally occurring gas sources.
- *Stable isotopes of  $\delta D$  and  $\delta^{18}O$  in water (if dissolved methane concentrations exceed 2 mg/L)*: The stable isotopic content of water is routinely used to establish water provenance, mixing between aquifers, and brine contamination from either natural contaminant or pollutant sources. The deuterium data are also used to differentiate the reaction pathways that generate bacterial methane (fermentation vs. CO<sub>2</sub> reduction), and to determine whether bacterial methane is generated in-situ or migrated from another source.

## DISCUSSION: DATA DOCUMENTATION

The Protocols Report offers recommendations for documenting a large variety of data and illustrates with examples what types of data table structures can be used to store the many field observations, field data, photographs, and lab data collected. A relational database structure is recommended. Examples of table structure are given for tables that can be queried to generate formatted data useful for spreadsheet analysis, plotting data on GIS maps, and other reports.

## DISCUSSION: QUALITY ASSURANCE / QUALITY CONTROL

Quality control measures and protocols for environmental sampling are too extensive to be covered in great detail here. Essentially, the Protocols Report suggests that every sampling program should make provisions to document the protocols required for checking data quality:

- Checklists are to include calibration checks, lists of interview questions to ask property owners, lists of field parameters to record, and a list of materials, equipment, and supplies needed for sampling.
- Records should be kept of field instrument calibration (minimum daily, using appropriate fresh standards).
- Submissions for laboratory analysis should include at least one blind sample duplicate for every twenty samples (i.e., 5% of samples).
- Records should indicate whether split duplicate or consecutive paired sample collection was used.
- The use of trip and equipment blanks should be anticipated and collected.
- The quality of laboratory results should be evaluated.

## CONCLUSION

The advent of baseline groundwater sampling, analysis, and monitoring in the oil and gas industry in advance of drilling new wells is a relatively new concept; however, the protocols recommended in the Protocols Report have been gradually developed and successfully tested for 15 years. Observing consistent sampling and analysis protocols will minimize natural variability that can sometimes be mistaken for trends of either decreasing or increasing contaminant concentrations in groundwater. Observing a consistent set of analytical measurements will facilitate the forensic analysis required to reliably determine whether a contaminant plume is increasing or decreasing in intensity. Maintaining a consistent and standardized data-reporting format will allow all stakeholders to compare results obtained by different service providers and operating companies. This will make it easier for all stakeholders to reliably evaluate whether groundwater in a producing basin is being adversely affected by oil and gas operations. And finally, maintaining consistent quality control and assurance practices will ensure that available data are defensible when subjected to public or scientific scrutiny.

Interested parties are welcome to contact the Resource Development and Geoscience Branch for a copy of the full-length report.



# ORGANIC GEOCHEMISTRY OF LATE TRIASSIC TO EARLY JURASSIC SEDIMENTARY ROCKS IN NORTHERN VANCOUVER ISLAND

Filippo Ferri<sup>1</sup>, Graham T. Nixon<sup>2</sup> and Julito Reyes<sup>3</sup>

---

## ABSTRACT

*Regional mapping in northern Vancouver Island has recognized the presence near the Triassic-Jurassic boundary of an organic-rich horizon up to 50 m thick. Detailed sampling of a section exposed in road cuts overlooking Neroutsos Inlet was undertaken to determine the thermal maturity and organic geochemistry of this horizon. Thermal maturity of these rocks, based on Ro reflectance analysis, indicates that the section is at or near the upper limit of the dry gas preservation zone, and results from Rock-Eval pyrolysis show residual organic carbon contents as high as 34%, with an average of approximately 6%. Very little or no generative capacity is present in these rocks due to the high thermal maturity, and, based on Rock-Eval results no information can be obtained concerning the original type of organic material present. Sampling of a horizon within this section at or near the Triassic-Jurassic boundary was carried out in an attempt to obtain from a Re-Os isochron a more accurate absolute age of this boundary; preliminary analysis suggests several of these samples will have high enough Re levels for this procedure and that further sampling is warranted.*

Ferri, F., Nixon, G.T. and Reyes, J. (2008): Organic geochemistry of Late Triassic to Early Jurassic sedimentary rocks in northern Vancouver Island; Geoscience Reports 2008, *B.C. Ministry of Energy, Mines and Petroleum Resources*, pages 13-23.

<sup>1</sup>Resource Development and Geoscience Branch, BC Ministry of Energy, Mines and Petroleum Resources; 250-952-0377; fil.ferri@gov.bc.ca

<sup>2</sup>Geological Survey Branch, BC Ministry of Energy, Mines and Petroleum Resources

<sup>3</sup>Geological Survey of Canada, Calgary, AB.

**Keywords:** Vancouver Island, organic carbon, hydrocarbons, source bed, Bonanza Group, Triassic, Jurassic.

---

## INTRODUCTION

Regional mapping in northern Vancouver Island has delineated an organic-rich sequence of latest Triassic to earliest Jurassic age at the base of the Bonanza Group (Nixon and Orr 2007). This package of sedimentary and lesser volcanic rocks is time-equivalent to parts of the Kunga Group, which contains one of several hydrocarbon source beds within the Queen Charlotte Basin. In order to assess the organic richness of these sediments and the hydrocarbon generation potential of this horizon, a series of samples were taken across the unit and analyzed via a Rock-Eval 6 pyrolysis apparatus at the Geological Survey of Canada laboratories in Calgary, Alberta.

In addition, regional mapping in northern Vancouver Island has led to a refinement of the Early Mesozoic stratigraphic framework (Nixon and Orr 2007). In particular, geochronological data from the sequence containing these organic-rich sediments has increased the resolution of the absolute age of the Triassic-Jurassic boundary (Nixon et al. 2000). Bonanza Group organic-rich shales straddle

this boundary; a horizon very close to the Triassic-Jurassic boundary was sampled in hopes of further refining the age of this boundary through use of the Re-Os geochronometer (see Creaser et al. 2002; Selby and Creaser 2005).

This paper presents Rock-Eval pyrolysis and vitrinite reflectance data for samples taken within these organic-rich sediments. A description and location of samples taken towards a Re-Os isochron are also shown, together with major, minor, and trace element data for these samples.

The study area is located on the west shore of Neroutsos Inlet, approximately 5 km northwest of Port Alice (Figure 1). Access from Port Alice is afforded by a series of logging roads that lead south from the town and around the southern end of the inlet.

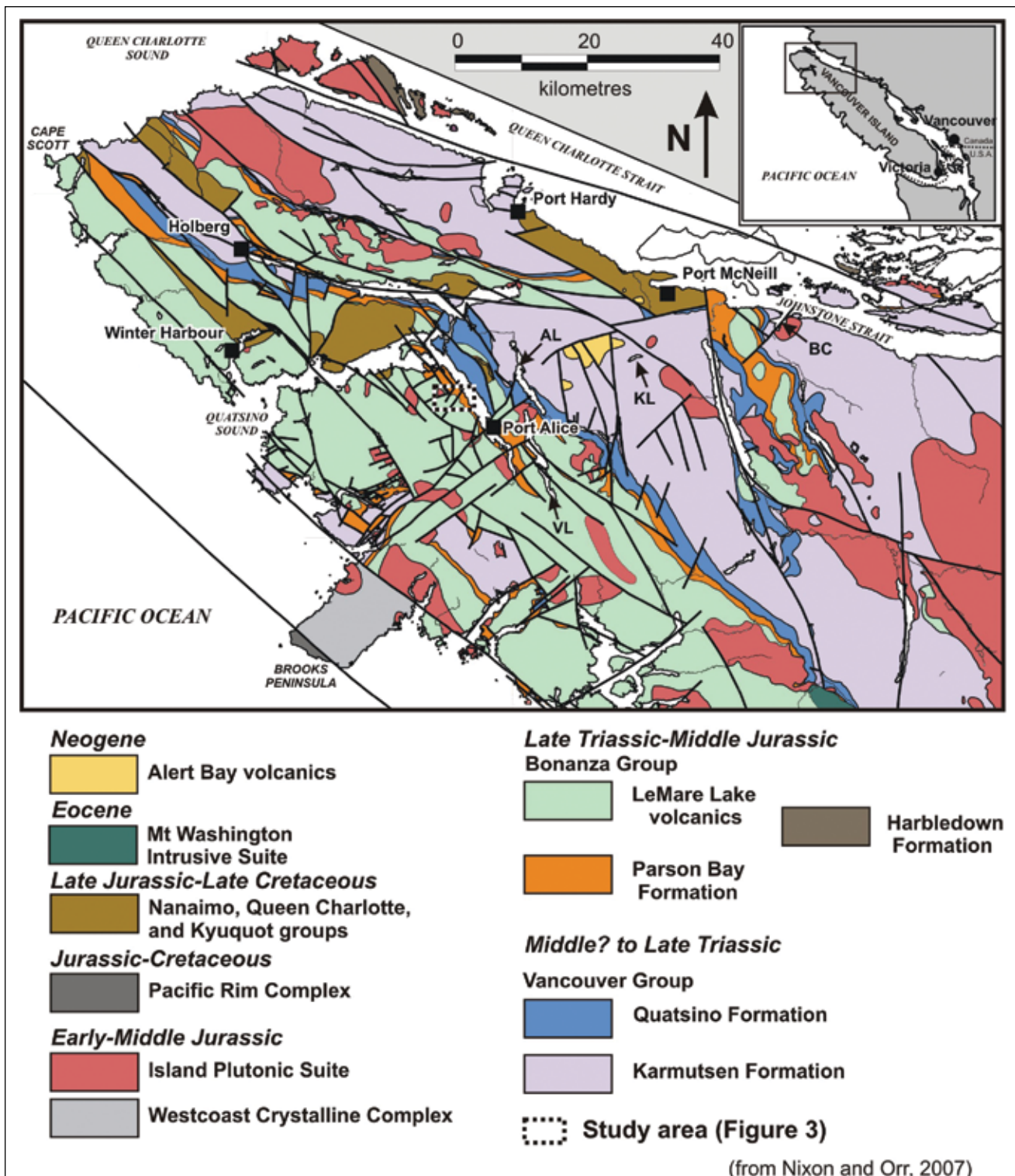


Figure 1: Regional geology of northern Vancouver Island (after Massey et al., 2005). AL, Alice Lake; BC, Beaver Cove; KL, Keogh Lake; VL, Victoria Lake.

## REGIONAL GEOLOGY

Late Paleozoic to Early Mesozoic rocks on Vancouver Island belong to Wrangellia, a tectonostratigraphic terrane that encompasses the southern Coast area and the Queen Charlotte Islands and underlies the Queen Charlotte Basin (Figure 1; Wheeler and McFeely 1991). These rocks began amalgamating with the northern Alexander Terrane in Pennsylvanian times, forming the Insular Belt, which was then juxtaposed against Coast and Intermontane belt rocks to the west either as early as the Middle Jurassic (van der Heyden 1991; Monger and Journey 1994) or as late as the mid-Cretaceous (Monger et al. 1982).

In the study area, bedrock stratigraphy is dominated by Late Triassic to Early Jurassic volcanic and sedimentary rocks of the Vancouver and Bonanza Groups. Although not exposed in the area, Devonian to Early Permian island-arc volcanic and sedimentary rocks of the Sicker and Buttle Lake Groups form the basement of Wrangellia (Massey 1995a, b, c). Nixon and Orr (2007) provide a revision of the Early Mesozoic stratigraphy for northern Vancouver Island, which is adhered to in this report.

The structural history of northern Vancouver Island and the Queen Charlotte Basin is complex and includes Jurassic to Cretaceous contractional or transpressional tectonics followed by Tertiary extension. A major angular unconformity separates Bonanza Group rocks from succeeding Jura-Cretaceous sequences.

## LOCAL GEOLOGY

In northern Vancouver Island, Vancouver Group rocks are represented by Mid(?) to Late Triassic flood basalts of the Karmutsen Formation and succeeding massive to well bedded micritic and bioclastic limestone of the Quatsino Formation (Figure 2). These are followed by Latest Triassic (Norian to Rhaetian) rocks of the marine Parson Bay Formation, an intermixed package of intermediate, aphanitic to augite-plagioclase phyric lava flows and volcanoclastic rocks together with impure limestone, siltstone, mudstone, shale, and epiclastic rocks. The uppermost part of the Parson Bay Formation contains a thin, pale grey, locally coralline limestone provisionally correlated with the Sutton limestone of the Lake Cowichan area, southern Vancouver Island. These rocks give way to Early to Middle Jurassic subaerial basaltic to rhyolitic flows, related volcanoclastics, and minor marine clastics and limestone of the LeMare Lake volcanics. Bonanza Group rocks, particularly the LeMare Lake volcanics, represent an island arc sequence.

The transition between the Parson Bay Formation and LeMare Lake volcanics is represented by an interbedded sequence of volcanoclastic and sedimentary rocks together with minor volcanic rocks. This unit straddles the Triassic-Jurassic boundary and is informally referred to as the

‘volcanoclastic-sedimentary unit’ (Nixon and Orr 2007). The sequence is dominated by thickly bedded to laminated epiclastic rocks. Volcanoclastics and minor massive flows are similar to those within the LeMare Lake volcanics. This package is cut by numerous dikes and sills, which are feeders to overlying LeMare Lake volcanics. The base of this epiclastic succession occurs where carbonate rocks of the Parson Bay Formation are the dominant lithology. The upper contact is marked by the first occurrence of massive volcanic flows and breccias of the LeMare Lake volcanics.

Epiclastic rocks are dominated by dark grey to grey-green lithic and feldspathic wacke, dark grey siltstone, mudstone, and shale. These all can be calcareous and associated with dark, impure limestone. The central 30 to 50 m of this unit is characterized by interbedded dark grey to rusty weathering, dark grey to black, blocky siltstone and fissile, dark grey to black, locally carbonaceous shale. Sections of dark grey to black, fetid limestone up to 3.5 m thick are found in the lower part of the sequence.

The upper 3 m of the interval is composed of rusty weathering, slightly fetid, dark grey to black, fissile shale to blocky siltstone containing calcareous (and fossiliferous) nodules up to 50 cm in size and located along a horizon several metres from the top of the section. Identification of pelecypod fauna within the nodules indicates that this sequence is Early Jurassic (Hettangian) in age and likely within a few tens of metres above the Triassic-Jurassic boundary. Six samples were taken along a horizon in the centre of the section for the purposes of obtaining a Re-Os radiometric age and more accurately determining the absolute age of the Triassic-Jurassic boundary.

## SAMPLING

Twenty samples of dark grey siltstone and limestone were obtained for Rock-Eval analysis from parts of the Parson Bay Formation and through the volcanoclastic-sedimentary unit at the transition between the Parson Bay and LeMare Lake units (Table 1). The bulk of the sampling was within the sedimentary-dominated portion of the volcanoclastic-sedimentary unit (Figure 3). In the central part of this sedimentary interval, a section some 8 m thick was sampled every 0.5 m at station 6, with the upper 3.5 m consisting of limestone to silty limestone. Sample FF07-6-1 occurs at the base of the section. The sample interval at map station 7 was across 3 m of section with samples taken approximately every 0.5 m. Samples at map station 8 (FF07-11) were taken every 1 m across a 3 m section, with sample 11-1 originating from the base of the section. In addition, 6 samples of Jurassic siltstone were taken at the top of the volcanoclastic-sedimentary unit (same locality as FF07-11) in hopes of obtaining an absolute age via a Re-Os isochron. Several analyses of thermal maturity were acquired through reflectance determinations on organic

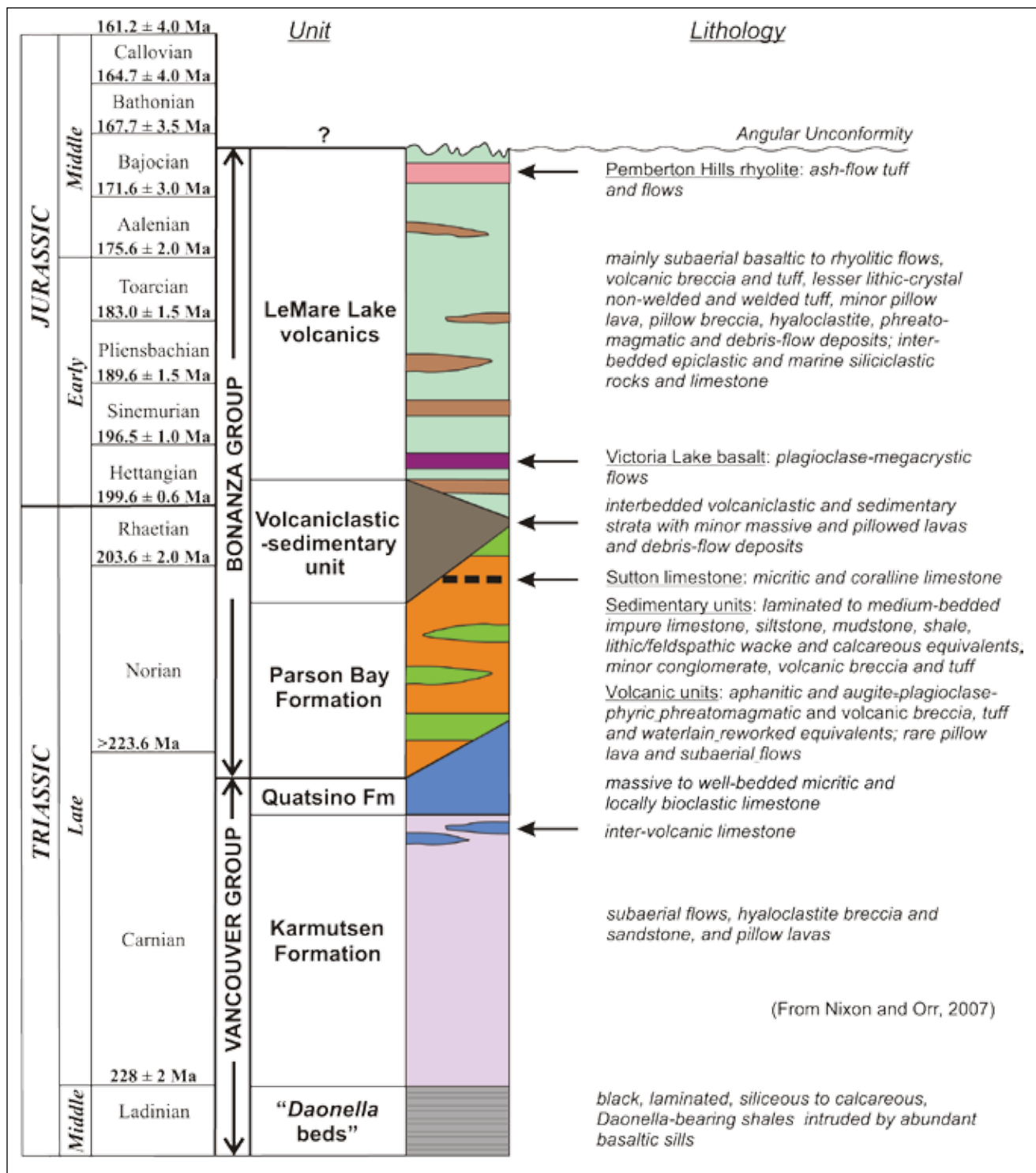


Figure 2: Schematic stratigraphy of northern Vancouver Island taken from Nixon and Orr (2007). The geological time scale is that of Gradstein et al. (2004), except for the Carnian-Norian Stage boundary, which is taken from Furin et al. (2006).

**TABLE 1: ROCK-EVAL PYROLYSIS RESULTS FOR SAMPLES OF SILTSTONE, SHALE, AND CARBONATE COLLECTED WITHIN THE VOLCANICLASTIC-SEDIMENTARY UNIT AND PARSONS BAY FORMATION. NUMBERS IN THE “MAP UNIT” COLUMN CORRELATE WITH SAMPLE LOCALITIES (PLOTTED IN FIGURE 3).**

Sample	Map		Easting	Northing	Mass	TOC(%)	S1	S2	S3	PI	S2/S3	PC(%)	Tmax	HI	OI
	Unit	Unit													
FF07-1	1	Parson Bay Fm.	603313	5589437	70.0	0.18	0.01	0.09	0.12	0.11	0.75	0.02	426	50	67
FF07-2	2	Parson Bay Fm.	603352	5589027	70.2	0.34	0.01	0.05	0.41	0.11	0.12	0.02	383	15	121
FF07-3	3	Sutton Lmst?	603174	5588607	70.1	0.21	0.01	0.06	0.08	0.14	0.75	0.01	386	29	38
FF07-4	4	Sutton Lmst?	603063	5588723	70.8	0.86	0.01	0.02	0.37	0.18	0.05	0.01	411	2	43
FF07-5A	5	Volc. Sed. Unit	602737	5588821	10.8	34.81	0.04	0.20	10.36	0.16	0.02	0.37	522	1	30
FF07-6-1	6	Volc. Sed. Unit	602670	5588918	20.2	7.41	0.02	0.03	1.38	0.37	0.02	0.05	342	0	19
FF07-6-2	6	Volc. Sed. Unit	602670	5588918	20.4	3.99	0.02	0.05	0.65	0.34	0.08	0.03	353	1	16
FF07-6-3	6	Volc. Sed. Unit	602670	5588918	20.5	4.95	0.01	0.01	0.46	0.66	0.02	0.02	302	0	9
FF07-6-4	6	Volc. Sed. Unit	602670	5588918	20.8	14.77	0.02	0.02	1.03	0.49	0.02	0.04	304	0	7
FF07-6-5	6	Volc. Sed. Unit	602670	5588918	20.8	4.16	0.01	0.02	1.28	0.41	0.02	0.05	330	0	31
FF07-6-6	6	Volc. Sed. Unit	602670	5588918	70.1	1.47	0.01	0.01	0.30	0.30	0.03	0.01	337	1	20
FF07-6-7	6	Volc. Sed. Unit	602670	5588918	70.1	1.76	0.00	0.01	0.39	0.40	0.03	0.01	336	1	22
FF07-6-8	6	Volc. Sed. Unit	602670	5588918	70.4	1.64	0.00	0.01	1.01	0.29	0.01	0.03	531	1	62
FF07-7	7	Volc. Sed. Unit	602600	5588877	70.0	4.15	0.01	0.01	0.15	0.49	0.07	0.01	324	0	4
FF07-8	7	Volc. Sed. Unit	602600	5588891	20.8	6.99	0.02	0.04	0.20	0.32	0.20	0.01	315	1	3
FF07-9	7	Volc. Sed. Unit	602603	5588882	50.4	16.45	0.01	0.04	0.35	0.27	0.11	0.02	309	0	2
FF07-10	7	Volc. Sed. Unit	602600	5588893	50.1	1.75	0.01	0.02	0.09	0.34	0.22	0.01	408	1	5
FF07-11-1	8	Volc. Sed. Unit	602430	5589259	50.9	4.46	0.03	0.03	0.13	0.52	0.23	0.01	368	1	3
FF07-11-2	8	Volc. Sed. Unit	602430	5589259	51.0	2.34	0.01	0.01	0.22	0.60	0.05	0.01	311	0	9
FF07-11-3	8	Volc. Sed. Unit	602430	5589259	50.5	4.37	0.01	0.03	1.94	0.32	0.02	0.07	329	1	44
7GNX-39-10-4	8	Volc. Sed. Unit	602430	5589259	50.7	3.03	0.01	0.03	0.28	0.28	0.11	0.01	295	1	9
7GNX-39-10-5	8	Volc. Sed. Unit	602430	5589259	50.3	3.37	0.01	0.01	0.40	0.30	0.03	0.01	334	0	12
7GNX-39-10-6	8	Volc. Sed. Unit	602430	5589259	50.9	4.25	0.01	0.03	0.21	0.31	0.14	0.01	489	1	5
7GNX-39-10-7	8	Volc. Sed. Unit	602430	5589259	69.9	2.83	0.01	0.01	0.15	0.35	0.07	0.01	550	0	5
7GNX-39-10-8	8	Volc. Sed. Unit	602430	5589259	70.6	2.70	0.01	0.02	0.16	0.25	0.13	0.01	327	1	6
7GNX-39-10-9	8	Volc. Sed. Unit	602465	5589234	50.3	2.52	0.00	0.01	0.11	0.41	0.09	0.01	339	0	4

Mass = mg; TOC = Total Organic Carbon, weight per cent; S1, S2 = mg hydrocarbons (HC)/g rock; S3 = mg CO<sub>2</sub>/g rock;

PI = Production Index = S1/(S1+S2); PC = Pyrolyzable Carbon(weight per cent) = ((0.83\*(S1+S2))+(S3\*.273)+ ((S3CO+(S3\*CO/2))\*0.4286))/10

Tmax = °C; HI = Hydrogen Index = (100\*S2)/TOC; OI = Oxygen Index = (100\*S3)/TOC

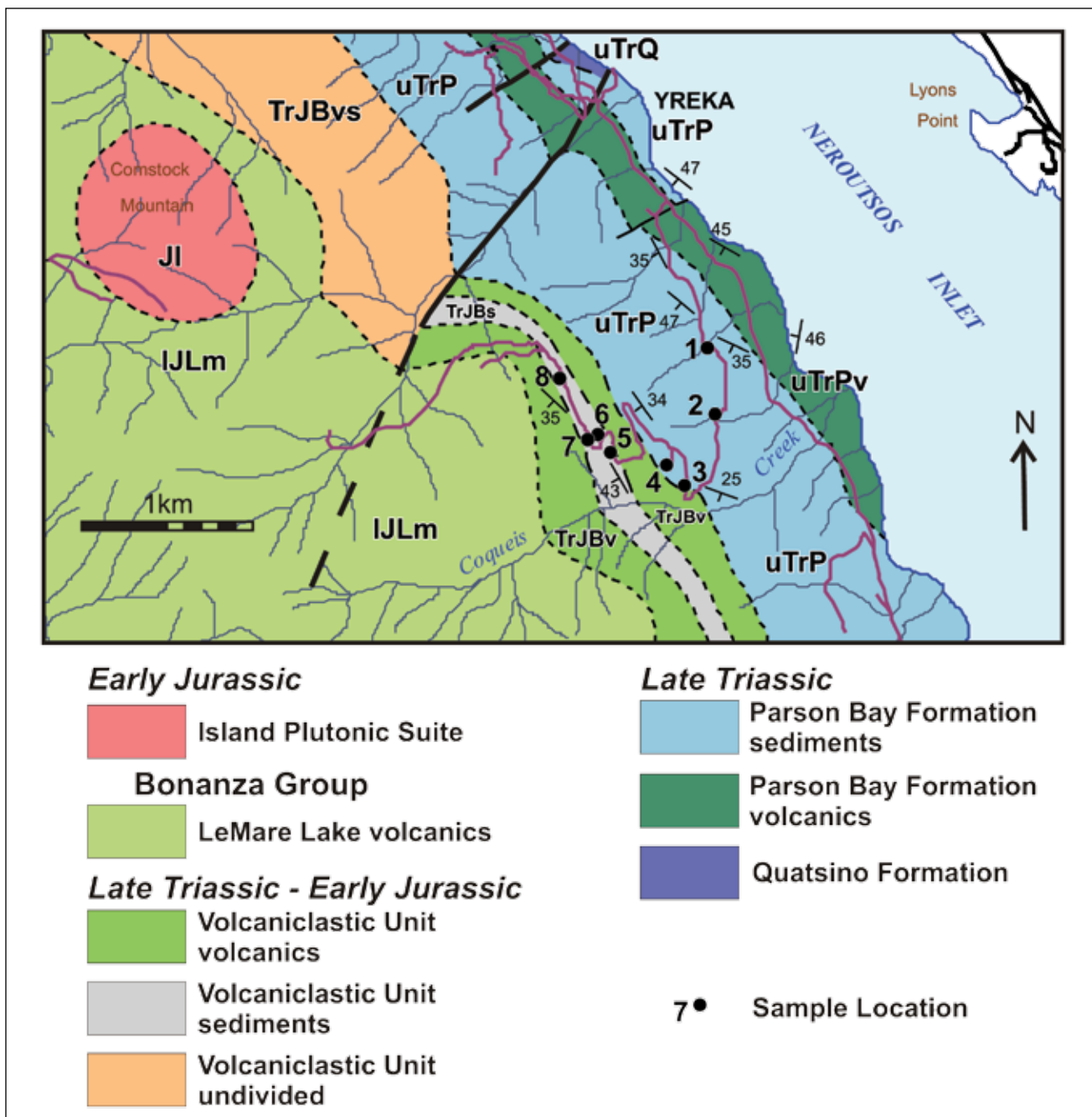


Figure 3: Detailed geological map of the study area showing location of sample sites. Sample locations correspond to “Map Unit” column in Table 1. Geological description of units can be found in Nixon et al. (2006).

matter (Table 2). In addition, 6 samples obtained for Re-Os geochronometry were analyzed by inductively coupled plasma mass spectrometry (ICP-MS) to determine if specific elemental concentrations were high enough to warrant proceeding further with this radiometric dating technique (Table 3).

## RESULTS AND DISCUSSION

### Organic Geochemistry

Thermal maturity levels, based on reflectance data from 2 samples, indicate the section reached or exceeded the dry gas preservation zone (%Ro equivalent 3.33 and 4.21; Table 2, Figure 4). High thermal maturity levels may be related to the abundant number of mafic to intermediate sills and dykes that cut the volcaniclastic-sedimentary unit

**TABLE 2: RO EQUIVALENT VALUES FROM ORGANIC MATERIAL FOUND WITHIN SELECT SAMPLES OF THE VOLCANICLASTIC-SEDIMENTARY UNIT. SAMPLE LOCALITIES CAN BE SEEN IN FIGURE 3.**

Sample	Easting	Northing	OT <sup>1</sup>	%R <sub>oR</sub>	SD	N	%R <sub>o</sub> max	%R <sub>o</sub> equiv <sup>2</sup>	%R <sub>o</sub> min	SD	COMMENTS
FF07-5b	602737	5588821	21	5.73	0.30	29		3.94			Mainly pyrobitumen showing signs of oxidation. Some are very fine to fine grain anisotropic pyrobitumen.
			21,30	4.75	0.19	8		3.33			Some are oxidized and some are min %Ro of anisotropic bitumen matrix. See organic type 33 %R <sub>o</sub> .
			21,30	6.63	0.11	14		4.50			
			33				5.7		4.70		
FF07-6-9	602670	5588918	30, 33	4.91	0.44	39	5.45		4.64	0.19	Mostly very to fine grain pyrobitumen (organic type 33) and granular pyrobitumen (organic type 30) within carbonate fractures and pores.
			21	6.17	0.16	3		4.21			

OT = organic type; SD = standard deviation; N = number of analysis

<sup>1</sup>Grint and March (1981), White (1976); <sup>2</sup>0.618\*%R<sub>oR</sub> + 0.4; Jacob (1989)

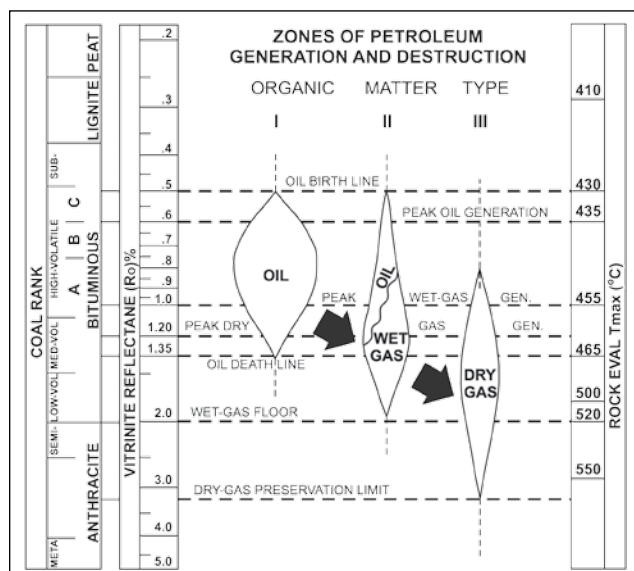


**Figure 4: Zones of hydrocarbon generation and destruction with respect to coal rank, vitrinite reflectance, and Tmax values from Rock-Eval pyrolysis. Modified from Leckie et al. (1988) and Dow (1977).**

and were most likely feeders to LeMare Lake volcanism. In addition, Jurassic volcanism and plutonism was likely accompanied by elevated heat flows.

Organic carbon levels for these rocks are generally over 2%, with some samples returning concentrations as high as 35%. The high organic carbon levels in these later samples suggest coaly material, although petrographic work indicates it is mostly pyrobitumen (Table 2; figures 5 and 6). The high thermal maturities in these samples, together with S2 and HI values (Table 1), also indicate that much of the hydrocarbons have been expelled and suggest that initial organic carbon levels were significantly higher. Consequently, based on pyrolysis results, very little can be

deduced about the original nature of the organic material. Characterization of this organic material could be achieved by further petrographic work.

Correlations of this stratigraphy with strata along northernmost parts of Vancouver Island and the Queen Charlotte Basin suggest this organic-rich horizon is most likely time-equivalent to parts of the Kunga and Maude Groups. These latter 2 units have organic-rich horizons containing Type II kerogens that were sources of oils found within the Queen Charlotte Basin (see Bustin 1997; Vellutini and Bustin 1991; Hamilton 1989). If this correlation is correct, the carbonaceous shales and siltstones of the volcanoclastic-sedimentary unit may have produced significant quantities of oil early in the thermal history of this area.

### Re-Os Geochronometry

The ability to use the Re-Os geochronometer depends on high enough levels of these elements for accurate analysis. The reducing environment represented by these black shales would have facilitated the incorporation of various elements, such as Re, from the sea water during their deposition. Creaser et al. (2002) indicate that Re and Os levels within organic-rich shales are up to 2 orders of magnitude higher than average continental crustal rocks. As such, a first step in determining the suitability of the Re-Os geochronometer in a sedimentary sequence is to establish if sea water conditions were reducing during sediment deposition. An indirect means of establishing this is an analysis of total organic carbon (TOC) content. Typically, TOC contents of 2% or higher result from preservation of organic material in reducing environments. Direct measurement of Re through ICP-MS analysis is suspect due to the volatile nature of this element during sample preparation and analysis; as such, its relative abundance is determined by measuring the levels

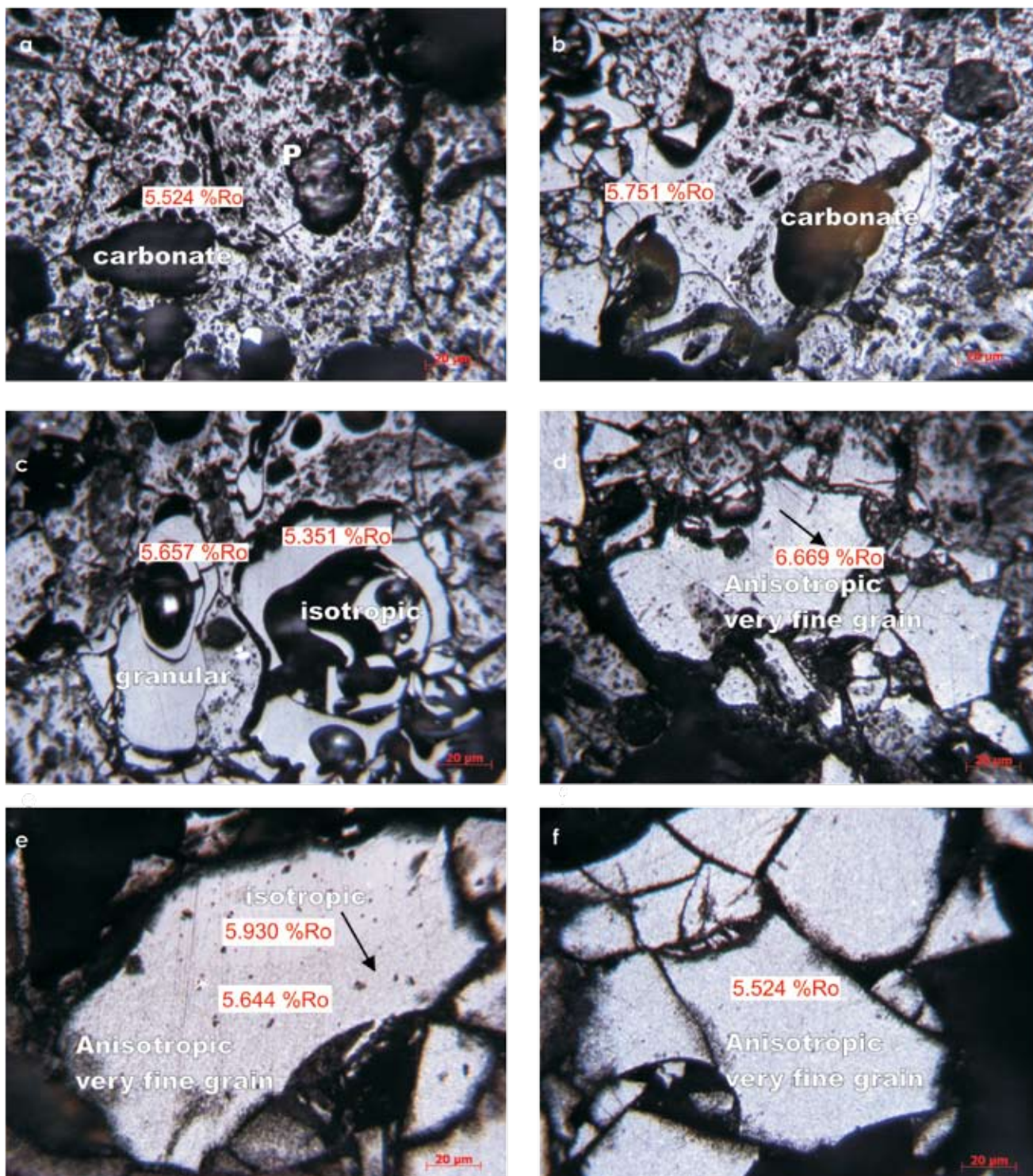
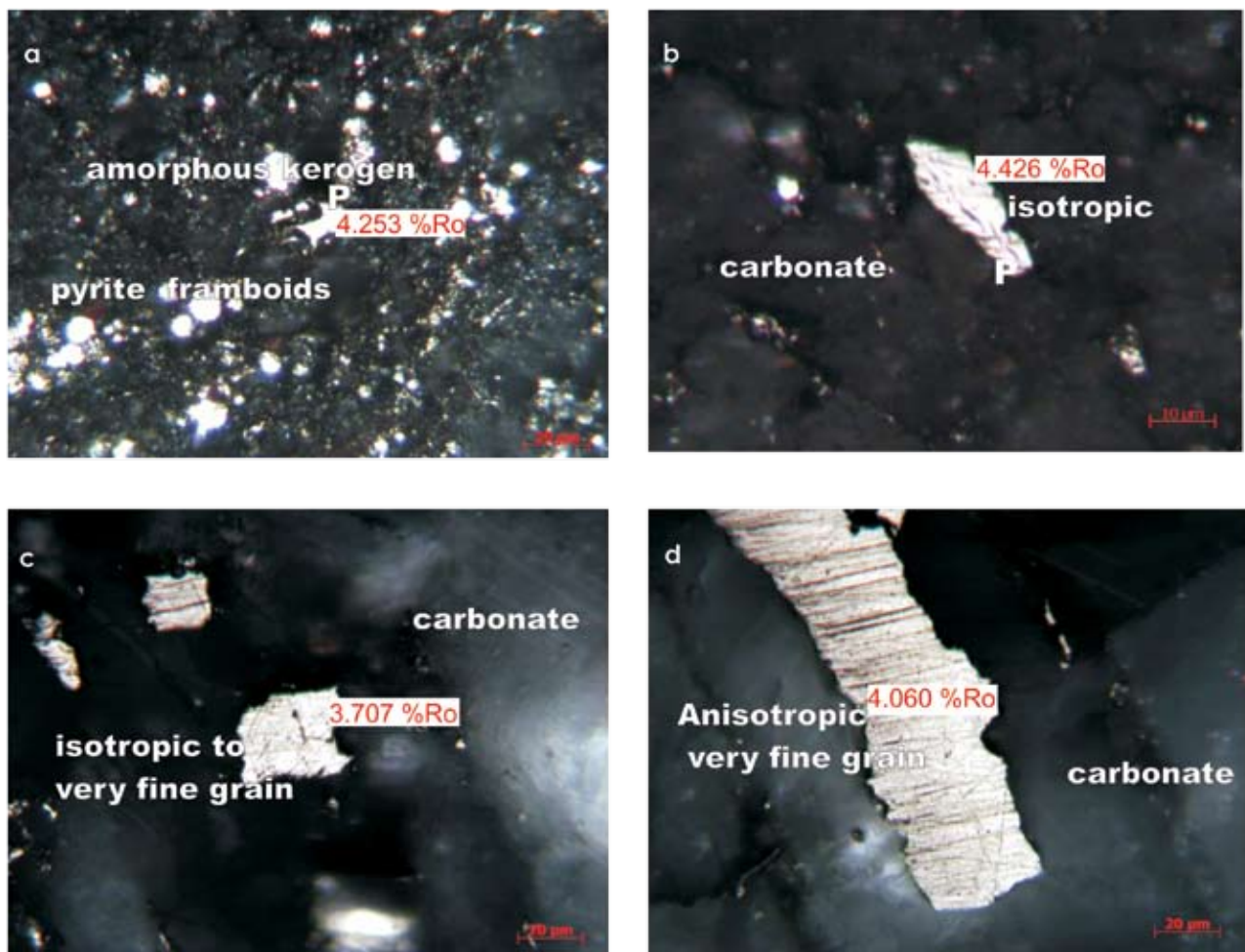


Figure 5: The high percentage of organic carbon in this sample is from bitumen/pyrobitumen consisting of; (a and c) networks of partially oxidized isotropic solid pyrobitumen; (c and d) very fine grain anisotropic pyrobitumen, and (e and f) large matrix of both isotropic and anisotropic and fine grained pyrobitumen. P – pyrobitumen.



**Figure 6: Mainly brecciated amorphous kerogen within carbonate matrix (a). Isotropic pyrobitumen (b) to anisotropic very fine grain pyrobitumen (c and d) migrated into the pores and fractures of the carbonate matrix. P – pyrobitumen.**

of other elements (Mo, V, Cr, Cd, U) that are incorporated into the sediment in levels proportional to Re. On average, Mo concentrations are 1000 times those of Re (R. Creaser, personal communication 2008).

Whole rock geochemistry of the 6 samples near the top of the sequence is shown in Table 3. The concentrations of Mo within the 6 samples indicates that only 4 samples (07GNX-39-10-4, 5, 6, 9) have levels high enough to suggest corresponding Re concentrations suitable for Re-Os geochronometry (R. Creaser, personal communication 2008). These samples are currently being analyzed and further samples will be acquired along this horizon to better constrain the isochron and obtain a more precise age.

## CONCLUSIONS

- In northern Vancouver Island, an organic-rich sequence of Late Triassic to Early Jurassic age and up to 50 m thick is present within the upper part of the volcanoclastic-sedimentary unit, transitional between the Parsons Bay Formation and LeMare Lake volcanics of the Bonanza Group.
- Organic carbon contents within this horizon are up to 34% and average approximately 6%.
- Thermal maturity, based on Ro analysis of organic matter, suggests the sequence is at or above the upper limit of the dry gas preservation zone.
- Preliminary analysis of 6 samples collected for Re-Os geochronometry to better constrain the absolute age of the Triassic-Jurassic boundary suggests that several of these will be suitable for delineating an isochron and that further sampling and analysis is justified.

**TABLE 3: SELECT MAJOR, MINOR, AND TRACE ELEMENT CONCENTRATIONS WITHIN SAMPLES COLLECTED FOR RE-OS GEOCHRONOLOGY.\***

Element		Det. limit	07GNX-39-10-4	07GNX-39-10-5	07GNX-39-10-6	07GNX-39-10-7	07GNX-39-10-8	07GNX-39-10-9
			VSU	VSU	VSU	VSU	VSU	VSU
			Siltstone 602430N 5589259E	Limestone 602465N 5589234E				
P	%	0.001	0.014	0.027	0.013	0.04	0.036	0.018
Ti	%	0.01	0.21	0.28	0.28	0.45	0.42	0.23
S	%	0.01	2.86	4.6	3.75	4.68	5.31	3.59
Fe	%	0.01	3.09	5.01	4.58	5.51	4.79	2.95
Na	%	0.001	1.49	1.88	1.51	2.16	1.96	1.24
Mg	%	0.01	0.68	0.49	0.31	0.74	0.8	0.25
Al	%	0.01	5.5	7.56	6.83	> 10.0	9.94	4.77
K	%	0.01	0.9	1.49	1.44	2.82	2.23	0.88
Ca	%	0.01	0.62	4.93	0.15	0.54	3.78	5.46
Mn	ppm	1	277	496	218	357	434	398
Cu	ppm	0.2	21.8	28	33.9	28.1	24.1	19
Pb	ppm	0.5	5.4	2.9	3.4	4	3.5	2.5
Zn	ppm	0.2	60	76.6	29.2	40	69.3	53.7
Ag	ppm	0.05	< 0.05	0.05	0.05	< 0.05	< 0.05	< 0.05
Mo	ppm	0.1	13.9	30.3	23.4	7.1	6.7	17
Ni	ppm	0.5	11.8	20.9	17.9	13.1	14.6	12.8
Cd	ppm	0.1	0.3	0.6	0.3	0.2	0.6	0.5
V	ppm	1	41	91	85	151	133	46
Cr	ppm	0.5	22.7	37.4	33.3	59.1	41.4	18.4
Ba	ppm	1	88	70	24	26	49	98
Li	ppm	0.5	9.7	6.9	4.7	9	8.4	3.6
B	ppm	1	24	5	5	7	4	3
Hf	ppm	0.1	1.5	2	2.1	2	1.8	1.4
Cs	ppm	0.05	0.8	1.1	1.5	2.2	1.8	0.7
Co	ppm	0.1	4.9	11.3	6.4	7.3	10.6	5.7
Eu	ppm	0.05	0.6	1	0.5	0.9	1	0.6
Bi	ppm	0.02	0.15	0.39	0.13	0.12	0.12	0.1
Se	ppm	0.1	1.6	2.4	1.9	3.1	1.8	1.6
Ga	ppm	0.1	6.7	10.1	8.4	16.9	14.5	6.2
As	ppm	0.1	8.4	12.7	12.8	8.9	7.2	7.6
Rb	ppm	0.2	27.2	38.6	41.7	76.8	64.1	22.7
Y	ppm	0.1	13.6	24.5	12	24	23.3	14.6
Sr	ppm	0.2	286	381	178	426	461	511
Zr	ppm	1	31	52	54	54	48	34
Nb	ppm	0.1	1	2	1.2	3.4	2.6	1.4
Er	ppm	0.1	1.7	2.9	1.5	3	2.8	1.9
Be	ppm	0.1	0.4	0.6	0.5	0.7	0.7	0.4
Ho	ppm	0.1	0.6	1	0.5	1	1	0.6
In	ppm	0.1	< 0.1	< 0.1	< 0.1	< 0.1	< 0.1	< 0.1
Sn	ppm	1	< 1	1	1	1	< 1	< 1
Sb	ppm	0.1	1.1	1.2	1.3	0.6	0.8	0.7
Te	ppm	0.1	< 0.1	< 0.1	0.2	< 0.1	< 0.1	< 0.1
La	ppm	0.1	5	9.6	4.6	8.7	10.9	6.9
Ce	ppm	0.1	10.6	18.3	10.9	19.6	22.1	13.3
Pr	ppm	0.1	1.8	3.1	1.7	3.4	3.6	2.1
Nd	ppm	0.1	8.3	14.9	7.7	15.5	16.4	9.8
Sm	ppm	0.1	2	3.4	1.7	3.5	3.6	2.2
Gd	ppm	0.1	2.5	4.4	2.1	4.4	4.6	2.7
Tb	ppm	0.1	0.4	0.6	0.3	0.7	0.6	0.4
Dy	ppm	0.1	2.1	3.7	1.9	3.8	3.7	2.3
Ge	ppm	0.1	0.1	0.1	0.1	0.1	0.1	0.1
Tm	ppm	0.1	0.2	0.4	0.2	0.4	0.4	0.3
Yb	ppm	0.1	1.6	2.7	1.5	2.9	2.6	1.8
Lu	ppm	0.1	0.2	0.4	0.2	0.4	0.4	0.3
Ta	ppm	0.1	< 0.1	0.1	0.1	0.2	0.2	0.1
W	ppm	0.1	1	1	0.8	0.9	0.6	0.4
Re	ppm	0.001	0.029	0.05	0.042	0.022	0.022	0.033
Tl	ppm	0.05	0.34	0.59	0.75	0.58	0.48	0.34
Th	ppm	0.1	1.1	1.2	1.7	1.9	1.8	1
U	ppm	0.1	3.7	6.9	5.8	4.5	3.9	2.5

VSU = Volcanic Sedimentary Unit  
 All samples steel milled at ACTLABS, Ancaster, Ontario.  
 All samples digested by HF-HClO4-HNO3-HCl  
 P, Ti and S determined by inductively coupled plasma emission spectrometry  
 All other elements determined by inductively coupled plasma mass spectrometry  
 % - per cent; ppm - parts per million

*\*These analyses were determined by inductively coupled plasma mass and emission spectrometry at Activation Laboratories in Ontario. Sample locations shown in Figure 3.*

## ACKNOWLEDGEMENTS

The senior author would like to acknowledge the assistance of Ray Lett in the preparation and submission of samples for analysis. Robert Creaser's willingness to undertake the analysis for a Re-Os isochron along this horizon and his help in trying to determine suitable samples is also appreciated.

## REFERENCES

- Bustin, R.M. (1997): Petroleum source rocks, organic maturation and thermal history of the Queen Charlotte Basin, British Columbia; *Bulletin of Canadian Petroleum Geology*, Volume 45, pages 255–278.
- Creaser, R.A., Sannigrahi, P., Chacko, T., and Selby, D. (2002): Further evaluation of the Re-Os geochronometer in organic-rich sedimentary rocks: A test of hydrocarbon maturation effects in the Exshaw Formation, Western Canada Sedimentary Basin; *Geochimica et Cosmochimica Acta*, Volume 66, pages 3441–3452.
- Dow, W. (1977): Kerogen studies and geological interpretations; *Journal of Geochemical Exploration*, Volume 7, pages 79–99.
- Furin, S., Preto, N., Rigo, M., Roghi, G., Gianolla, P., Crowley, J.L., and Bowring, S.A. (2006): High-precision U-Pb zircon age from the Triassic of Italy: implications for the Triassic time scale and the Carnian origin of calcareous nannoplankton and dinosaurs; *Geology*, Volume 34, pages 1009–1012.
- Gradstein, F.M., Ogg, J.G., and Smith, A.G. (2004): A geologic time scale 2004; *Cambridge University Press*, Cambridge, UK, 610 pages.
- Grint, A. and March, H. (1981): Carbonization of coal blends mesophase formation. *Fuel*, Volume 60, pages 1115–1120.
- Hamilton, T.S. (1989): Hydrocarbon occurrences on the western margin of the Queen Charlotte Basin; *Bulletin of Canadian Petroleum Geology*, Volume 37, pages 443–466.
- Jacob, H. (1989): Classification, structure, genesis and practical importance of natural solid bitumen (migrabitumen). *International Journal of Coal Geology*, Volume 11, pages 65–69.
- Leckie, D.A., Kalkreuth, W.G., and Snowdon, L.R. (1988): Source rock potential and thermal maturity of Lower Cretaceous strata: Monkman Pass area, British Columbia; *American Association of Petroleum Geologists Bulletin*; Volume 72, pages 820–838.
- Massey, N.W.D. (1995a): Geology and mineral resources of the Alberni-Nanaimo lakes sheet, Vancouver Island, 92F/1W, 92F/2E and part of 92F/7E; *BC Ministry of Energy, Mines and Petroleum Resources*, Paper 1992-2, 132 pages.
- Massey, N.W.D. (1995b): Geology and mineral resources of the Cowichan Lake sheet, Vancouver Island, 92C/16; *BC Ministry of Energy, Mines and Petroleum Resources*, Paper 1992-3, 112 pages.
- Massey, N.W.D. (1995c): Geology and mineral resources of the Duncan sheet, Vancouver Island, 92B/13; *BC Ministry of Energy, Mines and Petroleum Resources*, Paper 1992-4, 112 pages.
- Massey, N.W.D., McIntyre, D.G., Desjardins, P.J., and Cooney, R.T. (2005): Digital geology map of British Columbia: whole province; *BC Ministry of Energy, Mines and Petroleum Resources*, Geofile 2005-1.
- Resources, Geofile 2005-1. Monger, J.W.H. and Journeay, J.M. (1994): Basement geology and tectonic evolution of the Vancouver region; in *Geology and Geological Hazards of the Vancouver Region, Southwestern British Columbia*, Monger, J.W.H., Editor, *Geological Survey of Canada*, Bulletin 481, pages 3–25.
- Monger, J.W.H., Price, R.A., and Tempelman-Kluit, D.J. (1982): Tectonic accretion and the origin of the two major metamorphic and plutonic belts in the Canadian Cordillera. *Geology*, Volume 10, pages 70–75.
- Nixon, G.T. and Orr, A.J. (2007): Recent Revisions to the Early Mesozoic Stratigraphy of Northern Vancouver Island (NTS 102I, 092L) and Metallogenic Implications, British Columbia; in *Geological Fieldwork 2006, BC Ministry of Energy, Mines and Petroleum Resources*, Paper 2007-1, pages 163–177.
- Nixon, G.T., Friedman, R.M., Archibald, D.A., Orchard, M.J., and Tozer, T. (2000): A contribution to the geologic time scale: the Triassic-Jurassic boundary, northern Vancouver Island, Canada; *Geological Society of America*, Cordilleran Section, Annual Meeting, Vancouver, BC, Abstract Number 80179.
- Nixon, G.T., Snyder, L.D., Payie, G.J., Long, S., Finnie, A., Friedman, R.M., Archibald D.A., Orchard, M.J., Tozer, T., Poulton, T.P., and Haggart, J.W. (2006): Geology of the Alice Lake area, northern Vancouver Island; *BC Ministry of Energy, Mines and Petroleum Resources*, Geoscience Map 2006-1, scale 1:50 000.
- Selby, D. and Creaser, R.A. (2005): Direct radiometric dating of the Devonian-Mississippian time-scale boundary using the Re-Os black shale geochronometer; *Geological Society of America*, Volume 33, pages 545–548.
- van der Heyden, P. (1991): A Middle Jurassic to Early Tertiary Andean-Sierran arc model for the Coast Belt of British Columbia; *Tectonics*, Volume 11, pages 82–97.
- Vellutini, D. and Bustin, R. (1991): Source rock potential of Mesozoic and Tertiary strata of the Queen Charlotte Islands, British Columbia; in *Evolution and Hydrocarbon Potential of the Queen Charlotte Basin, British Columbia*; Woodsworth, G. J. Editor, *Geological Survey of Canada*, Paper 1990-10, pages 381–409.
- Wheeler, J.O. and McFeely, P. (1991): Tectonic Assemblage Map of the Canadian Cordillera and adjacent parts of the United States of America, *Geological Survey of Canada*, Map 1712A.
- White, J.L. (1976): Mesophase mechanisms in the formation of the microstructure of petroleum coke; in *Petroleum-derived carbons*; M.L. Deviney and T.M. O'Grady, Editors, *American Chemical Society Symposium Series*, Number 21, pages 282–314.



# CARBON CAPTURE AND STORAGE IN BRITISH COLUMBIA

by Alf Hartling, P.Geo., Senior Petroleum Geologist<sup>1</sup>

## ABSTRACT

The British Columbia government has implemented ambitious targets to reduce atmospheric discharge of greenhouse gases. One possible mitigation strategy is carbon capture and storage - the collection of carbon dioxide (CO<sub>2</sub>) produced at large industrial facilities and its permanent sequestration deep underground in geological rock formations. Large sources of anthropogenic greenhouse gases in BC have been identified and matched where possible with potential storage sites.

Some industries, such as natural gas processing, are well suited for carbon capture because the technology is available with storage opportunities often located reasonably nearby. In northeastern BC, there are a number of large natural-gas processing plants and several commercial-scale sequestration projects and the Western Canada Sedimentary Basin (WCSB) provides suitable porous and permeable reservoirs for CO<sub>2</sub> storage in depleted natural gas pools and deep saline formations.

Hartling, A., (2008); Carbon capture and storage in British Columbia; in Geoscience Reports 2008, BC Ministry of Energy, Mines and Petroleum Resources, pages 25-31.

<sup>1</sup>British Columbia Ministry of Energy, Mines and Petroleum Resources, Resource Development and Geoscience Branch  
PO Box 9333 Stn. Prov. Govt., Victoria, BC, V8W 9N3; e-mail: alf.hartley@gov.bc.ca

**Key Words:** carbon dioxide, greenhouse gas, capture, storage, sequestration, northeastern British Columbia, Western Canada Sedimentary Basin, reservoir, monitoring.

## INTRODUCTION

Anthropogenic greenhouse gases include CO<sub>2</sub>, methane (CH<sub>4</sub>), nitrous oxide (N<sub>2</sub>O), and various fluorocarbon groups. In BC, CO<sub>2</sub> constitutes 80% of these anthropogenic emissions (Environment Canada 2007). Many scientists consider the significant increase in CO<sub>2</sub> concentration in the atmosphere to be responsible for enhancing the Earth's natural "greenhouse effect" and thus heightening global warming (IPCC 2007).

The Province of British Columbia has introduced legislation setting targets to reduce greenhouse gas emissions by 33% below 2007 levels by 2020, increasing to 80% by 2050. Figure 1 is a simplified illustration of this challenge. The "business as usual" trend could exceed 80 Mt CO<sub>2</sub> equivalent by 2020 if not constrained. The actual emissions level for 2007 is being stringently reviewed to provide a more accurate baseline. The 2007 value estimated in Figure 1 (69.5 Mt CO<sub>2</sub> equivalent) was projected using the most recent data available from Environment Canada (Environment Canada 2007). To achieve these aggressive targets, all available mitigation strategies must be utilized, including conservation, energy efficiency, use of alternative energy sources, and carbon capture and storage.

## Carbon Capture and Storage

Carbon capture and storage is a process to reduce the amount of anthropogenic CO<sub>2</sub> emitted into the atmosphere. It entails collecting CO<sub>2</sub> from large industrial sources and permanently storing it deep underground in the pore space of geological rock formations. The first step is to identify major CO<sub>2</sub> sources that are located within approximately 300 km of potential geological storage sites. A concentrated

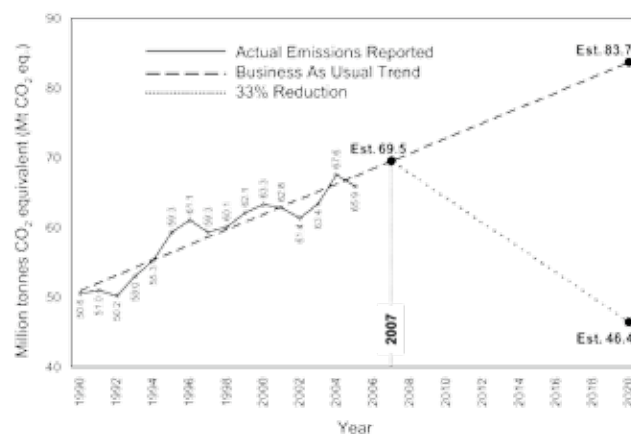


Figure 1: Greenhouse gas emissions in British Columbia (Environment Canada 2007), business as usual trend through 2020 based on historic data, and projection of a 33% reduction in emissions from an estimated 2007 value (69.5 Mt CO<sub>2</sub> equivalent) through 2020.

stream of CO<sub>2</sub> is captured at the source and compressed in preparation for transport (generally via pipeline) to a storage facility, where it is injected through a well bore into the pore space of a suitable geological reservoir. The storage reservoir must a) have enough capacity to contain the CO<sub>2</sub> delivered throughout the project life; b) have sufficient permeability to allow injection of CO<sub>2</sub> more-or-less as it arrives on-site; and c) be able to permanently confine the injected gas. The area surrounding the site should be monitored to track CO<sub>2</sub> movement within the geological formation and verify there is no leakage.

### Carbon Dioxide

CO<sub>2</sub> under normal surface conditions is a colourless, odourless, non-flammable gas that is denser than air. At elevated pressure and temperature the density increases, reaching a critical point at 7.38 MPa and 31.1 °C, where CO<sub>2</sub> behaves as a dense, supercritical fluid. These conditions are met across much of BC at burial depths below approximately 800 m. The solubility of CO<sub>2</sub> in water in-

creases with pressure (i.e., depth) while decreasing with rising temperature and/or salinity (i.e., depth). These characteristics are important parameters when selecting a storage reservoir. Storage efficiency is significantly improved if this dense, supercritical phase is maintained because more CO<sub>2</sub> can be injected into the rock's pore space. Supercritical CO<sub>2</sub> is less buoyant in formation fluid, thereby migrating more slowly in the subsurface.

### SOURCES

All Canadian companies that emit greenhouse gases in excess of 0.1 Mt CO<sub>2</sub> equivalent are required to report the volumes to Environment Canada under the *Canadian Environmental Protection Act, 1999*. In BC, 38 companies filed emission reports for 2006; their emissions totalled 12.3 Mt CO<sub>2</sub> equivalent (Environment Canada 2007) and represented 18.5% of the provincial emissions estimate of 69.5 Mt. Figure 2 shows the locations of these facilities, the relative amounts of CO<sub>2</sub> emitted, and the sedimentary basins found within BC.

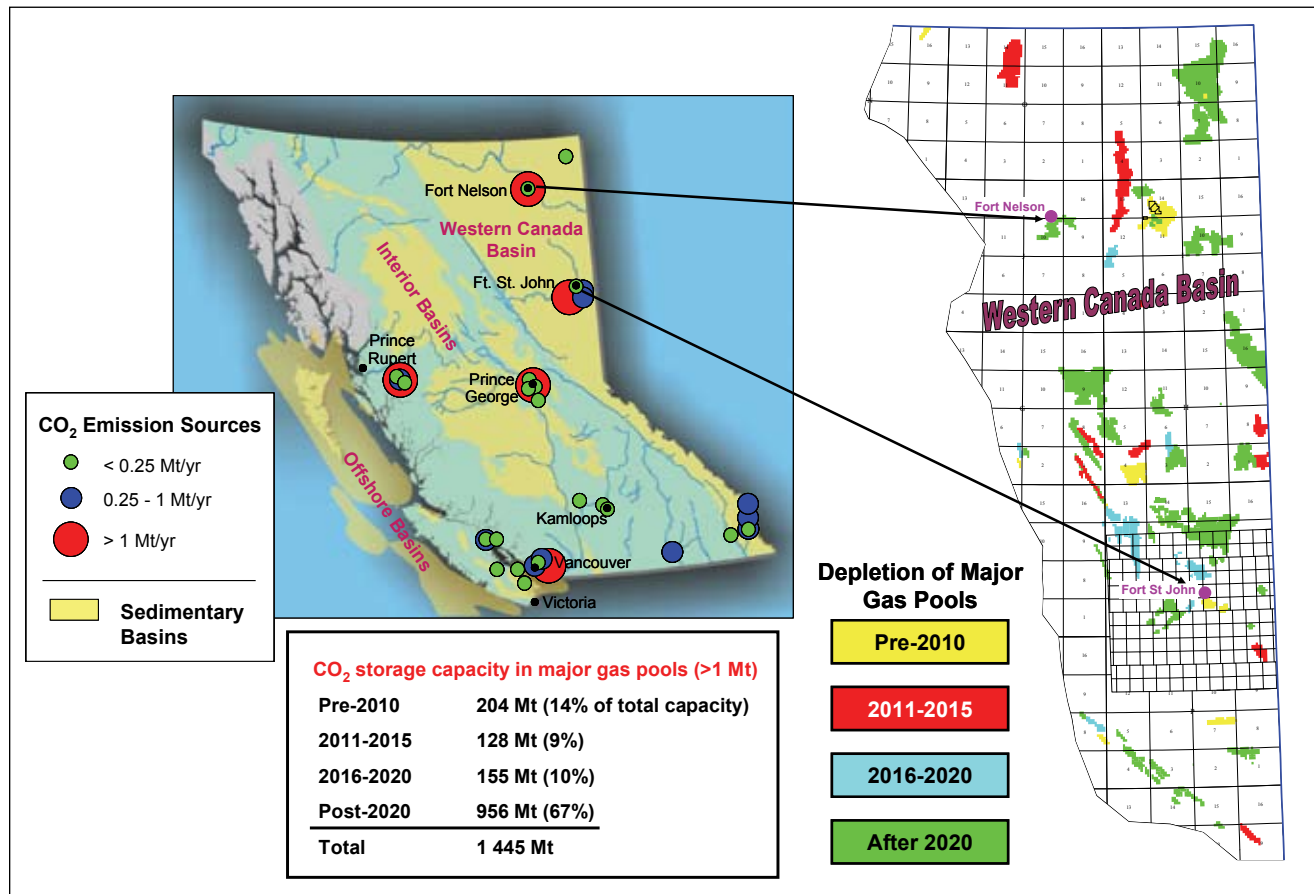


Figure 2: Sedimentary basins, large CO<sub>2</sub> emission sources, and the storage capacity and geographic distribution of depleting gas pools in British Columbia. (Data sources: Environment Canada 2007; Bachu 2006a, 2006b).

Major causes of anthropogenic CO<sub>2</sub> emissions include the combustion of fossil fuels (oil, gas, and coal), industrial processes, such as the “sweetening” of raw natural gas (removal of CO<sub>2</sub> and hydrogen sulphide, H<sub>2</sub>S), and deforestation.

## CAPTURE

Carbon capture is the collection of a concentrated stream of CO<sub>2</sub> using chemical reactions and/or physical means. CO<sub>2</sub> can be captured in a variety of ways from industrial processes or from combustion of fossil fuels.

Sour gas (greater than 0.5% H<sub>2</sub>S) produced from deeper pools in northeastern BC contains varying amounts of naturally occurring CO<sub>2</sub> and H<sub>2</sub>S. These impurities must be removed to improve the heating quality of the product and to meet pipeline specifications. Legislation prohibits the release of sulphur into the atmosphere; as a result, either sulphur is stripped out and retained at surface or the H<sub>2</sub>S is re-injected underground. Twelve sites have been approved (9 currently active) for acid gas disposal in northeastern BC. Approximately 40 sites are operational in similar settings in Alberta, all of which act as commercial-scale demonstration projects illustrating the feasibility of carbon capture and storage technology.

Flue gas emitted from industrial complexes because of the burning of fossil fuels generally has a low concentration of CO<sub>2</sub>, ranging from 5 to 15%. Other constituents, primarily nitrogen, oxygen, and water vapour, are not considered harmful to the environment and do not require abatement measures. It is impractical to capture, compress, transport, and store the entire flue gas stream, so CO<sub>2</sub> must be removed from the flue gas on-site.

There are 3 possible means of capturing CO<sub>2</sub> from flue gas:

- Post-combustion: CO<sub>2</sub> is removed using an amine solvent;
- Pre-combustion: fossil fuel is pre-mixed with steam and oxygen to produce carbon monoxide (CO) and hydrogen (H). The CO is combined with steam resulting in CO<sub>2</sub> (separated) and H (used as fuel); and
- Oxyfuel combustion: oxygen is used during initial combustion, creating water vapour and CO<sub>2</sub>. The water vapour is cooled and condensed, leaving relatively pure CO<sub>2</sub>.

Most CO<sub>2</sub> capture technology is available, though presently being applied to other industrial processes or for much smaller-scaled purposes. These CO<sub>2</sub> capture techniques can be more effective when applied to large, fossil fuel-fired industrial facilities, such as power generation plants. If CO<sub>2</sub> can be sequestered, emission levels from such facilities can be drastically reduced. These capture systems and compress-

ion necessary for transportation require an estimated 10 to 40% additional fuel consumption but can provide net emission reductions up to 80 to 90%. There are currently no large (500 MW) power plants employing CO<sub>2</sub> capture in the world, though a number are in the planning stage (outside BC).

## TRANSPORTATION

Relatively pure CO<sub>2</sub> is compressed into a supercritical state at source in preparation for transportation, usually via pipeline, to a storage site. To minimize metal corrosion, the gas is dehydrated before entering the pipeline. Transportation efficiency is improved by maintaining pipeline pressure above 8 MPa, keeping the CO<sub>2</sub> in its supercritical phase. Upstream compressors provide the drive mechanism, with booster stations installed as needed along the line.

There are several short acid gas (CO<sub>2</sub> + H<sub>2</sub>S) pipelines presently active in northeastern BC. There are more than 2 500 km of pipeline in the southern United States transporting greater than 45 Mt CO<sub>2</sub>/year for enhanced oil recovery (EOR) projects, mainly in Texas. Of note, a 320 km pipeline currently supplies roughly 6 500 tonnes/day CO<sub>2</sub> to an EOR project at Weyburn in southeastern Saskatchewan.

## GEOLOGICAL STORAGE

Geological storage requires a porous and permeable reservoir to contain the injected CO<sub>2</sub>. The sedimentary rocks most likely to have suitable reservoir characteristics are unique to sedimentary basins, of which there are a number throughout BC (Figure 2). The geological setting of a potential sequestration site must be well understood before its suitability can be determined; the Western Canada Sedimentary Basin in northeastern BC is promising because of the abundant geological data generated by the oil and gas industry.

Potential CO<sub>2</sub> storage reservoirs include depleted oil and gas pools, deep saline formations, unmineable coal beds, salt caverns, and abandoned gas storage facilities. In BC, the most feasible options are depleted gas pools and deep saline formations; these provide a good combination of storage capacity, cost effectiveness, minimal leakage risk, and public acceptance. There are also many existing oil pools at or near depletion that could potentially utilize CO<sub>2</sub> for enhanced oil recovery (EOR), extending their economic life by producing as much as 15% incremental reserves. The reservoirs can be filled with CO<sub>2</sub> prior to de-commissioning the EOR project.

Optimal conditions for CO<sub>2</sub> sequestration include:

- Proximity to large CO<sub>2</sub> source
- Existing wells in good condition
- Favourable reservoir characteristics to maximize storage efficiency (capacity and injectivity commensurate with project volumes, reservoir pressure and temperature above CO<sub>2</sub> critical point)
- Very low risk of leakage (stratigraphic isolation/competent seals)
- Minimal risk of contaminating nearby hydrocarbon pools
- Existing regulatory regime
- Expertise, knowledge, and workforce readily available
- Infrastructure available
- Potential for EOR or desulphurization projects to create economic value
- Tectonically stable area

Given these criteria, the best opportunities for early implementation of CO<sub>2</sub> storage exist in the northeast of the province - there are large CO<sub>2</sub> point sources (gas processing plants), and the Western Canada Sedimentary Basin provides ample storage space in gas pools that will be depleting over the next few decades as well as in deep saline formations. Also, there is infrastructure, expertise, a knowledgeable workforce, and existing regulations because of the active oil and gas industry and on-going acid gas re-injection operations.

Bachu (2006a) estimated a CO<sub>2</sub> storage capacity in northeastern BC of 1 935 Mt in 353 existing hydrocarbon pools. Of this volume, 1 440 Mt (approximately 75%) is found in the largest 80 pools, ranging in size from 1 Mt (minimum size considered) to 118 Mt. Virtually all of the capacity will be in depleted gas pools, with a very small contribution from depleted oil pools (5 Mt). The timing of availability for the 80 largest pools is not uniformly distributed, with 67% not accessible until after 2020 (Figure 2). Consequently, deep saline formations will have to be utilized to meet storage requirements in the short to intermediate term.

It is difficult to estimate the potential storage volume of deep saline formations as there is a significant shortage of data necessary for accurate calculation. There are a number of deep saline formations that could bridge the timing and areal distribution gap until more storage is available in depleted gas pools. These saline formations are sufficiently well understood to allow for safe usage. Key parameters such as porosity, permeability, reservoir pressure and temperature, and depth of burial can be obtained from existing well data (petrophysical well logs, core analyses) or estimated using information obtained from nearby hydrocarbon pools or similar formations analysed elsewhere. When assessing the risk of CO<sub>2</sub> leakage, proxy data can be used to better understand cap rock competency and the effect of reservoir heterogeneity on fluid migration.

Bachu (1995, 1997) demonstrated very slow (cm/year) regional-scale hydrodynamic flow up-dip to the northeast (Figure 3) in the BC portion of the Western Canada Sedimentary Basin. The flow is topographically driven from a

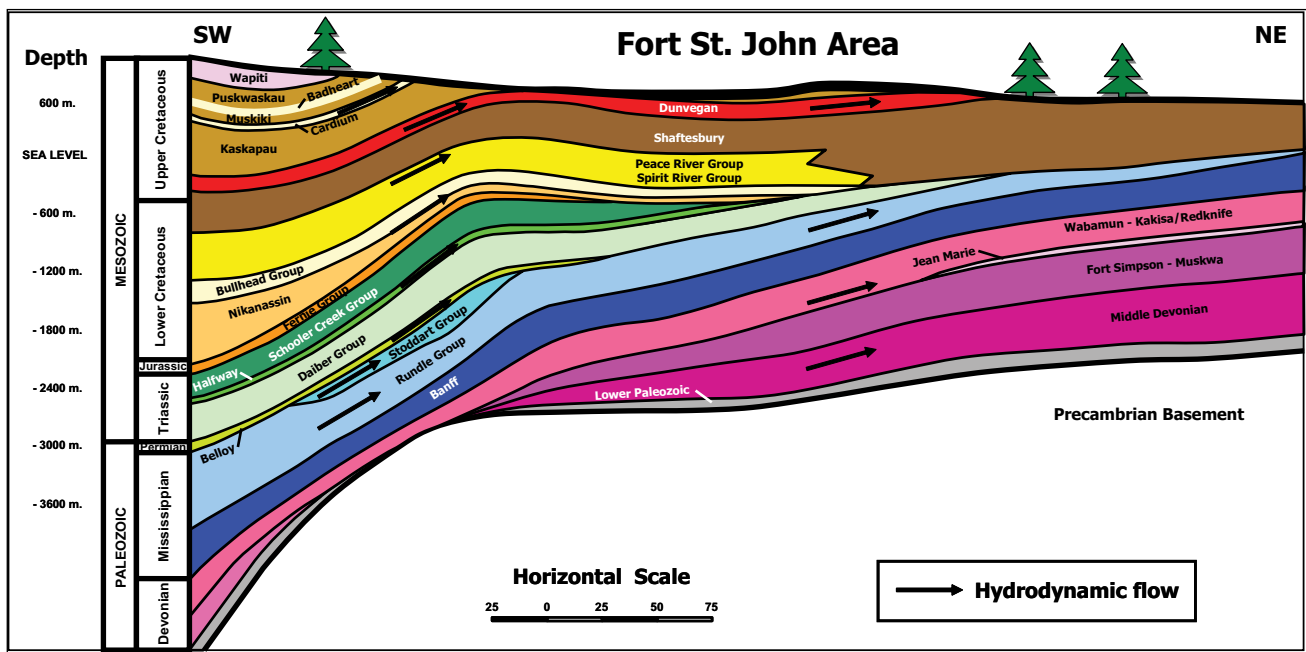


Figure 3: Diagrammatic structural cross-section of geological formations, northeastern British Columbia (modified from BC Ministry of Energy, Mines and Petroleum Resources, Oil and Gas Division 2008).

recharge area in the elevated southwest thrust belt to discharge in the low-lying Great Slave Lake region, Northwest Territories. Supercritical CO<sub>2</sub> injected into a deep saline formation is slightly less dense than formation brine and will gradually migrate up-dip, driven by its buoyant force and the regional hydrodynamic movement.

Optimal conditions must prevail for saline formations to be considered for CO<sub>2</sub> sequestration. There are a number of deep saline formations in northeastern BC with appropriate reservoir characteristics and competent stratigraphic barriers that make them excellent candidates (Table 1).

Any of these deep saline formations could be used for CO<sub>2</sub> sequestration on a site-specific basis, with the likely exception of the Upper Cretaceous. Overall, in the southern half of northeastern BC the Carboniferous-Triassic aquifer has the most beneficial CO<sub>2</sub> storage characteristics, while in the northern area the Lower Devonian aquifer offers the best potential.

Advantages of the Carboniferous-Triassic aquifer in the south:

- porosity developed over large geographic regions (significant capacity available);
- depth of burial often greater than 1 000 m and favourable to maintaining CO<sub>2</sub> as supercritical fluid;
- shallow enough to provide lower drilling, completion and CO<sub>2</sub> compression costs;
- stratigraphically isolated by regionally extensive, thick shales of the Fernie and Banff-Exshaw aquitards.

Advantages of the Devonian aquifer in the north:

- porosity well developed in some areas (need geological/geophysical mapping to establish porosity fairways and estimate capacity);
- depth of burial conducive to maintaining CO<sub>2</sub> as supercritical fluid (often more than 2000 m);
- stratigraphically isolated by areally extensive thick shales of the Banff-Eshaw, Fort Simpson-Waterways, and Chinchaga aquitards;

Physical and geochemical trapping will retain the CO<sub>2</sub> within these geological formations more-or-less permanently. Physical trapping mechanisms include:

- Structural/stratigraphic: containment within naturally formed fluid traps along migration pathway; reservoir heterogeneities form vertical and lateral boundaries that restrict migration rate.
- Hydrodynamic: residual traps form as some of the CO<sub>2</sub> is retained in the pore space by capillary forces; slow migration rate of injected CO<sub>2</sub> (because of buoyancy and hydrodynamic flow) provides more time for geochemical trapping to occur.

Geochemical traps include:

- Solubility trapping: CO<sub>2</sub> dissolves in formation fluid, loses buoyancy, and is carried by the prevailing hydrodynamic flow; CO<sub>2</sub>-rich brine may be denser than formation fluid and sink to the base of the storage reservoir.

**TABLE 1: CO<sub>2</sub> SEQUESTRATION OPPORTUNITIES IN SALINE FORMATIONS, NORTHEASTERN BRITISH COLUMBIA.**

Age	Group/Formation	CO <sub>2</sub> Sequestration Opportunity
Upper Cretaceous	Dunvegan Fm. Cardium Fm.	Generally inadequate depth to maintain optimal reservoir pressure and temperature. Outcropping nearby (increased risk of leakage to surface).
Lower Cretaceous	Paddy/Cadotte Fm. Notikewin/Falher Fm. Bullhead Gp.	Hydrocarbon-rich, especially Deep Basin area (risk of pool contamination). Shale prone and shallow to the north and northeast (poor reservoir development).
Carboniferous-Triassic	Pardonet-Baldonnel, Halfway, Montney, Belloy Fm. Rundle & Stoddart Gp.	Burial depths more-or-less optimal throughout southern area. Strata eroded to the north. Hydrocarbon-rich (risk of pool contamination).
Upper Devonian	Wabamun Gp.  Jean Marie Fm.	Good reservoir development in southern-most area; very argillaceous in northern portion.  Often shallow in the north (CO <sub>2</sub> in gas phase); large capacity reservoirs.
Lower Devonian	Keg River, Sulphur Point, Slave Point Fm. Pine Point and Elk Point Gp.	Porosity not uniformly developed (site specific—best developed near shelf/reef edges as a result of dolomitization). Optimal reservoir conditions in north; too deeply buried with poor reservoir characteristics in the south. Hydrocarbon-rich in north (risk of pool contamination).

- Mineral trapping (carbonation): stable minerals precipitate as acidic, CO<sub>2</sub>-rich water interacts with formation fluids and rock.
- Adsorption trapping: CO<sub>2</sub> is preferentially adsorbed by organic matter present in the formation (may include coal and organic-rich shales).

## MONITORING AND VERIFICATION

Monitoring provides a means for tracking movement of CO<sub>2</sub> in the subsurface. The goals of a monitoring program include a) early detection of CO<sub>2</sub> escaping from the storage reservoir (identifies a possible need for remedial work); b) ensuring public safety and environmental protection at or near surface; and c) verifying that CO<sub>2</sub> is being retained. Monitoring is required to comply with government regulations in BC. It may also play a vital role in establishing liability for damages incurred as a result of leakage or for verification of permanent storage associated with the trading of carbon credits.

A monitoring program begins with a reservoir simulation model run before start-up. This establishes an area of interest surrounding the storage site by identifying most likely CO<sub>2</sub> migration pathways. Various methods and tools can be utilized to track subsurface movement, including:

- Seismic surveys: imaging the subsurface movement of CO<sub>2</sub> using standard 2D, 3D, or 4D seismic techniques; cross-well bore vertical profiling to track CO<sub>2</sub> movement between injection and observation wells.
- Atmospheric, soil, and groundwater sampling: direct measurement using existing sampling methods and tools to identify escaping CO<sub>2</sub> at or near surface (tracer minerals mixed with the CO<sub>2</sub> can improve resolution).
- Reservoir pressure and temperature measurements: indirect means of tracking CO<sub>2</sub> between injection and observation wells within the storage reservoir or into overlying formations.
- Well bore fluid sampling: direct measurement of CO<sub>2</sub> content in fluid samples collected from observation wells, including samples from overlying formations.
- Passive geophysical: standard electromagnetic and gravity surveys to image CO<sub>2</sub> movement.

## RISK

The primary risk associated with CO<sub>2</sub> sequestration is leakage from the storage reservoir. Also, CO<sub>2</sub> escaping to surface may adversely affect human health or the environment, and encroachment of CO<sub>2</sub> into adjacent stratigraphic zones can result in contamination of commercial assets such as hydrocarbon pools or gas storage facilities.

The risk of CO<sub>2</sub> leaking from an appropriately selected storage site is minimal. Secure confinement is ensured by the interplay between physical and geochemical trapping mechanisms, the stratigraphic isolation of storage reservoirs by thick aquitards and by a rigorous inspection of the integrity of nearby well bores that may become exposed to migrating CO<sub>2</sub>. The most likely leakage pathways are identified in the initial design, and monitoring of the site provides for early detection of escaping CO<sub>2</sub>. Remedial work can rectify breaches.

Many geotechnical factors provide a high level of confidence in the safety of CO<sub>2</sub> storage in northeastern BC:

- Potential storage reservoirs are isolated from surface and other stratigraphic zones by competent seals provided by thick aquitards (shale and evaporate deposits).
- The slow-moving regional hydrodynamic system allows time for CO<sub>2</sub> to dissolve in formation water or precipitate as stable minerals.
- The tortuous path created by the regional geology and hydrology significantly impairs upward movement.
- Dense, supercritical CO<sub>2</sub> has relatively little buoyancy in formation water.

The most significant risk of leakage is from existing well bores, which may provide conduits to surface. The integrity of the cement and metal casings in existing wells must be ensured prior to injection and monitored for degradation as the casings are exposed to newly formed acidic CO<sub>2</sub>-rich formation fluid.

## CONCLUSION

Northeastern BC has significant geological CO<sub>2</sub> sequestration potential in depleted gas pools and deep saline formations. The storage space in depleted gas pools cannot be realized until production operations more-or-less cease (estimated to be decades away). Deep saline formations can be utilized to bridge the timing gap for short- to intermediate-term requirements. The technology, expertise, regulatory regime, and infrastructure are in place. The risk to human health, safety, and the environment is low.

## REFERENCES

- Bachu, S. (1995): Synthesis and model of formation-water flow, Alberta Basin, Canada; *AAPG Bulletin*, Volume 79, pages 1159–1178.
- Bachu, S. (1997): Flow of formation waters, aquifer characteristics, and their relation to hydrocarbon accumulations, northern Alberta Basin; *AAPG Bulletin*, Volume 81, pages 712–733.
- Bachu, S. (2006a): The potential for geological storage of carbon dioxide in northeast British Columbia; *Report to the B.C. Ministry of Energy, Mines and Petroleum Resources*, 71 pages.
- Bachu, S. (2006b): Timing of availability for carbon dioxide storage of the largest gas reservoirs in northeastern British Columbia; *Report to the B.C. Ministry of Energy, Mines and Petroleum Resources*, 22 pages.
- British Columbia Ministry of Energy, Mines and Petroleum Resources, Oil and Gas Division (2008): Diagrammatic southwest to northeastern geologic section through northeastern BC; [http://www.em.gov.bc.ca/dl/oilgas/cog/nebc\\_geo.pdf](http://www.em.gov.bc.ca/dl/oilgas/cog/nebc_geo.pdf).
- Environment Canada (2007): National inventory report 1990–2005, greenhouse gas sources and sinks in Canada: The Canadian government's submission to the United Nations Framework Convention on Climate Change; *Greenhouse Gas Division, Environment Canada*, 643 pages.
- IPCC (2005): Carbon dioxide capture and storage; *Intergovernmental Panel on Climate Change, Special Report*; Bert Metz, Ogunlade Davidson, Heleen de Coninck, Manuela Loos and Leo Meyer (Editors), Cambridge University Press, UK, 431 pages.



# NORTHEASTERN BRITISH COLUMBIA DISPOSAL WELL STUDIES

*Ed Janicki<sup>1</sup>*

---

Janicki, E., (2008); Northeastern British Columbia Disposal Well Studies; in Geoscience Reports 2008, *BC Ministry of Energy, Mines and Petroleum Resources*, pages 33-39.

<sup>1</sup>British Columbia Ministry of Energy, Mines and Petroleum Resources, Oil and Gas Division, Resource Development and Geoscience Branch, PO Box 9333 Stn. Prov. Govt., Victoria, BC, V8W 9N3; e-mail ed.janicki@gov.bc.ca ed.janicki@gov.bc.ca

**Key words:** waste-water disposal, disposal well, volumes, engineering and geological parameters, volumetric calculations, reservoir modelling, well files, pressure, tubing, completion.

---

## INTRODUCTION

Water is a vital commodity and certain to become more important as demand grows and the number of clean sources shrinks. British Columbia has an abundance of clean fresh water not only in its plentiful rivers and lakes but also in its groundwater. Both types of valuable fresh water are susceptible to contamination from waters produced as a result of hydrocarbon production.

Water that is produced incidental to oil and gas production is typically re-injected into isolated formations using dedicated water-disposal wells. Sometimes this is done only to avoid contaminating the surface with oily and brackish water; often it serves the dual purpose of waste removal and pressure maintenance of depleting hydrocarbon reservoirs. If done correctly, subsurface water disposal can avoid contaminating either surface water or groundwater. An understanding of the practice is necessary to ensure proper procedures are followed to mitigate leakages up-hole into potable reservoirs.

As a first step in understanding the practice of waste-water disposal in the subsurface of BC, a set of studies of representative disposal wells is being prepared. A sample study for one well (BRC HTR Beau Beg D-25-G/94-G-1) has been presented here to show the proposed style and level of content. Any comments or suggestions from readers will be taken into account while working on the additional well studies. The more comprehensive report will include studies of disposal wells from different pools and formations throughout northeastern BC. This information should provide insights into which formations are most useful for the practice and which formations have the greatest limitations. Also to be provided is a brief summary of the technical aspects of water disposal and an overview of the current practice within BC.

Included for each individual well study will be a brief geological description, a history of the well, potential disposal volumes, and engineering and geological parameters needed for volumetric calculations or reservoir modelling. A well-plan showing the construction details of the well bore and a log showing the injection zone will also be included whenever possible. More or less detail and features will be included in the future, depending on input from readers.

The well files for this location contain a wide range of information, and that is partly why it was selected for study. BRC HTR Beau Beg is typical for water disposal wells in BC because it was not drilled specifically for that purpose. It began as a Halfway Formation gas well and was later converted to Baldonnel Formation water disposal when production became uneconomic due to a high water cut.

All information for the disposal well studies will be taken from publicly available well files.

## SAMPLE WATER DISPOSAL WELL STUDY: BRC HTR BEAU BEG

Location:	200 / D-25-G/94-G-1 / 02
Pool:	Baldonnel (as designated by the British Columbia Oil and Gas Commission)
Formation:	Baldonnel Formation
Formation Age:	Triassic
Rig Release:	February 28, 2000
Status (October 2007):	Water Disposal

## Development Details

This well was drilled for potential gas production in both the Halfway and Baldonnel Formations. After a period of production from the Halfway Formation between 2001 and 2002, the well was suspended due to a high water cut. The Baldonnel Formation was never produced because testing showed it to be wet with only small volumes of sour gas. The original well operator, Canadian Hunter Exploration Ltd., applied to convert the well to water disposal in the Baldonnel Formation, and permission was granted by British Columbia's Oil and Gas Commission on July 30, 2001. This was followed by injectivity testing that confirmed its suitability.

During testing, water was injected at rates of up to 190 m<sup>3</sup> per day with a pressure of 13 996 kPa. Pressure dropped off satisfactorily after pumping stopped, demonstrating the presence of an aquifer-supported constant-pressure boundary. Water disposal began in 2002 and has continued at least until the date of the latest records of 2007.

Figure 1 shows the original well completion scheme for this well, which is typical for this region. Surface casing was set to a depth of 255 m, presumably below the depth of the lowest potable aquifer. Production casing was set to total depth. A plug was set to isolate the Halfway Formation from the Baldonnel Formation, and a sleeve was included within the tubing to allow the flexibility of dual- or

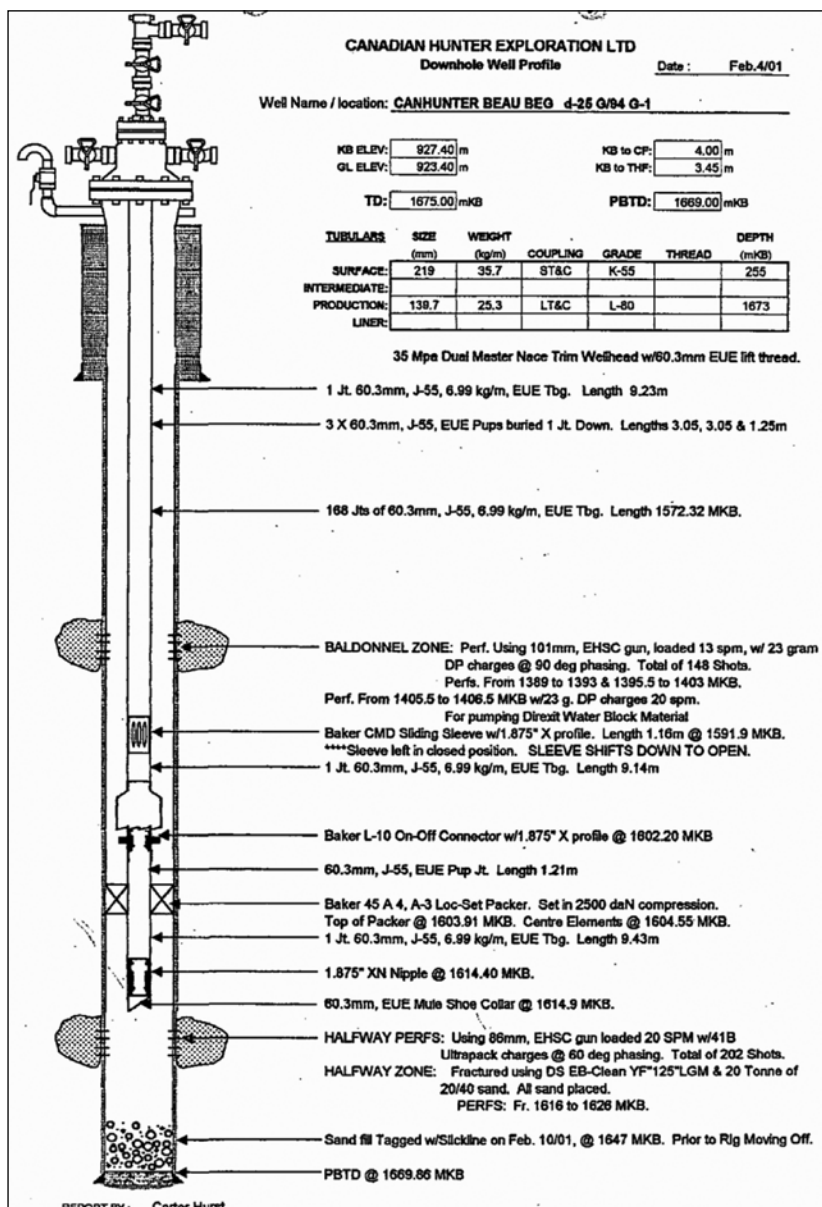


Figure 1: Well Completion Plan for d-25-G/94-G-1. This is taken from the wellfile for this location. The Halfway and Baldonnel Formations were both perforated, but the Halfway was sealed off by a plug and a sleeve was left in the closed position.

single-zone production. Figure 2 shows the revised completion scheme designed to isolate the Halfway from the Baldonnel. Separate tubing strings allowed dual Halfway Formation gas production and Baldonnel water disposal until the gas production was suspended.

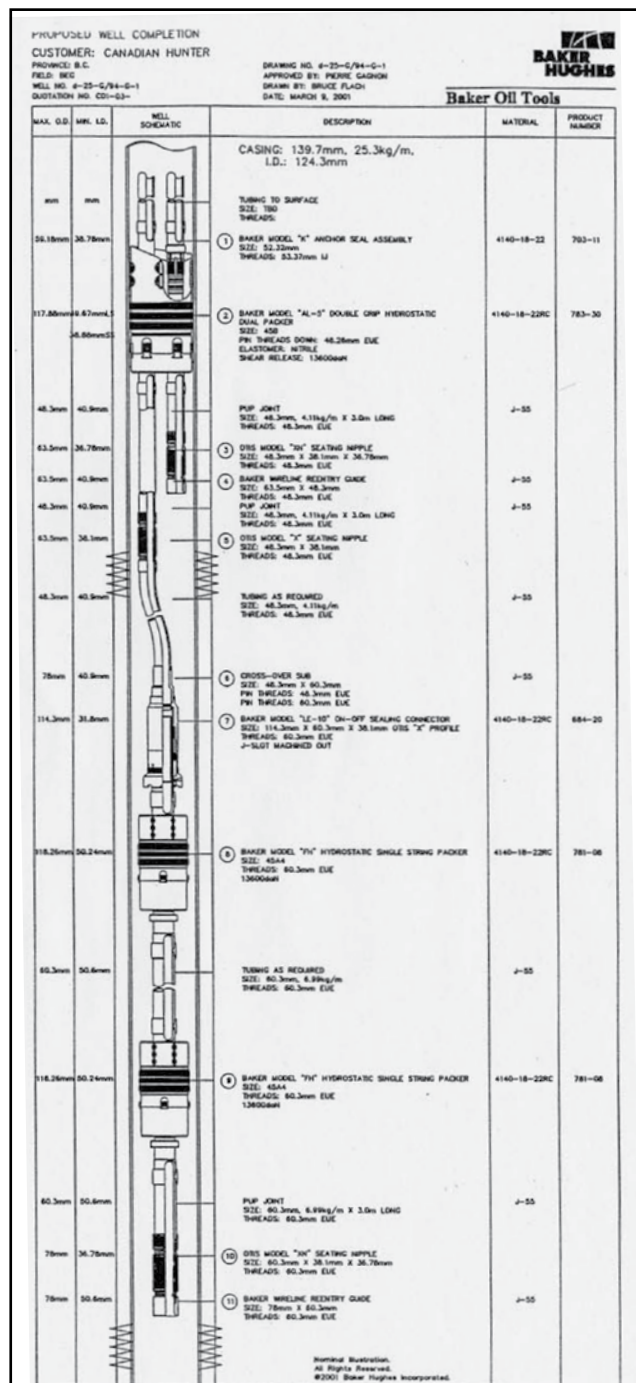


Figure 2: Revised Well Completion Plan d-25-G/94-G-1. This setup allows for isolation of the Halfway Formation from the Baldonnel Formation so that production and disposal could occur concurrently. Halfway gas production was suspended in 2002.

## Geology

Hydrodynamic flow mapping (confidential consultant report) shows a general aquifer flow direction conforming to the regional dip of southwest to northeast. Trapping is also generally to the northeast, where relatively porous facies pinch out or are eroded. Post-Triassic exposure eroded the Triassic surface very unevenly and created considerable subsurface relief. Trapping is therefore determined not just by facies, but also by amount of erosion and regional dip. If only the stratigraphically lowest portions of the Baldonnel Formation remain uneroded, the chances for economic gas accumulations are less because the better porosity is generally in the upper units. At this location, the Pardonet Formation is missing, which suggests that at least some of the Baldonnel has been eroded. Normally the Pardonet provides sealing, but in this case the overlying trap is provided by the Nordegg Formation.

Figure 3 is a map of the structural elevations of the Baldonnel Formation, which are characterized by long linear northwest trends of ridges and valleys interrupted by what appear to be erosional re-entrants. The tops of Baldonnel in the linear gas fields just to the west of location d-25-G (near centre of Figure 3) follow trends at generally higher structural elevations on a relatively raised ridge. Location d-25-G appears to be in a trough or possibly an erosional re-entrant. Location c-35-G is producing gas from the Baldonnel and is located on a structurally higher spur that projects into the trough. Completions within the Baldonnel in this region are usually near the top of the formation, where porosity tends to be higher and water saturations lower.

Reservoir porosity for the Baldonnel averages 10% to 12%; in this case the facies is relatively non-porous with pinpoint porosity of between 3% and 8% (Figure 4). In places the facies appears to be tight. The wellfile sample log describes the Baldonnel as a finely crystalline, argillaceous dolomite. Originally it was deposited as an argillaceous mudstone under stable, shallow-shelf environmental conditions; later it was uniformly dolomitized.

The density log response shows that the completed interval has variable reservoir quality. At best, reservoir parameters yield a water saturation calculation of 30%; other parts of the completed interval clearly are tight or wet. No core was cut across the reservoir interval, but based on local knowledge, permeability is likely poor except where enhanced by fracturing. Long-term disposal into this zone will probably be limited by the poor to fair porosity and low permeability.

Figure 5 shows water-disposal data up to November 2007. The curves suggest that volumes of disposal water have remained fairly constant except for annual monthly dips. However, hours on pump have been rising steadily. Wellhead pressures (Table 1) have been reported since only 2006 and do not show a clear trend of increase or decrease.

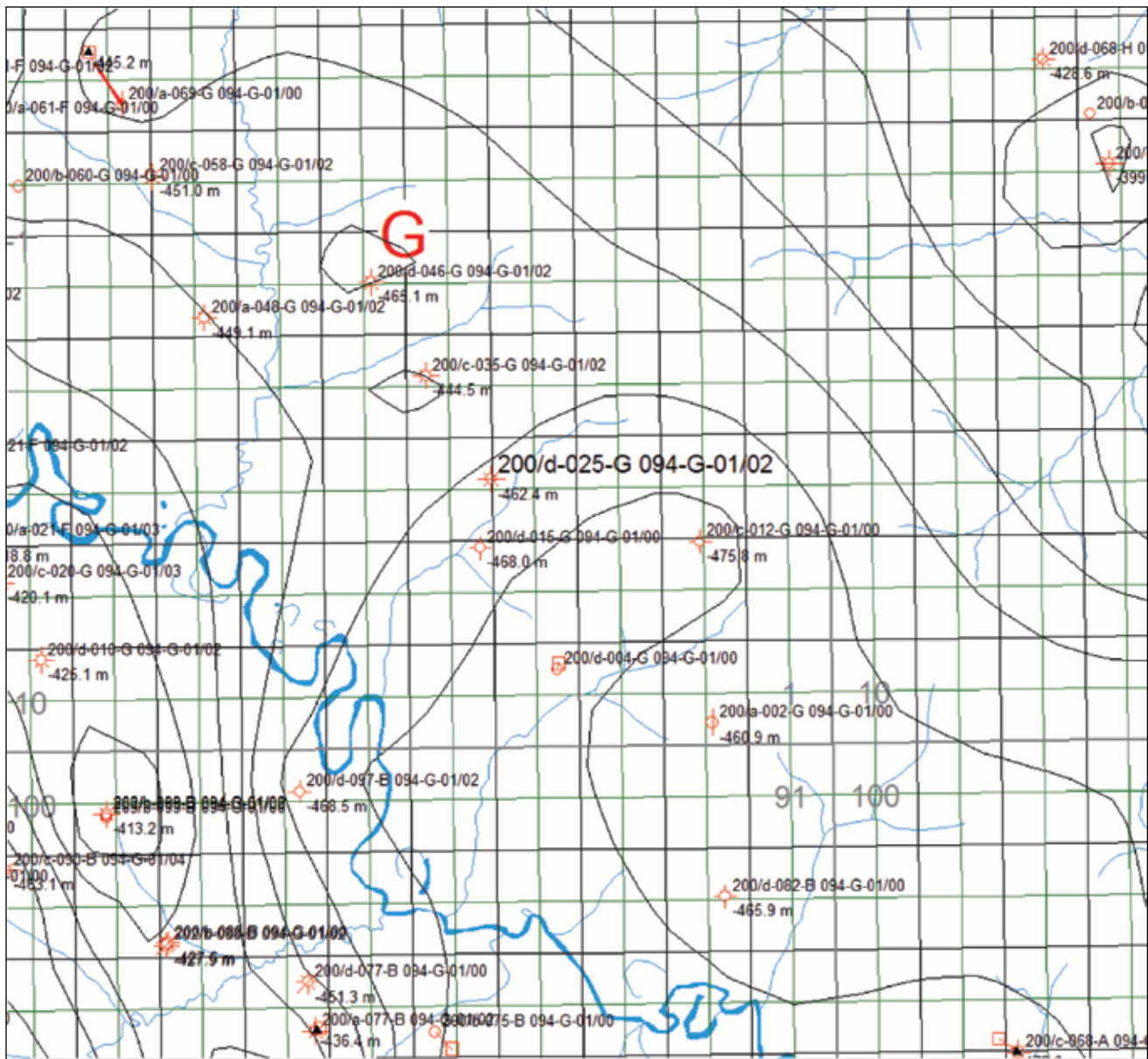


Figure 3: Structural Elevation of the Baldonnell Formation. Contour interval is 10 m. Structural elevations are shown below the well locations. Location d-25-G is shown to be in an intermediate structural position: it is between the elevation of the gas producers to the northwest (e.g., c-35-G) and the wet wells to the southeast (e.g., c-12-G). Although the scale of this illustration is not regional, it is possible to note the linear northwest-southeast trend of drilling and production.

Maximum wellhead pressures appear to be well below the estimated fracture pressure of roughly 25 000 kPa.

Figure 6 shows a cement bond log over the Baldonnell Formation and surrounding zones. A generally good bond between casing and borehole is indicated, although some weaker signals are present over the Nordegg Formation.

The bond might be less complete here, likely due to the possibility of sloughing in this shale formation. Overlying bonds appear to be strong, so any leaks between the Baldonnell Formation and annulus would likely not get past the Nordegg Formation shales.

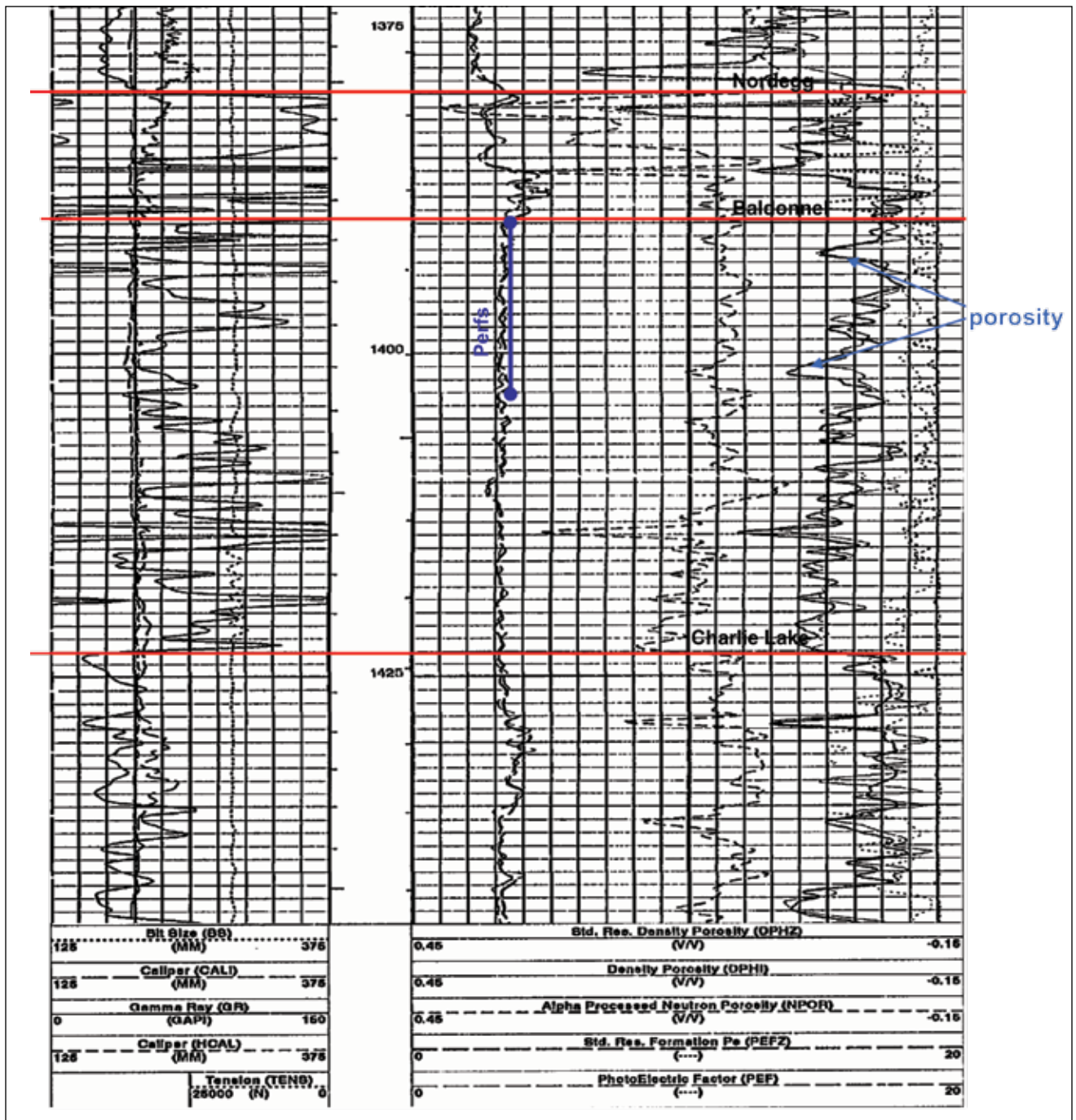


Figure 4: Neutron-Density Log d-25-G/94-G-1. Porosity is scaled in sandstone units, so through the perforation interval porosity peaks at roughly 8% when converted to limestone. Much of the interval is tight. The Pardonet Formation is missing, so the Nordegg Formation shale is acting as the seal.

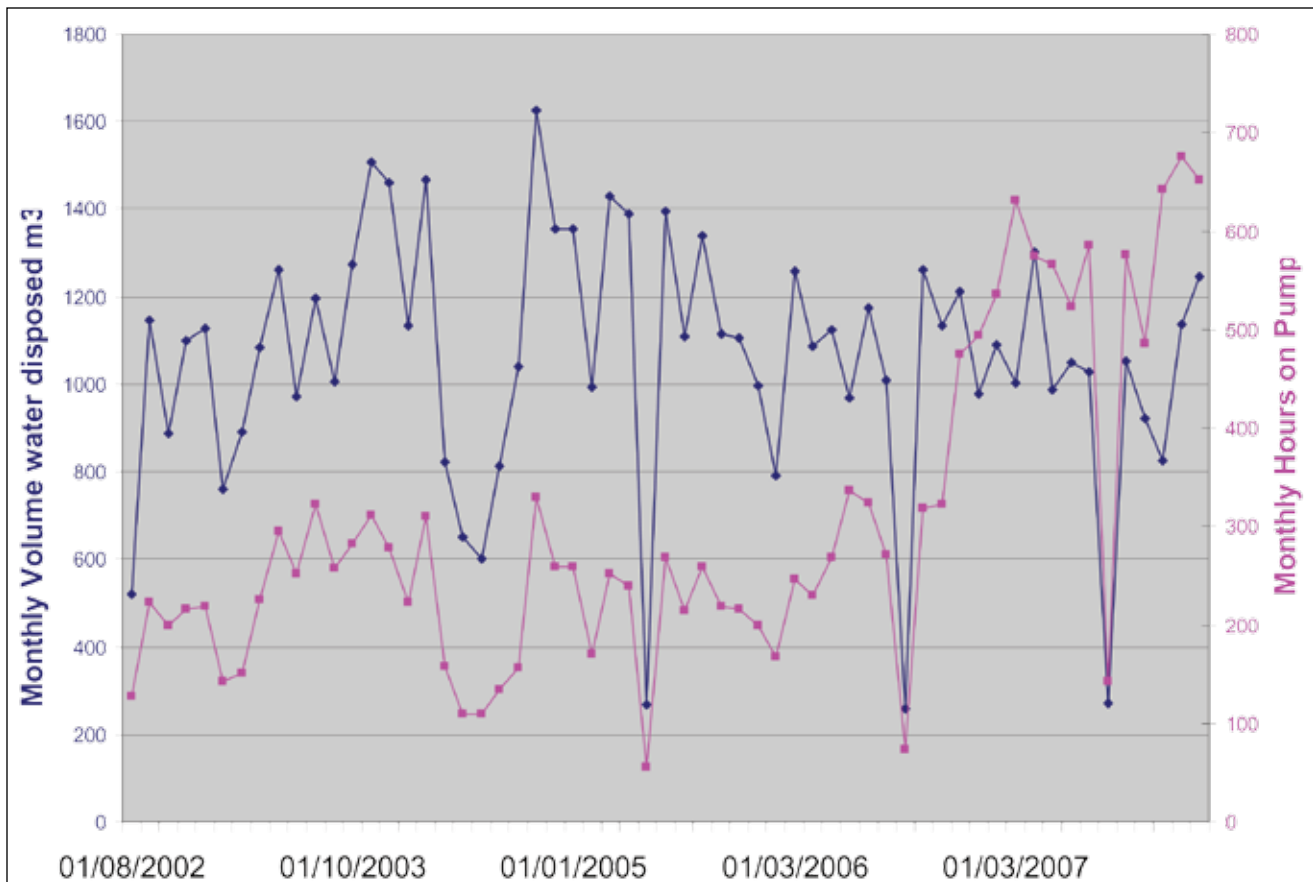


Figure 5: Water Disposal Plot for d-25-G/94-G-1. As volumes seem to be decreasing slightly, monthly hours on pump appear to be increasing. Data has been taken from the IRIS database of the Oil and Gas Commission of British Columbia.

***Drilling, Formation Evaluation, And Completion Practices***

Casing:	255 m @ 219 mm 1673 m @ 140 mm
Log Suite:	Sonic, Compensated Neutron, Induction, Gamma Ray, Cement Bond, Temperature
Completion:	Perfs 1389–1393 m, 1395.5–1403 m
Stimulation:	acid wash

**Reservoir Data**

Depth:	1389 m KB
Lithology:	Dolomite
Trapping:	Stratigraphic/Structural
Net porosity:	7 metres
Porosity:	7%
Water Saturation:	30% (optimal)
Initial Pressure:	11 473 kPa
Reservoir Temperature:	70 °C

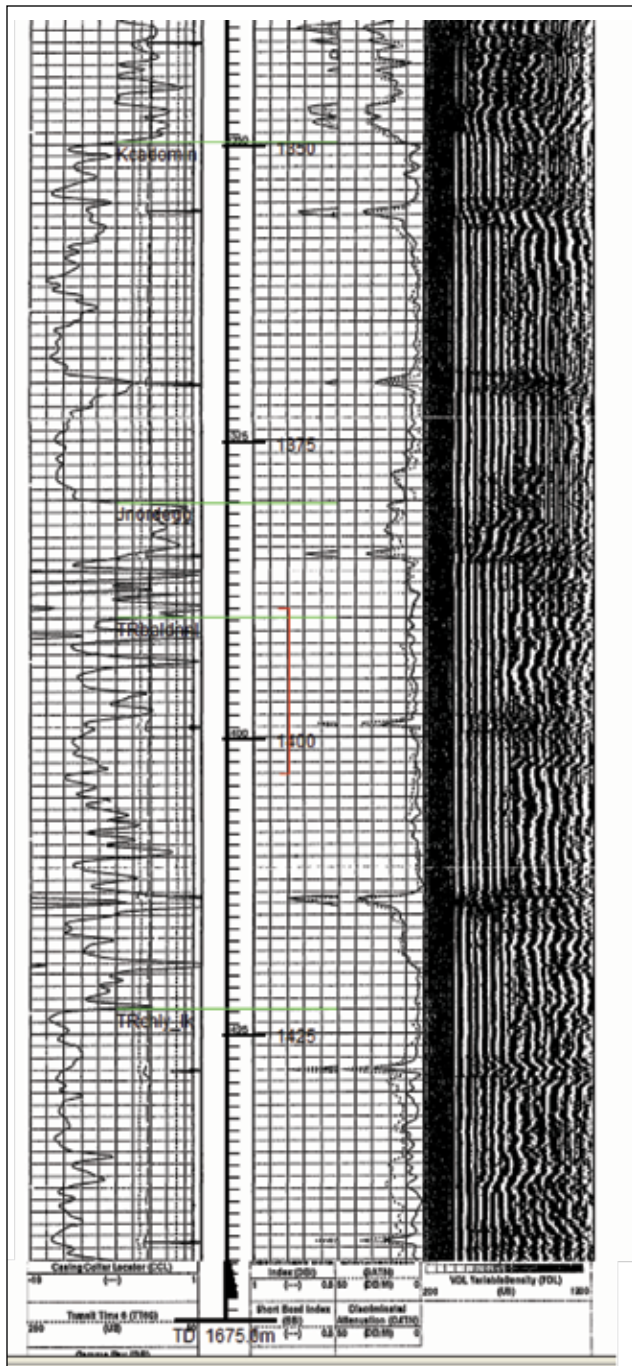


Figure 6: Cement Bond Log d-25-G/94-G-1. Generally strong amplitudes indicate good cement bond and low likelihood of leaks behind casing. Some weakness of bond is suggested by weaker returns at around 1380 m in the Nordegg Formation. Overlying bonds appear to be good, so leaks would likely not go far up-hole.

TABLE 1. MONTHS ON PUMP VS. WELL HEAD PRESSURE (KPA) D-25-G/94-G-1.\*

Months on Pump	Well Head Pressure (kPa)
01/07/2006	6900
01/08/2006	5150
01/09/2006	3000
01/10/2006	6900
01/11/2006	3500
01/12/2006	4600
01/01/2007	2900
01/02/2007	4200
01/03/2007	6000
01/04/2007	8400
01/05/2007	4500
01/06/2007	8500
01/07/2007	8100
01/08/2007	5000
01/09/2007	5300
01/10/2007	7900
01/11/2007	4500
01/12/2007	5600
01/01/2008	7200

\*This data is from the IRIS database of the Oil and Gas Commission. Values began to be reported in 2006. Few wells in British Columbia have complete records for wellhead pressure. When graphed, the values do not yet show a clear trend of increase or decrease. If a rule-of-thumb fracture gradient of 18 kPa/m is applied (approximately 25 000 kPa at 1400 m), the maximum wellhead pressure so far has been well below the limit.



# PETROLEUM EXPLORATION HISTORY OF NORTHEASTERN BRITISH COLUMBIA

*Ed Janicki<sup>1</sup>*

---

## ABSTRACT

*A decade-by-decade analysis of the history of petroleum exploration in northeastern British Columbia attempts to understand why some regions remain relatively unexplored. Most development followed the trends of previous discoveries or the construction of infrastructure such as roads. Some portions of the unexplored regions are now opening up due to technical advancements in drilling and completions. Exploration patterns were largely influenced by events outside the province, such as the two world wars and discoveries in other parts of the Western Canada Sedimentary Basin.*

Janicki, E., (2008); Petroleum Exploration History of Northeastern British Columbia; in Geoscience Reports 2008, BC Ministry of Energy, Mines and Petroleum Resources, pages 41-57.

<sup>1</sup>British Columbia Ministry of Energy, Mines and Petroleum Resources, Oil and Gas Division, Resource Development and Geoscience Branch, PO Box 9333 Stn. Prov. Govt., Victoria, BC, V8W 9N3; e-mail ed.janicki@gov.bc.ca

**Key Words:** patterns, white area, surface structure, seep, Peace River, cycles, Leduc, Alexander McKenzie, reefs, Alaska Highway, Boundary Lake, Fort St. John, Clarke Lake, Cordova Embayment, Presqu'île, Triassic, Devonian, deep basin, resource play, National Energy Program, seismic, resistivity.

---

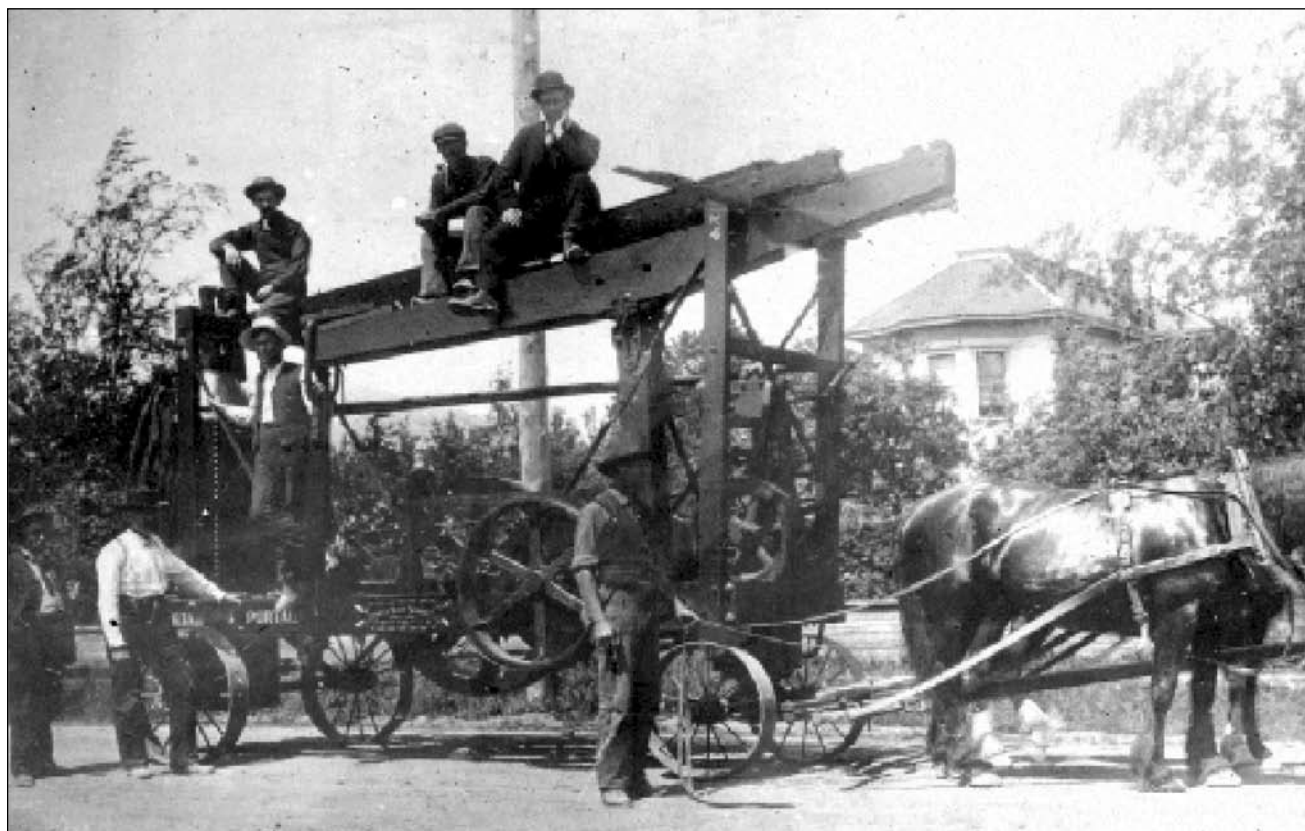


Figure 1: Oil drilling rig in Chilliwack, BC, ca. 1906. Photo courtesy of BC Archives collections; call number G-07686.

## INTRODUCTION

Understanding the historical patterns of oil and gas development of a petroleum region is perhaps as important a method of deciphering the subsurface as trying to see underground with sophisticated geological and geophysical methods. It is a method that is vastly easier to implement and should not be ignored.

Aside from considering this historical analysis as a valid exploration method, it is a response to a desire of the British Columbia Ministry of Energy, Mines and Petroleum Resources to know why some regions in northeastern BC have remained relatively unexplored and undeveloped for oil and gas. These areas are referred to throughout as “white areas” because they remain white on maps heavily dotted with oil and gas wells.

Before the current age of 3D seismic, horizontal drilling and sequence stratigraphy, most of the big oil and gas discoveries in Canada and around the world were made on the basis of the simple observation of seeps or surface structures. Seismic imaging of subsurface structures was not needed to discover the Middle Devonian reefal oilfield at Norman Wells in the Northwest Territories—its existence was known hundreds of years ago to the First Nations people by the presence of oil seeping from bluffs overlooking the Mackenzie River. The supergiant Baku oilfields in Azerbaijan did not require high-tech horizontal drilling rigs to become economic—hand-dug wells sufficed at first. Simple cable-tool rigs were adequate to get the oil industry going in southern Ontario more than 150 years ago because oil was obviously close to the surface. BC’s petroleum potential was signalled in the 1920s by noting the presence of oil seeps along the Peace River; test drilling led to confirmation of potential and to the eventual development of BC’s best oilfields. For many highly productive regions, such as the Sirte Basin in Libya, which lacked seeps or structures observable at surface, rudimentary seismic technology was sufficient to make very large discoveries.

Early exploration in British Columbia was marked by sparse and sporadic drilling, mostly in accessible parts of the province such as the Fraser Delta (Figure 1; Galloway 1915) or Crowsnest Pass (Hume 1933), where interest had been sparked by dubious reports of oil seeps or gas blows. Lack of positive results eventually shifted interest to the northeastern parts of the province, where drilling did lead to discoveries.

Once a new petroleum region has been discovered—often by relatively simple means—it is usually followed with additional discoveries in the vicinity. It is in the further development of initial discoveries that high technology and increasingly refined geological thinking have their greatest application. Traditionally, oil and gas discoveries have led geological studies, rather than the reverse.

## METHODOLOGY

This report divides the past century of exploration activity in northeastern British Columbia into discrete five-year time intervals that are not entirely arbitrary—they reflect typical cycles of drilling activity. Historically, a cycle began with one or two years when a promising new play or a geopolitical or economic force translated into peaks of drilling activity; then, when something happened to force prices downward, a lag time of one year or so would precede the bottom of the cycle. Therefore, cycles of roughly five years duration are typical. More recently, with the maturation of the Western Canada Sedimentary Basin, those cycles may be lengthening or shortening—time will tell. But despite the pace of activity, they are likely to lengthen because true discoveries are not happening very often.

This report focuses on drilling activity (rather than other types of activity such as pipeline or gathering facility construction, seismic exploration, or field mapping) mainly because it is the most direct indicator of economic interest and results. Future revisions of this report may take a more comprehensive approach to gain a deeper overall understanding.

Much information about exploration activity came from annual public reports of year-to-year oil industry activity published by the Government of British Columbia beginning in the early 1950s. These reports also reveal the shifts of governmental priorities with the stages of exploration. As time went by the reports were published by various government divisions, depending upon the prevailing organizational structure. Formats and level of content varied with each organizational change. The earliest reports of the young oil industry contain much useful information; later on, government turned more to the role of promoter and so less detailed information about exploration was provided. All reports can be found (usually as a section within a mining report) online at: [http://www.em.gov.bc.ca/Mining/Geosurv/Publications/catalog/cat\\_rpts.htm](http://www.em.gov.bc.ca/Mining/Geosurv/Publications/catalog/cat_rpts.htm)

Another valuable source of detailed historical information for individual wells is the publicly available well files, available through the BC Ministry of Energy, Mines and Petroleum Resources. Sometimes individual well files give glimpses of the strategy used for the development of entire regions.

A map for each time interval has been provided (Figures 2–13). Only the wells drilled during each respective interval have been shown so the trends can be clearly seen.

Significant events in BC’s exploration history have been linked with the wider world. World history for the past century has been heavily influenced by the search for oil, and that also applies for BC.

## EXPLORATION DEVELOPMENTS

### Pre-1948

In 1920 the first five or six exploration wells of northeastern BC were drilled in the Peace River area, just west of the townships, by the provincial government. They were part of a test-hole program and not intended to be producers. This drilling effort had been preceded the year before by field mapping that revealed promising structures and rock formations capable of forming hydrocarbon reservoirs. Similar activity was occurring in adjacent parts of Alberta for the same reasons. The test-hole drilling program did provide promising shows of oil and gas from Cretaceous clastic formations. At the time, no infrastructure was available to enable further development.

Early settlers had reported the presence of oil seeps, and because most petroleum discoveries in the world had been made near seeps, interest in the area was high before any geological field mapping had been done. At the same time as oil was discovered in the Northwest Territories (on oil seeps at Norman Wells), a well was drilled by Imperial Oil near Pouce Coupe near the site of oil seeps reported by an early settler (Clare 2003). A small quantity of oil was

encountered at shallow depths but substantial amounts of gas were unexpectedly found at greater depths. The inexperienced and poorly equipped drilling crew was unprepared for the ensuing blow-out, which left killed one and severely burned several others.

In the early 1930s, the BC government took a different turn from its neighbour Alberta. Reflective of its divergent political philosophy, BC placed all the Peace River lands under reserve to discourage control by American interests, while Alberta continued to actively promote development, although the potential of the region at that time was largely unknown.

The BC government began to change its non-development stance in the latter part of the 1930s. As part of the war effort to find more oil, a well was drilled by the provincial government in 1941 near Pine Pass. This location was politically contentious because of the expense and lack of private interest. It had been recommended on the basis of surface mapping and the presence of an existing road from Dawson Creek to East Pine, but it did not provide promising results. Further activity in northeastern BC waited until after the 1947 Leduc discovery and improvement of transportation infrastructure with the building of the Alaska Highway and other roads.

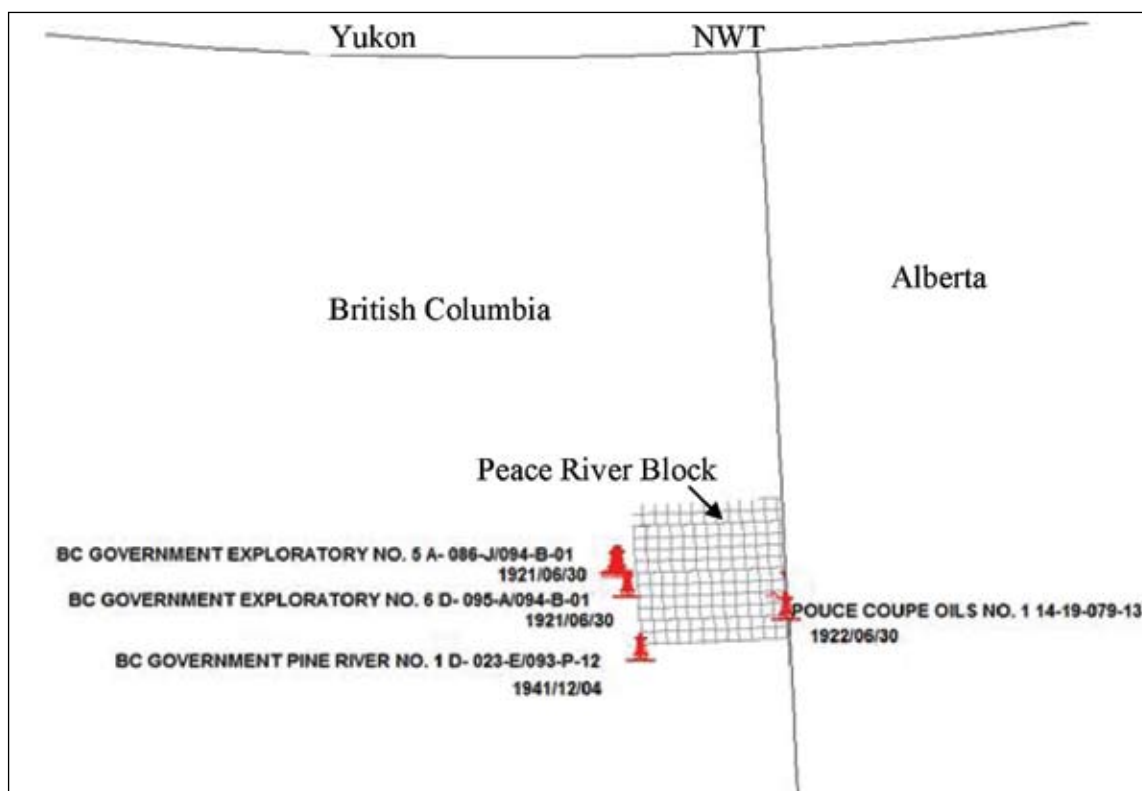


**Figure 2: Drilling before 1948**

*In 1920–21 the first five or six exploration wells of northeastern BC were drilled in the Peace River area, just west of the townships, by the BC government; the township block was placed off-limits from American interests. Pouce Coupe Oils drilled a shallow well near the Alberta border to investigate signs of hydrocarbons at surface.*

### 1948–1950

This was a brief interval of seminal importance for Canada's oil industry because of the discovery of the Middle Devonian reefal oil play at Leduc, Alberta. No better oil producer has since been discovered in Canada in terms of productivity and access. Many "dry holes" were drilled before this, but faith in eventual success was provided by previous reefal discoveries at Norman Wells, Northwest Territories, and Midale, Saskatchewan (Gould 1976). Many of those "dry holes" were not actually dry but simply not economic at that time. They provided information for later successful exploration efforts throughout Alberta and extending into BC; for example, the Leduc discovery led to the delineation of Middle Devonian reef trends, which helped lead to the discovery of the Clarke Lake Field in BC.

After the Leduc discovery, drilling extended into regions that had shown promise from test holes or field mapping. The opening up of more remote regions (such as the Peace River) with roads built to serve agricultural expansion also helped. In the late 1940s, a number of wells were drilled in Alberta, extending into BC just north of Dawson Creek, to follow up earlier observed shows in the Lower Cretaceous Paddy and Cadotte Formations. An east-west trend was quickly established by drilling for these gas-bearing shoreface to foreshore prograding sands.

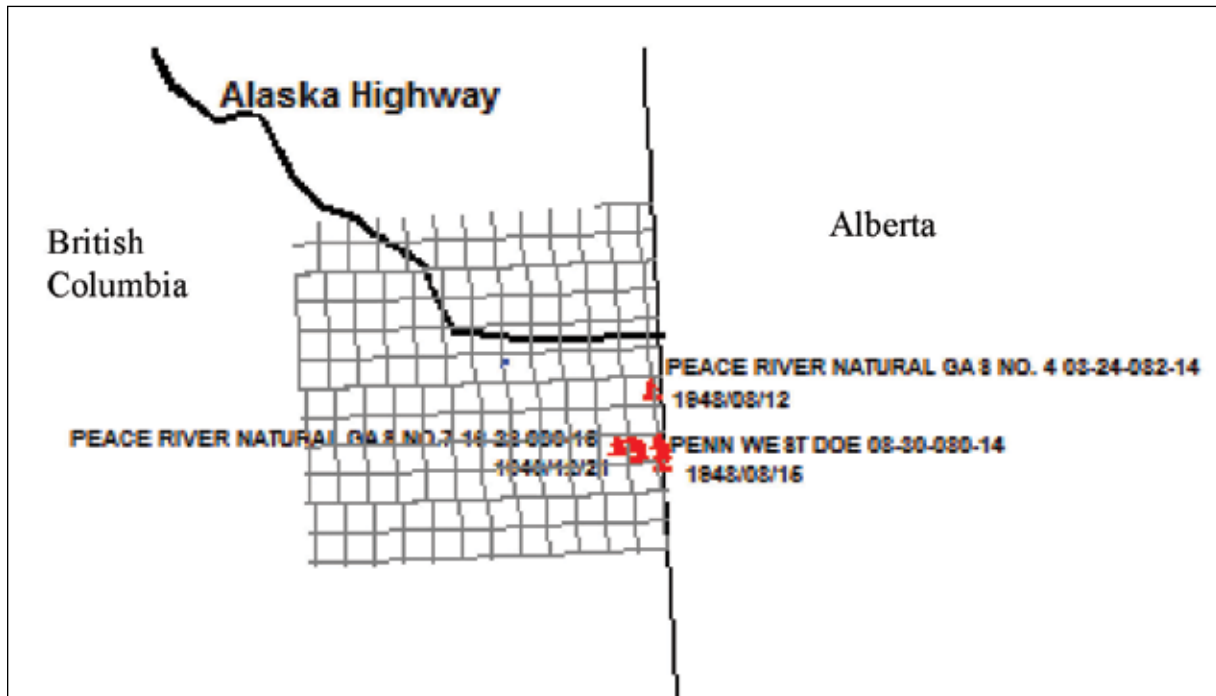


Figure 3: Drilling 1948–1950

*Wells drilled during this period were pursuing shallow Lower Cretaceous gas plays found across the Alberta border.*

## 1950–1955

By the early 1950s, operators were showing that northeastern BC held potential in multiple zones of different geological ages. It outlined a basic reality that still applies: if hydrocarbons are discovered in one formation in a region, they are usually present in other formations because it proves a source. The corollary has also generally held true: wells with only one hydrocarbon-bearing formation or interval are uncommon, at least in regions with substantial stratigraphic sections.

More wells were drilled for Lower Cretaceous gas in the previously established trend north of Dawson Creek. It did not meet with the same success as it had in Alberta; on the edge of the adjacent white area are a few dry holes. Many wells tested gas from the deeper Lower Cretaceous shoreface clastic Cadomin and Nikanassin Formations.

A number of wells were drilled deeper, perhaps in hope of there being another Leduc-style reef in the Devonian section. Nothing like that was found in northeastern BC at that time; instead—and of great significance for the oil industry in the region—was the discovery of gas in the Triassic Halfway and Baldonnel Formations. A northwest trend, parallel to the cratonic shorelines of the Triassic, was quickly delineated by drilling. Drilling along this trend was facilitated by the Alaska Highway, which more-or-less followed it. A few of these deeper wells also established other targets, with gas discoveries in Permo-Pennsylvanian formations.

Maybe the most significant event for the oil industry in northeastern BC at this time was the completion of Boundary Lake No.1 well in 1955 in the Triassic Schooler Creek Formation. Initially it was shut-in pending arrangements to bring the oil to market, but it later became the first well of a very important oilfield for the province. Development was aided by its location near the Alberta border with good existing road access.

Activity was still hampered by a shortage of passable roads. Aside from the Alaska Highway and roads in the vicinity of Fort St. John and Dawson Creek, only a few bush roads existed, and they were usable by heavy equipment only in the winter and the driest portions of the summer. Therefore, drilling and exploration were restricted to proximity of the better roads.

A few remote, scattered wildcats were attempted at greater distances from the main trends. Abandoned well d-82-L/94-J-2 tested significant amounts of gas from Middle Devonian formations. Access was no problem as it was located very close to the Alaska Highway. It is not clear why this particular spot was chosen for such a rank wildcat, except for its proximity to a good road. Perhaps by this time drilling throughout northern Alberta and the southern Northwest Territories was revealing the shape of the Presqu'ile Middle Devonian carbonate barrier.

In 1953, the Administration Branch of the former Department of Mines assumed the role of administering oil and gas activity in BC.

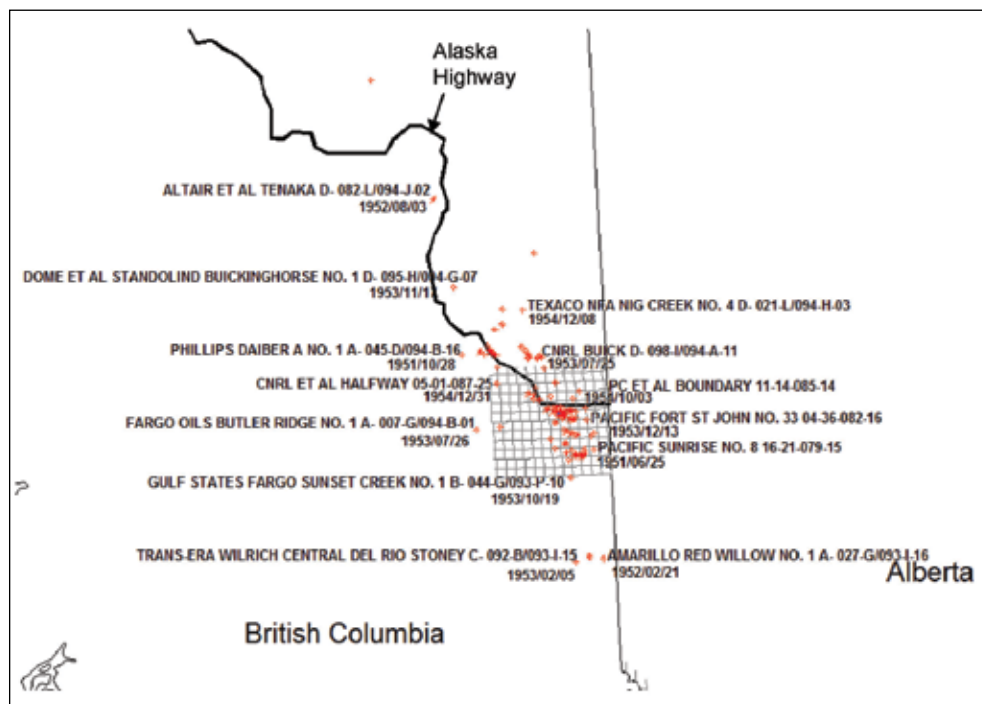


**Figure 4: Drilling 1950–1955**

*Drilling expanded from its initial foothold in the Peace District near the Alberta border. Many fields were found in these early days of exploration, including significant oil finds near Fort St. John. Many of the discoveries were conveniently close to the Alaska Highway built for strategic purposes during World War II.*

## 1955–1960

In 1956, the Boundary Lake oilfield—British Columbia's first—was put into continuous production. Ten wells were producing oil by the end of the year.

Exploration for Halfway, Baldonnel, and other Triassic formations pushed the producing fields further northward and north-westward. Fields such as Jedney and Bubbles began producing from the Baldonnel Formation at the edge of the deformed belt. Several wells were the first to be drilled directly within the BC foothills. None of these were completed as producers.

Other unexplored areas (white areas) were tested between the Halfway and Baldonnel trends and the foothills as well as to the north, where a big gap exists to this time.

Oil and gas were also found in the Lower Cretaceous Bluesky and Gething Formations in the Milligan Creek and

Beatton River areas north of Fort St. John.

The previous discovery of gas in the Middle Devonian Slave Point Formation near Fort Nelson at Clarke Lake led to a flurry of activity chasing after this new trend. Several wells were completed, but no gathering system was yet available to bring the gas to market. Drilling was also constrained by the lack of roads in the area, other than the Alaska Highway. Several wells were drilled in the currently defined white area north of the Clarke Lake discovery, probably in the hope of extending the Middle Devonian gas play northward, but these did not provide positive results and the wells were abandoned.

The Petitot River discovery (d-24-D/94-P-13) in the Slave Point Formation at the northern boundary of the province would eventually become very important for providing a new Middle Devonian carbonate trend for explorationists.

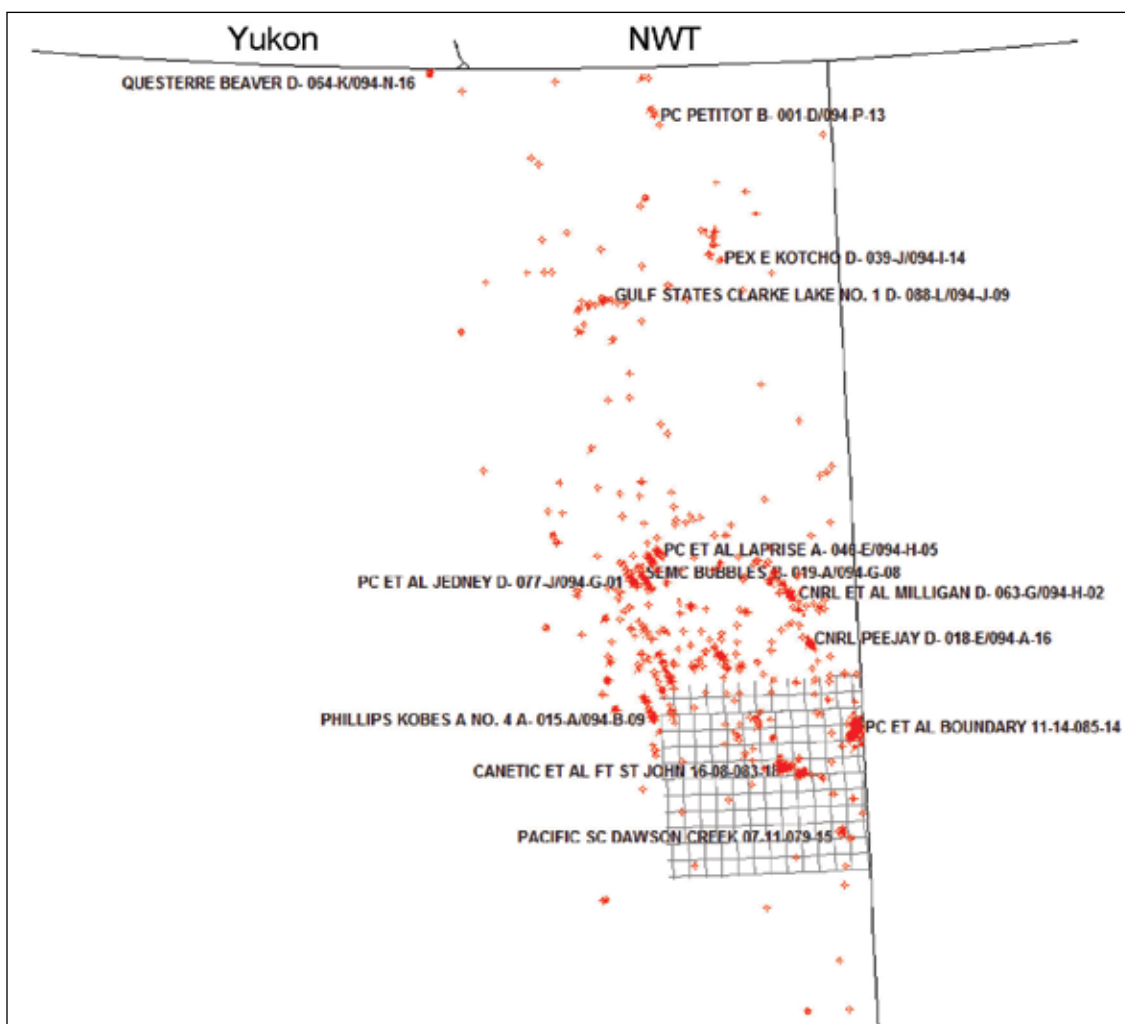


**Figure 5: Drilling 1955–1960**

Many of the fields familiar to BC explorationists were discovered. Clarke Lake—a Middle Devonian carbonate gas play—was discovered as explorationists scrambled to find more reefal plays like Leduc in Alberta. The Beaver Creek discovery near the Yukon border is close to the Alaska Highway within the disturbed belt.

## 1960–1965

By the late 1950s, the number of cores and drill cuttings turned over to the government by industry, as required by regulation, greatly exceeded the space available in a temporary storage shed in Pouce Coupe. In 1961, a new core storage facility opened in Charlie Lake, near Fort St. John. This was an essential step for facilitating the orderly further exploration and development of the province's hydrocarbon resources.

Drilling extended northward as multiple potential zones allowed the Triassic trend to broaden. The first wells were drilled in the Tommy Lakes area, also for Triassic gas. These wells were not successful producers at that time, but improved technology in later years enabled production from the relatively tight reservoir rocks from the lower portions of the Triassic section. One or two wells extended from Tommy Lakes into a white area to the north.

The new linear north-south trend at Petitot River was followed up with a number of wells. Another trend splayed off to the southeast at Kotcho Lake and Yoyo. Gas was also found in the Devonian Jean Marie Formation at Gunnell Creek.

In the far northwest of the region, in an area sparsely drilled even now, a discovery was made in the Nahanni Formation at d-73-K/94-N-16 at Beaver River. This well was directionally drilled into rock within the deformed belt. Very substantial gas recoveries were made from drill-stem tests in Middle Devonian formations, and that provided impetus for the building of infrastructure to deliver the gas to market. At around this time, gas was discovered on the Yukon side of the border along the same trend.

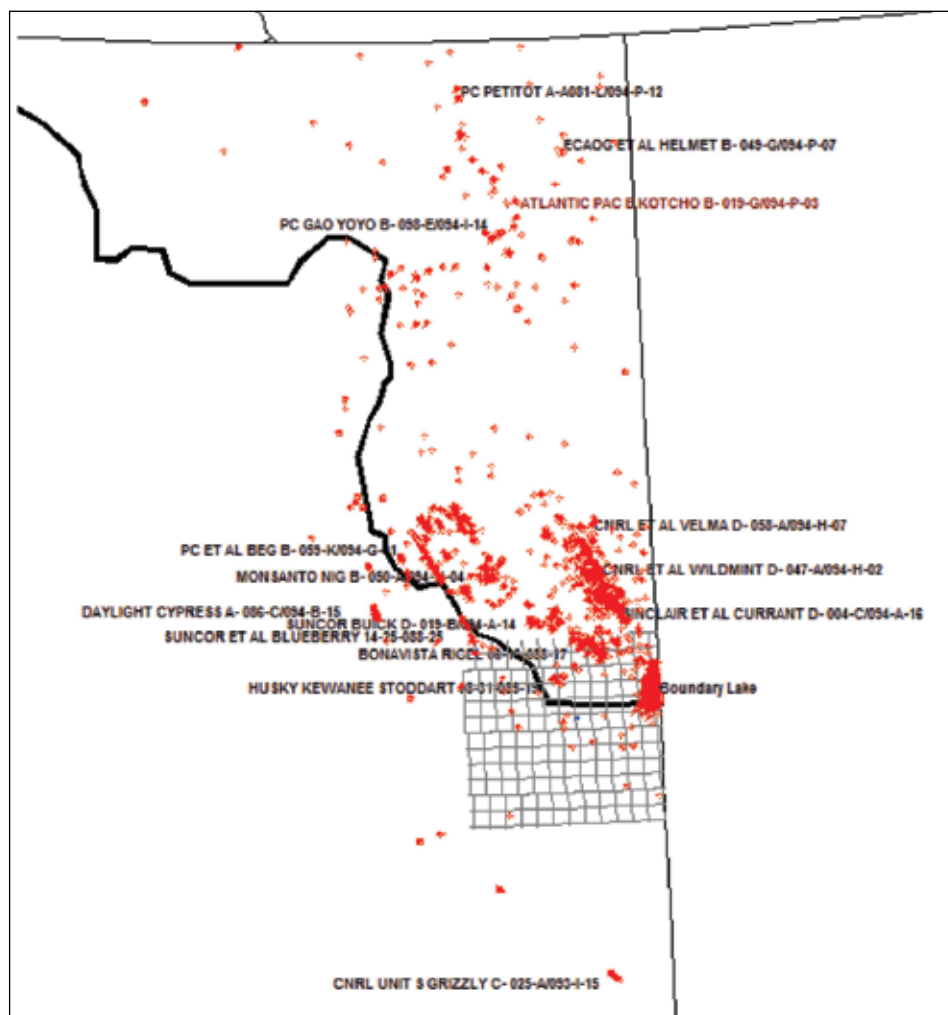


**Figure 6: Drilling 1960–1965**

*A new linear north-south trend at Petitot River was followed up with a number of wells. Another trend splayed off to the southeast at Kotcho Lake and Yoyo.*

## 1965–1970

Activity had settled into predictable patterns close to the major discoveries, and the rate of discovery had slowed. Most of the big discoveries, of which many are still in production, were being exploited or were in the process of expansion through step-outs. The progression of field development followed the northwest-trending Triassic reservoirs, such as the Inga Field in the Fort St. John region. To the north, discoveries followed the trends of porous Middle Devonian rocks at Clarke Lake. While drilling for the Triassic and Devonian formations, discoveries were being made in the shallower Lower Cretaceous. Extensive drilling revealed that the Lower Cretaceous clastic fields, such as the Dahl Field, followed a northwest trend similar to the Triassic shoreface clastics.

In the north-easternmost corner of the province, which was remote from established roads, follow-up wells were drilled for discoveries made in the Upper Devonian Jean

Marie Formation. Exploration had been underway on the Northwest Territory side of the border, and these Jean Marie wells were drilled as part of the hunt for Devonian plays on the Presqu'île Barrier that extends into the southern territories. At about this time, the Rainbow Reef Middle Devonian carbonate play in northwestern Alberta was discovered, and development quickly ensued. Reefal plays were still at the top of mind for many explorationists in the Western Canada Sedimentary Basin, as they had been since the Leduc discovery, which was not yet in the distant past.

The white area in the extreme northeast defines the extent of the Cordova Embayment, a basin shale correlative portion of the Devonian section. A handful of wells had been drilled there to explore the edges of the shale basin and define the fringes of the Middle Devonian carbonate barrier reef.

Other significant developments of this time included a gas discovery from the Mississippian Debolt Formation at a-75-D/94-G-7 in the Grassy Field.

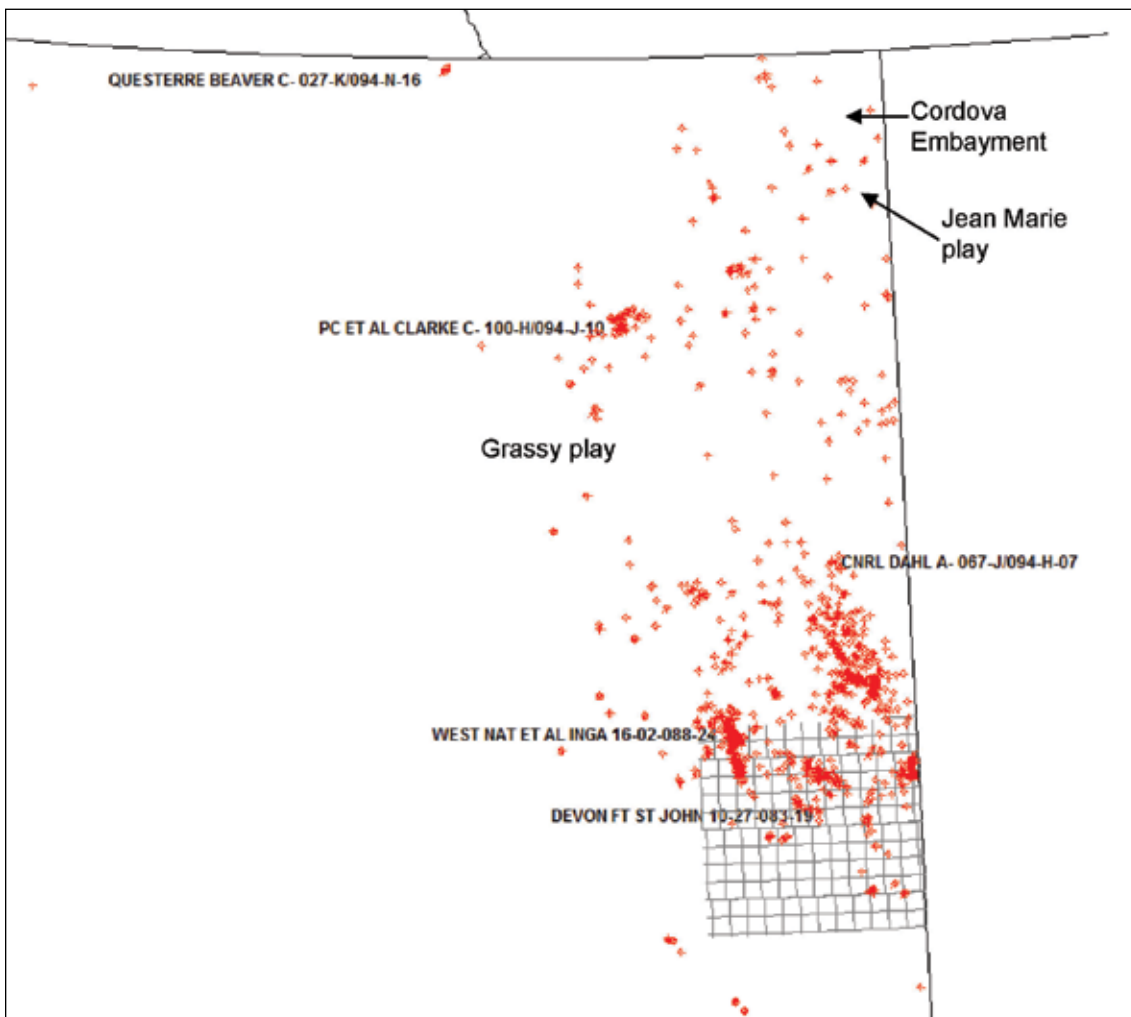


**Figure 7: Drilling 1965–1970**

*Activity included further developments of the Clarke Lake carbonate play and extensions to the Dahl Field; it was moving away from rank exploration and instead clustering around existing fields.*

## 1970–1975

This was a time of discord between the federal government and western oil producers. As a bargaining tactic, production was withheld, and therefore activity levels were low for part of this period. Also, the pace of discovery had slowed; most of the major discoveries we know about now had already been made. Some exploration wells were drilled in the white areas without success.

Drilling continued to expand the Triassic trend further to the north-northeast. The pace of activity for this trend did not match the march of development in adjacent parts of Alberta. Tensions between the BC New Democrat government and industry were high, as compared with the pro-business Conservatives in Alberta.

Possibly the most significant exploratory development was the discovery and drilling of Mississippian and Cretaceous shallow gas in the northernmost part of the province, just to the east of the linear Nahanni Formation gas trend in the foothills. Many wells were also drilled for Debolt Formation gas at Helmet Field, which would later expand to the edge of the Cordova Embayment.

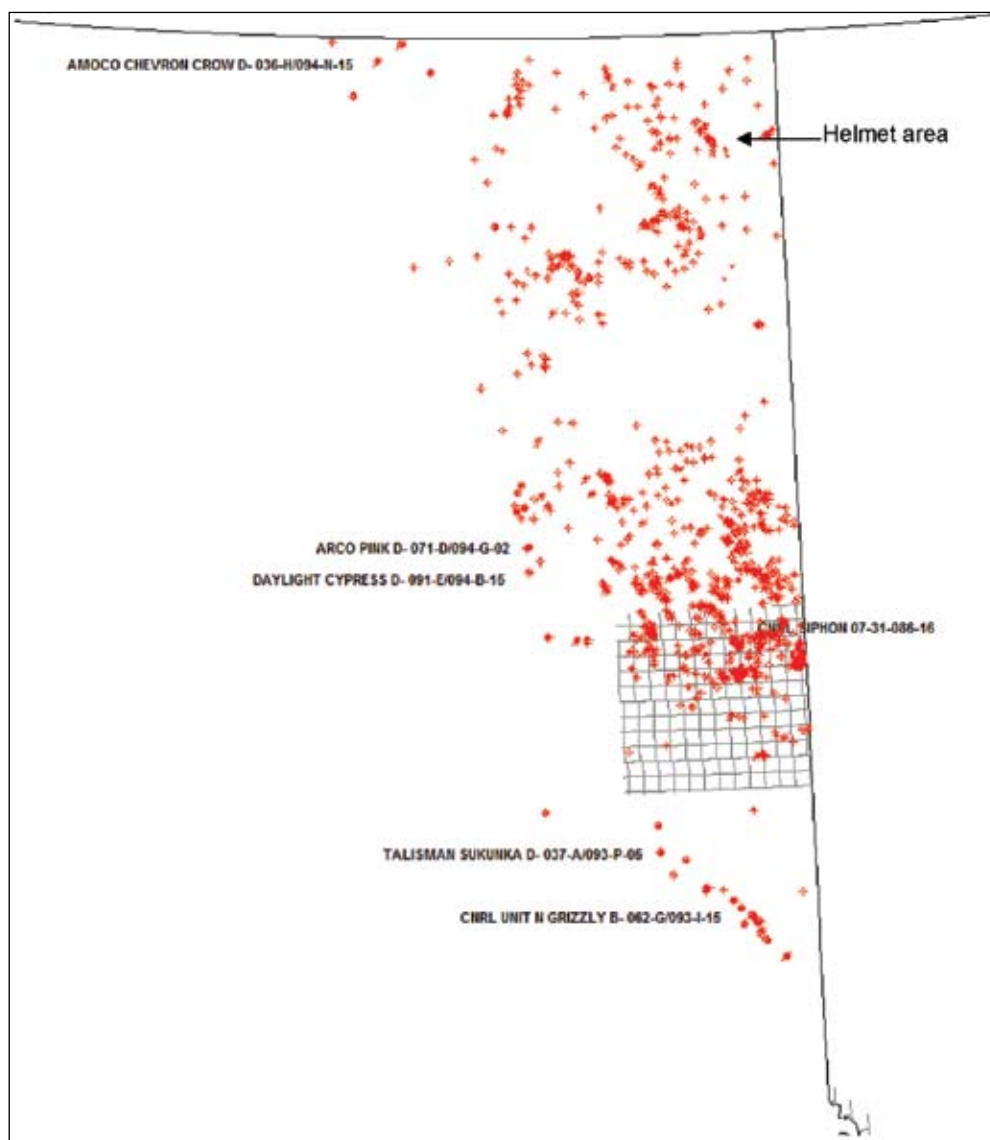


**Figure 8: Drilling 1970–1975**

*New discoveries, such as Pink, Sukunka, and Crow, were made in the disturbed belt along the western fringe of northeastern BC. Helmet was another significant development in the far northeast. Most activity centred on existing fields as oil companies stuck to safe prospects.*

## 1975–1980

The first of many wells to follow were drilled during this period in the “Deep Basin” region of northeastern BC, south of Dawson Creek and adjacent to the Alberta border. On the Alberta side, drilling was very intense for the tight Lower Cretaceous reservoirs recently made economic by advances in fracing technology. This play is among the earliest prototypes of the so-called “resource plays” that have attracted more attention as the more mature basins run out of conventional targets.

Although northeastern BC was slowly running out of conventional wildcat targets, many small fields were still being found and existing play trends were expanding.

More drilling took place to define the linear foothill

trends. Compared with “resource plays”, these targets could be considered conventional despite being expensive and dependent on advances in seismic and drilling technology. The numbers of such wells drilled in any given year will always be low due to their expense and the technical difficulties in defining a location.

A new trend started to take shape at the Dahl Field (in block NTS 094H adjacent to the Alberta border) with the discovery of gas from the Bluesky Formation.

Most of the existing plays within northeastern BC were heavily drilled during this period because an oil boom caused by Middle Eastern political tensions was at its height. Despite the prevailing speculative frenzy for any reasonable play, only a few wells (unsuccessful) were drilled within the increasingly clearly defined white areas.

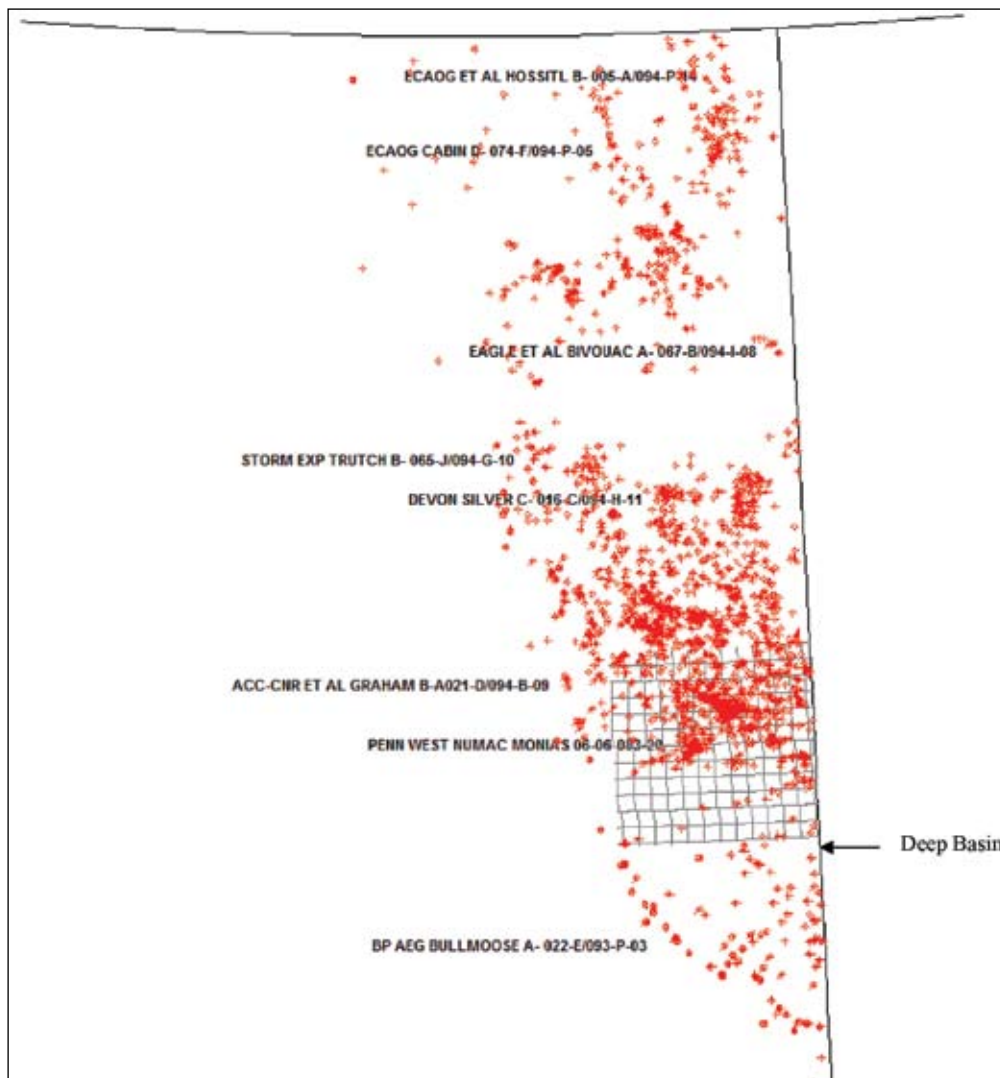


**Figure 9: Drilling 1975–1980**

*Perhaps the most exciting new development was the drilling and production of gas from tight Cretaceous sands in the Deep Basin. A number of small fields in proximity to existing ones were also brought into production. A large number of wells were drilled during this period due to increases in oil prices caused by tensions in the Middle East.*

## 1980–1985

This period was one of the most volatile of all time for the oil industry, both within Canada and worldwide. In the early part of the decade, oil prices remained near the record levels of 1979; before long, prices began a steady drop that lasted for the rest of the period. Activity and speculative fever peaked at the beginning but dropped very quickly by 1985. In Canada, the effects of oil price volatility were compounded by the National Energy Program, which imposed new taxes on production. One of the effects of this new policy was the diversion of significant amounts of investment from conventional plays in the Western Canada Sedimentary Basin to much more risky frontier plays on the north and east coasts. As a result, drilling activity slumped drastically from the peaks of the late 1970s.

One area in northeastern BC that did not suffer a drop in activity was the Deep Basin, where well density began to approach that on the Alberta side. The Helmet and Desan Fields also did not lack for activity where drilling density increased and drainage extended almost to the Alberta border.

Gas prices also were very low during this period. Many newly drilled gas wells were shut-in indefinitely because tie-in costs were high and no markets existed for the gas. A number of existing producers in more remote regions also were shut-in because low gas prices rendered them uneconomic.

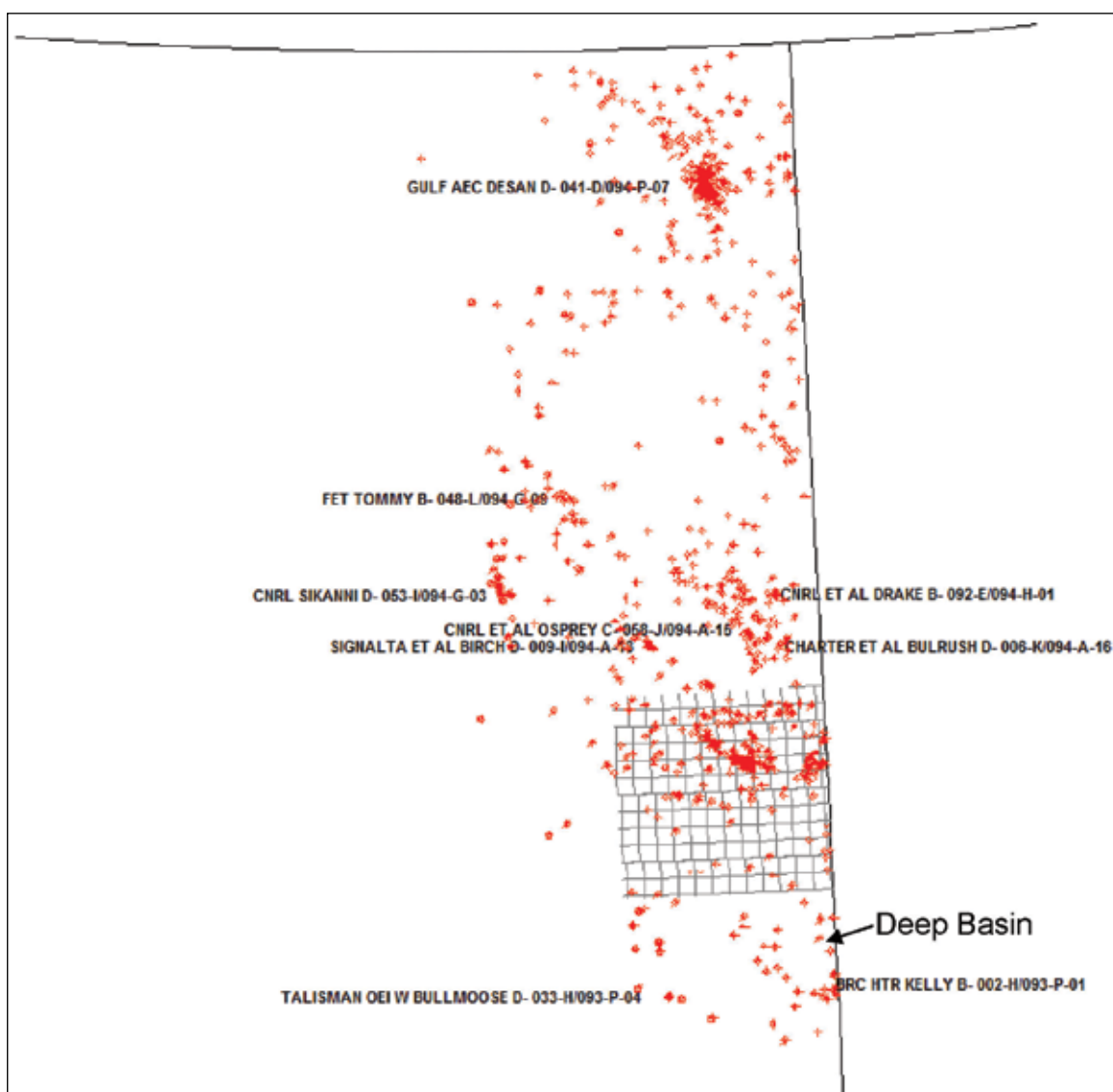


**Figure 10: Drilling 1980–1985**

*The number of wells (1104) dropped considerably from the previous period due to a collapse in world oil prices and the National Energy Program in Canada.*

## 1985–1990

The volatility of the previous period was followed by even greater volatility as the price of oil went from a steady decline to the steepest plunge of all time for one year in 1986. While oil consumers revelled in cheaper fuel prices, countries, regions, and individuals that had grown dependant on abundant revenues faced a stark new reality. Prices began to recover in 1987, but they did not approach former levels until they shot up briefly when Iraq invaded Kuwait at the start of the first Gulf War in 1990.

In BC, the downturn in oil prices led to a 40% drop in drilling activity in 1986 from 1985. Despite the drop in prices, infill drilling of oilfields continued. Toward the end of the decade, gas prices recovered, leading to a re-emphasis on gas.

Significant additions or extensions to existing play types were made in this period at Blueberry, Brassey, and Boundary Lake Fields and other areas. Although many new fields were brought into production, most of that occurred near other producers and no dramatically new play concept brought drilling into the white areas.

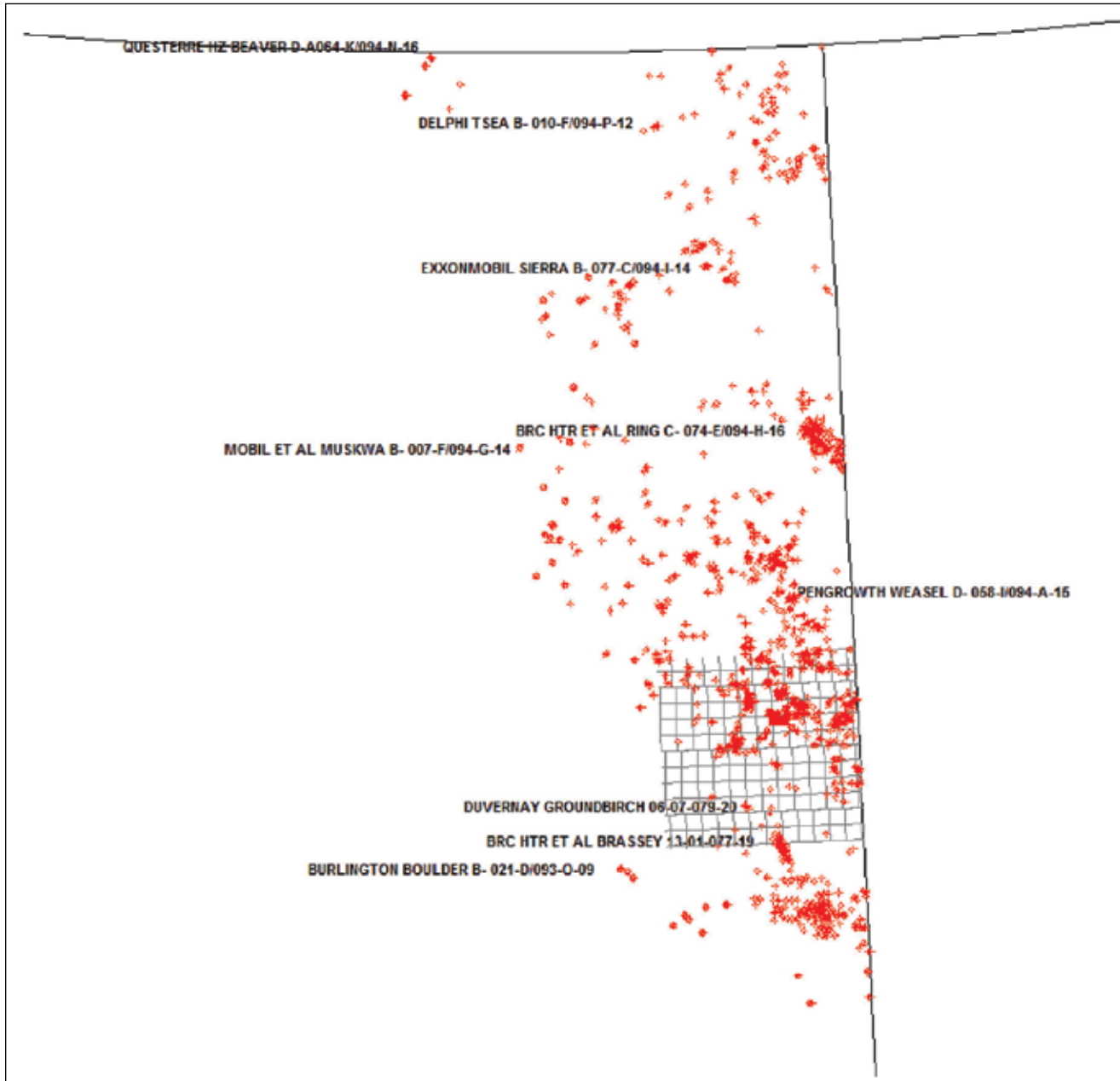


**Figure 11: Drilling 1985–1990**

*Only a few small fields were found at this time. Most drilling (1274 wells) concentrated on safe infills. Low oil and gas prices suppressed activity.*

## 1990–2000

Technology began to play an increasingly important role in the exploration of northeastern BC. Seismic imaging, especially 3D, continued to improve. Horizontal drilling opened up possibilities for exploiting previously uneconomic plays or extending the life of oilfields. Within exploration departments, computers appeared on the desktops of all geologists—the mapping capabilities of the personal computer were by this time greater than the most powerful mainframe of the previous decade.

Coinciding with a recession in Asia—and before the emergence of China as an economic superpower—oil prices

hit rock bottom in 1998. They had never been so low in dollars adjusted for inflation. This depression lasted only a year, and by the end of the 20th century, oil prices began the more-or-less uninterrupted climb that continues today.

In northeastern BC, uncertainty over oil and gas prices restrained drilling activity until after the price collapse of 1998.

A small tongue of drilling extended into a white area with the development of shallow Montney Formation gas at the Kahntah River Field. Many new wells were also drilled for Lower Cretaceous Chinkeh Formation at the Maxhamish Field in the structurally deformed north-westernmost part of northeastern BC.



**Figure 12: Drilling 1990–2000**

Drilling activity remained low until around 1998, when it took off due to increasing oil prices. Activity concentrated around known developments and the white areas remained dotted with only a few outposts.

## 2000–January 2008

The steady rise in energy prices led to record levels of drilling activity throughout northeastern BC in the first part of this century. Most of the drilling took place within established areas, which began to resemble the mature petroleum regions of Alberta and the US. Only a relatively small number of wells were attempted in the white areas, despite the overall number of wells drilled and the availability of sophisticated new exploration technologies.

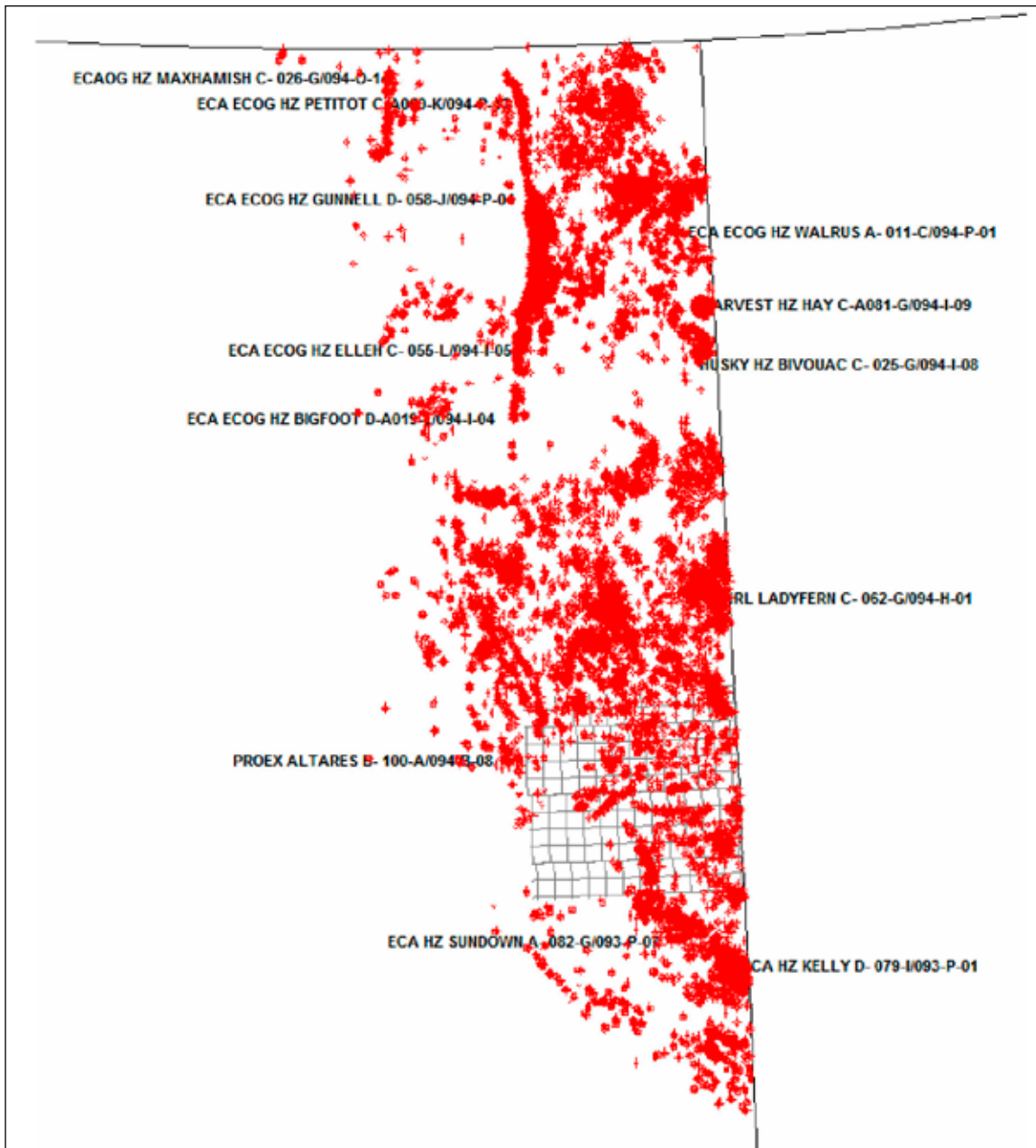


**Figure 13: Drilling 2000–January 2008**

*Drilling reached all-time highs due to steadily rising oil prices. The Gunnell trend of the Jean Marie Formation became hotly pursued as technology improved to enable production from tight carbonates. The white areas received little new attention despite improvements in exploration and production technologies. Activity levels were strong in the demanding foothills areas.*

## SUMMARY AND CONCLUSIONS

The earliest wells in northeastern BC were drilled in the 1920s and 1930s in the Peace River area (which had already been thinly populated by settlers). Like elsewhere in the rapidly growing oil industry throughout the world, the earliest wells, and often still the best, were drilled on surface indications like seeps or obvious structures.

A non-seep discovery, the Leduc Field in Alberta, influenced the exploratory pursuit of the deep Devonian reefal trends in northeastern BC. Deeper drilling for Devonian targets near Fort Nelson also resulted in finding multiple potential producing zones in the Lower Cretaceous, Triassic, and Mississippian. The original Triassic discoveries near Fort St. John and Dawson Creek provided expanding trends to the north and northeast.

By the late 1960s, almost every corner of northeastern BC had been penetrated by a drill bit. Not all attempts found commercial shows of hydrocarbons. However, the areas around Fort St. John and Dawson Creek, with multiple pay zones in the Lower Cretaceous and Triassic, quickly became densely developed.

In the late 20th and the early 21st centuries, new technologies enabled the development of some of the previously discovered but uneconomic resource-type plays, such as the tight sands of the Deep Basin and the widespread Jean Marie Formation carbonates of the far northeast.

The primary play fairways within northeastern BC were largely well established by the late 1960s, and for economic reasons most exploration was concentrated on finding extensions to already well understood plays. The most daring and expensive wildcats were drilled in the foothills, but their risk was mitigated by increasingly precise seismic imaging and the promise of quick returns on investment with their substantial potential reserves. By contrast, in the more central parts of northeastern BC, including the white areas, the hopes of finding another huge discovery like Leduc were gone by the 1980s, so exploration focused on relatively low risk extensions to known plays.

During this latest extended boom in exploration, explorers have apparently not been tempted to drill extensively in the white areas, nor have any new exciting discoveries been made there.

## SELECTED HISTORICAL HIGHLIGHTS IN WORLDWIDE PETROLEUM EXPLORATION

**1789:** Sir Alexander Mackenzie noted tar springs on cliffs above the eponymous Mackenzie River, near the present-day site of Norman Wells, Northwest Territories

**1846:** Abraham Gesner of Canada distilled kerosene from coal.

**1853:** Ignacy Lukaszewicz, a Polish pharmacist, developed a process to distil kerosene from seep oil. This was the start of the oil industry as we know it today.

**1854:** The use of kerosene for lighting provided incentive to dig several wells of roughly 50 m depth at the foot of the Carpathian Mountains in Poland. They are termed “oil mines”.

**1857:** Arguably the first oil wells in North America were drilled (dug?) in southwestern Ontario near Sarnia. Production for the first wells came from oil trapped above the bedrock beneath thick layers of peat and clay.

**1859:** The first wells to produce directly from consolidated bedrock were drilled in Titusville, Pennsylvania.

**1870:** The first supergiant field was initiated in Baku, Azerbaijan, to exploit the abundant oil seeping to surface.

**1878:** The first recession in the oil industry occurred when the invention of the electric light bulb by Thomas Edison negated the need for kerosene for lighting.

**1886:** Oil markets rebounded with the introduction of gas-powered automobiles in Europe by Karl Benz. The use of oil for steam locomotives also began.

**1898:** Automobiles made their appearance in Canada; consumption of oil grew rapidly, as did reliance on American sources for the Canadian market.

**1901:** Texas was ushered in as a major oil producer with the “Spindletop Gusher”. Its prodigious productivity sparked a worldwide frenzy in oil exploration.

**1902:** The first oil exploration well in Alberta was drilled at the site of an oil seep in Waterton Park (Cameron Creek).

**1906:** First recorded well (Steveston No. 1) drilled in the Fraser River delta; it was abandoned at 1200 feet.

**1906:** The first wells in British Columbia were drilled in the Fraser Delta on what were thought to be oil seeps and on a reported gas blow from a diamond-drill hole.

**1908:** Beaver Valley No. 1 was drilled, Cariboo area.

**1909:** Akamina No. 1 was drilled, Flathead area, southeastern BC.

**1909:** Natural gas was discovered in a well drilled near Calgary at Bow Island; the first gas pipeline was constructed to Calgary shortly after.

**1909:** Oil was discovered in Persia, now known as Iran.

**1910:** Oil was discovered in the “Golden Lane” of Mexico.

**1914:** Oil was discovered at Turner Valley south of Calgary, near the site of gas seeps and perpetual surface flares. An oil seep was discovered near Rolla in northeastern BC.

**1914–1918:** Oil became a strategically important commodity with the highly mechanized armies deployed during World War I. A shortage of steel and manpower prevented the exploration of prospects like the oil seep near Rolla.

**1919:** A well was drilled near Crowsnest Pass of southeastern BC to test the obvious structures and oil seeps of the area.

**1920:** Imperial Oil discovered oil at Norman Wells, NT, at the location noted by Alexander Mackenzie.

**1921–1922:** Several test holes were drilled in the Peace River district of BC based upon reported oil seeps and structures observed from surface mapping. One well drilled at Pouce Coupe blew out and killed a crew member. The presence of oil was confirmed.

**1924:** The second oil boom at Turner Valley, Alberta, started with the blow-out at Royalite No.4.

**1927:** Conrad and Marcel Schlumberger recorded the first electrical resistivity well log in Pechelbronn, France. It would be difficult to overstate the importance of this technological development for geologists and the oil industry in general.

**1930:** A well that did not provide encouraging shows was drilled to 2355 feet, six miles south of Kelowna.

**Ca. 1930s:** Vast oilfields were discovered in the Middle East, giving it great strategic and geopolitical importance.

**1942:** Adolf Hitler’s ambitious plans to take the Russian oilfields in the Caucasus were stalled and eventually thwarted, on the battlefields of Stalingrad.

**1943:** Oil began to flow from Norman Wells to Whitehorse in the CANOL pipeline as a strategic supply for the US Army. The pipeline was dismantled after the war.

**Ca. 1947:** The first seismic surveys were conducted in the Aquitaine Basin of France. Exploration entered a new phase because subsurface structures could be visualized in two dimensions.

**1947:** Imperial Oil discovered oil at Leduc No.1 near Edmonton (after many dry holes drilled without the benefit of the new technology of seismic imaging). As a result, the Canadian oil industry was set upon a solid footing and exploration accelerated to other parts of the Western Canada Sedimentary Basin, including northeastern BC. In the years following the Leduc discovery, pipeline construction boomed, opening up more lands for exploration.

**1953:** The Pembina Field, the largest in western Canada, was discovered in a sandstone reservoir in north-central Alberta. Explorationists in western Canada realized that oil could be found not just in reefs or large structures such as thrust sheets but in a great variety of rocks and trap types.

**1953:** Oil supply problems during the Korean War led to the development of the Trans-Mountain pipeline from Edmonton to Vancouver and Seattle. A number of feeder lines were created to supply this pipeline.

**1955:** The first McDonald’s, symbolic of the post-war, fuel-consuming, suburban lifestyle, opened outside Chicago.

**1955:** The first commercial oil well in British Columbia was completed at Boundary Lake.

**1956:** The geopolitical importance of oil was underlined when President Nasser of Egypt expropriated the Suez Canal. Supplies of oil to Europe were threatened until tensions were diffused by United Nations peacekeeping troops.

**1957:** A pipeline was built from the Peace River area of BC and Alberta to carry natural gas to the American market.

**1959:** After several years of discouraging results, oil was discovered in the North African country of Libya. Several other major sources of oil, such as a revitalized industry in the former Soviet Union, came into the market at roughly the same time and caused a softening of oil prices.

**1960:** OPEC (Organization of Petroleum Exporting Countries) was formed in an effort to control oversupply of oil to the market and thereby exert some control on prices. Western Canadian oil producers sought market protection from the federal government.

**1960:** The deepest well in Canada (to that time) was drilled to a depth of 16,540 feet in the Crowsnest Pass area of southeastern BC. Compressed air rather than mud was used as the circulating medium.

**1960:** A facility dedicated to the storage and viewing of drill cores cut in BC is opened at Charlie Lake.

**1965:** Substantial oil discoveries were made in Devonian reefs of Rainbow Lake, northwestern Alberta. This intensified exploration along the Devonian barrier reef trend extending into northeastern BC.

**1968:** A confirmation well at Prudhoe Bay, Alaska, was drilled to demonstrate the potential of this very substantial oilfield. This led to the construction of the Alaska Pipeline and an intensification of exploration in Canada’s Beaufort Sea and Mackenzie Delta.

**1970:** Following the lead of Prudhoe Bay, Imperial Oil made a large oil discovery at Atkinson Point in the Mackenzie Delta.

**1971:** Large discoveries of natural gas were made in the Mackenzie Delta.

**1973:** The first sharp rise in oil prices, in constant dollars, since the beginning of the oil industry began when Arab states tightened supplies to anyone who supported Israel in the Yom Kippur War.

**1973–1975:** Despite the spike in oil prices, activity in northeastern BC declined due to the drop in gas prices and the lack of significant oil discoveries. Bickering between the federal government and provinces over exports to the US also dampened activity as companies withheld investment in exploration.

**1975:** Activity jumped in northeastern BC and the rest of western Canada with a rise in gas prices. The boom of the late 1970s was on.

**1979:** The second energy crisis started when Americans were taken hostage at the American Embassy in Iran and Ayatollah Khomeini replaces the Shah. The price of oil reached the highest level of all time in constant dollars in December (\$100.28 US in January 2007 dollars).

**1980:** The Canadian federal government imposed the National Energy Program. This resulted in a sudden and big drop in activity in northeastern BC and most of western Canada except the far north.

**1982:** Oil prices began a steady drop to the levels before the 1973 energy crisis. Activity in western Canada was not severely affected until 1986 when prices reached their nadir.

**Ca. 1982:** Vast improvements in computing power allowed the development of 3D seismic technology. This enabled far more precision in imaging the size, shape, and location of hydrocarbon reservoirs than did 2D seismic.

**1985:** A pipeline was constructed from Norman Wells to bring oil down to Zama in Alberta.

**1986:** A dramatic drop in world oil prices to the levels found prior to the first energy crisis led to company amalgamations, layoffs, re-evaluations of exploration projects, and a general drastic cut-back in activity.

**Ca. 1988:** Horizontal drilling technology opened up new possibilities for exploiting tight but continuous formations.

**1990:** A brief spike in oil prices occurred with the invasion of Kuwait by Iraq. Prices dove back down as Iraq was repelled.

**1995:** Around the mid-nineties the Asian economies went into a recession, which caused oil prices to fall to their lowest level ever, in constant dollars, around 1998. Another round of consolidations and layoffs ensued.

**1998:** Oil prices reached their nadir in adjusted dollar value and began their long climb up as OPEC instituted cuts in production. Asian economies recovered, and industrial production grew in China.

**2000:** The discovery of gas in hydrothermal dolomites in a remote part of BC (Ladyfern) leads to a mini-boom in exploration.

**2001:** The suicide bombings of the World Trade Centre and Pentagon raised the profile for North American energy security ever higher. Increased investment flowed in BC and western Canada.

**2005:** British Columbia raises a record amount of money in disposition of oil and gas rights.

**2007 (late):** British Columbia set a new annual record for money raised in disposition of mineral rights. This was due mainly to new interest in shale gas in shale basins in the northernmost regions of the province. “Resource plays” attract increasing attention in BC, Alberta, and the western US as conventional reserves run down and prove more difficult to replace.

**2007:** Tightening supplies due to increasing demand combined with continuing tensions in the Middle East led to an oil price of almost \$100 per barrel—close to the adjusted record set in 1979.

**2008:** Interest in BC potential increases due to changes in royalty regimes on production in neighbouring Alberta. Changing demographics and political climate in Alberta pressures the government to make changes.

## REFERENCES

- Clare, G. (2003): History of the Oil and Gas Industry in the South Peace. An address to the Oil and Gas Conference, Dawson Creek, BC, September 2003.
- Galloway, J.D. (1915): Drilling for Oil at Port Haney; Minister of Mines, B.C., Annual Report, 1914, pages 392–396.
- Gould, E. (1976): The History of Canada’s Oil and Gas Industry; Hancock House Publisher, 288 pages.
- Hume, G.S. (1933): Oil and Gas in Western Canada (second edition); Canada Department of Mines, Geological Survey, Economic Geology Series, No.8.



# TRIASSIC POROSITY TRENDS IN NORTHEASTERN BRITISH COLUMBIA

Ed Janicki<sup>1</sup>

---

## ABSTRACT

*Interest has increased recently in finding suitable locations for subsurface disposal (sequestration) of carbon dioxide (CO<sub>2</sub>) and water incidental to hydrocarbon production. Wireline logs from approximately 600 wells in northeastern British Columbia were evaluated for porosity of Triassic formations with the goal of outlining possible disposal sites. Total porosity for the Doig, Halfway, and Baldonnel Formations was mapped for much of the area with known Triassic sedimentation. Strong northwest trends, roughly coincident with Triassic shorelines, appear for the Halfway Formation. A number of isolated occurrences of porosity (especially wet porosity) have also been outlined for further study. Maps for the Baldonnel and Doig Formations also show potential disposal/sequestration sites within those formations.*

Janicki, E., (2008); Triassic Porosity Trends in Northeastern British Columbia; in Geoscience Reports 2008, BC Ministry of Energy, Mines and Petroleum Resources, pages 59-65.

<sup>1</sup>British Columbia Ministry of Energy, Mines and Petroleum Resources, Oil and Gas Division, Resource Development and Geoscience Branch, PO Box 9333 Stn. Prov. Govt., Victoria, BC, V8W 9N3; e-mail ed.janicki@gov.bc.ca

Key words: subsurface disposal, Triassic, trends, sequestration, reservoir, logs, porosity, cut-offs, picks.

---

## INTRODUCTION

The Triassic Period has so far been the most important geological interval for hydrocarbon production in British Columbia. Its productivity and rapid pace of development over the past five decades have led to exploratory maturity and concomitant decreases in the size and frequency of new discoveries. This project is not aimed at reversing the decline, but it does make use of the wealth of data accumulated in developing this resource to examine an issue related to intense hydrocarbon development: the disposal of production waters and CO<sub>2</sub>. If the Triassic has provided BC with many good hydrocarbon reservoirs, it should also be able to provide suitable reservoirs for accepting unwanted gases or fluids; this potential might also extend to the temporary storage of excess gas production.

The maps presented here are intended to illustrate trends in porosity for the major producing formations of the Triassic. Because the maps are regional in extent, it is unlikely that they will do more than help in targeting certain areas for further study of disposal possibilities. Figure 1 places the study area within the context of western Canada.

These maps have not yet been refined to resolve inconsistencies in data. With additional data and critical scrutiny of the output, the maps could evolve to look considerably different. Approximately 600 locations were evaluated in no particular order. These 600 represent only a small portion of the total number of wells with suitable logs available in the area, so more detail would likely add complexity and

texture to the contoured trends displayed here. The edges of the maps may eventually be extended to include more area with Triassic sediments. The area mapped represents the most accessible region with likely the greatest need for water disposal and CO<sub>2</sub> sequestration.

Determinations of porosity accurate enough for volumetric calculations were not within the scope of this project. By applying consistent criteria over vast differences in log vintages and quality, a regional picture is presented that shows relative differences in porosity.

The database used to generate the maps in this publication is available upon request. Comments, corrections, or new ideas to improve the product would be appreciated.

## METHODOLOGY

To ensure an adequate distribution of well density, approximately two wells per township or NTS block were selected, at diagonally opposite corners wherever possible. Before selection, available logs were previewed and then printed. Recently drilled wells with modern Compensated Neutron Formation Density (CNFD) logs were preferred. Older wells were used if necessary. If no CNFD logs were available, sonic logs were chosen. Some blocks were not sampled at all because they lacked wells with adequate porosity logs. The actual evaluations were done on printed hardcopies of the logs.

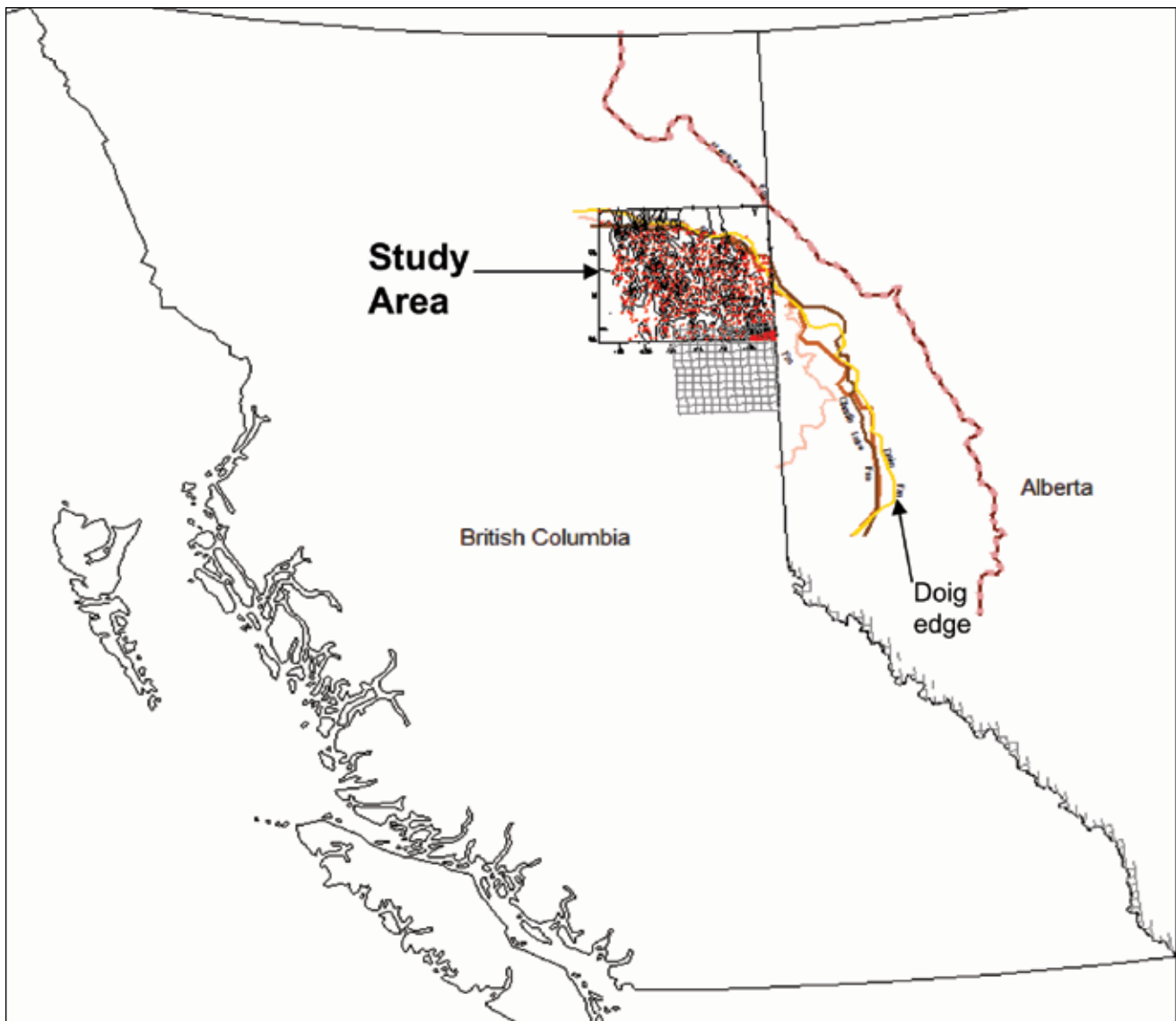


**Figure 1: Triassic Porosity Trends in Northeastern British Columbia.** The study extends from the northern portion of the township block near Fort St. John to the edge of Doig Formation sedimentation.

The following generally accepted porosity cut-offs were applied for productive Triassic formations in northeastern BC:

- Halfway Formation 10%
- Charlie Lake Formation 6%
- Baldonnel Formation 6%
- Doig Formation 6%
- Montney Formation 6%

A gamma ray cut-off for shale content was applied for each formation, but especially for Charlie Lake, because otherwise the porosity thickness would be excessively high in many wells, as confirmed by their poor results on drill-stem tests. This cut-off was not applied on a strict numerical basis, but rather by drawing a baseline through the gamma ray curve on a case-by-case basis, depending on

the apparent quality of the potential reservoir rock. In most cases, locations with abundant porosity had been tested and/or produced, which was a tip-off that porosity exists. Abandoned locations usually have little or no porosity, except for those that clearly are wet (i.e., have high water saturations).

To eliminate bias, each well location was evaluated independently without knowledge of its geographical location. This was possible because the logs were printed and stacked in essentially random order—one location did not influence the values given to the next because they were usually randomly scattered and not closely offsetting. Mapping and contouring the results were not begun until all 600 wells were evaluated. Contouring was done with Golden Software's Surfer using the kriging technique.

Many holes examined were in poor condition with large and frequent washed-out sections. Under those conditions, the primary porosity tools (density and sonic logs) do not give accurate results—they overstate porosity because the tools are measuring the extra space in the washed-out sections rather than rock properties. For that reason, porosity was not counted for sections that were badly washed out, and therefore porosity is likely understated for some wells. However, this omission can be rationalized for the purpose of this study because rock sections prone to wash-out would probably not be ideal for either CO<sub>2</sub> sequestration or water disposal anyway. Those washed-out sections not included in porosity totals are indicated on the paper logs, which have been retained in files for reference.

More recently drilled wells tended to be less washed out (another reason for choosing them in preference to older wells). The biggest offenders in this respect seemed to be those drilled during the last “big boom” of the late 1970s and early 1980s.

Porosity totals for the Charlie Lake Formation were measured but have not yet been mapped because it would probably not be a viable formation for CO<sub>2</sub> sequestration or water disposal. Porosity for the formation (all members were lumped together) is usually dispersed over a number of thin streaks of marginal quality. It seldom has more than three continuous metres of good porosity. Log presentation also poses a problem because very large sections of Charlie Lake appear to be well above the 6% porosity cut-off. Much of this apparent high porosity for Charlie Lake should probably not be included in the porosity total because it is of marginal quality. Poor drill-stem-test results usually confirm this suspicion. A strict gamma ray cut-off was applied to ensure that only the most viable, effective porosity has been included in the total.

Formation picks were provided by IHS Accumap. Their picks appear to be reliable for the more straightforward picks for the Halfway and Baldonnel Formations. These formations also happen to present the best sequestration potential in the Triassic. The Doig Formation can easily be confused with the base of the Halfway Formation; those locations with good porosity mapped in the Doig Formation could be added to Halfway Formation porosity if so desired by users of this data. Members of the Charlie Lake Formation are difficult to pick, so they were grouped together.

Porosity totals might be greater for formations only partly penetrated, especially for the Doig Formation, where many wells were drilled only deep enough to pick a top.

The Montney Formation was evaluated but not mapped because it is generally very shaley and contains only scattered lenses of cleaner sand and good porosity.

## INTERPRETATION

### *Halfway Formation Porosity*

This formation probably presents the best potential for either CO<sub>2</sub> sequestration or water disposal in the Triassic in BC. It has been proven to be a very good oil and gas producer with favourable reservoir qualities of porosity and permeability. It has also been used successfully in a number of places (Janicki 2008) for water disposal. Figure 2 shows that it is widespread in extent but not uniformly porous. Changes in facies from clean sand to relatively dirty or tight sands would aid trapping and isolation of disposed fluids or gases but are not adequate without suitable structure. Where it is porous enough to exceed the cut-off limit (10%), it usually approaches 20% or more for at least a portion of the section. Total thickness of reservoir quality sand ranges from zero to 8 m. Figure 2 shows a northwest-southeast trend of semi-isolated pods of relatively thick porous Halfway Formation sand stretching across the entire mapped area. This conforms roughly with what is generally accepted as the trend of the original Triassic shoreline. Porosity thins to zero at the depositional edge (Cant 1988) to the northeast. A secondary weaker north-south trend appears to splay off the main trend passing through NTS 094A/16, 094H/2, 094H/7, and 094H/10.

A second map for the Halfway Formation (Figure 3) is based upon total porosity-metres where it is clearly wet, as indicated by log responses and/or drill-stem-test results. Low total porosity on this map does not mean the Halfway is non-porous—it just indicates where thick, wet Halfway occurs. The locations with large total thickness values shown on this map should be of interest for either water disposal or CO<sub>2</sub> sequestration because injection into those intervals would not interfere with existing production and wet locations tend to be more isolated than clusters of productive wells—another advantage. Some of the thickest examples of porous Halfway Formation sand often happen to be wet. Many locations with thick sand sections fell only slightly below the cut-off and therefore were mapped with little or no total porosity. Optimistic tweaking of the cut-offs could result in many more metres of porosity for many locations.

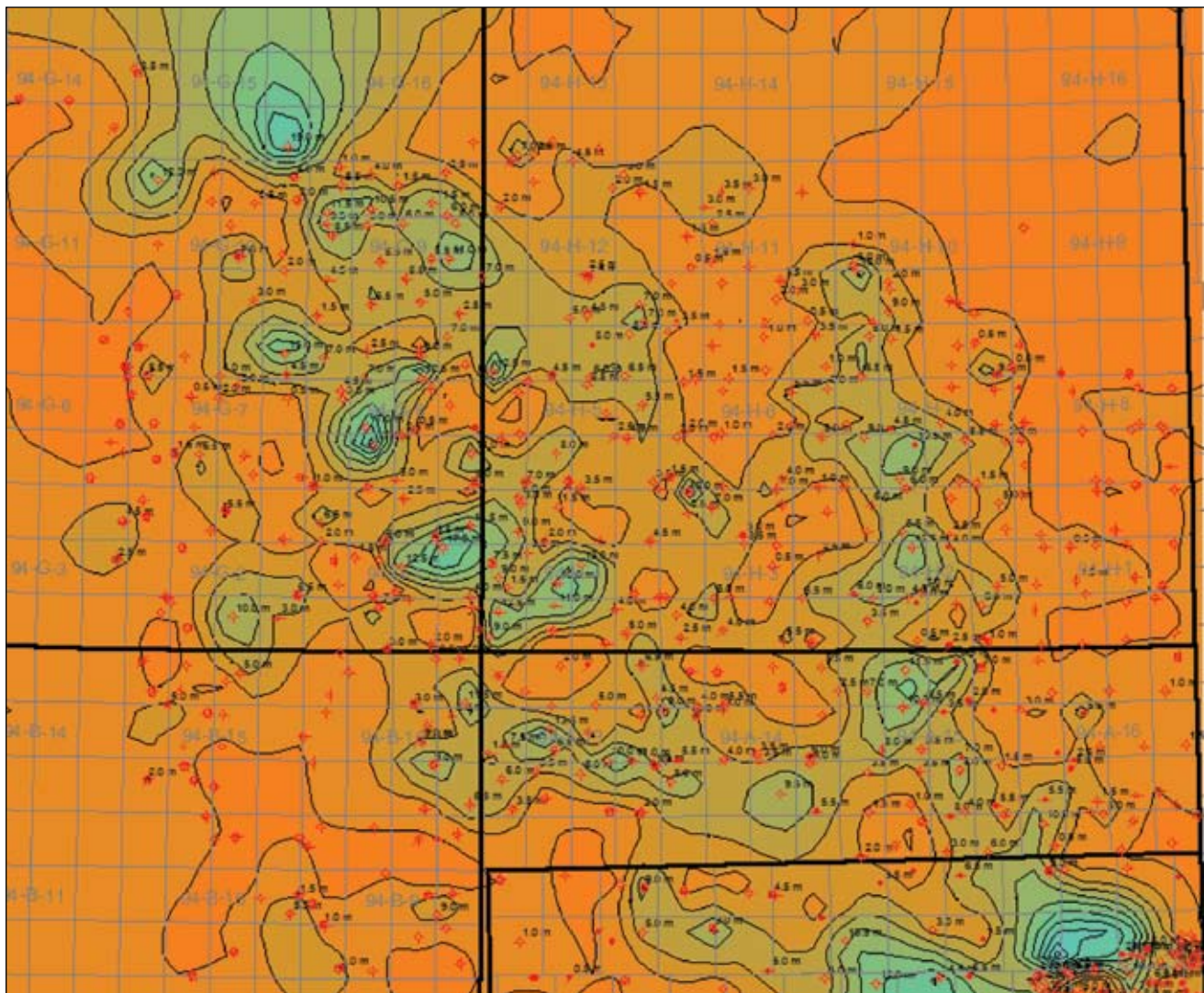


Figure 2: Halfway Formation Porosity (contour interval 2 m). Green represents thick porosity. Orange and brown represent low totals. Porosity cut-off is 10%.

### ***Baldonnell Formation Porosity***

The northwest-southeast trend for porosity-metres (Figure 4) for the Baldonnell Formation is generally consistent with the ancient Triassic shoreline, which advanced and retreated over a low-relief slope. The trend is muted and irregular in comparison to the Halfway because erosion removed the top rock units in many locations towards the northeastern limits of deposition. The upper units tend to be the most porous. In many locations, the Baldonnell section has too little matrix porosity to be counted. The Baldonnell often appears to be fractured; therefore porosity that was included in the totals might not be just matrix porosity. Even where clearly enhanced by fracturing, measured porosity is often just above cut-off.

Fracture porosity is probably not ideal for containing waste water or CO<sub>2</sub> because fractures could cause wastes to flow in unpredictable paths. The increase in pressure introduced by injecting waste streams could enlarge and extend existing fractures into and beyond the formations intended to seal them in place.

The best sites to consider for disposal into the Baldonnell Formation appear to lie west and north of the Siphon and Boundary Lake Fields, respectively. Another potential area of interest lies near the Birley Field in NTS Block 094H/3. The Boundary Lake Field itself appears to be of relatively little interest, but it would be problematic for disposal because it is known to be dissected by many normal faults, which could act as conduits into overlying formations.

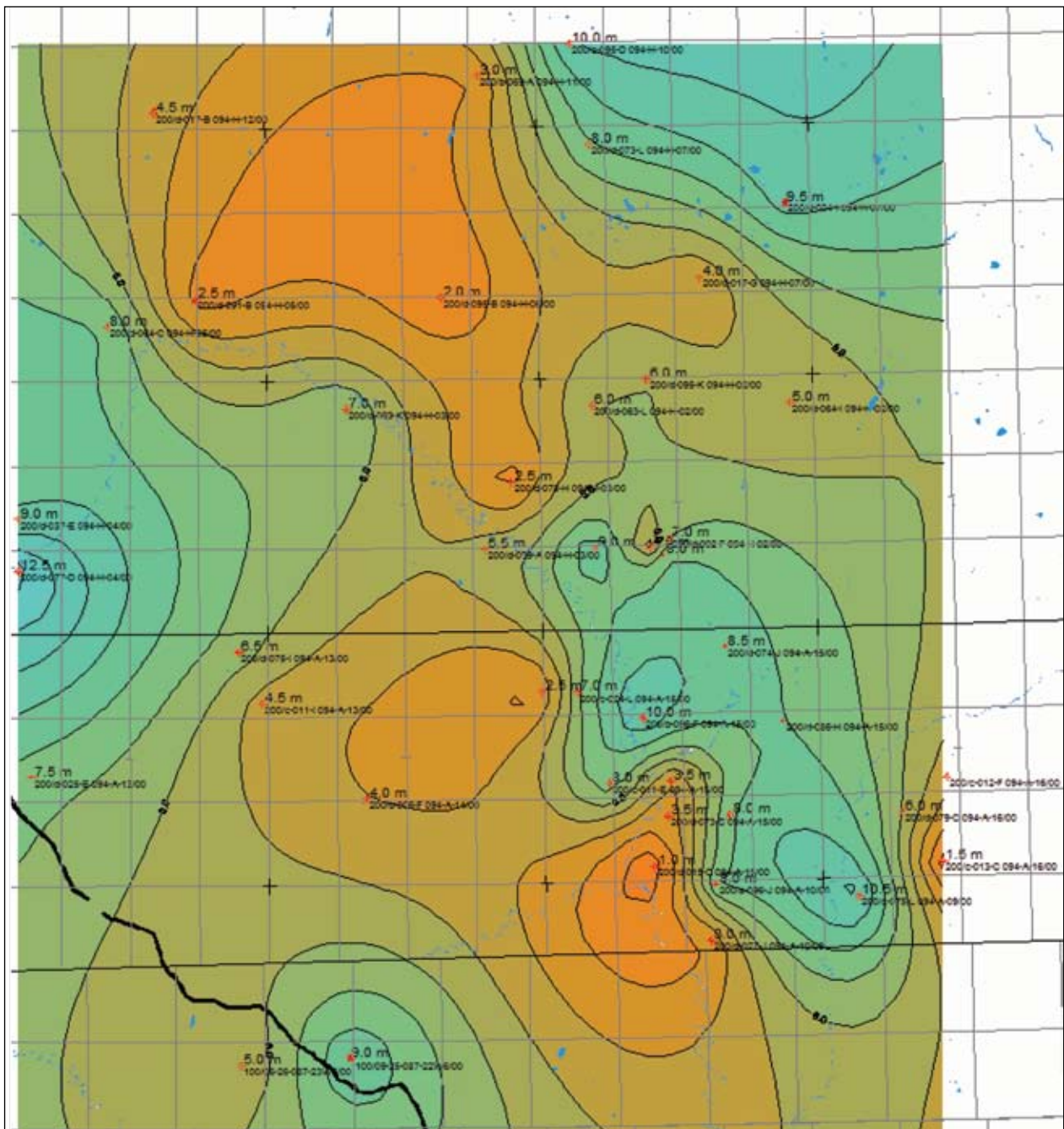


**Figure 3: Wet Halfway Formation Porosity (contour interval 2 m). A strong northwest trend of thick, wet and porous Halfway occurs to the north of the township block. Isolated occurrences, such as the 9 m in 9-25-87-22W6, might be of greatest value for water disposal or CO<sub>2</sub> sequestration.**

### ***Doig Formation Porosity***

The Doig Formation can easily be confused with the Halfway (as discussed above), so porosity-metres might not be valid in all cases. Despite that possibility, the Doig Formation, or the rock that occurs at the stratigraphic level picked as Doig in these wells, shows some promise because the thickest porosity-metres appear to be isolated in scattered, discrete pods. This would be favourable be-

cause good porosity in one or several wells would tend to be surrounded by wells with little or no Doig porosity. There would be less chance, therefore, of injected wastes interfering with current production or escaping into uphole formations.

No clear trend is discernable for the Doig Formation, at least for the area covered (Figure 5). This lack of a trend might be an indication of poorly defined stratigraphic picks; on the other hand, it might simply indicate that the natural

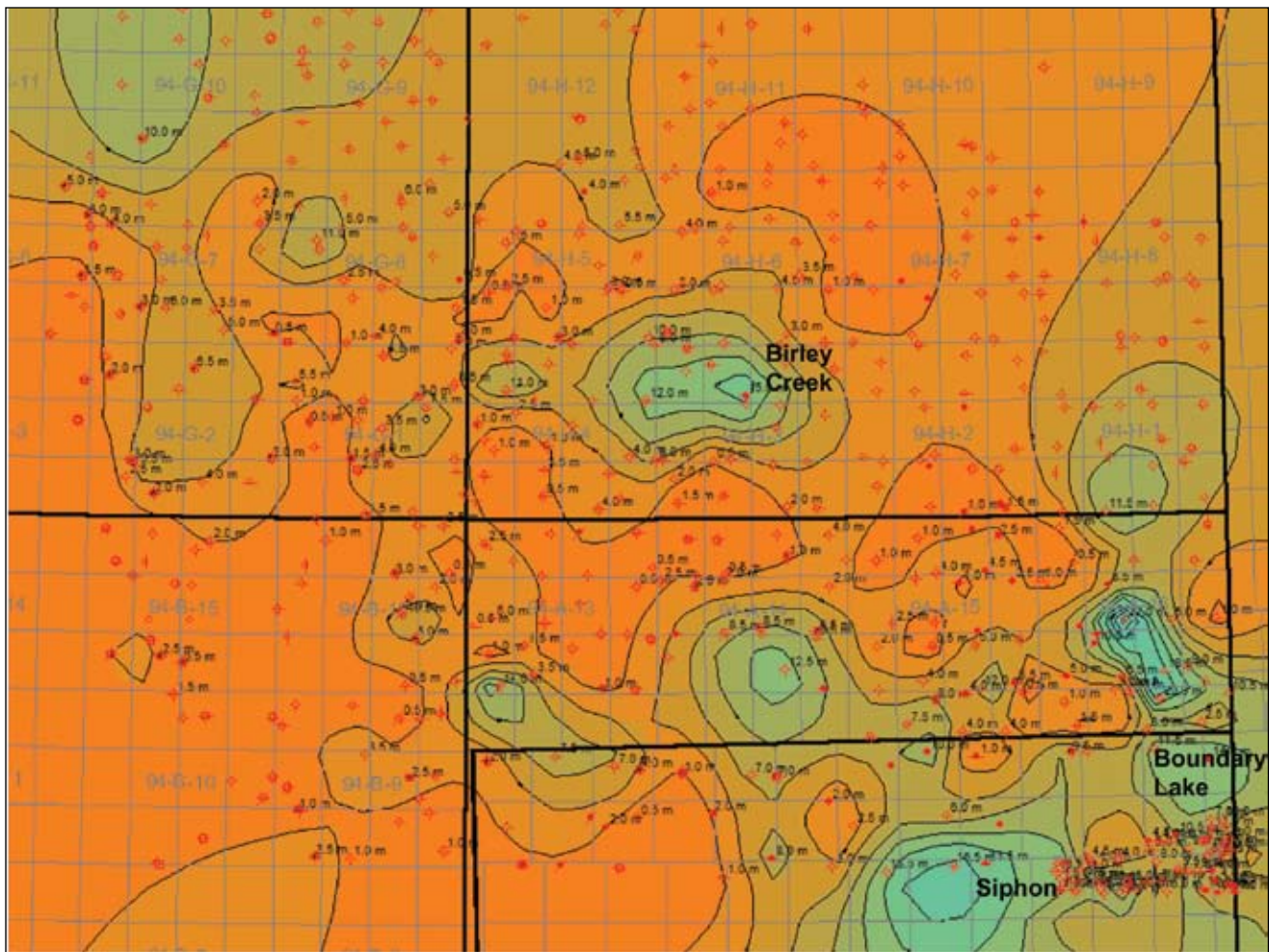


Figure 4: Baldonnell Formation Porosity (contour interval 2 m). Green represents the thickest accumulations of porous Baldonnell. The best sites to consider for disposal into the Baldonnell Formation appear to lie west and north of the Siphon and Boundary Lake Fields, respectively.

tendency of the Doig Formation is to be less clean and porous than the overlying Halfway Formation and that porosity, when it occurs, requires special geological conditions. This apparent randomness of porosity might be advantageous when considering disposal sites because isolation is beneficial in containing wastes.

While most of the Doig Formation appears to have low porosity, in a few places it does have among the thickest

occurrences of any of the Triassic formations considered. The northeast trend (some might break this trend into two isolated pods) in NTS Block 094A/14 and the north-westernmost portion of the township block shows very good porosity totals of up to 29 m. Several isolated but relatively thick pods of up to 15 m and surrounded by low porosity occur to the northwest.

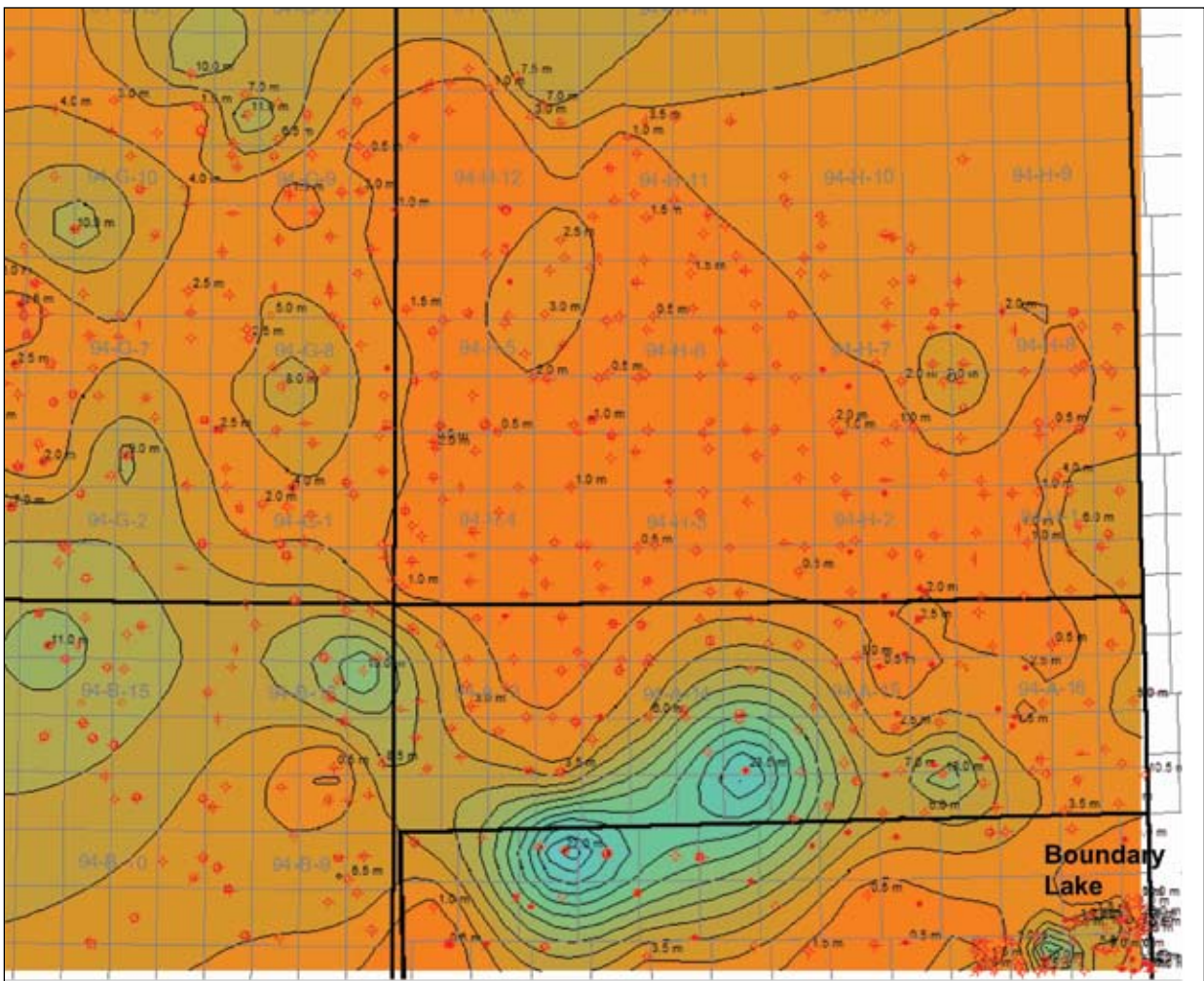


Figure 5: Doig Formation Porosity (contour interval 2 m). Thick Doig porosity, highlighted in green, occurs at the north-west edge of the township block. Another small but thick occurrence is present in the Boundary Lake Field. An overall strong trend does not appear to be present.

## CONCLUSIONS

This project attempts to identify potential sites for disposal of produced waters or CO<sub>2</sub> in northeastern British Columbia by mapping porosity of Triassic formations. Roughly 600 evenly distributed locations were selected for evaluation of Triassic porosity. Maps showing porosity-metres for the Halfway, Baldonnel, and Doig Formations were drawn. More work will be done to refine the mapping presented here.

Overall, the Halfway has the greatest number of potential disposal sites because many locations have good sections of continuous porosity. A number of locations with wet Halfway were segregated and mapped separately. The trends of thick porosity shown by this map should receive special consideration because wet locations tend to be more isolated and disposal into those areas would not be disruptive to production.

The Baldonnel Formation has generally less-favourable characteristics for waste disposal, but some porous trends are present, and it does have a local history of accepting significant volumes of produced waters.

## REFERENCES

- Cant, D.J. (1988): Regional structure and development of the Peace River Arch, Alberta: A Paleozoic failed rift system? *Bulletin of Canadian Petroleum Geology*, Volume 36, no. 3, pages 284–295.
- Janicki, E. P. (2008): Northeastern British Columbia water disposal well studies. Geoscience Reports 2008, *BC Ministry of Energy, Mines and Petroleum Resources*, pages 47-53.



# NECHAKO PROJECT UPDATE

Janet Riddell<sup>1</sup> and Filippo Ferri<sup>1</sup>

## ABSTRACT

*Evaluation of the oil and gas potential of the Nechako Basin continued for the third consecutive year. Fieldwork during the 2007 season was concentrated in the northwesternmost part of the basin and in the Skeena Arch. The Jurassic Smithers and Ashman Formations and the Early Cretaceous Skeena Group were evaluated for source and reservoir potential. Source potential is very poor in the Smithers Formation but is fair to good in the Ashman Formation and in the shale members of the Skeena Group. Thermal maturation data indicate Skeena rocks are currently in the oil window and Ashman and Smithers units are in the peak to upper dry gas zone. Results are pending for analysis of the Skeena Group coarse clastics, but indications for good reservoir quality in these rocks are lacking. Two new U-Pb dates from andesites on the southern fringe of the basin indicate that these volcanics are latest Early Cretaceous rather than Middle to Late Jurassic as previously thought.*

Riddell, R. and Ferri, F., (2008); Nechako Project Update; in Geoscience Reports 2008, BC Ministry of Energy, Mines and Petroleum Resources, pages 67-77.

<sup>1</sup>British Columbia Ministry of Energy, Mines and Petroleum Resources, Oil and Gas Division, Resource Development and Geoscience Branch, PO Box 9333 Stn. Prov. Govt., Victoria, BC, V8W 9N3; e-mail janet.riddell@gov.bc.ca

**Key Words:** Nechako Basin, oil and gas, petroleum, hydrocarbons, Rock-Eval, source beds, thermal maturity, vitrinite reflectance, reservoir, porosity, U-Pb dates, apatite fission track (AFT) thermochronometry, Skeena Group, Hazelton Group, Bowser Lake Group, Spences Bridge Group, Smithers Formation, Ashman Formation, Powell Creek volcanics.

## INTRODUCTION

Evaluation of the oil and gas potential of the Nechako Basin (Figure 1) continued for the third consecutive year. The focus of the 2007 field season was the northwesternmost part of the basin and the Skeena Arch, following investigation of the more highly prospective southern part of the basin in previous years (Riddell et al. 2007; Ferri et al. 2006). Two new U-Pb dates of volcanic rocks in the western Chilcotin have improved our understanding of the underlying basement in the southern part of the basin. We continue to build a thermal history of the Nechako region using apatite fission track (AFT) thermochronometry.

## 2007 FIELD SEASON

The 2-person field crew spent 2 weeks in the field during the summer of 2007 (Figure 2). We visited outcrops of Jurassic and Cretaceous clastic units in the northwestern Nechako basin and the Skeena Arch to sample units with potential as source or reservoir rocks, expanding the database compilation initiated by the work of Hunt (1992). New data presented in this report include Rock-Eval analyses for 20 shale and siltstone samples and vitrinite reflectance analyses for 24 samples.

## Reconnaissance In The Northwestern Nechako Basin And Skeena Arch Areas

We conducted reconnaissance of the Jurassic and Cretaceous clastic units in the northwestern part of the Whitesail Lake mapsheet (NTS 093E) and the southwestern part of the Smithers sheet (NTS 093L), from Tahtsa Lake and Tahtsa Reach on the south to the Morice River on the north. We visited isolated outcrops in the Skeena Arch area at the

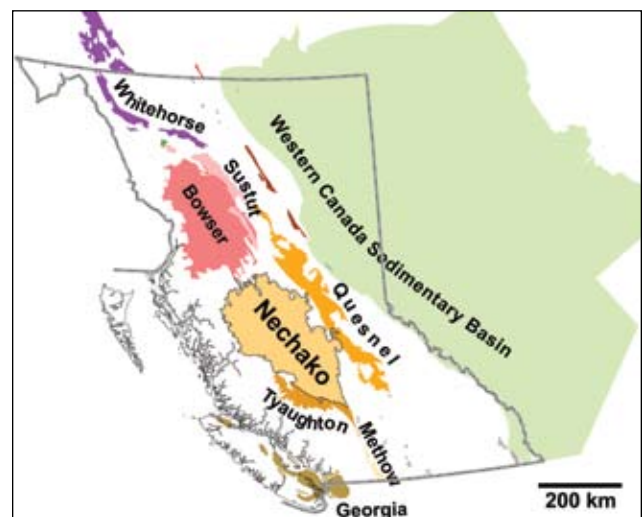


Figure 1: Sedimentary basins of British Columbia.

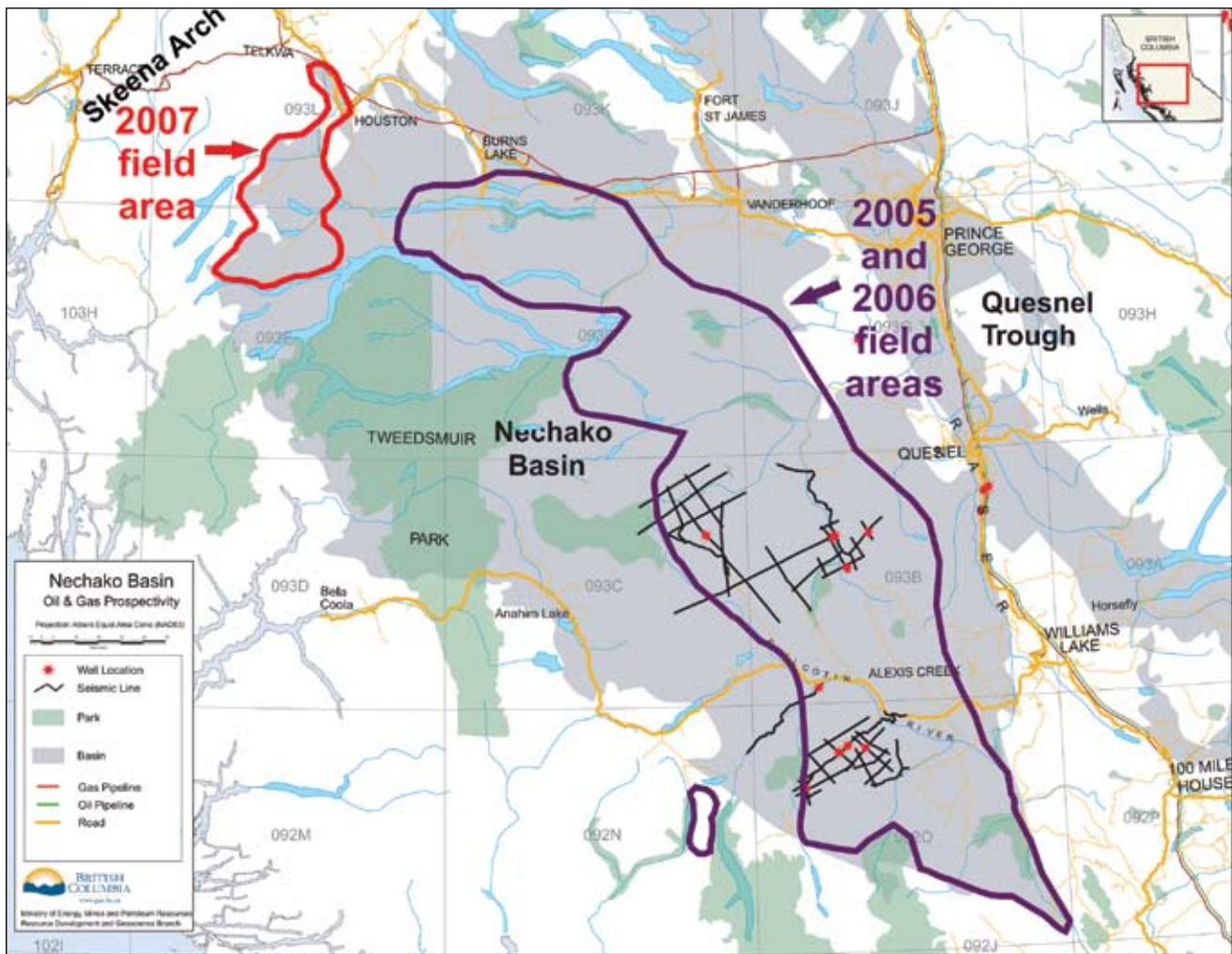


Figure 2: The 2007 field season was conducted in the northwesternmost part of the Nechako Basin.

community of Walcott, and on Ashman Ridge.

The region shares some stratigraphic elements with the Bowser Basin (Table 1). A portion of the geological map of Tipper et al. (1974) in Figure 3 shows the distribution of the major map units. Andesitic volcanics and sedimentary rocks of the Early to Middle Jurassic Hazelton Group are the oldest units in the region (MacIntyre 1985a). The Bowser Lake Group is represented by sparse exposures of the Middle Jurassic Ashman Formation. Late Jurassic to Early Cretaceous members of the Bowser Lake Group are not represented in this region. Early to Middle Cretaceous Skeena Group rocks are exposed south of Tahtsa Lake, around Collins and Nadina Lakes (Desjardins et al. 1991), and along the Morice River. Volcanic rocks of the Late Cretaceous Kasalka Group unconformably overlie the Skeena Group locally (MacIntyre 1985a). Exposures of the Paleocene to Eocene Ootsa Lake and Endako volcanic sequences are scattered and isolated in the reconnaissance area; they are more widespread and continuous further east, between Houston and Ootsa Lake (Figure 3).

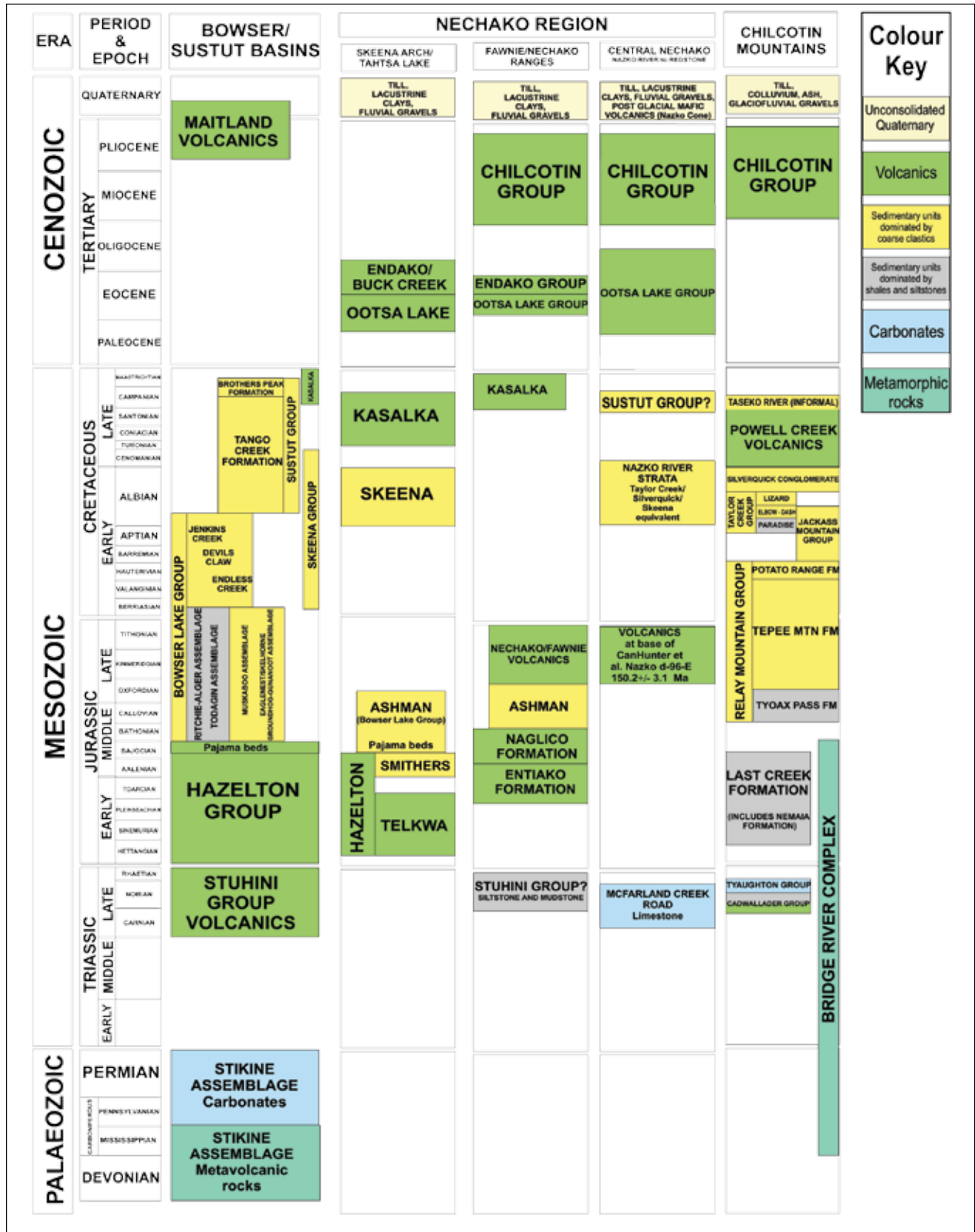
Layered rocks are intruded by granitic rocks of Late Cretaceous and Tertiary ages, which are especially abundant in the Tahtsa Lake area. Porphyry copper and molybdenum deposits, including the Huckleberry Mine, are associated with these plutons.

The Smithers Formation of the Hazelton Group, the Ashman Formation of the Bowser Lake Group, and shales and sandstones of the Skeena Group were examined and sampled for Rock-Eval analysis, reservoir quality, vitrinite reflectance, apatite fission track thermochronometry, and palynology. Clastic rocks are sparse relative to volumetrically abundant volcanic and plutonic rocks in the area.

### SMITHERS FORMATION

The Smithers Formation of the Hazelton Group is well exposed in the region (Diakow 2006). We examined it on Mount Sweeney and in the Mosquito Hills north of Tahtsa Reach. It is a shallow marine sedimentary unit consisting predominantly of pale coloured grey to tan feldspar greywacke, arkosic arenite, and siltstone. Locally

TABLE 1: CORRELATION CHART, NECHAKO BASIN.



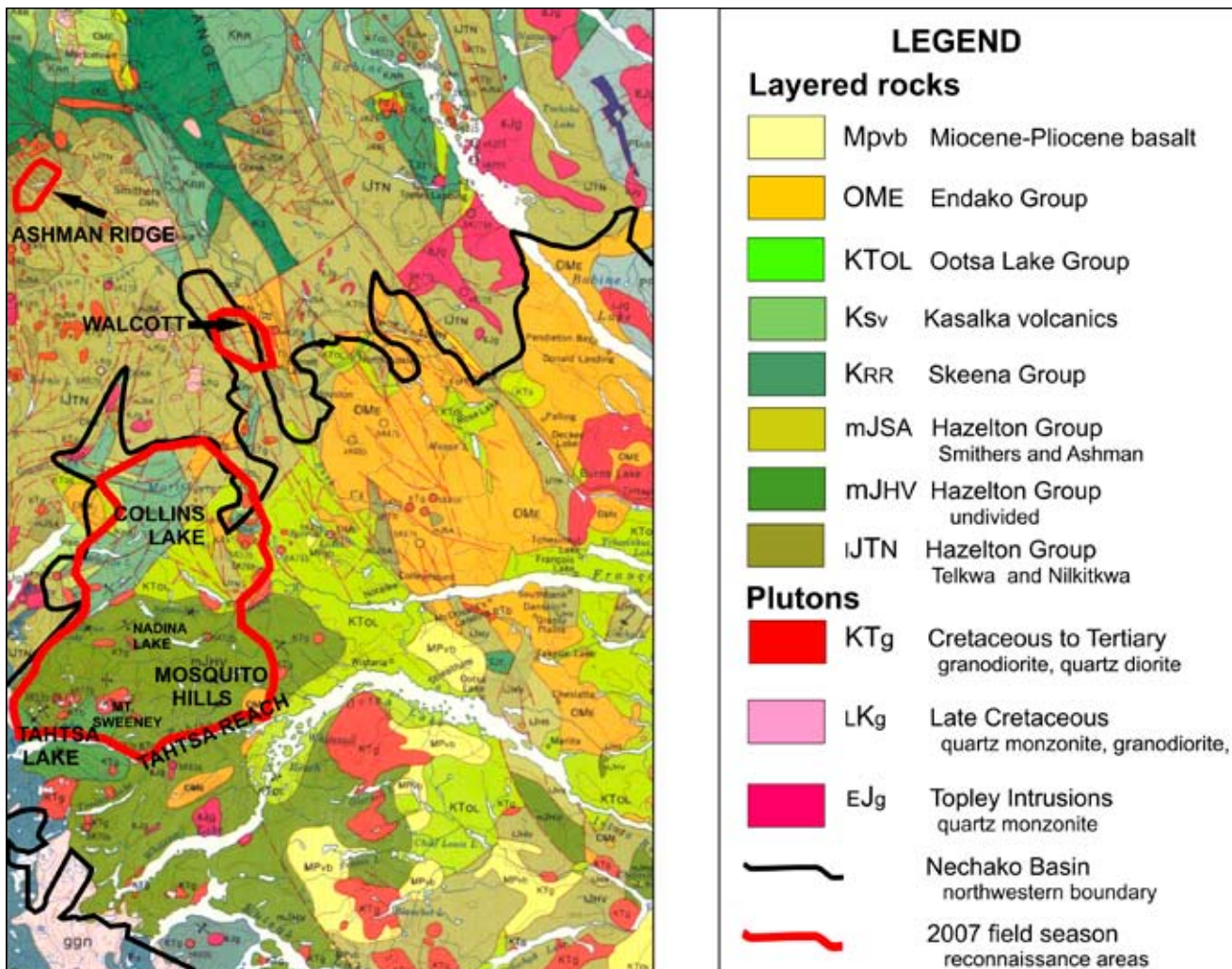


Figure 3: Reconnaissance was conducted in 2007 in the areas outlined in red. Geological map by Tipper et al. (1974); legend adapted from MacIntyre (1985).

it is rich in a distinctive Aalenian to Bajocian macrofossil assemblage that includes trigoniids, belemnites, bivalves, and ammonites. The pale colours indicate that the Smithers Formation likely has low potential as a source rock. A sample collected at Mount Sweeney contained very low levels of organic carbon (see Rock-Eval results below).

### ASHMAN FORMATION

The Ashman Formation of the Bowser Lake Group, as defined by Tipper and Richards (1976), comprises mainly dark grey to black shale with lesser coarse clastics of Middle to Late Jurassic (late Bajocian to early Oxfordian) ages. Ashman Formation siltstones and shales were sampled at Walcott in the Skeena Arch; exposures in the Tahtsa Lake region were deemed to be too strongly affected by abundant Cretaceous and Tertiary plutons to provide reliable thermal and Rock-Eval data.

We also collected samples of the Ashman Formation and the underlying so-called “pyjama beds” at the top of the Hazelton Group at Ashman Ridge on the southern fringe of the Bowser Basin as part of a larger study underway by Ferri (Filippo Ferri, personal communication 2008).

Recent work in the Bowser Basin by Evenchick and others (see Evenchick and Thorkelson 2005 and references therein) has refined and redefined Jurassic and Early Cretaceous stratigraphic nomenclature and has recommended that use of the term Ashman be discontinued. A detailed discussion of the redefinition of the units at Ashman Ridge is provided by Gagnon and Waldron (2008). However, south of the Bowser Basin, in the Skeena Arch (Smithers mapsheet NTS 093L) and in the northern Nechako basin region (Nechako River mapsheet NTS 093F and north half of the Whitesail Lake mapsheet 093E) the Ashman forms a distinctive late Middle Jurassic black clastic/chert conglomerate.

erate assemblage. In these areas, the Upper Jurassic/Lower Cretaceous facies of the Bowser Basin do not exist and use of the term Ashman Formation is well-entrenched and will likely persist (T.A. Richards, written communication 2008; D.G. MacIntyre, written communication 2008).

## SKEENA GROUP

The Skeena Group includes marine and nonmarine sedimentary rocks and volcanic strata (Tipper and Richards 1976) of Early Cretaceous to earliest Late Cretaceous (Albian to Cenomanian) ages. They are exposed in the southeastern part of the Bowser Basin and in the northwestern corner of the Nechako Basin. A discussion of the history of Skeena Group nomenclature is provided by Ferri et al. (2005). In the 2007 reconnaissance area, the Skeena Group is represented by the mainly basaltic Mount Ney volcanic sequence overlain by a sedimentary sequence dominated by blocky weathering sandstones with interbedded shales. The sedimentary sequences are best exposed in the areas around Collins Lake. The sandstones are fine-grained, greenish-grey and blocky weathering and generally massive or with barely discernible bedding. White muscovite flakes (1 to 2 mm-size) are almost ubiquitous in proportions ranging from 1 to 5 per cent. The most abundant clast type is green chert; also present are black chert, black lithic fragments, feldspar crystals, and rare pink chert. Plant material and carbonaceous wisps are abundant. The sandstones appear to have low potential as a reservoir unit due to their dense textures and the abundance of feldspar; however, 10 samples were collected for analysis, which has not yet been completed. The sandstones were also sampled for vitrinite reflectance and apatite fission track thermochronometry analyses.

The Skeena Group shales are exposed only in road cuts and roadside pits, where they have been quarried for local road fill. In the Collins Lake area, the shale is black, spheroidally weathered, and either brittly fractured into small pieces or soft and crumbly. Competent shale blocks with well-preserved ammonite fossils were encountered in road fill in the forestry clear cuts; however, we did not see these textures (or fossils) in place. The shales were sampled for Rock-Eval and vitrinite reflectance analyses.

## RESULTS

The northwestern part of the Nechako basin has received minimal investigation of its oil and gas potential (Hunt 1992; Hayes 2003) and has seen no oil and gas exploration industry activity. Rock-Eval and vitrinite data from the Ashman Formation and the Skeena Group shales collected by Hunt (1992) and this study indicate that units with reasonably good carbon content do occur in the north-west Nechako basin and Skeena Arch areas, and some have undergone thermal maturation within the oil to gas window.

However, potential source beds (the Ashman Formation, and Skeena Group shales) are thinner here than in the Bowser Basin, and the Rock-Eval data indicate that the quality of the organic material is poor. Furthermore, no promising reservoir unit has been identified by this project. Rock-Eval and vitrinite maturity data in the Tahtsa Lake/Tahtsa Reach areas are probably influenced by the abundant intrusions and volcanic rocks that post-date potential source rocks.

## ROCK-EVAL

Rock-Eval analysis provides information about the amount, quality, type, and maturity of organic carbon in the sample. Of the units sampled during the 2007 field season, those from the Skeena Group and Ashman Formations contain reasonably good amounts of organic carbon but are low in oil and gas generative quality.

The Rock-Eval analyses for 20 samples collected in 2007 are presented in Table 2 and graphed on Figure 4. Total organic carbon (TOC) values for the samples from shales of the Skeena Group yielded fair to good organic carbon amounts. Results from the Ashman Formation and from the “pyjama beds” at the top of the Hazelton Group at Ashman Ridge fall mainly into the “fair” range for hydrocarbon potential, with a few in the “good” range. However, low S1 and S2 values (Table 2) for all samples indicate that the quality of the organic material is poor. Plots of various Rock-Eval data ratios on the 2 diagrams in Figure 4 indicate that kerogen from all sampled units is Type 3 (gas-prone) (Langford and Blanc-Valleron 1990; Peters 1986).

## VITRINITE REFLECTANCE

Twenty-four new vitrinite samples (mainly sandstones with visible carbonaceous material) were collected; the resulting thermal maturation data are presented in Table 3 and Figure 5. Sample symbols are placed on the oil and gas window diagram of Dow (2000) based on their reflectance (%R<sub>o</sub>) values. Note that the sample symbols are placed toward the right-hand side of the diagram, reflecting the Rock-Eval data that suggests kerogen in the Nechako region tends to be Type 3. Skeena Group rocks collected in the Collins Lake show maturity in the oil window. The values near Nadina Lake in the Skeena Group and at Ashman Ridge in the upper Hazelton and Ashman Formations show higher maturity—in the dry gas window. The high (overmature) values for thermal maturity for the Tahtsa Lake/Mosquito Hills area should be regarded with caution due to their proximity to abundant younger igneous rocks.

These new data will be used to calibrate results from new apatite fission track samples collected concurrently.

**TABLE 2: ROCK-EVAL DATA FROM SURFACE SAMPLES COLLECTED IN THE NORTHWESTERN NECHAKO BASIN IN 2007. \***

Sample	Formation	Area	Easting	Northing	TOC	S1	S2	PI	S3	Tmax	Tpeak	S3CO	PC(%)	RC%	HI	OICO	OI	MINC%
JR07-1	Skeena	McKendrick Ck	643196	6079027	1.01	0.02	0.02	0.52	0.60	310	349	0.20	0.03	0.98	2	20	59	0.1
JR07-2A	Ashman	Walcott	639436	6044083	1.91	0.14	0.08	0.62	0.49	312	351	0.01	0.03	1.88	4	1	26	2.0
JR07-2B	Ashman	Walcott	639436	6044083	1.17	0.04	0.02	0.61	0.63	448	487	0.02	0.03	1.14	2	2	54	0.1
JR07-9	Smithers	Mt. Sweeney	615111	5954846	0.10	0.01	0.02	0.28	0.14	348	387	0.30	0.02	0.08	20	300	140	0.5
JR07-16	Skeena	Nadina Lake	634620	5974792	0.68	0.01	0.03	0.22	0.50	495	534	0.02	0.02	0.66	4	3	74	0.1
JR07-26	Skeena	Nadina Lake	634313	5974572	0.80	0.01	0.02	0.36	0.88	421	460	0.21	0.04	0.76	2	26	110	0.1
JR07-46	Skeena	McBride Lake	613484	5988284	0.64	0.05	0.32	0.13	0.12	452	491	0.01	0.04	0.60	50	2	19	0.0
JR07-48	Skeena	McBride Lake	615350	5991769	0.58	0.04	0.26	0.14	0.20	468	507	0.02	0.04	0.54	45	3	34	0.2
JR07-51	Skeena	Collins Lake	615958	5995296	1.26	0.02	0.33	0.06	0.47	508	547	0.02	0.05	1.21	26	2	37	0.1
JR07-52	Skeena	Collins Lake	616458	5995630	1.09	0.03	0.27	0.10	0.89	516	555	0.04	0.06	1.03	25	4	82	0.1
JR07-68	Hazelton PJ beds	Ashman Ridge	573273	6078679	1.06	0.04	0.07	0.39	0.23	561	600	0.15	0.03	1.03	7	14	22	0.1
JR07-70	Hazelton PJ beds	Ashman Ridge	573286	6078735	0.65	0.04	0.07	0.32	0.18	539	578	0.02	0.01	0.64	11	3	28	0.1
JR07-71	Hazelton PJ beds	Ashman Ridge	573302	6078812	0.47	0.02	0.07	0.25	0.58	557	596	0.34	0.04	0.43	15	72	123	0.4
JR07-72	Ashman	Ashman Ridge	573309	6078862	0.59	0.02	0.05	0.29	0.30	559	598	0.16	0.02	0.57	8	27	51	0.1
JR07-73	Ashman	Ashman Ridge	573284	6078860	0.42	0.03	0.06	0.34	0.19	531	570	0.02	0.01	0.41	14	5	45	0.2
JR07-74	Ashman	Ashman Ridge	573246	6078891	0.96	0.01	0.06	0.15	0.48	598	637	0.08	0.02	0.94	6	8	50	0.1
JR07-76	Ashman	Ashman Ridge	573267	6079278	0.71	0.03	0.08	0.28	0.15	546	585	0.03	0.02	0.69	11	4	21	0.1
JR07-77	Ashman	Ashman Ridge	573278	6079476	1.06	0.02	0.12	0.13	0.98	542	581	0.51	0.06	1.00	11	48	92	0.1
JR07-78	Ashman	Ashman Ridge	573291	6079564	1.79	0.01	0.07	0.10	1.63	529	568	0.04	0.06	1.73	4	2	91	0.2
JR07-79	Skeena	Collins Lk quarry	615586	5997350	1.06	0.07	0.69	0.09	0.17	457	496	0.19	0.08	0.98	65	18	16	0.1

Standard criteria for rating potential source rocks (Peters 1986)			
Rating	Total organic carbon (TOC) wt. %	S1 mg HC/g rock	S2 mg HC/g rock
Poor	0 - .5	0 - .5	0 - 2.5
Fair	.5 - 1	.5 - 1	2.5 - 5
Good	1 - 2	1 - 2	5 - 10
Very good	2+	2+	10+

\*During Rock-Eval analysis, a detector senses any organic compounds generated during pyrolysis. The results provide information about the amount, quality, type, and maturity of organic carbon in the sample. Definitions are from Peters 1986. TOC: Total Organic Carbon (weight per cent), a measure of the amount of organic carbon. S1: the amount of hydrocarbons that can be distilled from one gram of rock (mg/g rock). S2: the amount of hydrocarbons generated by pyrolytic degradation of the kerogen in one gram of rock (mg/g rock). S3: milligrams of carbon dioxide generated from a gram of rock during temperature programming up to 390 oC. S1, S2, and S3 are measures of the quality of the generative potential of the source rock. Tmax: is the temperature at which the maximum amount of S2 hydrocarbons is generated, an indication of thermal maturity. HI and OI are calculated from S2, S3, and TOC analytical data and are plotted to provide an indication of kerogen type (see Figure 4).

## MAGNETIC SUSCEPTIBILITY

The field crew collected 42 magnetic susceptibility readings from all formations that we encountered during the field season (Table 4). These measurements form a contribution to a new database of physical and paleomagnetic properties that is being compiled for south-central British Columbia by the Geological Survey of Canada. See Enkin et al. (2008) for a discussion of the development of this new database, which will be used to calibrate geophysical models and facilitate accurate interpretations of old and new geophysical data.

## ONGOING STUDIES

### *New U-Pb Dates*

The project continues to acquire new geochronological data in the Nechako region. Four new U-Pb zircon ages were determined from samples of previously undated volcanic sequences that we collected during fieldwork in 2005 and 2006. The supporting data will be presented in detail in an upcoming publication, along with that of new dates described in Riddell et al. (2007). All new ages cited below are from Paul O’Sullivan (written communication 2007; see “Acknowledgements”).

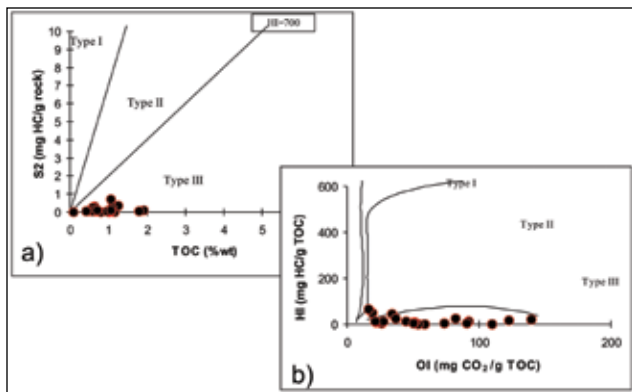


Figure 4: Graphs of Rock-Eval data for kerogen from surface samples collected in 2007 from the northwestern Nechako basin. Data points are presented in Table 2. These graphs give an indication of the kerogen type; Type I is very oil-prone, Type II is oil-prone, Type III is gas-prone. These samples fall in the Type III (gas prone) fields. a) S2 versus TOC (total organic carbon); (Langford and Blanc-Valleron 1990); b) HI (hydrogen index) versus OI (oxygen index); (Peters 1986) See Table 2 for definitions of S2, S3 and TOC. HI and OI are calculated from S2, S3, and TOC values.  $HI = (S2/TOC) \times 100$  (mg HC/g Corg);  $OI = (S3/TOC) \times 100$  (mg HC/g Corg);

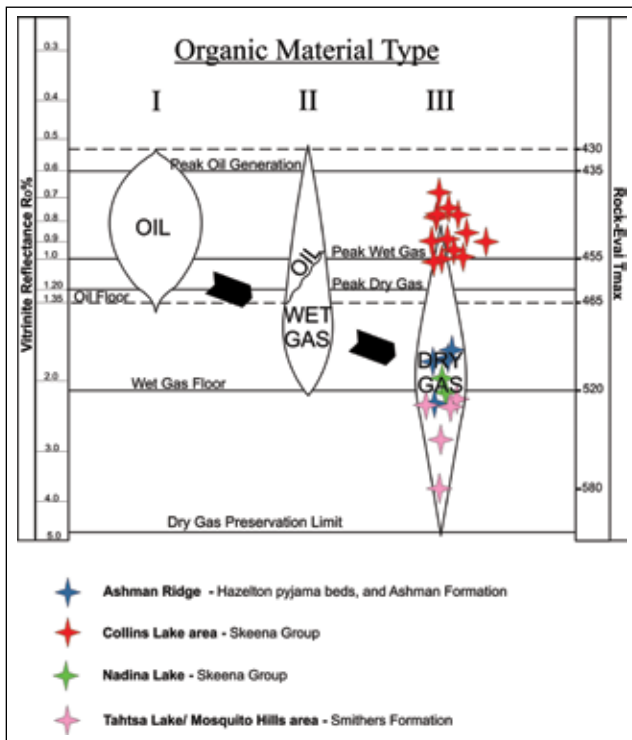


Figure 5: Thermal maturation ( $R_o$ ) values from 2007 vitrinite reflectance data for areas of the northwestern Nechako basin and the Skeena Arch, plotted on a graph of the oil and gas generative window. Diagram adapted from Dow (2000). Refer to Figure 3 for sample location areas.

TABLE 3: VITRINITE REFLECTANCE DATA; SURFACE SAMPLES COLLECTED IN THE NORTHWESTERN NECHAKO BASIN IN 2007.\*

Station ID	VR Ro %	Formation	Location name	Easting	Northing	Rock type
JR07-5	2.38	Smithers	Mt. Sweeney	614885	5955034	sandstone
JR07-9	2.49	Smithers	Mt. Sweeney	615087	5954494	siltstone
JR07-16	2.13	Skeena	Nadina Lake	634620	5974792	siltstone
JR07-18	2.21	Smithers	Tahtsa Reach	639801	5955840	sandstone
JR07-20	2.86	Smithers	Tahtsa Reach	637153	5955739	siltstone
JR07-24	3.81	Smithers	Mosquito Hills	644564	5963819	sandstone
JR07-26	1.98	Skeena	Nadina Lake	634313	5974572	siltstone/shale
JR07-42	0.68	Skeena	McBride Lake	614015	5986720	sandstone
JR07-43	0.74	Skeena	McBride Lake	613886	5986794	sandstone
JR07-44	0.77	Skeena	McBride Lake	613738	5986834	sandstone
JR07-46	0.79	Skeena	McBride Lake	613484	5988284	shale
JR07-47	0.86	Skeena	McBride Lake	614667	5990358	sandstone
JR07-50	0.89	Skeena	McBride Lake	614576	5993426	sandstone
JR07-51	1.00	Skeena	Collins Lake	615958	5995296	siltstone
JR07-53	0.79	Skeena	Lamprey Creek	621450	5998507	sandstone
JR07-54	0.95	Skeena	Collins Lake	612559	5993131	sandstone
JR07-55	0.99	Skeena	Collins Lake	612914	5993405	sandstone
JR07-62	1.03	Skeena	Lamprey Creek	619260	5998870	sandstone
JR07-63	0.89	Skeena	Lamprey Creek	621427	5998511	sandstone
JR07-66	1.88	Smithers	Ashman Ridge	573598	6078381	siltstone
JR07-70	1.72	Hazellon PJ beds	Ashman Ridge	573286	6078735	siltstone
JR07-72	1.85	Ashman	Ashman Ridge	573309	6078862	brown shale
JR07-75	2.28	Ashman	Ashman Ridge	573202	6078989	sandstone
JR07-79	0.90	Skeena	Collins Lake	615585	5997350	shale

\* $R_o$  is a measure of fraction of the incident beam that is reflected coherently from the vitrinite and is an indication of thermal maturity.

Two of the new samples were collected from the Batnuni Cone area; they each provided confirmation of expected ages. A rhyolite mapped as Ootsa Lake Group by Tipper (1962) produced a weighted mean age of approximately  $49 \pm 1$  Ma, which falls within the time constraints for Ootsa Lake events (approximately 53 to 47 Ma) provided by Grainger et al. (2001). A tuff collected at Taiuk Creek just west of Klunchatistli Lake yielded a late Middle Jurassic age of approximately  $162 \pm 2$  Ma, consistent with the Middle Jurassic fossil age determination of Tipper (1962) from a nearby outcrop.

Two new dates have been obtained from andesite flows exposed on the southwestern fringe of the Nechako region. Both samples are from outcrops that were interpreted as lower Middle Jurassic Hazelton Group volcanics by Tipper (1959 and 1969), Roddick and Tipper (1985), and on subsequent compilations (Massey et al. 2005 and Riddell 2006). These units are labeled ImJHz and coloured orange on Figure 6; however, the 2 new dates, marked by purple stars at Choelquoit Lake and Puntzi Lake, indicate that at least some of these rocks are too young to correlate with the Hazelton Group. The sample from the north shore of Puntzi Lake contained 2 populations of zircons; the older has a weighted mean age of approximately  $152 \pm 4$  Ma, and the younger population is approximately  $101 \pm 2$  Ma, suggesting that latest Early Cretaceous andesitic melts assimilated zircons from Hazelton volcanic rocks while moving up through the crust. The sample from Choelquoit Lake produced poor quality grains; however, a weighted

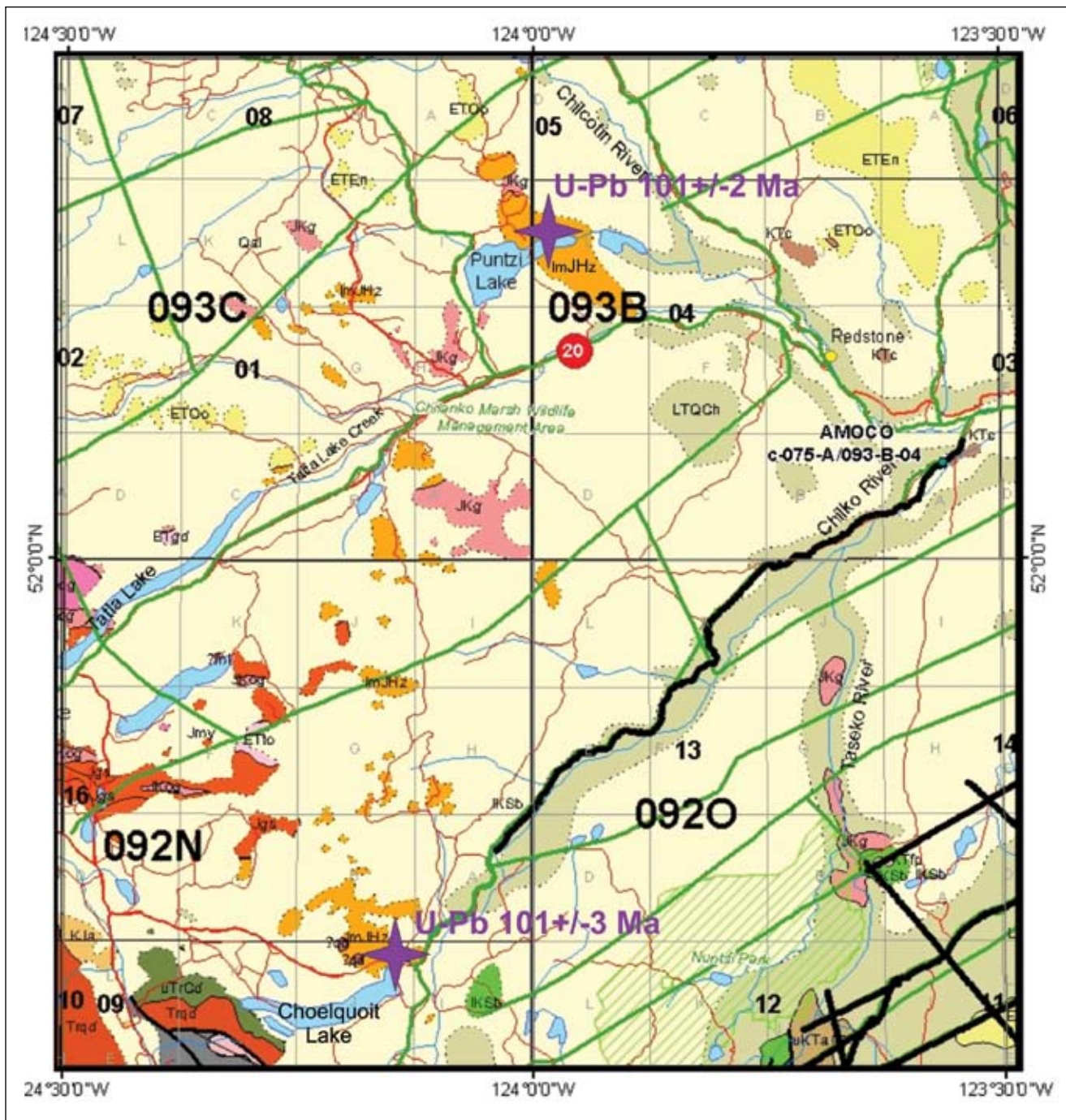


Figure 6: Locations for which 2 new U-Pb dates have been established. Base geology from Riddell (2006). The new dates indicate that at least some dark orange-coloured outcrops labeled ImJHz are latest Early Cretaceous in age—too young to correlate with the Hazelton Group. They are more likely to be correlative with the Spences Bridge volcanics or possibly the Powell Creek volcanics.

**TABLE 4: MAGNETIC SUSCEPTIBILITY DATA COLLECTED IN THE NORTHWESTERN NECHAKO BASIN IN 2007. \***

Station_ID	Formation	Rock type	EASTING	NORTHING	MS (X10 <sup>-3</sup> SI)
JR07-2	Hazelton-Smithers	black limy shale	639436	6044083	0.70
JR07-3	Hazelton-Smithers	fsp sandstone	615061	5955165	0.27
JR07-4	Hazelton-Telkwa	basalt flow & bx	615277	5955359	2.10
JR07-5	Hazelton-Smithers	sandstone	614885	5955034	0.35
JR07-6	Hazelton-Smithers	conglomerate	615096	5954909	0.47
JR07-8	Hazelton-Smithers	sandstone	615127	5954784	0.21
JR07-9	Hazelton-Smithers	siltstone	615087	5954494	0.29
JR07-10	Hazelton-Telkwa	andesite porphyry	615178	5954207	13.60
JR07-11	Hazelton-Telkwa	andesite	615237	5954077	0.25
JR07-12	Endako?or Skeena volc	pyroxene basalt	632600	5966359	6.53
JR07-13	Endako?or Skeena volc	pyroxene basalt	636433	5966881	12.40
JR07-14	Endako	basalt	638375	5974277	27.10
JR07-15	Mount Ney volcs (Skeena)	basalt breccia	640587	5981921	9.50
JR07-16	Skeena	siltstone/shale	634620	5974792	0.28
JR07-17	Goosly Intrusive	quartz monzonite	642922	5956244	4.76
JR07-18	Hazelton-Smithers	fsp sandstone	639801	5955840	0.44
JR07-19	Hazelton-Smithers	fsp tuff	640039	5955754	0.16
JR07-21	Hazelton??	serpentinite	636777	5962980	6.58
JR07-22a	Hazelton??	calcareous siltstone	636903	5962897	0.27
JR07-22b	Hazelton??	pillow basalt	636903	5962897	0.42
JR07-24	Hazelton-Smithers	fsp sandstone	644564	5963819	14.30
JR07-25	Mount Ney volcs (Skeena)	pyroxene crystal tuff	634719	5974948	0.28
JR07-40	Bridge River Group	greenstone- ropy lava	515967	5656400	0.34
JR07-42	Skeena	sandstone	614015	5986720	0.27
JR07-43	Skeena	sandstone	613886	5986794	0.46
JR07-44	Skeena	sandstone	613738	5986834	0.55
JR07-45	Skeena	siltstone	612896	5987195	0.23
JR07-46	Skeena	shale/slst/sst	613484	5988284	0.23
JR07-47	Skeena	sandstone	614667	5990358	2.39
JR07-48	Skeena	siltstone/shale	615350	5991769	0.21
JR07-49	Skeena	sandstone	614099	5991516	0.26
JR07-50	Skeena	sandstone	614576	5993426	0.59
JR07-52	Skeena	shale	616458	5995630	0.26
JR07-53	Skeena	sandstone	621450	5998507	0.17
JR07-54	Skeena	sandstone	612559	5993131	0.45
JR07-55	Skeena	sandstone	612914	5993405	5.36
JR07-56	Skeena	sandstone	612977	5993456	1.19
JR07-57	Skeena	sandstone	612990	5993783	0.30
JR07-58	Skeena	sandstone	613013	5993990	0.41
JR07-59	Skeena	sandstone	613092	5994242	0.45
JR07-60	Skeena	sandstone	613118	5994303	0.33
JR07-61	Skeena	sandstone	612759	5993389	0.20

*\*These data form a contribution to a new database of physical and paleomagnetic properties that is being compiled for south-central British Columbia by the Geological Survey of Canada. See Enkin et al. (2008) for discussion of the development of this new database.*

mean age of approximately  $101 \pm 3$  Ma was determined. These latest Early Cretaceous rocks may correlate with the Spences Bridge Group (bright green unit on Figure 6) or the Powell Creek volcanics.

### ***Thermal History***

Nine new apatite fission track (AFT) samples were collected in 2007 between Tahsta Reach and Collins Lake. Results will contribute to a larger AFT thermal history study of the Nechako region that will include 50 samples collected in 2005 from the Nazko River and Redstone areas (Riddell et al. 2007) and 9 samples collected in 2006 from the Fawnie and Nechako ranges and Batnuni Lake.

### ***Reservoir Study***

In contrast to many proven clastic reservoir units in the Western Canada Sedimentary Basin, the clastic units in the Nechako region tend to be mineralogically and texturally immature. Volcanic lithic fragments and detrital feldspars are locally abundant, and sorting is highly variable. Primary porosity is almost absent in surface and core samples. However, multiple factors (including early compaction that inhibited the precipitation of diagenetic products, the development of secondary porosity, and mineral leaching) conspire to create local zones of good porosity. Lithologically similar units do form productive oil and gas reservoirs in other basins; one example is the Rewan Group in the Bowen Basin of Queensland Australia (Bashari 1998).

A detailed petrographic study of samples of potential reservoir units collected during the 2005 and 2006 field seasons and from archived exploration drill cores is available as a separate report (Brown et al. in press).

### **CONCLUSIONS**

- Rock-Eval analyses of shaly horizons indicate that the Skeena Group and Ashman Formation contain fair to good amounts of organic carbon.
- Thermal maturation data indicate that Skeena shales in the Collins Lake are within the oil window while rocks of the Smithers and Ashman formations bracket the peak to upper dry gas zone.
- New U/Pb dates of andesites near Puntzi and Choelquoit Lakes in the southern Nechako region indicate that these volcanics are late Early Cretaceous, too young to belong to the Lower Jurassic Hazelton Group. They may be correlative to either the Spences Bridge Group or the Powell Creek volcanics.

- Petrographic analysis of coarser clastics within the Nechako Basin show them to be mineralogically and texturally immature with little primary porosity. Much of the observed porosity in surface and core samples is the result of secondary porosity.

### **ACKNOWLEDGEMENTS**

Matt Sawatzky provided excellent field support and assistance during the challenging blackfly season of 2007. We are most grateful to Don MacIntyre for answering endless questions about the geology of the Smithers, Houston, and Tahtsa Lake areas and to both Don and Jackie MacIntyre for their kind hospitality. We thank the Thompson family for logistical help and hospitality during our stay at Nadina Lake Lodge. Pat and Tania Rooney of Highland Helicopters provided safe helicopter transportation and reliable service. Jenny Wong of GSC Calgary provided prompt lab analyses of Rock-Eval and vitrinite reflectance samples. Margaret and Raymond Donelick and Paul O'Sullivan of Apatite to Zircon Labs continue to provide timely fission track and U/Pb geochronology analyses.

### **REFERENCES**

- Bashari, A. (1998): Diagenesis and reservoir development of sandstones in the Triassic Rewan Group, Bowen Basin, Australia, *Journal of Petroleum Geology*, Volume 21 (4), pages 445–465.
- Brown, D., Simpson, J., Daniels, H., and Riddell, J. (in press): Two reports on petrographic analyses of clastic rocks from the Nechako region of British Columbia; *British Columbia Ministry of Energy, Mines and Petroleum Resources*; Open File.
- Desjardins, P.J., Arksey, R.L., and MacIntyre, D.G., (1991): Geology of the Lamprey Creek map sheet (93L/3); in Geological Fieldwork 1990, *British Columbia Ministry of Energy, Mines and Petroleum Resources*, Paper 1991-1, pages 111–119.
- Diakow, L.J. compiler (2006): Geology of the Tahtsa Ranges between Eutsuk Lake and Morice Lake, Whitesail Lake map Area, west-central British Columbia (Parts of NTS 093E/5, 6, 7, 9, 10, 11, 13, 14 and 15), *British Columbia Ministry of Energy, Mines and Petroleum Resources*, Geoscience Map 2006-5, 1:150 000 scale.
- Dow, W.G. (2000): Geochemical analysis of outcrop samples from Tingmerkpuk 1998 project; *State of Alaska Department of Natural Resources*, Division of Geological and Geophysical Surveys, Raw Data File 200-3, 64 pages.
- Enkin, R.J., Vidal, B.S., Baker, J., and Struyk, N.M. (2008): Physical properties and paleomagnetic database for south-central British Columbia; in Geological Fieldwork 2007, *British Columbia Ministry of Energy, Mines and Petroleum Resources*, Paper 2008-1, pages 5–7.

- Evenchick, C.A. and Thorkelson, D.J. (2005): Geology of the Spatsizi River map area, north-central British Columbia; *Geological Survey of Canada Bulletin* 577, 276 pages.
- Ferri, F., Mustard, P.S., McMechan, M., Ritcey, D., Smith, G.T., Boddy, M. and Evenchick C. (2005): Skeena and Bowser Lake Groups, west half Hazelton map area (NTS 093M): in Summary of Activities 2005, *BC Ministry of Energy, Mines and Petroleum Resources*, pages 113-131.
- Ferri, F. and Riddell, J. (2006): The Nechako Basin project; new insights from the southern Nechako basin; in Resource Development and Geoscience Branch, Summary of Activities, *British Columbia Ministry of Energy, Mines and Petroleum Resources*, pages 89–124.
- Gagnon, J-F. and Waldron, J.W.F. (2008): Ashman Ridge section revisited: new insights for the evolution of the Bowser Basin, northwestern British Columbia (93L/13); Geoscience BC Summary of Activities 2007, *Geoscience BC Report* 2008-1, pages 121–128.
- Grainger, N.C., Villeneuve, M.E., Heaman, L.M., and Anderson, R.G. (2001): New U-Pb and Ar/Ar isotopic age constraints on the timing of Eocene magmatism, Fort Fraser and Nechako River map areas, central British Columbia; *Canadian Journal of Earth Sciences*, Volume 38, Number 4, pages 679–696.
- Hayes, Brad (2002): Petroleum exploration potential of the Nechako Basin, British Columbia, *British Columbia Ministry of Energy, Mines and Petroleum Resources*, Petroleum Geology Special Paper 2002-3, 52 pages.
- Hunt, J.A. (1992): Stratigraphy, maturation and source rock potential of Cretaceous strata in the Chilcotin-Nechako region of British Columbia; *University of British Columbia*, unpublished Master's thesis, 448 pages.
- Langford, F.F. and Blanc-Valleron, M.M. (1990): Interpreting Rock-Eval pyrolysis data using graphs of pyrolyzable hydrocarbons vs. total organic carbon; *American Association of Petroleum Geologists Bulletin* Volume 74, pages 799–804.
- MacIntyre, D.G. (1985a): Geology and mineral deposits of the Tahtsa Lake district, west central British Columbia; *British Columbia Ministry of Energy, Mines and Petroleum Resources*, Bulletin 75, 82 pages.
- MacIntyre, Don G. (1985b): Geology of the Tahtsa Lake District; Figure 2 in Bulletin 75, *British Columbia Ministry of Energy, Mines and Petroleum Resources*, 1:50 000 scale.
- Massey, N.W.D, MacIntyre, D.G., Desjardins, P.J., and Cooney, R.T. (2005): Geology of British Columbia; *British Columbia Ministry of Energy, Mines and Petroleum Resources*, Geoscience Map 2005-3, 1:1 000 000 scale.
- Osadetz, K.G., Snowdon, L.R. and Mark Obermajer (2003): Rock-Eval/TOC data for eleven northern British Columbia boreholes; *Geological Survey of Canada*, Open File 1550.
- Peters, K.E. (1986): Guidelines for evaluating petroleum source rock using programmed pyrolysis; *American Association of Petroleum Geologists*, Bulletin Volume 70, pages 318–329.
- Riddell, J.M., compiler (2006): Geology of the southern Nechako Basin, NTS 92N, 92O, 93B, 93C, 93F, 93G; *British Columbia Ministry of Energy, Mines and Petroleum Resources*, Petroleum Geology Map 2006-1, 1:400 000 scale.
- Riddell, J., Ferri, F., Sweet, A. and O'Sullivan, P. (2007): New geoscience data from the Nechako basin project; in The Nechako Initiative – Geoscience Update 2007; *British Columbia Ministry of Energy, Mines and Petroleum Resources*, Petroleum Geology Open File 2007-1, pages 59–98.
- Roddick, J.A. and Tipper, H.W. (1985): Geology, Mount Waddington 92N; *Geological Survey of Canada*, Open File 1163 map, 1:250 000 scale.
- Tipper, H.W. (1959): Geology, Quesnel map area; *Geological Survey of Canada*, Map 12-1959, 1:253 440 (1 inch to four miles).
- Tipper, H.W. (1962): Geology, Nechako River; *Geological Survey of Canada*, Map 1131A, 1:253 440 scale (1 inch to four miles).
- Tipper, H.W. (1969): Geology, Anahim Lake, British Columbia; *Geological Survey of Canada*, Map 1202A, 1:253 440 scale (1 inch to four miles).
- Tipper, H.W., Campbell, R.B., Taylor, G.C. and D.F. Stott (1974): Geology, Parsnip River, British Columbia; *Geological Survey of Canada Map* 1424A, 1:1 000 000 scale.
- Tipper, H.W. and Richards, T.A. (1976): Jurassic stratigraphy and history of north-central British Columbia; *Geological Survey of Canada Bulletin* 270, 73 pages.



# DIFFUSIVITY AND DIFFUSION COEFFICIENTS OF ANTHRACITE

Barry Ryan<sup>1</sup> and Karin Mannhardt<sup>2</sup>

## ABSTRACT

Permeability is one of the most important properties influencing the produceability of a coal seam. Generally diffusivity is given less consideration; however, if diffusivity is low then it may be as important as permeability. Anthracites like the maceral vitrinite are often considered to have low diffusivity, which may affect produceability. There is little data on the direct measurement of methane diffusivity in coal and even less on the direct measurement of methane diffusivity in anthracites. This paper uses transient adsorption and transient desorption data obtained during isotherm experiments to investigate methane diffusivity in an anthracite sample.

Ryan, B. and Mannhardt, K., (2008): Diffusivity and Diffusion Coefficients of Anthracite; Geoscience Reports 2008, B.C. Ministry of Energy, Mines and Petroleum Resources, pages 79-98.

<sup>1</sup> British Columbia Ministry of Energy, Mines and Petroleum Resources, Victoria, BC, 250-952-0377; barry.d.ryan@gov.bc.ca.

<sup>2</sup> Tomographic Imaging and Porous Media Laboratory, TIPM, University of Calgary, Alberta.

**Key Words:** Anthracite, diffusivity, diffusion coefficients, isotherms, unipore equation, Airey equation, diffusion grain size, initial concentration gradient.

## INTRODUCTION

Permeability is often considered the most important parameter controlling the produceability of coalbed gas (CBG), also known as coalbed methane (CBM). Certainly without permeability there is zero chance of success, but even with good permeability, other factors can spell disaster. Another important factor, generally less well understood than permeability, is diffusion, which describes the movement of gas molecules through coal to cleat or microfracture surfaces. It may not be possible to produce CBM from seams with extremely low diffusivity even if they have adequate permeability. Initial production may result in rapid removal of free gas and a decrease in hydrostatic pressure, which will be accompanied by an increase in effective stress. Coal will respond by deforming, generally in such a way as to decrease permeability. Without matrix shrinkage (triggered by desorption and diffusion of gas to cleat or microfracture surfaces) to counter the decrease in permeability, it may not be possible to produce CBM from the seam.

Sawyer et al. (1987) demonstrated the sensitivity of production to changes in diffusivity, which is often calculated from Tau, sorption time (the time to 63.2% desorption of all gas). The simulator they used indicated that higher values of Tau, equivalent to lower diffusivity, decreased early production rates but did not affect long-term production rates by much (Figure 1). The increase in Tau by an order of magnitude decreases diffusivity by the same factor. The simulator modelled the relationship between permeability, porosity, seam compressibility, and hydrostatic pres-

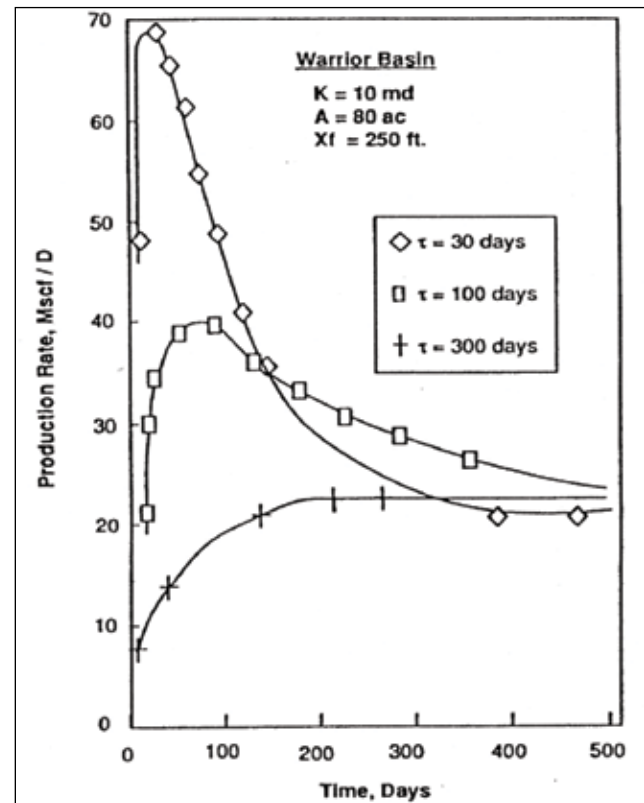


Figure 1: Effect of varying diffusivity on gas production; Figure from Sawyer et al. (1987).

sure but did not consider the effects of matrix shrinkage. Matrix shrinkage, which is related to gas desorption, would amplify the effects of diffusion on production profiles by increasing permeability and probably decreasing diffusivity. The delayed gas production extends the time over which the coal is experiencing increased effective stress without compensating matrix shrinkage to help maintain permeability. The model predicted that long-term production rates are not sensitive to diffusivity but that diffusivity affected short-term production rates; this means that diffusivity influences cumulative production and does influence economics, which are sensitive to initial production.

There is limited data on diffusivity in anthracites; however, there is a general perception in literature that anthracites have lower diffusion coefficients compared to other ranks of coal (Ettinger et al. 1966; Laximinarayana and Crosdale 1999). Nandi and Walker (1974) compared diffusivity of coals of different rank, and for some conditions anthracite had the lowest diffusivity. Laximinarayana and Crosdale (1999) used a gravimetric method to do isotherms on dry 0.212 mm samples and calculated diffusivity using a unipore spherical model. They documented decreases in diffusivity for bright and dull coal as rank increased.

It is often not possible to compare diffusivity values from different papers because of differences in laboratory approaches; consequently, there is little comparative data. Low diffusivities of anthracite may counter the advantage of the high adsorption capacities of anthracites that make them attractive targets for exploration compared to lower-rank coals; it is therefore important to prove or disprove this perception.

Ettinger et al. (1966) suggest that diffusivity may be related to the volume of macropores present in coal, whereas adsorption capacity may be related to the volume or surface area of the micropores. At a constant porosity volume, the surface area increases as the pore size decreases. It is therefore important to appreciate as coal rank increases the significance of changes in:

- a) total volume porosity,
- b) distribution of this volume by pore size, and
- c) the total surface area resulting from the combination of total porosity and size distribution of pores.

A number of authors have documented total volume porosity distributions in coal (Rodrigues and Lemos de Sousa 2002); overall porosity volume is high for low-rank coals, minimum for mid-rank coals, and moderately high for high-rank coals. The total internal surface area of coals tends to follow a similar relationship, decreasing from a maximum at low rank to a minimum at intermediate rank before increasing again at high rank (Thomas and Damberger 1976; Moffat and Weale 1955). Maximum surface area is attained for low-rank coals because of their high porosity. Total surface area is very dependent on the volume

percent of micropores, which tends to increase with rank at the expense of macropore volume (Gan et al. 1972).

As a useful generalization, micropore surface area is a good measure of adsorption capacity and diffusivity probably correlates in part with the amount of macropore porosity. This means that in many cases there may be an inverse relationship between adsorption capacity and diffusivity. These possible relationships may be confused by the variable preferential adsorption of water as rank increases (Ryan 2006)

Diffusion is described by Fick's Law, which describes the movement of molecules through a solid and along a constant concentration gradient. The unipore diffusion equation derived from Fick's Law does not model variation in pore size and does not take into account variation in temperature or changing concentration gradients over time, which define unsteady state conditions. Diffusion is variously described using either:

- a) the diffusion coefficient ( $D$ ), which has units of  $L^2/T$ , or
- b) diffusivity ( $De$ ), also sometimes called effective diffusivity, which has units of  $1/T$  and is related to  $D$  as  $De = D \times s$ , where  $s$  is the shape factor, which is related to the particle geometry. As an example, for a spherical particle  $s = 15/r^2$ , where  $r$  is the radius of the particle through which diffusion is occurring. Other denominator values for the shape factor are 8 for cylinders and 3 for slabs. Spherical diffusion is the simplest model used to describe diffusion in coal and works moderately well for crushed coal samples. In a cleated coal seam, the matchstick or cylinder model may be better for describing diffusion, and in this case the shape factor is  $s = 8/r^2$ .

Spherical diffusion is often combined with the unipore diffusion model derived from Fick's Law (Smith and Williams 1984):

$$V_t/V_\infty = 1 - (6/\pi^2) \sum_{n=1}^{\infty} [(1/n^2) \exp(-De \times n^2 \times \pi^2 \times t)]$$

Smith and Williams stated that the unipore equation described the early stages of desorption well and could be fitted to desorption data to provide a solution for diffusivity ( $De$ ). They found that for  $V_t/V_\infty$  values less than 0.5, the unipore equation fitted desorption data well, but for values above 0.5, it predicted values of  $V_t/V_\infty$  that diverge from the actual desorption data. The diffusion coefficient ( $D$ ) can be calculated if the grain size controlling diffusion (the diffusion grain size) is known. It is relatively easy to collect data from desorption or adsorption experiments and curve-fit to the data using the unipore equation to provide a best fit solution for  $De$ , which is the combined effect of diffusion and diffusion grain size. If the diffusion grain size is also

the size of the grains in the experiment, then the diffusion coefficient is also easy to calculate.

There are 2 ways commonly used to calculate diffusivity ( $De$ ) from desorption curves. It can be calculated from the slope of the lost-gas plot (gas cumulative fraction versus  $(t)^{1/2}$ , where  $t$  is the time in seconds) (Smith and Williams 1984). The slope of the line on a plot of  $V_t/V_\infty$  versus  $(t)^{1/2}$  is

$$6 \times (D/r^2)^{1/2}/(\pi)^{1/2}$$

or

$$D/r^2 = \text{slope}^2 \times \pi/36.$$

In this instance  $D/r^2 = De$ , and there is no shape factor involved because spherical diffusion is assumed in the equation. Diffusivity is also calculated from the sorption time,  $\tau$  (which is  $1/s \times D$ ), where  $\tau$  is the time taken for 63.2% of the total gas to desorb from a sample. For spherical diffusion  $s = 15/r^2$  and  $De = (1/\tau)/15$  (Graham 1998).

Airey (1968) developed an empirical equation that has 2 constants. The first constant,  $T_0$ , is equivalent to  $\tau$  and is dependent on grain size, concentration gradient, adsorption properties, and temperature. The second constant, a power term,  $n$ , is dependent in part on the size distribution of the diffusion grain sizes that combine to make up the coal fragments. The Airey equation was developed using Darcy's Law to describe gas movement through a permeable solid. As discussed later, the equation provides a better fit to desorption and adsorption data than does the unipore model. The equation has the form:

$$V_t/V_\infty = 1 - \exp[-(t/T_0)^n]$$

The constant  $T_0$  in the Airey Equation provides another way to derive a value for diffusivity of samples. It is possible to curve-fit the Airey equation to desorption or adsorption data in such a way as to solve for the constants  $n$  and  $T_0$ .

Since the discussion by Sawyer et al. (1987), many authors have discussed the significance of diffusion of gas molecules through coal. Clarkson (1998) confirmed the results of Smith and Williams (1984), indicating that the unipore model does not adequately explain diffusion in coals with multimodal pore distribution. In fact, Smith and Williams (1984) using the bi-disperse pore model developed by Ruckenstein et al. (1971) found that it produced a much better fit of calculated  $V_t/V_\infty$  values to measured  $V_t/V_\infty$  values. The model assumes that coal fragments contain pores of 2 sizes, each with a different diffusivity. A good fit to desorption data was achieved, based on using the 2 diffusivities and a gas distribution factor.

Clarkson (1998) and Clarkson and Bustin (1999) compared the bi-disperse model to the unipore model and also found that the bi-disperse model provided a better fit to the data. They comment that the unipore model may be appropriate for samples containing a high proportion of vitrinite. Lennan (2004) states that the model may provide useful approximate results.

As noted later, the anthracite used in this study is composed mainly of vitrinite and mineral matter. Also, both the range of pore sizes and the pore sizes themselves probably decrease for higher-rank coals (Bustin and Clarkson 1999). The bi-disperse equation is not easy to solve and requires knowledge of coal constants, such as surface area and pore-size distribution. These equations incorporate diffusivity for micro- and macropores and a constant describing the distribution of the 2 pore sizes. Bell (2003) uses a more general form of the unipore spherical diffusion model to provide a curve-fit to desorption data.

Busch et al. (2004) found that using 2 first-order rate functions provided a better fit to  $CH_4$  and  $CO_2$  desorption data than did the bi-disperse model.

In this paper, 3 equations are fitted to the transient adsorption and transient desorption data acquired during isotherm experiments—these are the unipore equation, the Airey equation and an equation similar to that used by Busch (2004). In the Busch equation, the 2-component unipore equation assumes that data can be described using 2 unipore equations with different diffusivities added together based on a distribution factor. In real terms, the equation assumes that a sample is composed of fragments of either vitrinite with slow diffusivity or inertinite with faster diffusivity. The equation is then simply the sum of 2 unipore equations with a distribution factor ( $d$ ) defining proportions of the 2 components as  $(d)$  and  $(1-d)$ . Most coals are mixtures of vitrinite and inertinite macerals, though as the coal fragment size increases, the fragments are less likely to be composed of 100% vitrinite or 100% inertinite.

Any attempt to fit a theoretical curve to desorption or transient adsorption data assumes that a single gas is involved. This is true in experimental transient adsorption data but may not be the case for exploration desorption data. Some coals from southeastern British Columbia contain a significant amount of  $CO_2$ , and for these samples, desorption curves must reflect the presence of 2 gases with distinctly different diffusivities. A simple test for the presence of more than 1 gas may be the difference in  $De$  calculated from the initial slope of the desorption curve compared to the value calculated from  $\tau$ . Large differences probably confirm the presence of 2 gases with different diffusivities desorbing simultaneously. If the desorbing gas is mainly methane, then large differences in  $De$  calculated from the slope of the lost gas line and from  $\tau$  may flag problems with the lost gas calculation.

## SAMPLE PREPARATION AND ANALYSIS

A single sample of anthracite core was provided for the project (Photo 1). Prior to laboratory work, the sample was coarsely crushed and high-ash fragments hand-picked and discarded. Some coal fragments up to 1 cm<sup>3</sup> in size were mounted in plastic and polished to provide samples for reflecting microscope and scanning electron microscope studies of cleats and larger-scale textures. The rest of the sample was then crushed and screened to provide 6 sized samples (less than 0.25 mm, 0.25 to 1mm, 1 to 2 mm, 2 to 3.35 mm, 3.35 to 4 mm, and 4 to 6 mm). Splits from each size were mounted and polished in preparation for reflectance and petrographic studies. Most isotherm canisters hold about 100g of coal; for a 100g sample, this means a grain count of about 500 to 10 million grains in each sized sample, depending on the size range (Table 1).

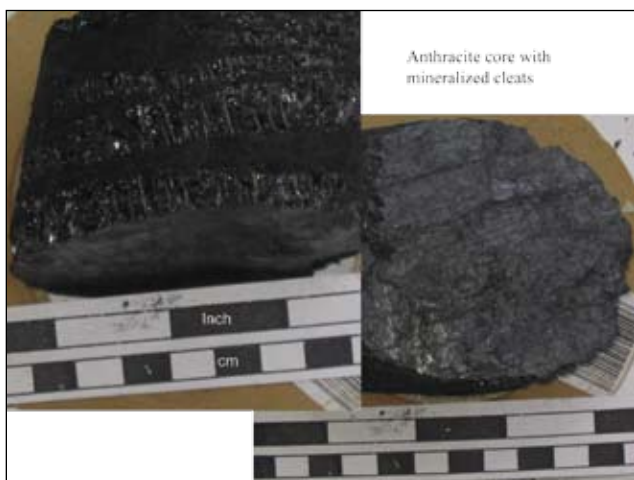


**Photo 1: Anthracite sample prior to crushing, showing cemented face cleats and butt cleats.**

Polished sections of the sized samples indicate that the size distribution matches that indicated by the mesh sizes; however, the mean size is probably less than the average radius used for plotting the data  $\{(top\ screen\ size + bottom\ screen\ size)/4\}$  in preceding sections. Even at the small size, many grains are obviously partially fractured into smaller subgrains.

The 6 samples were sent to the Tomographic Imaging and Porous Media (TIPM) Laboratory, University of Calgary, for analysis. Five adsorption isotherms were run on samples at 25 °C and one sample at 40 °C. Transient pressure data were collected, for a number of pressure steps on each sample, to provide data for  $V_t/V_\infty$  versus time plots. In addition, some samples were allowed to desorb at atmospheric pressure to simulate a desorption experiment. The resulting data suite provides a number of ways to calculate diffusivity ( $D_e$ ) and diffusion coefficients ( $D$ ); these include the slope of the early adsorb or desorb curves; curve-fitting

**TABLE 1: MESH SIZE, SAMPLE SIZE, AND EXAMPLE OF GRAIN COUNTS FOR THE PREPARED SAMPLES.**

sample number	mesh	mesh	from mm	to mm	radius cm
		>5	10	6	
1	5	6	6	4	0.25
2	6	7	4	3.35	0.18375
3	7	10	3.35	2	0.13375
4	10	18	2	1	0.075
5	18	60	1	0.25	0.03125
6		<60	0.25	0	0.00625

Estimated grain count based on sample mass of 50 g and specific gravity of 1.4				
mesh	diameter cm	radius cm	grain count	mass gm
3	0.673	0.3365	2.24E+02	2.23E-01
3.5	0.57	0.285	3.68E+02	1.36E-01
5	0.4	0.2	1.07E+03	4.69E-02
7	0.283	0.1415	3.01E+03	1.66E-02
10	0.2	0.1	8.53E+03	5.86E-03
18	0.1	0.05	6.82E+04	7.33E-04
20	0.085	0.0425	1.11E+05	4.50E-04
60	0.025	0.0125	4.37E+06	1.15E-05
100	0.015	0.0075	2.02E+07	2.47E-06
200	0.0075	0.00375	1.62E+08	3.09E-07

using the unipore equation, the Airey equation, or the 2-component unipore equation; and Tau values.

## SAMPLE PETROGRAPHY

The estimated mean maximum vitrinite reflectance of the anthracite sample is 4.0%. The standards used in the laboratory do not bracket a reflectance this high, and consequently the value is only an estimate of mean maximum reflectance.

The sample is composed of collotelinite, which is generally structureless with occasional pseudo-vitrinite slits, dispersed mineral matter, and very little inertinite. Mineral matter occurs as filling in fractures, as finely dispersed grains in layers, as zoned inclusions, and as fine spherulitic pyrite or forms a granular matrix enclosing fragments of collotelinite (Photo 2). The mineral composition is discussed in the *SEM Results* section (following), as it is easier to identify the composition using a scanning electron microscope than an optical reflecting microscope.

The form of mineral matter probably influences the size of the grains that gas must diffuse out of (diffusion grain size). In samples examined here, there are often microfractures radiating out from dispersed mineral fragments. These fractures may form by differential compaction or differential contraction during cooling and uplift (Photo 3). Either way, their presence and the degree of dispersion of the mineral matter grains probably help define the diffusion grain size. This means that the more dispersed the mineral matter, the smaller the diffusion grain size and the larger the value of  $D_e$ . The differential compaction also provides

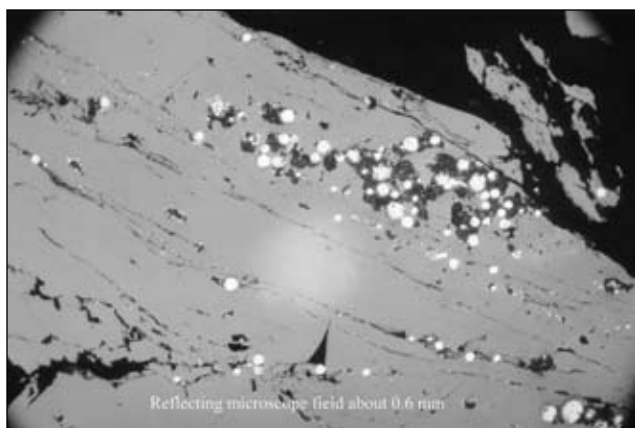


**Photo 2: Reflecting microscope field of view 0.6 mm. Collotelinite with early-formed spherulitic pyrite.**

a relative time sequence between growth of the autogenic minerals and deformation. Other factors that influence  $D_e$  by providing interconnecting microfractures include the thickness of microlithotype banding; the spacing of microfractures in these bands is proportional to the thickness of the bands, and fractures are often restricted to the collotelinite bands (Photo 4). The presence of pseudo-vitrinite slits in core samples indicates that they did not form near surface and are available to help limit the diffusion grain size.

Diffusivity is dependent on diffusion grain size, and this is in part dependent on the microtexture of the coal, which is readily studied under the microscope. In this context it is probably more important to study 0.5 to 1 cm sized fragments of coal to develop an appreciation of the microtexture of the coal than to do traditional maceral determinations on 20-mesh coal fragments.

It is also interesting to consider the effects on the size of diffusion grains of de-stressing, cooling, and contraction of substances with different coefficients of thermal expansion and Poisson's ratios. During uplift, a coal may adsorb or desorb gas based on the changing relationship between depth and saturated gas content, and this may be accompanied by matrix shrinkage or expansion. At intermediate and shallow depths, adsorption ability decreases during uplift, and the coal (if saturated) expels gas and undergoes matrix shrinkage. Anthracites will undergo more matrix shrinkage at shallower depths than lower rank coals because of the shape of the isotherm (low Langmuir pressure and high Langmuir volume). There is some evidence, discussed later, that indicates that diffusivity is less during desorption and matrix shrinkage than it is during adsorption and matrix expansion.

Optical microscope studies will not provide direct information on pore sizes that influence adsorption; the field of view for the optical microscope is about 0.4 mm ( $10\times 50$  magnification), which means that the resolution is about 0.4 mm/100 ( $4\ \mu\text{m}$ ) compared to the maximum mesopores size of  $0.04\ \mu\text{m}$ . Alternatively, a 0.1 mm sized grain has a diameter equivalent to over 10 000 pores.

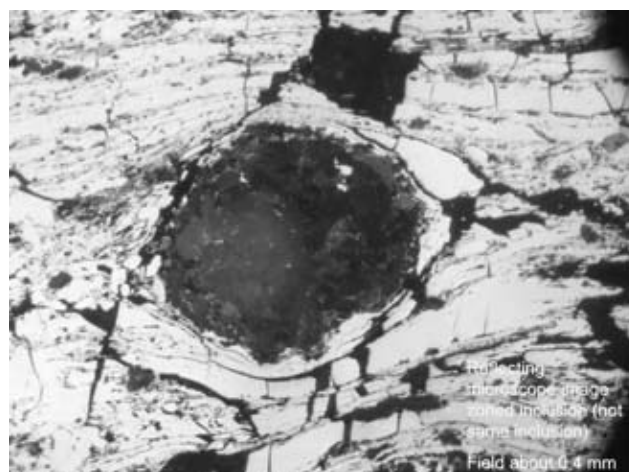


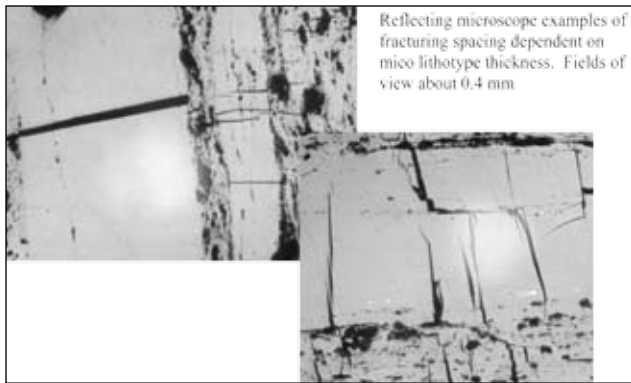
**Photo 3: Reflecting microscope field of view 0.6 mm. Zoned spherulite with differential compaction and associated microfractures.**

## SCANNING ELECTRON MICROSCOPE (SEM) RESULTS

Fragments of coal approximately 1 cm<sup>3</sup> in size were mounted in a plastic binder and polished until large flat areas of coal fragments were exposed. Three samples were taken to the University of British Columbia, Earth and Ocean Sciences department, for electron SEM analysis. The SEM provides a powerful semi-quantitative way of identifying non-coal minerals in samples and is useful for identifying the mineralogy and form of inclusions, cell fillings, and cleat-cementing minerals. Minerals are identified by partial XRF spectra, which provide very rough estimates of the proportions of elements present, based on peak heights. A number of video photos and XRF spot scans were taken for elemental analysis of samples.

In some situations, non-coal minerals occur as filling in fractures, which may or may not be cleats. It is important to identify planar sides and degree and type of branching because these features help differentiate early replacement origin from late brittle origin. Inward zonation provides a time sequence for mineralization of the coal. Similar time sequences are revealed by zonation of inclusions. Late mineralization is identified when it fills fine fractures that clearly have an extensional origin. Authigenic mineral matter is finely dispersed in coal and defines bedding.

Dispersed mineral matter that appears to be authigenic is a mixture of 70% carbonate (approximate elemental weight ratios  $\text{Ca} = 1$ ,  $\text{Mg} = 0.3$ ,  $\text{Fe} = 0.2$ ) and 30% quartz. Finely dispersed mineral matter is usually a clay mineral with elemental ratios of about  $\text{Al} = 1$ ,  $\text{Si} = 1$ ,  $\text{Fe} = 0.5$ , and  $\text{Mg} = 0.3$ . The absence of K and presence of Fe and Mg indicate a chlorite-type clay. Finely dispersed and isolated grains of mineral matter include carbonates—sometimes siderite surrounded by calcite ( $\text{Mg} = 1$ ,  $\text{Ca} = 1$ ,  $\text{Fe} = 1$ ) and dolomite ( $\text{Mg} = 1$ ,  $\text{Ca} = 0.8$ ,  $\text{Fe} = 0.7$ ) and occasional grains



Reflecting microscope examples of fracturing spacing dependent on micro lithotype thickness. Fields of view about 0.4 mm

**Photo 4: Reflecting microscope field of view 0.6 mm. Bands of collotelinite with micro fractures that are generally restricted to bands.**

of aluminophosphate and apatite (Ca = 1, P = 0.8; no Al or Sr). Occasional grains of pyrite are present—some angular and some spherulitic. Large 2-component spherulites were observed with dull cores of quartz (dull in back-scattered image) and outer rims of clay (brighter in back-scattered image) (Photo 5).

Fracture-filling minerals include quartz, carbonate, clay, kaolinite/illite, and apatite. An approximate sequence of mineralization is established based on relationships of minerals in a number of fractures (Table 2). A major fracture, about 0.5 mm thick with planar sides, contains walls of quartz (dull grey) with infillings of carbonate (Ca with minor Fe and Mg; bright), clay (Si = 1, Al = 0.9, Fe = 0.5, Mg = 0.3; less grey) and apatite (brightest; Ca = 1, P = 0.8) in that order of emplacement (Photo 6). Fine fractures are often filled with quartz and kaolinite, and if a sequence is apparent, then quartz is earlier. Other associations include carbonate and kaolinite, with the carbonate earlier (Photo 7). Other fillings include carbonates, with pure calcite being earlier. Carbonate filling predates kaolinite or clay filling.

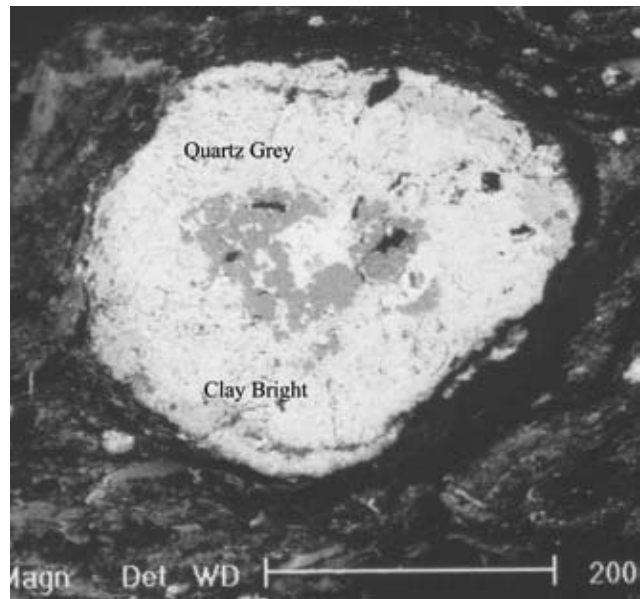


**Photo 5: Large 2-component spherulites with dull cores of quartz (dull in back scattered image) and outer rims of clay (brighter in back scattered image).**

It appears that there was an early flooding of silica that cemented cleats and formed inclusions in the coal. The silica may have originated during deep burial from the breakdown of smectite clays in coal or non-coal lithologies. Silica cementation was followed by introduction or remobilization of carbonate—mainly calcite, but also carbonates containing Mg and Fe and, in some cases, siderite. Siderite is the earliest carbonate and in places is rimmed by calcite. Early quartz inclusions have reacted to form rims of clay. Kaolinite appears to have been introduced later. It fills fine fractures, some looking like pseudo-vitrinite slits, which may form in a partially desiccated environment at depth (Ryan 2003).

**TABLE 2: VARIOUS MINERAL SEQUENCES SEEN IN FRACTURES AND AUTHIGENIC INCLUSIONS.**

diagenesis	→				uplift				→
Time	→								
	1	2	3	4	5	6	7	8	9
pyrite			Quartz			clay			pyrite
			Quartz		calcite	clay		apatite	
					calcite		kaolinite		
			Quartz	carbonate					
siderite					calcite				
			Quartz			clay		kaolinite	

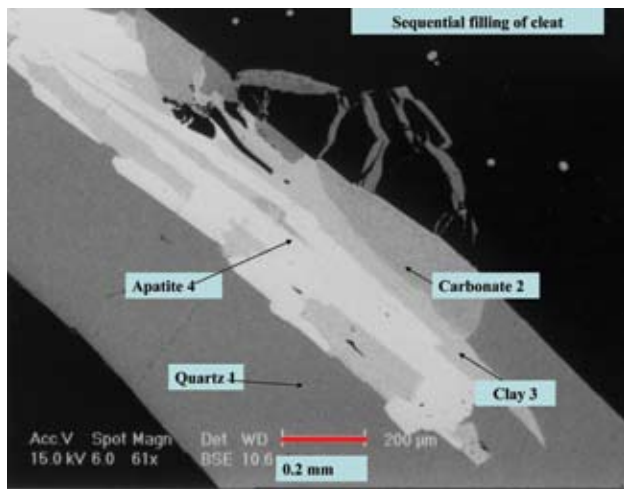


**Photo 6:** Major fracture, about 0.5 mm thick, with planar sides contains walls of quartz (dull grey) with infillings of carbonate (Ca, minor Fe, and Mg; bright), clay (Si = 1, Al = 0.9, Fe = 0.5, Mg = 0.3; less grey), and apatite (brightest; Ca = 1, P = 0.8), in that order of emplacement.

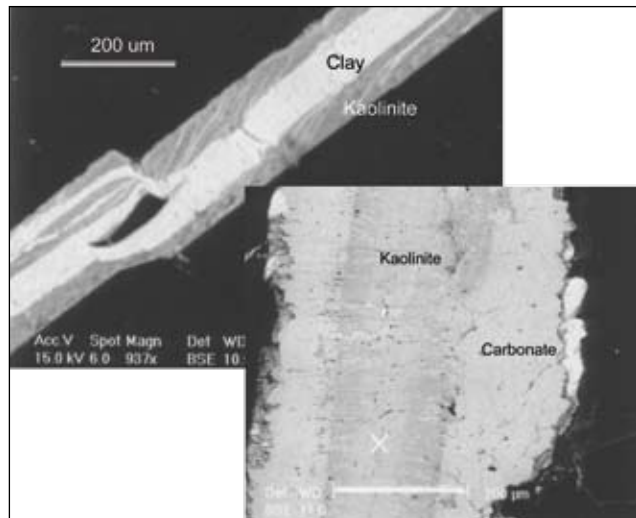


**Photo 7:** Fine fractures filled with carbonate and kaolinite. If a sequence is apparent, then carbonate is earlier.

Some branching fractures with rough sides have the appearance of early replacement features. They have inner zones that are a mixture of carbonate and clay and outer zones that are more carbonate rich (Photo 8). The composition of the inner zone varies from mainly carbonate to a mixture of kaolinite and illite. Planar-sided late fractures are filled with kaolinite or an inner zone of clay with an outer zone of kaolinite.

## ISOTHERM DATA

Five isotherms were run on sized coal samples at 25 °C and one isotherm was run at 40 °C on the 3.35 to 4 mm sized sample (Table 3). Anthracite adsorbs more gas than

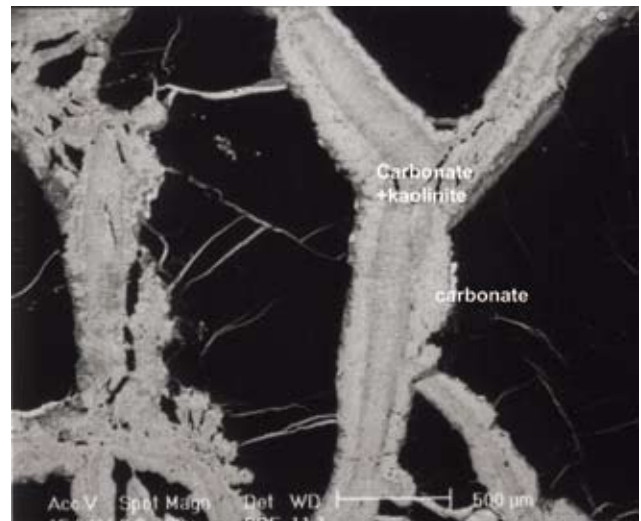


**Photo 8:** Early replacement branching fractures with rough sides. Inner zones are a mixture of carbonate and clay; outer zones are more carbonate rich.

do lower-rank coals and generally has lower Langmuir pressure (PI) values. In theory, increase in temperature should not affect Langmuir volume (VI) but should increase PI. In practice, data sets generally indicate some decrease in VI with increasing temperature but a marked increase in PI.

Isotherm data may be based on calculations that either:

- assume that adsorbed gas has the density of liquid CH<sub>4</sub> at the boiling point (0.421 g/cm<sup>3</sup>) or
- are made using a calculation of the surface excess gas (Mannhardt 2005).

The latter method does not require any assumptions about the density of the adsorbed phase. The method illustrates that as the density of the gas phase approaches that of the adsorbed phase, the concept of adsorption is no longer valid. Below the critical point, calculations of surface excess probably underestimate the amount of adsorbed gas. On the other hand, calculation of adsorbed gas using a liquid density may overestimate the amount of adsorbed gas (Figure 2); it is apparent that the value of Langmuir pressure (PI) predicted using the liquid density is much larger than that calculated using the excess surface model. This has major implications when considering the relationship between de-pressuring and gas production. The excess surface method may be more applicable for multi-layer adsorption where it is probably not realistic to assume that all the adsorbed gas has a density of 0.421 g/cm<sup>3</sup>.

It is also important to attempt to correct data to a mineral-matter-free (mmf) basis when the ash contents of samples are high, as is the case in this study. The spread in ash concentrations for the sized samples is not large, but based on a plot of the inverse of specific gravity versus ash (Figure 3), which incorporates related data from exploration drill-

**TABLE 3: ISOTHERM DATA ON SIZED SAMPLES.**

size mm	temp °C	weight g	Ash% EQ basis	moisture% EQ	V <sub>t</sub> daf cm <sup>3</sup> /gm	PI MPa	V <sub>t</sub> ar cc/gm
250-0.25	25	150.5	40.7	3.8	28.72	1.76	15.94
0.25-1.0	25	148.7	31.4	4.2	35.12	2.13	22.61
1.0-2.0	25	150.6	31.0	5.1	35.34	1.65	22.57
2-3.35	not run						
3.35-4	25	112.74	32.6	3.9	37.76	2.52	23.99
3.35-4	40	108.08	32.6	3.93	30.03	1.81	19.06
4-6	25	107.52	30.6	4.66	28.6533	1.16	18.55

daf = dry ash free; ar = as received

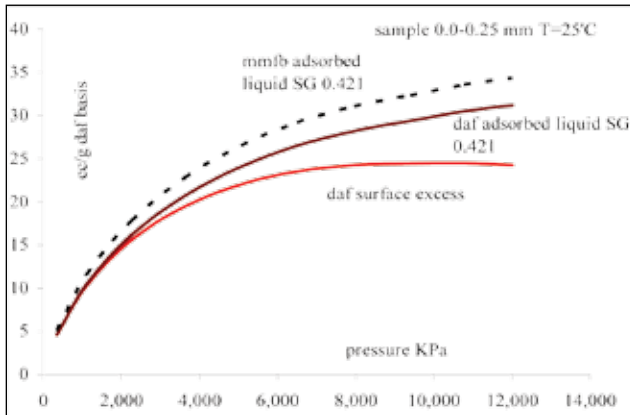


**Figure 2: Isotherms for 0.25 mm sample, using excess surface adsorbed model and liquid density adsorbed model calculated to daf (dry ash-free) and mmf (mineral-matter-free) basis.**

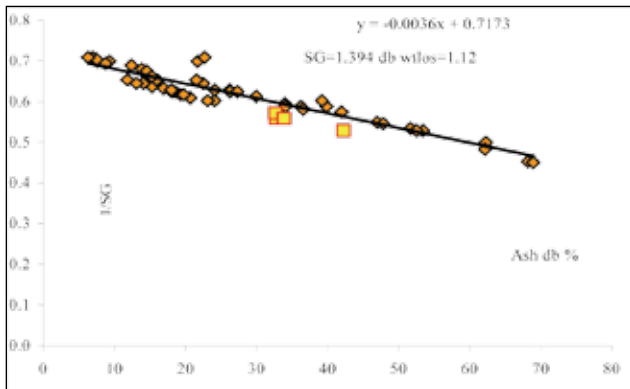


**Figure 3: Ash versus 1/SG plot for samples in this study and related exploration samples, indicating a zero ash SG of about 1.457 and a wtos value (mineral matter/ash ratio) of 1.2 at a mineral matter SG of 2.66.**

ing, the zero-ash specific gravity is about 1.39 g/cm<sup>3</sup> and the wtos ratio (weight mineral matter/weight ash) required to correct data to a mineral-matter-free basis is about 1.10.

## COMMENTS ON CURVE-FITTING AND CALCULATING DIFFUSIVITY

Mavor et al. (1990) analysed isotherm data, and they discuss how the diffusion coefficient ( $D$ ) may be derived by measuring the pressure change over time as samples equilibrate to new pressure steps during isotherm analysis. They

discuss derivation of  $D$  using the unipore model, but in fact they are assuming that grain radius is the same as the radius of the sphere controlling spherical diffusion (diffusion grain size). They illustrate 2 solutions; one uses the initial slope of the  $V_t/V_\infty$  versus time plot, and the other is referred to as the sorption diagnostic graph and plots fractional volume change (or the derivative of same) against time on log-log paper. This second plot has the advantage that the trajectory for ideal spherical diffusion can be plotted, and this allows comparison of real data to an ideal diffusion model. Both these methods have the advantage over a single desorption plot of calculating diffusion coefficients for a number of initial pressures. They can also provide estimates of diffusion coefficients over pressure ranges and concentration gradients that better model production.

In this study, curves were fitted to the experimental data with minimal cumulative error calculated as the sum of  $[(V_t/V_\infty \text{ measured} - V_t/V_\infty \text{ predicted})^2]^{1/2}$ . The individual errors were weighted based on the percentage of total time that each individual data point represented. This corrected for the fact that there are a lot of data points defining the initial part of the adsorption curve and fewer points defining later parts of the curve. Without the weighting, curves fitted to the real data would be biased towards matching low values of  $V_t/V_\infty$  and not larger values. Obviously different ways of calculating minimum error will predict slightly different values of  $D$ . Cumulative error values give a relative idea of the goodness of fit of the various equations to the experimental data (Table 4). Errors increase at higher pressure steps, in part because of noise in the experimental data; a curve-smoothing routine was used to try to remove some of the spikes in the data.

The unipore equation requires an iterative solution that usually converges after a few iterations to provide a value of diffusivity or diffusion coefficient if the diffusion grain size is known. The equation does not fit the experimental data very well. The equation is fitted to all the data and to the first part of the data, where spherical diffusion predicts that a  $V_t/V_\infty$  versus  $T^{1/2}$  plot is linear. The 2-component unipore model also requires an iterative approach and involves inputting 2 diffusion coefficients and a distribution factor. By a process of trial and error, good fits of the calculated curve to the data were obtained. The Airey equation has 2 constants ( $T_0$  and  $n$ ) that can be solved for by trial and error curve-fitting or directly using a derivative plot (Figure 4) where  $\ln(\text{time})$  is plotted against  $\ln[(dv/dt)1/(V_{\text{total}} - V_t)]$  or alternatively  $\ln(t)$  versus  $\ln(\ln[V_t/(V_t - v_t)])$ . Both provide direct solutions for  $n$  and  $T_0$ ; the second method is discussed in Harris et al. (1996).

**TABLE 4: RELATIVE ERRORS FOR CURVE FITTING DIFFERENT EQUATIONS TO PRESSURE STEP DATA.**

Relative error for curve fitting to data											
size	radius	temp	Equation	steps							
mm	cm	°C		1	2	3	4	5	6	7	
4-6	0.25	25	Airey		18	9	7				
			2C Unipore		11	6	16				
			Unipore		57	86	94				
3.35-4	0.18375	25	Airey		13	16	34				
			2C Unipore		9	8	15				
			Unipore		74	56	78				
3.35-4	0.18375	40	Airey		17	22	10	12			
			2C Unipore		13	15	7	11			
			Unipore		56	35	44	20			
1-2	0.075	25	Airey		4	12	5	6			
			2C Unipore		15	8	12	12			
			Unipore		74	45	127	73			
0.25-1	0.03125	25	Airey		6	9	8	7			
			2C Unipore		6	9	11	9			
			Unipore		24	23	22	24			
0-0.25	0.00625	25	Airey		5	7	4	7	18	31	36
			2C Unipore		7	5	6	8	16	31	35
			Unipore		37	15	10	16	22	32	40

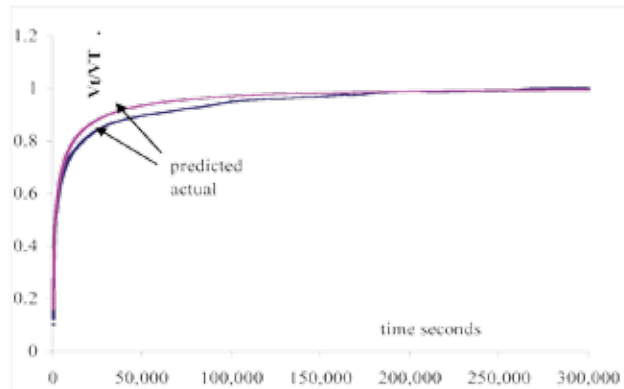
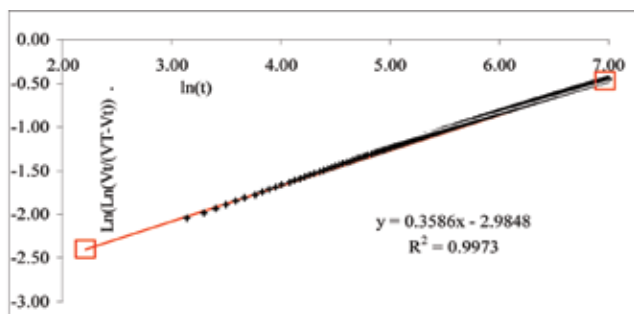


**Figure 4: Method of solving for  $T_0$  and  $n$  in the Airey equation. X axis is  $\ln(t)$  and Y axis is  $\ln[(dv/dt)1/Vr]$ . Slope of best-fit line is  $1+n$  and  $T_0 = [(1 + \text{slope})/2.718^{(1/n)}]^{\ln(1/n)}$ . An alternative solution from Harris et al. (1996) is derived from a plot of  $\ln(t)$  versus  $\ln(\ln(Vt/(VT-V)))$ ;  $n = \text{slope}$  and  $T_0 = \exp(\text{intercept}/\text{slope})$ .**

## TRANSIENT ADSORPTION RESULTS

Analysis of transient adsorption data requires collecting pressure data over the time interval that is required for the sample to equilibrate at each pressure step during isotherm analysis. As gas is introduced into the sample cell, the initial high rate of adsorption causes a brief rise in temperature that invalidates the first few measurements. The isosteric heat of adsorption of methane is 3 to 6 Kcal/mole. The time taken to equilibrate at each pressure step varies, in large

part based on the fragment size, and for the largest size (4 to 6 mm diameter), times range up to 5 days. Most adsorption analyses were conducted at 25 °C and a few at 40 °C.

Transient adsorption data were obtained for a total of 27 runs, representing a number of pressure steps for 5 sized samples (Table 4). Curves were fitted to the data using a number of macro programs in Excel.

Values of  $D$  and  $D_e$  were calculated:

- Using the unipore equation from the complete adsorption curve and from the initial part of the curve using the  $V_t/V_\infty$  versus  $T^{1/2}$  plot;
- Using the Airey equation and the value  $T_0$ , which is an averaged value for  $\tau$ ;
- Using the 2-component unipore model, which provides two values of  $D$  and  $D_e$  as well as a distribution factor  $R$ ;

The unipore equation provides 2 estimates of diffusivity. One is derived by curve-fitting to the first part of the  $V_t/V_\infty$  versus  $T^{1/2}$  plot and the second curve-fitting to the full curve. Values calculated from the full curve are lower than values calculated using the first part of the curve, and the difference decreases as diffusivity increases. The difference, as discussed later, is evidence that diffusivity and diffusion coefficients vary with initial concentration gradient, which varies with adsorption or desorption time and initial versus final pressures. The unipore equation generally does not fit the data well based on a comparison of curve-fitting errors (Table 4). This is despite the facts that the sample is composed almost entirely of collotelinite and mineral matter and that Clarkson and Bustin (1999) suggest that the unipore equation has the best chance of modelling diffusion from vitrinite-rich samples.

The Airey equation provides good fits to data for all pressure steps, as does the 2-component unipore model; the unipore model provides the worst fit to the data (Table 4; Figure 5). The flexibility of the Airey equation using only 2 constants ( $T_0$  and  $n$ ) to provide excellent fits to measured adsorption or desorption data is remarkable. The Airey equation models data well because, if the form of the equation is compared to the unipore equation, then the power term  $n$  is equivalent in the unipore model to allowing  $D_e$  to vary with time. In fact, values of  $D_e$  would be higher at the start and lower towards the end of adsorption or desorption. Airey (1968) indicated that the value  $n$  did not vary much and may be related to the size distribution of grains in a sample, with larger values indicating a wider size distribution. In this study  $n$  acts to vary  $D_e$  over time, based on effects of initial concentration gradient.

In the following discussion, most of the diffusivity values discussed were calculated using  $T_0$  from the Airey equation and using a spherical shape factor of 15, which provides better agreement than slab or cylinder shape fac-

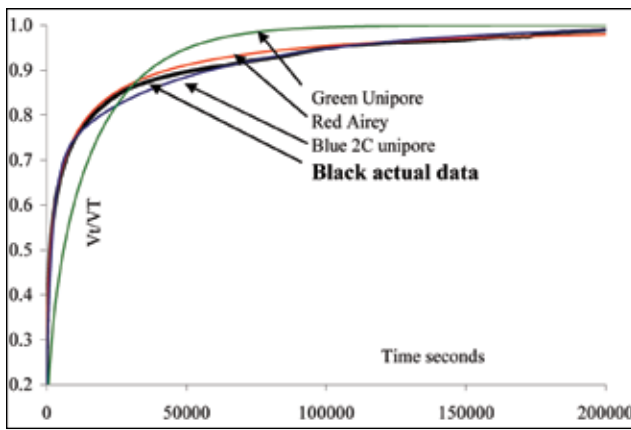


**Figure 5: Comparison of curve-fitting unipore, 2-component unipore, and Airey equations to data.**

tors. Diffusivity values calculated from the Airey equation are consistently higher than those calculated using the unipore equation but are similar to values calculated using the unipore equation and the initial part of the adsorption curve (Figure 6).

A number of papers (Ettinger et al. 1966; Gamson et al. 1996; Laximinarayana and Crosdale 1999) suggest that the

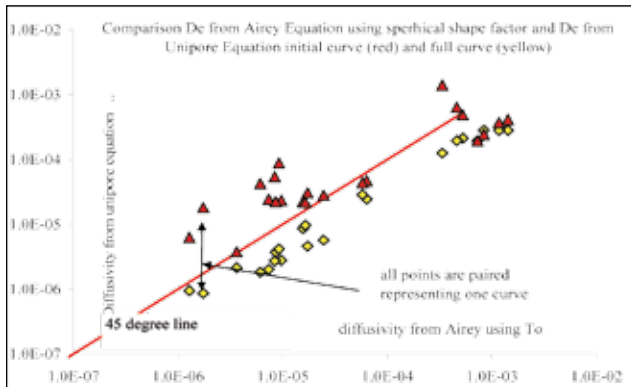


**Figure 6: Comparison of  $D_e$  calculated using the 2-component unipore equation and the Airey equation for different pressure steps; sample 0 to 0.25 mm.**

diffusivity of inertinite is greater than that of vitrinite, probably because, at least at lower ranks, inertinite has more macroporosity than vitrinite. It is therefore reasonable to assume that there are 2 components mixed together in a sample and that gas is diffusing out of both components independently. One component is slow-diffusing (vitrinite?) with micropores and the other is fast-diffusing (inertinite?) with meso- or macropores. Each component accesses microfractures within the composite sample independently of the other. In this case, the unipore model is used with 2 diffusivities and a fractional proportion for each component. When this is done, it is possible to obtain a reasonable fit of the 2-component unipore model to adsorption data. Obviously this implies that diffusivity is independent of initial concentration gradient.

Fitting the 2-component unipore equation to the experimental data requires finding the best combination of 2 diffusion coefficients and the distribution factor ( $R$ ) to minimise the sum of the errors. The process is trial and error, and it is not clear that there is a single solution; however, in cases where there appears to be a wide difference in the 2 diffusivities, there appears to be a single “vitrinite” fraction that permits a good fit to the data. The fractional proportion of vitrinite required to produce a fit is much lower than that measured by petrography, which indicates a mineral-matter-free vitrinite content of close to 100%. If the model is identifying something real in the samples, it is not related to obvious changes in maceral composition; in fact it may simply be responding to changes in concentration gradient over time, which requires an early faster diffusion and a later slower diffusion.

Diffusivities calculated using the slope of the lost gas plot model the fast-diffusing component, and diffusivities calculated from Tau tend to model the slow-diffusing components. The application of 2 diffusivities to modelling adsorption data is intuitively satisfying in terms of petrography; however, considering that there is probably a range of diffusion grain sizes controlling diffusion, then there will also be a range of diffusivities related solely to grain size.

Both the Airey and 2-component unipore models are able to model data well. The 2-component unipore model provides 2 diffusivities that straddle the diffusivity calculated using the Airey equation (Figure 5). The proportions of the two components ( $R$  in Table 5) do not seem to vary with the initial concentration gradient for the various pressure steps.

In the following discussion, values of  $D$ ,  $D_e$ ,  $T_o$ , and  $n$  are calculated using the Airey equation, and these values allow the impact on diffusivity, diffusion grain size, pressure step, initial concentration gradient, and initial pressure and temperature to be investigated.

## DIFFUSION GRAIN SIZE, DIFFUSIVITY, AND DIFFUSION COEFFICIENTS

Probably the most important physical variable controlling diffusion in coal is grain size (diffusion grain size). Diffusion grain size is usually smaller than the grain size defined by cleating and fracturing in coal and is related to the degree of microfracturing in each coal fragment. Diffusion grain size is required to calculate diffusion coefficients ( $D$ ) that are used in various CBM simulators. Diffusion grain size may vary within a seam and based on location in folds (deformation history). Other parameters influencing diffusion include initial pressure, initial concentration gradient, and temperature. It is important, if possible, to separate out the effects of these 4 variables on diffusivity.

**TABLE 5: SUMMARY OF DIFFUSIVITY AND DIFFUSION COEFFICIENT RESULTS.**

Ash EQ basis EQ %	range mm	temp °C	radius cm	diffusivity l/sec	steps							
					1	2	3	4	5	6	7	
30.6 4.7	4--6 2C unipore	25	0.25	De v		1.14E-06	1.12E-06	2.08E-05				
				De i		1.60E-05	2.64E-05	1.28E-06				
				R		0.4	0.42	0.6				
				Airey n		9.75E-06 0.350	8.42E-06 0.360	9.26E-06 0.359				
Unipore	De		2.78E-06	2.72E-06	4.16E-06							
32.6 3.9	3.35--4 2C unipore	25	0.18375	De v		1.10E-06	1.04E-06	5.92E-07	7.11E-07			
				De i		2.96E-05	2.67E-05	2.55E-05	5.03E-06			
				R		0.485	0.5	0.64	0.76			
				Airey n		7.35E-06 0.350	6.11E-06 0.365	1.75E-06 0.450	1.29E-06 0.600			
Unipore	De		2.01E-06	1.82E-06	8.60E-07	9.48E-07						
31 5.1	1--2 2C unipore	25	0.075	De v		2.20E-06	1.56E-06	1.42E-06	1.03E-06			
				De i		1.16E-04	4.62E-05	2.84E-05	6.76E-06			
				R		0.415	0.4	0.48	0.48			
				Airey n		2.47E-05 0.300	1.73E-05 0.345	8.61E-06 0.345	3.63E-06 0.480			
Unipore	De		5.69E-06	4.62E-06	3.73E-06	2.13E-06						
31.4 4.2	.25--1 2C unipore	25	0.03125	De v		9.01E-06	1.74E-05	4.35E-06	4.61E-06			
				De i		2.05E-04	1.54E-04	2.05E-05	2.15E-05			
				R		0.415	0.49	0.39	0.39			
				Airey n		6.39E-05 0.380	5.79E-05 0.480	1.57E-05 0.495	1.65E-05 0.510			
Unipore	De		2.46E-05	2.87E-05	8.60E-06	9.73E-06						
40.7 3.8	0--.25 2C unipore	25	0.00625	De v		8.96E-05	7.17E-05	7.17E-05	6.40E-05	8.45E-05	8.45E-05	5.12E-05
				De i		2.56E-03	2.00E-03	2.00E-03	8.96E-04	1.18E-03	1.18E-03	3.07E-04
				R		0.35	0.337	0.337	0.34	0.44	0.44	0.37
				Airey n		1.42E-03 0.300	1.17E-03 0.304	8.42E-04 0.310	7.28E-04 0.325	5.29E-04 0.380	4.63E-04 0.410	3.37E-04 0.400
Unipore	De		2.82E-04	2.82E-04	2.82E-04	1.95E-04	2.12E-04	1.95E-04	1.25E-04			
32.6 3.9	3.35--4 2C unipore	40	0.18375	De v		2.37E-06	2.37E-06	4.44E-06	1.48E-06	3.55E-06		
				De i		1.63E-04	1.72E-04	7.40E-05	2.96E-05	1.60E-05		
				R		0.5	0.4	0.46	0.5	0.49		
				Airey n		2.32E-05 0.350	2.46E-05 0.360	2.77E-05 0.400	8.83E-06 0.410	9.94E-06 0.570		
Unipore	De		5.03E-06	5.63E-06	8.89E-06	2.96E-06	6.22E-06					

Diffusivity (De) is proportional to (diffusion coefficient)/(square of diffusion grain radius). If the diffusion grain size is known, then it should be possible to estimate values of *D*. In this study, variations in the values of De and *D* are apparent when comparing results from samples screened to various sizes. To limit the effect of the variables initial concentration gradient and pressure gradient, each sized sample was pressured to similar initial methane concentrations so that values of De for each sample reflect changes in the size of the spheres controlling diffusion (diffusion grain size). Values of *D* are independent of grain size and should not change as long as the diffusion grain size is the same as the actual grain size for the sample. Eventually as the screened grain size increases, a point is reached where the sample grain size is greater than the diffusion grain size and grains are actually composites of a number of diffusion grains. At this point calculated values of *D* start to increase, values of De stop decreasing, and the sample grain size defines the actual diffusion grain size that is controlling diffusivity in the coal. As sample grain size increases further, De remains constant and values of *D* starts to increase, because it is calculated using the actual

grain size and not the smaller diffusion grain size that is controlling diffusion.

Data in this study indicate that the grain size controlling diffusion is 0.1 to 0.15 cm (Figure 7). The field of view for a petrographic microscope using 10 × 50 power is about 0.4 mm, so the microfracturing defining diffusion gain size should be apparent as long as sample preparation has not introduced new microfractures.

For samples crushed to less than the diffusion grain size, there is less variation in diffusion grain sizes, and values of *n* in the Airey equation are low. As the actual grain size increases, there is a wider spread in the diffusion grain sizes, with the average defined as above, and when the actual grain size is greater than the average diffusion grain size, then there is a wide spread in diffusion grain sizes, and *n* increases further. How well the break in the diffusivity versus grain size plot is defined depends on how well an average diffusion grain size is defined.

The diffusion coefficients vary based on pressure steps (Figure 7) but are in the range of 10<sup>-7</sup> to 10<sup>-8</sup> cm<sup>2</sup>/s. As mentioned, the average grain radius is probably less than [(top size + bottom size)/4] because grains are biased towards

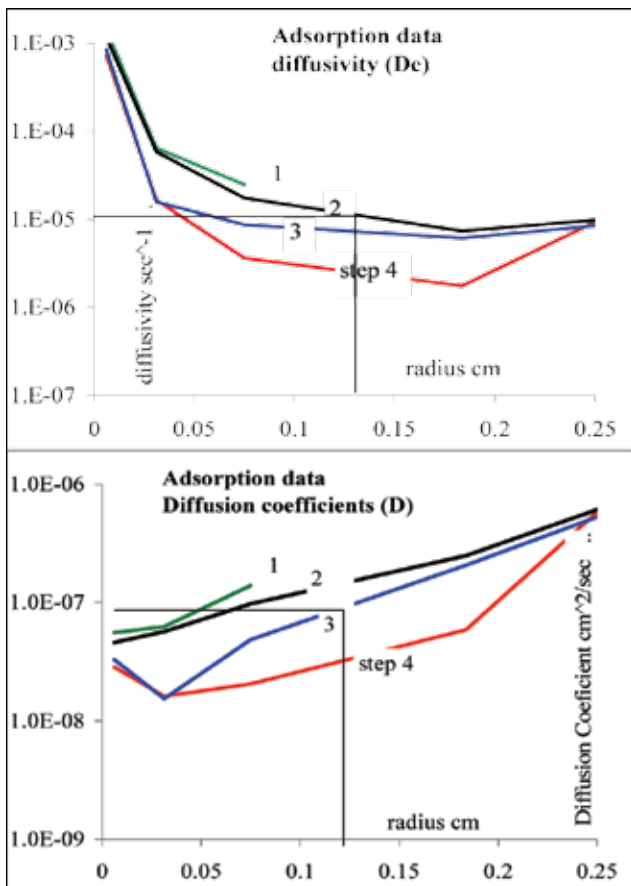


**Figure 7: Diffusivity and diffusion coefficients for each pressure step plotted against increasing grain radius, cm.**

the minimum mesh size; consequently, the diffusion grain size is almost certainly less than 0.1 mm. The 7 pressure steps used in Figure 7 correlate loosely with actual initial pressure for isotherm construction (Figure 8) and therefore provide a good way of grouping data. Initial concentration gradients also influence diffusivity (Figure 9), but the effect on diffusivity is less than for diffusion grain size, as indicated by the 0.0625 mm sample (Figure 9), which plots along a low-slope line.

There is little diffusivity data on anthracites in the literature; however, Harris et al. (1996) report  $T_0$  values for sheared anthracite samples from Wales. Values of  $T_0$  are generally lower than values in this study, indicating either faster diffusivity or small diffusion grain sizes.

Airey (1968) investigated the desorption behaviour of sized coal samples from the Sherwood Colliery in England. Samples were maintained at 60% to 75% of equilibrium moisture and, based on grain size, experienced initial concentration gradients that ranged from about 13 to over 2000  $\text{cm}^3/\text{g}/\text{cm}$  radius. The rank of the coal is not given, but based on estimated equilibrium moisture contents, it was probably high-volatile bituminous to sub-bituminous. Data in the paper are recalculated and plotted as diffusivity and diffusion coefficients versus grain radius (Figure 10).

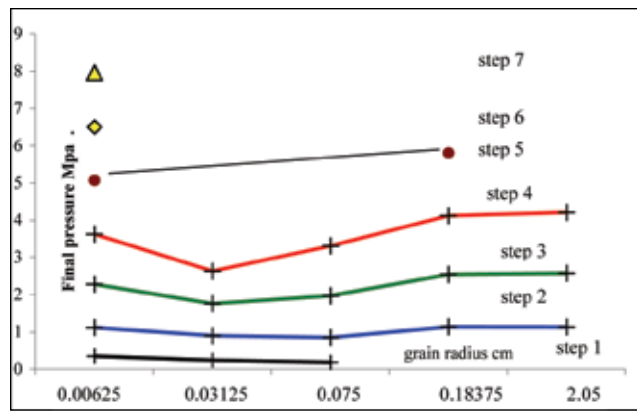


**Figure 8: Comparison of pressure step number and actual isotherm pressure for the various grain sizes.**

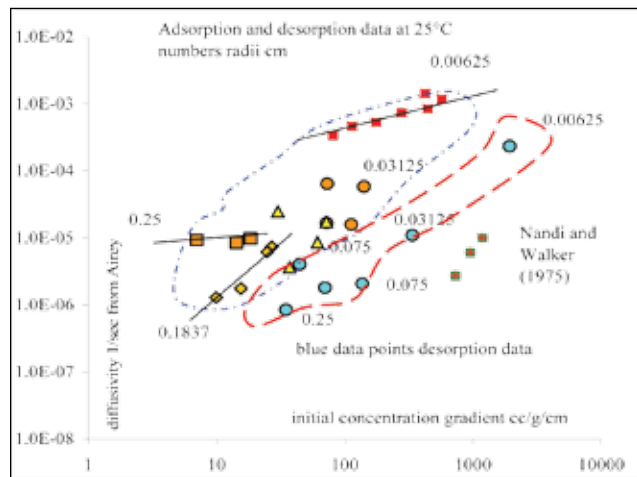


**Figure 9: Diffusivity versus initial concentration gradients for transient adsorption and desorption data, with grain radii indicated.**

There is a break in the slope of the plot, indicating that the diffusion grain size is about 0.4 cm and grains larger than this are composite grains. At this size, the diffusion coefficient is between  $10^{-8}$  and  $10^{-9}$   $\text{cm}^2/\text{s}$  compared to  $10^{-7}$  to  $10^{-8}$   $\text{cm}^2/\text{s}$  for the samples in this study. The difference may relate to rank or the fact that samples in this study appear to have a smaller diffusion grain size.

Nandi and Walker (1975) analysed the desorption behaviour of a number of coals, including an anthracite sample. Their data indicate that a radius size of 0.1 to 0.2 cm was controlling diffusivity (Figure 11), with predicted diffusion coefficients in the range  $10^{-8}$  to  $10^{-9}$   $\text{cm}^2/\text{s}$ , which are an order of magnitude lower than values in this study.

Laximinarayana and Crosdale (1999) provide diffusivity values (recalculated to diffusion coefficients using 0.212 mm) of  $3 \times 10^{-5}$  to  $1 \times 10^{-5}$   $\text{cm}^2/\text{s}$  on dry coal with a rank of 3.0%  $R_{\text{max}}$ . The values are high compared to this study because samples were dried as is required for isotherms measured using balances.

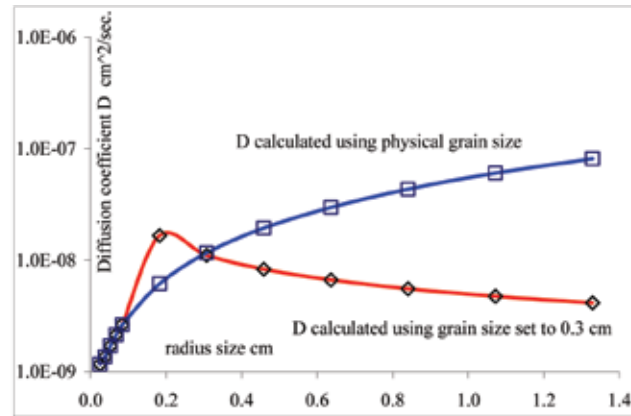
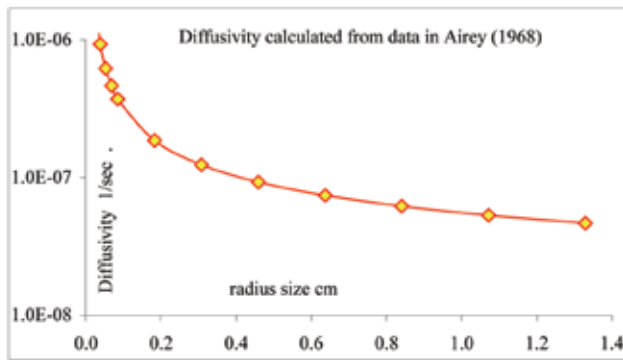


Figure 10: Plot of diffusivity and diffusion coefficients versus grain size; data recalculated from Airey (1968).

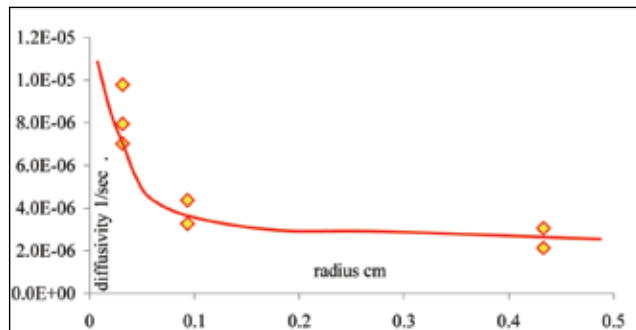


Figure 11: Plot of diffusivity versus grain size; data from Nandi and Walker (1975).

It is apparent that diffusion coefficients estimated in this study for anthracites are higher than values in the literature. All analyses in this study were run at equilibrium moisture contents. Some data from older literature were derived from samples dried below equilibrium moisture (Nandi and Walker 1975), which may explain the difference between their data and this study. However Airey (1968) did not find a variation of diffusivity over a moisture range of 5% to 6.2%. Clarkson and Bustin (1999) found faster diffusion through dry coal than moist coal, as did Busch et al. (2004). They found that the diffusion grain sizes for their samples were less than 0.2 mm.

## EFFECTS OF INITIAL CONCENTRATION GRADIENT ON DIFFUSIVITY

A number of studies (Nandi and Walker 1975; Harpalani and Ouang 1999) documented the dependence of diffusivity on either initial concentration gradient or initial pressure gradient. In their studies, and for exploration data, the final pressure is atmospheric, so that initial concentration gradient  $[(\text{final adsorbed gas content} - \text{initial adsorbed gas content})/\text{grain radius, cm}]$  and initial pressure gradient  $[(\text{initial pressure} - \text{final pressure})/\text{grain radius, cm}]$  are generally closely related. This is not the case if the 2 are measured over a number of pressure steps required for the collection of data to plot an isotherm. Initial concentration gradients are high at low pressures (steep part of isotherm) and then decrease at higher pressures; in contrast, pressure gradients between isotherm steps tend to increase with each step (Figure 12). Diffusivity tends to increase as initial concentration gradients increase but decrease as pressure gradients or initial pressures increase (Figure 13). This implies that the mechanism controlling gas movement in coal is diffusion controlled by initial concentration gradient and not Darcy flow controlled by pressure gradient. The positive correlation of pressure gradient and diffusivity is valid only when the final pressure is atmospheric and diffusion is occurring over the initial part of the isotherm.

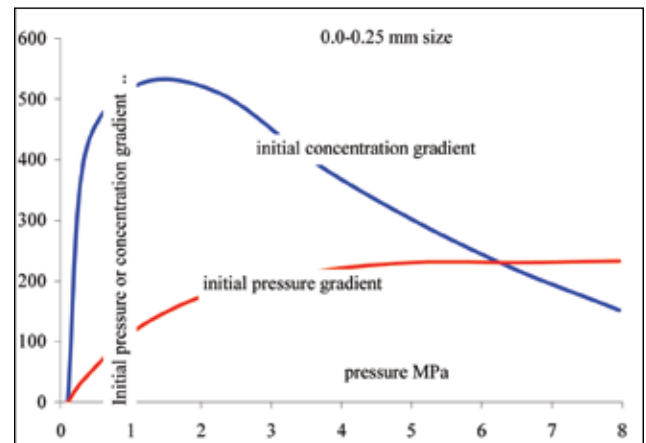
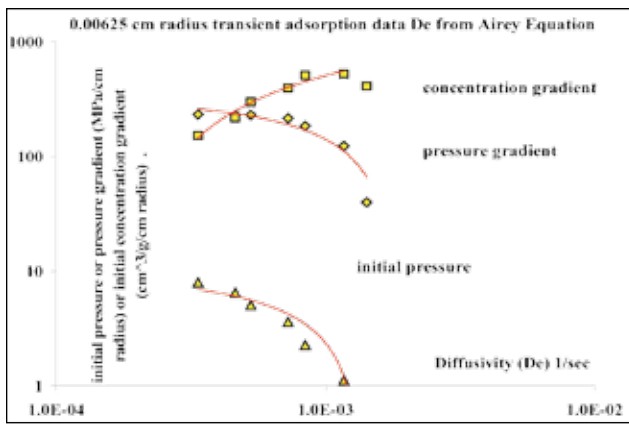


Figure 12: Plot of initial concentration gradients and initial pressure gradients versus pressure.

Diffusivity varies with concentration gradient and therefore must vary over time as the concentration gradient changes. This means that any diffusivity calculated from a desorption or an adsorption curve is an average. Values calculated from the first part of the curve will always be greater than values calculated from the full curve (Figure 6). The Airey equation provides the best average of diffusivity but is biased towards representing the early stages of adsorption or desorption when the concentration gradient is high.



**Figure 13: Plot of diffusivity versus initial concentration gradient, initial pressure gradient, and initial pressure.**

Harpalani and Ouang (1999) measured diffusivity for a sample at constant pressure but varying partial pressures of methane. They found that  $D_e$  decreased as the mean concentration of methane in the coal decreased. They discussed the possible effect of matrix shrinkage on diffusivity. The decrease in diffusion coefficient as concentration gradient decreases may be related to decrease in pore size caused by loss of gas and matrix shrinkage. As desorption progresses, decrease in pore size decreases diffusivity.

During desorption of exploration samples, the initial concentration gradient is determined by gas content at atmospheric pressure and initial gas content—it is therefore nearly always much greater than the initial concentration gradient that is in effect during production. Consequently, diffusivity or diffusion coefficients calculated from exploration data may be much higher than those in effect during production, and these values will change over time as concentration gradients change. The difference in diffusivity between desorption data and production data may be over one order of magnitude, based on the potential change in initial concentration gradients. This is estimated by calculating the difference between  $D_e$  calculated from the  $V_i/V_\infty$  versus  $T^{1/2}$  plot and the Tau value of the full curve (Figure 6).

In this study, it appears that the sensitivity of diffusion coefficients to initial concentration gradients is similar to that outlined by Harpalani and Ouang (1999) and is in the range of a doubling of  $D$ , which corresponds to a tripling in concentration gradient (Figure 9).

Nandi and Walker (1975) measured the desorption characteristics of an anthracite sample starting at different levels of saturation and for temperatures of 0 °C, 25 °C, and 50 °C. The grain diameter was 0.0315 cm. They dried samples under vacuum before starting the experiments and calculated diffusivity using the slope of the first part of the desorption curve and the unipore equation. Based on their data, sensitivity of diffusivity to initial concentration gradients is greater for anthracite than for other ranks of coals

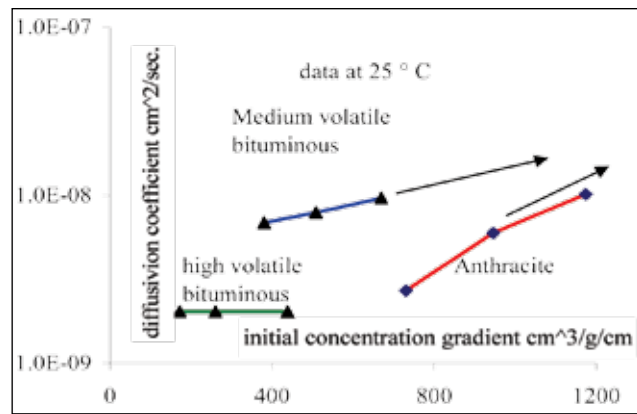


**Figure 14: Diffusion coefficients versus concentration gradient for different rank coals; data from Nandi and Walker (1975).**

(Figure 14), and for anthracite there is a tenfold increase in  $D$  for a threefold increase in concentration gradient.

In a production scenario, producing at lower pressures with large concentration gradients increases the diffusion coefficient of anthracite more than other ranks of coal, and at high concentration gradients, anthracite diffusivity may exceed even that of lower-rank coals.

Based on the pressure gradient that extends outwards from a hole and the shape of isotherms, initial concentration gradients and diffusion coefficients will decrease outwards away from the hole. If diffusion cannot deliver gas to the grain surfaces, where it will be transported by Darcy flow, then there may be a rapid decrease in pore pressure, an increase in effective stress, and a decrease in permeability. It is important that de-pressuring a well take into account the interplay between Darcy flow and diffusion at different distances along a seam away from the well head.

## DESORPTION DATA

Once a sample, as part of an isotherm experiment, has been pressurized with gas in a sample canister, it is possible to desorb gas back at atmospheric pressure and construct a desorption curve that does not have a lost-gas component. The data therefore provide information on the validity of lost-gas corrections as well as calculated diffusivity values using the full desorption curve compared to values calculated using the first part of the desorption curve.

Ten desorption experiments were run: six 6 at 25 °C and 4 at 40 °C. All 6 size ranges are represented by the data. Values of  $D$ ,  $D_e$ ,  $T_o$ , and  $n$  were calculated using the Airey equation (Table 6). Diffusivity values decrease as grain size increases (Figure 15) up to a size of about 0.1 to 0.15 cm, which defines a similar diffusion grain size as the adsorption data. Diffusion coefficients are in the range  $10^{-7}$  to  $10^{-8}$   $\text{cm}^2/\text{s}$  for the smaller sizes, which is similar to but

TABLE 6: DIFFUSIVITY AND DIFFUSION COEFFICIENTS CALCULATED FROM DESORPTION DATA.

temperature	25°C	25°C	25°C	25°C	25°C	25°C	40°C	40°C	40°C	40°C
radius cm	0.00625	0.03125	0.075	0.13375	0.18375	0.25	0.03125	0.075	0.13375	0.18375
ash db	42.3	34	32.7	34.1	33.9	32.1	34	32.7	34.1	33.9
EQ moisture	3.84	4.1	5.1	4.6	3.9	4.7	4.1	5.1	4.6	3.9
start pressure KPa	5582	2646	2620	2800	2823	3278	2993	2915	3138	3224
adsorbed gas cm <sup>3</sup>	603.1	579.7	584.8	547.4	530.7	334.9	432.7	442.8	373.8	347.4
desorbed gas cm <sup>3</sup>	492.7	487.0	483.1	431.6	364.6	380.4	558.2	524.2	503.8	483.9
conc gradient cm <sup>3</sup> /g/cm	1933.58	337.63	137.19	70.37	44.62	34.92	386.97	148.86	82.64	59.22
n from Airey Equation	0.41	0.48	0.52	0.56	0.52	0.53	0.39	0.48	0.46	0.38
To hours Airey Equation	0.08	1.7	8.9	10.3	4.6	22	0.85	4.7	5.5	3.2
diffusivity De	2.31E-04	1.09E-05	2.06E-06	1.80E-06	4.03E-06	8.42E-07	2.18E-05	3.94E-06	3.37E-06	5.79E-06
diffusion coefficient D	9.04E-09	1.06E-08	1.17E-08	3.22E-08	1.36E-07	5.26E-08	2.13E-08	2.22E-08	6.02E-08	1.95E-07
diffusivity from t <sup>1/2</sup> plot	2.14E-04	1.10E-05	6.67E-06	5.43E-06	6.54E-06	5.96E-07	7.07E-05	2.94E-05	2.91E-05	3.62E-05
linear T <sup>1/2</sup> plot time sec	168	111	98	67	75	74	125	112	98	106
linear T <sup>1/2</sup> plot Vt/V∞	0.51	0.147	0.068	0.053	0.065	0.04	0.245	0.152	0.152	0.172

db = dry basis

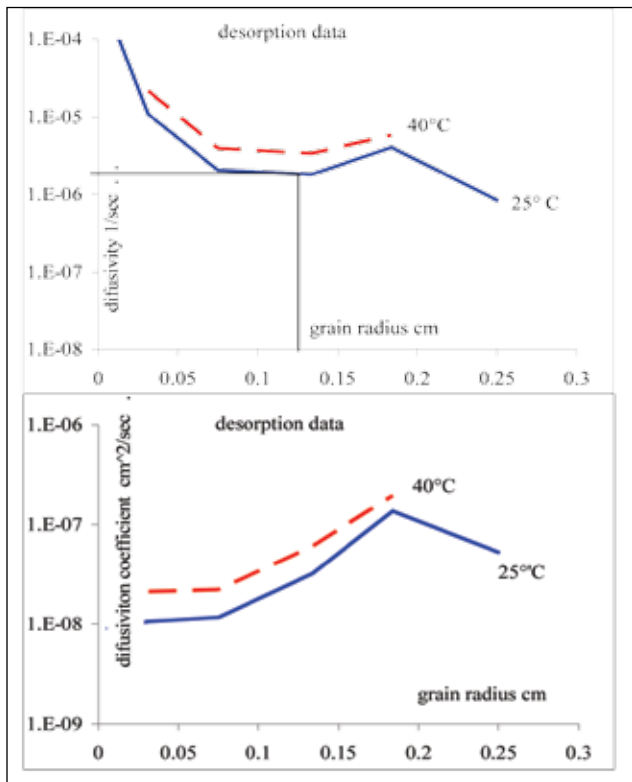


Figure 15: Diffusivity and diffusion coefficients versus grain size for desorption data; values calculated using the Airey equation.

a bit less than values calculated from the transient adsorption data. Diffusivity measured by desorption decreases at smaller initial concentration gradients than does diffusivity measured by adsorption.

The relationship of diffusivity to initial concentration gradient is similar for desorption data and for adsorption data (Figure 9), and generally diffusivity does not appear to be very sensitive to changes in initial concentration gradient. There is some indication that diffusivity decreases as initial concentration gradients decrease and that, for similar initial concentration gradients, diffusivity during desorption is lower than during adsorption. This may be related to the

effects of matrix swelling during adsorption versus matrix shrinkage during desorption.

Comparison of diffusivity and  $n$  values from the Airey equation derived from desorption and adsorption data indicate that at equivalent initial concentration gradients, values of  $n$  for desorption are higher than for adsorption (Figure 16). Diffusivity measured by desorption is less than that measured by transient adsorption, even when concentration gradients and grain sizes are the same (Figure 9). This has the effect of decreasing early diffusivity and increasing later diffusivity during desorption compared to the equivalent times during adsorption. The differences in the shape of desorption curves versus adsorption curves means that information from transient adsorption experiments may not be applied directly to modelling production situations.

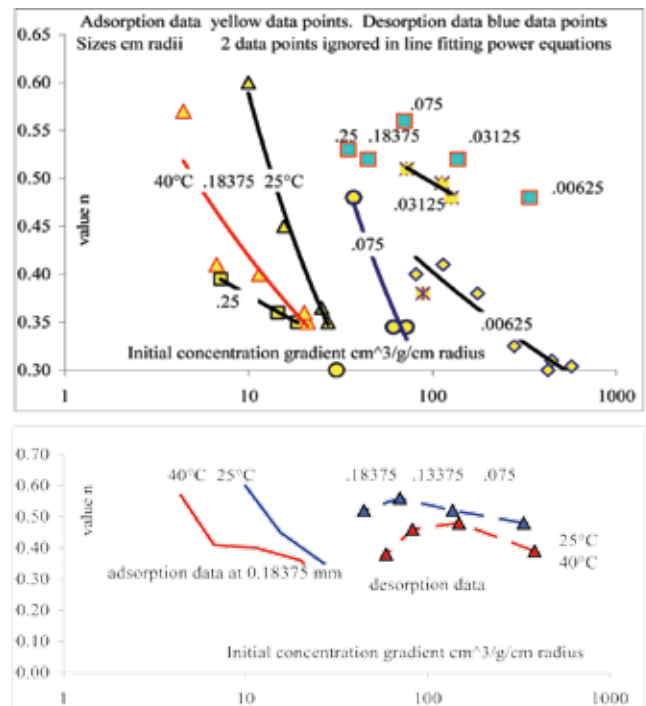


Figure 16: Variation of  $n$  from the Airey equation versus initial concentration gradient.

## EFFECT OF TEMPERATURE ON DIFFUSIVITY

Most of the experimental data were generated at a temperature of 25 °C and some at 40°C. Exploration desorption data were collected at temperatures generally less than 25 °C. Consequently, diffusivities from exploration desorption data are influenced by 3 variables: diffusion grain size, initial concentration gradient, and temperature.

The 3.35 to 4 mm size fraction was adsorbed at a number of steps at temperatures of 25 °C and 40 °C. The data indicate that diffusion coefficients increase by a factor of about 10 when the initial concentration gradient is about 75 cm<sup>3</sup>/g/cm and the temperature increases from 25 °C to 40 °C. The increase is a factor of 100 when the initial concentration gradient is 11 cm<sup>3</sup>/g/cm. This means that the ratio of  $D$  at 40 °C to  $D$  at 25 °C increases more as the initial concentration gradient decreases (Figure 17). The effect of temperature on diffusion coefficients will be greater during production (low initial concentration gradients) than may be estimated from desorption data (high initial concentration gradients).

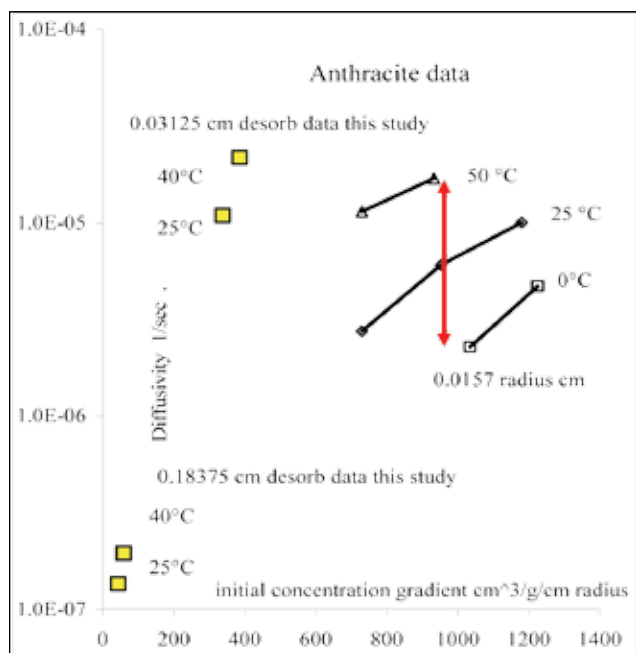


Figure 17: Effect of temperature on diffusivity; comparison of data from Nandi and Walker (1975) and this study.

Desorption tests were done at a single pressure step (but varying initial concentration gradients) for a range of sizes and temperatures of 25 °C and 40 °C (Table 6). It is not possible to separate the effects on diffusion coefficients of grain size and initial concentration gradient. The 15 °C increase in temperature has increased diffusivity (Figure 17) by about a factor of 5, which is less than the increase during adsorption. Data from Nandi and Walker (1975) (Figure

17) measured by desorbing gas from coal samples indicate that at a fixed initial concentration gradient, diffusivity changes by an order of magnitude for a 50 °C increase in temperature.

## LOST-GAS CORRECTIONS

Data from desorption experiments provide information on the validity of lost-gas corrections. It is possible to measure the time over which a plot of  $V_t/V_\infty$  versus  $T^{1/2}$  for desorption data is linear; i.e., the length of time over which the conventional lost-gas correction can be applied (Table 6). The times in minutes and  $V_t/V_\infty$  values were measured at the point at which the plot was no longer linear for the 6 desorption tests run at 25 °C. Plotting the results versus size provides an indication of what times and what particle sizes invalidate the lost-gas plot (Figure 18). As an example, for the 0.075 mm sized sample, if the lost time is more than 4 minutes, then the lost-gas correction may be invalid. It is also possible to estimate the relationship between total degassing of particles (represented by 80% loss of gas) and particle size (Figure 18). A 0.075 mm sized

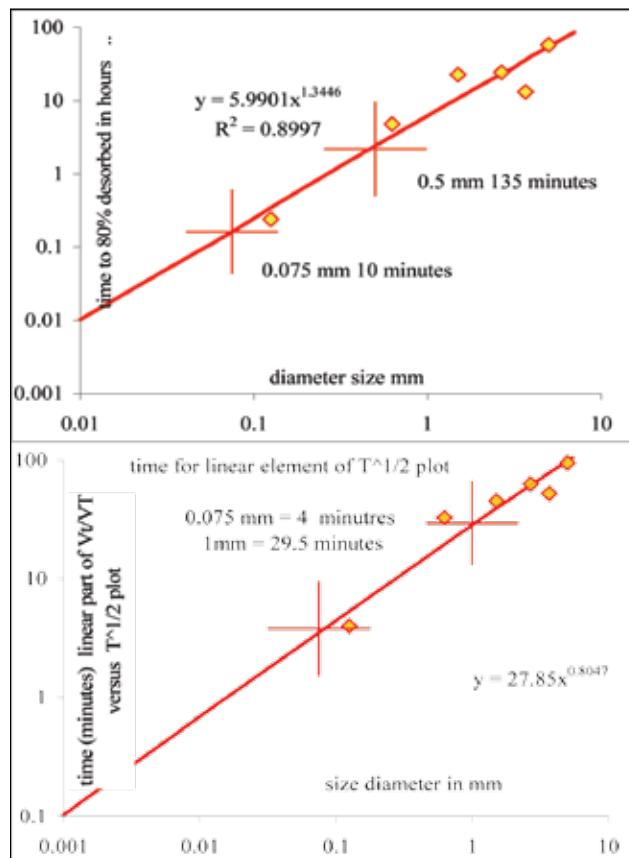
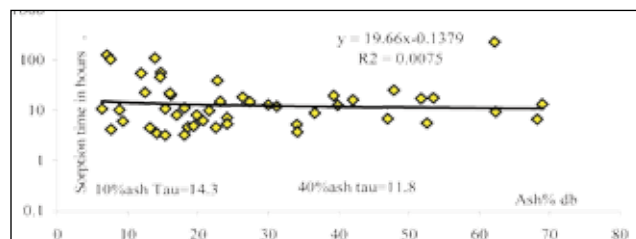


Figure 18: Validity of lost-gas plots; grain diameter (mm) versus linear element of lost gas plot and time for 80% degassing of grains.

sample has effectively lost all its gas in about 10 minutes. The time increases markedly as size increases, and for 0.5 mm sized fragments, the time is about 2 hours. This gives some idea as to what sized fragments should be considered to be dead (non-coal) during desorption. If this material is treated as coal when calculating the gas concentration of the total sample on an ash-free basis, then the gas concentration will be too low because there is no way of estimating the lost gas of the fine coal component.

## COMPARISON OF DIFFUSIVITY VALUES FROM EXPLORATION DESORPTION DATA AND EXPERIMENTAL DESORPTION AND ADSORPTION DATA

Exploration data for anthracite samples (from the same area as the core sample) are presented in Figure 19. Values of Tau for the anthracite exploration data do not appear to be very sensitive to varying ash content, though there is a slight increase in Tau (decrease in diffusivity) as ash content decreases. The lack of sensitivity of diffusivity to ash content is important because it removes one potential variable from consideration. It implies that ash is in large part contained in fragments external to the fragments controlling diffusion (diffusion grain size). The slight decrease in Tau (increase in  $D_e$ ) with increasing ash content (Figure 19) may indicate that as the amount of dispersed mineral matter increases, the diffusion grain size decreases because of more microfracturing surrounding mineral grains.



**Figure 19:** Plot of ash dry basis (db) versus sorption time (hours) for anthracite exploration samples.

The spread in Tau values at the same ash content may indicate a variation in diffusion grain size or changes in  $D$  that are related to variations in petrography in terms of contents of vitrinite (low diffusivity) and inertinite (high diffusivity).

If the diffusion grain size is estimated for core samples, then it is possible to calculate diffusion coefficients in a production scenario by using the appropriate diffusion grain size and diffusion coefficients (calculated from experimental data at the correct temperatures and over the correct initial concentration gradients). The 0 to 0.25 mm size data reflects the true change in diffusion coefficients versus initial concentration gradient over a wide range of

gradients because the grain size is less than the diffusion grain size, which appears to be about 0.15 cm radius. This is also true for desorption data sized 0.00625, 0.03125, and 0.075 cm radii. The range in initial concentration gradients for experimental data is similar to that for the exploration data over a wide range of assumed diffusion grain sizes. It is therefore possible to adjust the assumed diffusion grain size for exploration data (this changes both diffusion coefficients and initial concentration gradients) until the exploration data projects through the field outlined by the experimental data in the plot (Figure 20). This is achieved by fixing the diffusion grain size for the exploration data at about 0.10 cm radius. At this grain size, diffusion coefficients are in the range  $10^{-7}$  to  $10^{-8}$   $\text{cm}^2/\text{s}$ , which is a similar range as the experimental data. For comparison, data points are plotted for 0.05 and 0.5 cm diffusion grain sizes (Figure 20).

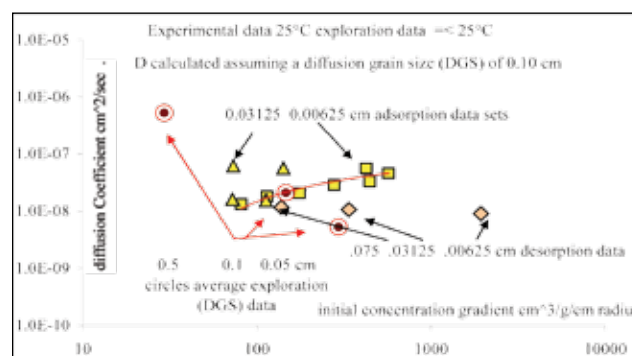


**Figure 20:** Comparison of diffusion coefficients and initial concentration gradients for anthracite experimental data and exploration data. The exploration data is averaged, and both  $D$  and initial concentration gradients vary based on the assumed diffusion grain radius.

The above process is used for experimental adsorption data; however, because of the difference between experimental adsorption and experimental desorption data, it should probably be used for experimental desorption data. Unfortunately in this study there is insufficient experimental desorption data, but it appears based on Figure 20 that the difference is not great. This method of estimating the diffusion grain size can be applied to individual samples. It may be possible to relate the variation in diffusion grain size to geological factors, such as regional structure and seam petrography.

Desorption times (Tau) and the value  $T_0$  from the Airey equation provide an estimate of diffusivity and indicate the combined effects of diffusion grain size and diffusion coefficient. The first is revealing physical information about the sample (core) and the second may be revealing something about the maceral composition. In the example illustrated (Figure 21), an order of magnitude change in  $T_0$  represents an order of magnitude change in  $D$  or a doubling in diffusion grain size. Large changes in  $T_0$  that do not obviously

relate to fragmentation of the core probably imply changes in  $D$  and maceral composition. Data from southeastern BC (Figure 21) indicate a fine structure to  $T_0$  (desorption time) values within a seam. Values of  $T_0$  decrease towards the hangingwall of the seam, as do dry, ash-free gas contents. The implication is that values of  $D$  are increasing near the hanging wall, possibly indicating either more inertinite (higher values of  $D$ ), lower saturated gas content, or more fragmentation (smaller diffusion grain size) associated with under-saturated coal.

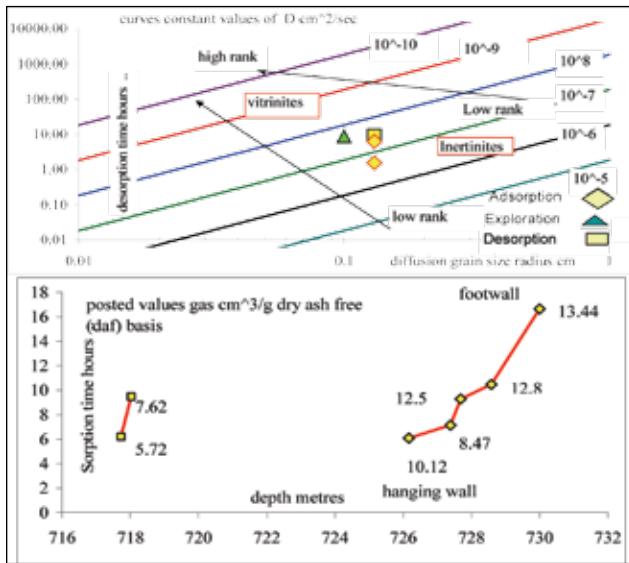


Figure 21: a) Relationship between diffusion coefficients, desorption time, and diffusion grain size. b) Variation in desorption time based on location in a seam.

## CONSTRUCTING A $V_t/V_\infty$ VERSUS TIME PLOT FOR A PRODUCTION ENVIRONMENT

In order to simulate production scenarios, it is necessary in part to predict actual  $V_t/V_\infty$  versus time plots in effect during production. This is not the same as being able to predict  $D_e$ , as knowing  $D_e$  alone is not sufficient to reconstruct the plots because the value of  $D_e$  varies during desorption. The unipore equation does not allow reconstruction of the real  $V_t/V_\infty$  versus time plots very well, whereas the Airey and 2-component unipore equations are more successful. The Airey equation has the advantage over the 2-component unipore equation because it introduces only 1 additional constant ( $n$ ) other than diffusivity, which is easily determined from  $T_0$  or  $\tau$ .

The method in the previous section illustrates a way of determining exploration diffusion coefficients and diffusion grain sizes by using experimental data gained during isotherm experiments. Determining an appropriate value of  $n$  is not easy. Airey (1968) found that the value  $n$  did not vary much and averaged about 0.31. In this study, values of

$n$  range from 0.3 to 0.65 and, for a fixed size, they increase as initial concentration gradients or temperatures decrease (Figure 16). Under similar conditions of size, temperature, or initial concentration gradient, values of  $n$  are larger for desorption data than for adsorption data (Figure 16).

There is no obvious easy way to predict values of  $n$  based on the fact that it varies with initial concentration gradient, grain size, and temperature and probably also based on the variability of grain sizes in a sample. However, once the diffusion grain size is determined for a seam using a plot similar to Figure 20, it is then possible to calculate the appropriate  $D_e$  value adjusted for the initial concentration gradient in effect during production. A value of  $n$  is derived from Figure 22 using the estimated  $D_e$  for the production scenario. Values of  $D_e$  from samples screened to grain sizes larger than the diffusion grain size are constant, and therefore the value derived from Figure 20 can be used in Figure 22 to provide a value of  $n$ . This is sufficient to construct a  $V_t/V_\infty$  versus time plot for an increment of production occurring over a limited pressure interval. In simple terms, increased values of  $n$  flatten the  $V_t/V_\infty$  versus time plot near the origin, while smaller values steepen it.

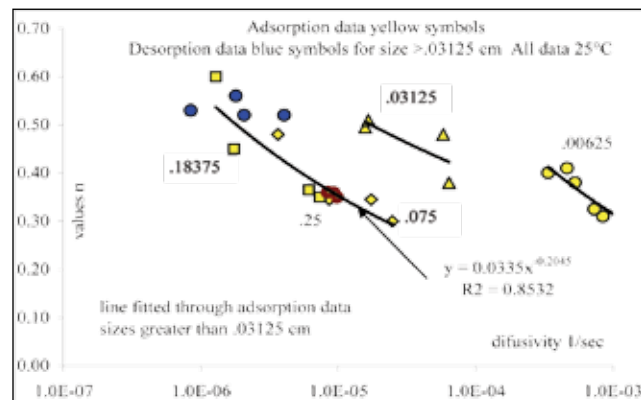


Figure 22: Values of  $n$  versus diffusivity, indicating a fairly predictable ratio as long as actual grain size is greater than diffusion grain size.

Values of  $n$  increase as  $D_e$  decreases, and the relationship is fairly good for grain sizes that are greater than the average diffusion grain size. For these samples,  $n$  is related to the degree of variability of diffusion grain sizes and is biasing the  $V_t/V_\infty$  curve by decreasing  $V_t/V_\infty$  values at earlier times as  $D_e$  decreases. Under similar conditions,  $D_e$  for desorption is lower than for adsorption and is accompanied by a larger value of  $n$ . The larger value of  $n$  is, as above, biasing the  $V_t/V_\infty$  versus time plots by decreasing  $V_t/V_\infty$  values at earlier times. Values of  $n$  decrease to correct desorption or adsorption curves to better model low  $D_e$  values, which would otherwise predict  $V_t/V_\infty$  values near the origin that are too low. This occurs for desorption data compared to adsorption data and for lower temperature data compared to higher temperature data.

## CONCLUSIONS

This study investigates the diffusion characteristics of a single sample of anthracite. Diffusivity values are calculated from transient adsorption and desorption data using the Airey equation, which has the flexibility to model the data well. By screening the sample to different sizes, the diffusion grain size and diffusion coefficients are determined. The diffusion grain size controlling diffusion is 1.0 to 1.5 mm. Diffusivity and diffusion coefficients are also partially dependent on initial concentration gradient.

The unipore equation does not model real data well. The equation may describe the early part of the adsorption or desorption curve, which provides the basis of a method for lost-gas corrections. However, it does not describe the full curve well and therefore cannot be used to predict diffusion behaviour during production.

Diffusion coefficients operating during transient adsorption determined using the Airey equation are in the range  $10^{-7}$  to  $10^{-8}$  cm<sup>2</sup>/s at a temperature of 25 °C and increase by a factor of about 5 for a 15 °C increase in temperature. There is little published anthracite diffusion data to compare to results in this paper, and often published data are not applicable because of different moisture levels. Diffusion coefficients increase as the initial concentration gradient increases. The initial concentration gradient is in part dependent on the external methane concentration but also on the diffusion grain size.

Exploration desorption data provides values of  $T_0$  and  $n$  using the Airey equation. This allows calculation of diffusivity, but without knowing the diffusion grain size, it is not possible to calculate diffusion coefficients. It is possible using the experimental data to determine the right combination of diffusion grain size and diffusion coefficient for the exploration data (Figure 20), and in this case it appears that average values are 0.1 cm and  $10^{-7}$  to  $10^{-8}$  cm<sup>2</sup>/s.

Even then, the concentration gradient operating on exploration desorption samples is generally much greater than that in effect during production. Consequently, diffusion coefficients calculated from exploration data may not be relevant for production data, even if the desorption data were measured at in situ temperature. Diffusion coefficients determined from transient adsorption data may be better because the initial concentration gradients are closer to production gradients. However, diffusion coefficients calculated from adsorption data are different from those calculated from desorption data even when initial concentration gradients are similar. The effect may be caused by matrix expansion during adsorption and shrinkage during desorption.

The diffusion behaviour during production is best modelled using the Airey equation, which requires the value  $T_0$  and  $n$  to construct the  $V_t/V_\infty$  versus time plot. The plot is important because it provides information on the amount

of gas being delivered to the cleat system and available for Darcy flow. Construction of the plot requires values of  $D$  and diffusion grain size to provide values of  $T_0$  and the value of  $n$ . Calculation of  $T_0$  requires doing transient adsorption or desorption experiments on sized samples. The appropriate diffusion coefficient is calculated based on the initial concentration gradient operating during production, which in turn is dependent on the diffusion grain size for the exploration samples and the methane concentrations in effect during production.

Once diffusivity and diffusion grain size values are known, it is possible to estimate a value of  $n$  (Figure 22) and then to construct a realistic time versus  $V_t/V_\infty$  plot for a production situation. This approach is empirical and avoids discussion of the validity of unipore or bipore models for diffusion in coal.

## ACKNOWLEDGEMENTS

This study evolved from discussions between me and Karin. I provided geology and some half-baked concepts, and Karin organized, making the equipment to produce the data, and kept me on track in terms of theory. During the study, Karin was diagnosed with cancer and, despite treatment, the disease progressed and she died 26th July 2006. She will be missed and I will miss the opportunity for more collaboration, fun, learning, and production. Rong Guo (Grace) helped with collating the data when Karin was no longer with us.

## REFERENCES

- Airey, E.M. (1968): Gas emission from broken coal. An experimental and theoretical investigation; *International Journal of Rock Mechanics and Mineral Science*, Volume 5, pages 475–494.
- Bell, G.J. (2003): Spherical diffusion analysis: an improved method for analyzing coal gas content; *Canadian Society of Unconventional Gas*, Conference Calgary October 24th 2002.
- Busch, A., Gensterblum, Y., Kroos, B.M. and Littke, R. (2004): Methane and carbon dioxide adsorption-diffusion experiments on coal: upscaling and modeling; *International Journal of Coal Geology*, pages 151–168.
- Bustin, R.M. and Clarkson, C.R.M. (1999): Free gas storage in matrix porosity: a potential significant coalbed resource in low rank coals; *International Coalbed Methane Symposium*, Proceedings May 3–7 1999, Bryant Conference Center University of Alabama, Alabama USA.
- Clarkson, C.R. (1998): The effect of coal composition moisture content and pore volume distribution upon single and binary gas equilibrium and non equilibrium adsorption implications for gas content determination; PhD Thesis, *University of British Columbia*; May 1998.

- Clarkson, C. R. and Bustin, R.M. (1999): The effect of pore structure and gas pressure upon the transport properties of coal: a laboratory and modeling study; 2. Adsorption rate modeling; *Fuel*, Volume 78, pages 1345–1362.
- Dawson, F.M., Marchioni, D.L., Anderson, T.C. and McDougall, W.J. (2000): An assessment of coalbed methane exploration projects in Canada; *Geological Survey of Canada*, Bulletin Number 549.
- Dawson F.M., and Clow, J.T. (1992): Coalbed methane research, Elk Valley Coalfield; in *Canadian Coal and Coalbed Methane Geoscience Conference*, Parksville BC, pages 57–71.
- Ettinger, I, Dimitriev, A and Lamba, E. (1966): Natural factors influencing coal sorption properties, V- Some special features of sorption properties of anthracite coals of eastern Donbass; *Fuel*, Volume 45, pages 363–366.
- Feng, K.K., Cheng, K.C. and Augsten, (1984): Preliminary evaluation of the methane production potential of coal seams at Greenhills Mine, Elkford, British Columbia; *Canadian Institute of Mining and Metallurgy*, Volume 77, pages 56–61.
- Feng, K.K. (1981): Desorption of gases from Canadian coals; *CanMet Report ERP/MRL81-20 (OP) (J)*.
- Gamson, P., Beamish, B., and Johnson, D. (1996): Coal microstructure and secondary mineralization: their effect on methane recovery; Coalbed Methane Geology, *Geological Society*, Special Publication Number 109, pages 165–179
- Gan, H., Nandi, S.P. and Walker, P.L. (1972): Nature of porosity in American coals; *Fuel*, Volume 51, pages 272–277.
- Graham, B.C. (1998): Determining coalbed gas content; Gas Research institute; GRI 98/0365.2
- Harpalani, S. and Ouyang, S. (1999): A new laboratory technique to estimate gas diffusion characteristics of coal; *International Coalbed Methane Symposium*, Tuscaloosa Alabama, pages 141–152.
- Harris, I.H., Davies, G.A., Gayer, R.A. and Williams, K. (1996): Enhanced methane desorption characteristics from South Wales anthracites affected by tectonically induced fracture sets; Coalbed Methane and Coal Geology, *Geological Society*, Special Publication Number 109, pages 181–196.
- Laximinarayana, C. and Crosdale, P.J. (1999): Role of coal type and rank on methane sorption characteristics of Bowen Basin, Australia coals; *International Journal of Coal Geology*, Volume 40, pages 309–325.
- Lennan, J.D., Schafer, P.S. and Pratt, T.T.J. (1995) A guide to determining coalbed gas content; *Gas Research Institute GRI-94/0396*
- Mannhardt, K. (2005): Adsorption and diffusion analysis of anthracite; Contract performed by TIPM for BC Ministry of Energy, Mines and Petroleum Resources, Progress report No. 1, 11 May 2005.
- Mavor, M.J., Owen, L.B., and Pratt, T.J. (1990): Measurement and evaluation of coal sorption isotherm data; *Society of Petroleum Engineers*, 65th Annual Conference, pages 157–170.
- Moffat, D.H. and Weale, K.E. (1955): Sorption of methane by coal at high pressures; *Fuel*, Volume 34, pages 449–462.
- Nandi, S.P. and Walker, P.L. (1975): Activated diffusion of methane from coals at elevated pressure; *Fuel*, Volume 54, pages 81–86.
- Rodrigues, C.F. and Lemos de Sousa, M.J. (2002): The measurement of coal porosity with different gases; *International Journal of Coal Geology*, Volume 48, pages 245–251.
- Ruckenstein, E., Vaidyanathan, A.S. and Youngquist, G.D. (1971): Sorption of solids with b-disperse pore structures; *Chemical Engineering Science*, Volume 26, 1305–1318.
- Ryan, B.D. (2003): Pseudovitrinite: possible implications for gas saturation in coals and surrounding rocks; *B.C. Ministry of Energy and Mines*, Geological Fieldwork, Paper 2003-1, pages 1–9.
- Ryan, B.D. (2006): A discussion on moisture in coal; implications for coalbed gas and coal utilization; *British Columbia, Ministry of Energy, Mines and Petroleum Resources*, Oil and Gas Division, Summary of Activities 2006.
- Sawyer, W.K., Zuber, M.D. and Kuskraa, V.A. (1987): Using reservoir simulation and field data to define mechanisms controlling coalbed methane production; *Proceedings of the 1987 Coalbed Methane Symposium*, Tuscaloosa, Alabama, November 16–19 1987.
- Smith, D.M. and Williams, F.L. (1984): Diffusion models for gas production from coals: Application of methane content determination; *Fuel*, Volume 63, pages 251–255.
- Thomas and Damberger (1976): Internal surface area moisture content and porosity of Illinois coals variation with coal rank; *Illinois State Geological Survey*, Circular 493.

# PRELIMINARY ANALYSES OF COAL REFUSE MATERIAL FROM VANCOUVER ISLAND

Barry Ryan<sup>1</sup>

---

## ABSTRACT

*The first period of coal mining on Vancouver Island lasted from 1847 to 1967, and during that period, waste material from the coal cleaning accumulated in a number of areas along the east coast of Vancouver Island. Three of these areas were sampled and analysed for coal related properties, major oxides, and trace metals. Results indicate that the material is generally similar in composition to average shale.*

Ryan, B., (2008): Preliminary Analyses of Coal Refuse Material from Vancouver Island; Geoscience Reports 2008, B.C. Ministry of Energy, Mines and Petroleum Resources, pages 99-118.

<sup>1</sup>Resource Development and Geosciences Branch; Oil and Gas Division; BC Ministry of Energy, Mines and Petroleum Resources; 250-952-0377; barry.d.ryan@gov.bc.ca.

**Key Words:** Waste coal, trace metals, coal refuse, Vancouver Island.

---

## THE EARLY VANCOUVER ISLAND COAL INDUSTRY

Coal mining on Vancouver Island started in 1847 near Port Hardy on the northeast coast. Subsequently mining moved south to the Nanaimo and Cumberland areas, where activity continued until 1967. This early period of coal mining activity has left a legacy of coal mine waste. There are a number of coal refuse piles on Vancouver Island, especially in the Nanaimo area, and the total accumulation may be as high as 2.5 million tonnes (Gardner 1997).

The early mines removed rock from raw coal using simple wash plants and hand picking tables to remove large rock fragments. This produced a waste product composed of large fragments of rock and high-ash coal and referred to as coarse rejects. In some areas where clean coal was being loaded onto barges, some fell off conveyors or trains to accumulate as finer, cleaner coaly material.

Coal waste in the Ladysmith area originates from the Extension Mine, which opened in the 1890s as an extension of the Wellington Mine. Workers were moved to the new town of Oyster Harbour, later to be called Ladysmith. A wash plant was built in the area, and waste from the plant now forms Slag Point. Coal from the wash plant was shipped out from the harbour.

## THE ENVIRONMENTAL HAZARDS OF COAL REFUSE

Coal in situ contains varying amounts of rock and water in addition to the organic carbon and associated volatile material. It is very difficult to totally separate the included rock and report a weight percent, so the organic material is burnt off and the remaining weight reported as percent ash, which is a bit less than the original weight of included rock. Thermal coals are shipped, after removal of rock, at ash concentrations up to about 15%. Coking coals (metallurgical coals), which are made into coke (the fuel in blast furnaces), are washed to ash contents generally less than 10%. The definition of coal varies, but generally anything over about 50% ash is not considered coal. This means that most coal mines, whether they are mining thermal or coking coal, have to process the coal to remove included rock. These wash plants usually produce two streams of waste material—coarse reject (greater than 0.6 mm) and tailings (less than 0.6 mm). Generally, modern wash plants have a yield of 65% to 85%, which means that 35% to 15% of the weight of raw material entering the wash plant becomes waste material dumped somewhere close to the mining activity. It is usually buried or re-contoured and vegetated, but it does represent a concentration of material from a specific geological environment.

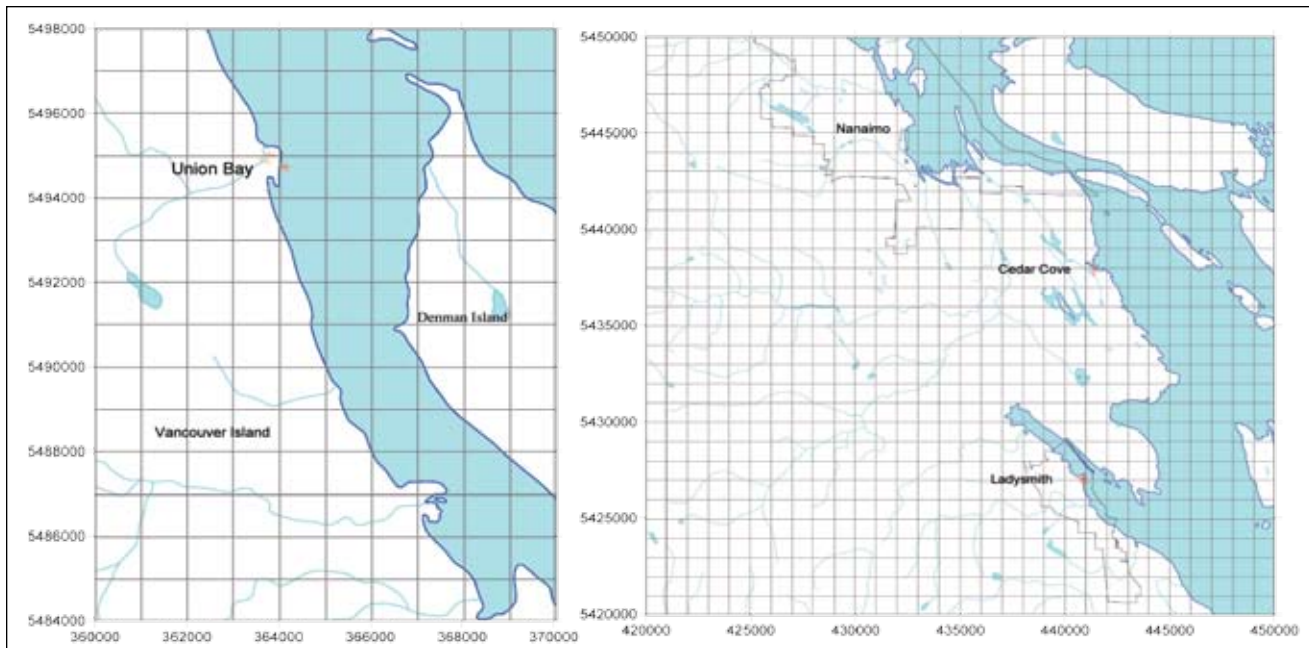


Figure 1: Sample locations north (Union Bay) and south (Cedar Cove and Ladysmith) of Nanaimo. UTM grid scale is 1 km.

Most of the concern about coal waste involves the possibility that the coal waste is leaching harmful trace metals into the environment. Coal itself is composed of environmentally benign organic carbon; unfortunately, coal and the rock closely associated with coal seams often contain appreciable amounts of sulphides and some trace elements. Sulphide minerals, predominantly pyrite ( $\text{FeS}_2$ ), often contain trace amounts of elements other than iron and will oxidize to produce acidic water that releases and mobilizes these elements. There may also be increased concentrations of certain trace elements in rock material associated with coal, which was deposited in conjunction with vegetation in an oxygen-deficient, slightly acid, swamp environment; some trace elements are bound in insoluble forms and concentrated in this type of environment.

It is important to clarify the terms trace metals and trace elements as they are used in literature. The term trace metal may refer either to a metal (element) that is indeed rare or to the amount that occurs in a particular environment. The term is often applied to metallic elements such as iron, magnesium, zinc, copper, chromium, nickel, cobalt, vanadium, arsenic, molybdenum, and selenium. Possibly only selenium and vanadium are actually rare in overall terms. In contrast, the term trace element is broader and generally is used to refer to any element that occurs in very small concentrations in a particular environment.

In 2007, BC coal mines were expected to produce over 25 million tonnes of clean coal and over 5 million tonnes of coarse and fine refuse. This material will be permanently sequestered within mine lease areas in such a way as to not cause environmental problems. The record for safe disposal of this material is good based on the fact that there

has been large-scale surface coal mining in BC for the last 40 years without major environmental problems related to coal waste handling.

## STUDY AREAS

Samples were collected in 3 areas along the east coast of Vancouver Island, including Union Bay, Cedar Cove (Canary Cove and Clam Bay), and Ladysmith Slag Point areas (Figure 1). Union Bay was the site of the major wash plant and load-out for coal mined in the Cumberland area. Mining started in the area in 1869 when Baynes Sound Coal Company started operations in the Tsable River area; however, most of the activity soon moved to the Cumberland area, where mining continued until 1953. The Tsable River Mine continued operation, finally by removing coal from mine pillars, until 1967, when it closed as the last operating coal mine on the island.

## SAMPLING AND ANALYSIS

Samples were collected from beaches, exposed banks of waste material, and from the top surface of piles of waste material. Fragment size varied from pebble to fine sand, and the mass of each sample collected varied based on fragment size and ranged from less than 1 kg to about 5 kg. Wherever possible, shallow holes up to 1 m deep were dug so that one or two samples could be collected to represent a simple stratigraphic section. On beaches, this required digging a hole up to 1 m deep (Figure 2). In some banks it was possible to sample a section up to 2 m thick (Figure



**Figure 2: Photo; Union Bay intertidal zone, location 646.**



**Figure 3: Photo; Union Bay; bank into waste coal pile, location 662.**

3). In some places (Union Bay intertidal zone), there was a heavy iron staining (Figure 4). A total of 43 samples were collected (Table 1). Larger samples were split, with one split screened into 2 sizes to provide coarse-sized and fine-sized samples.

Inspection of samples provided some information on amount of coal in samples, and those that were noticeably coaly were sent for coal-specific analyses as well as x-ray fluorescence (XRF) major oxide and ICP-MS analyses (Table 2). Other samples not visibly coal-rich were sent for ash, XRF (Table 3), and ICP-MS (using a hot aqua-regia digestion; Table 4) analyses.

The XRF analysis provides a good estimate of the amount of organic matter in samples because samples are fused prior to analysis and the loss of weight is a measure of organic carbon and the remaining weight correlates closely to American Society for Testing and Materials (ASTM) ash measurements (Figure 5). It appears that ash concentration determined by XRF is about 0.5% lower, but the correlation between the 2 methods is generally very good.



**Figure 4: Photo; Union Bay intertidal zone, location 646; heavy iron staining on surface.**

**TABLE 1: SAMPLE LOCATIONS AND DESCRIPTIONS.**

Sample No	lat	long	Zone 10		Notes
			easting	northing	
Union Bay					
641	49-35.209	124-53.083	363773	5494180	Vertical bluff Sample top 40 cm coaly
642					Vertical bluff Sample middle 1 m down from top coaly
643					Vertical bluff Sample bottom 2 m down from top coaly
Intertidal zone Sampling					
644	49-35.475	124-52.773	364159	5494663	top 3cm mdst+coaly
645					middle 8-12 cm mdst+coaly
646					bottom 15-20 cm mdst+coaly
647	49-35.512	124-52.763	364173	5494732	low inter tidal zone top 4 cm mdst+coaly
648					low inter tidal zone 10-15 cm middle sample mdst+coaly
649					low inter tidal zone aprox depth 40 cm mdst+coaly
Intertidal					
650	49-35.524	124-52.784	364148	5494754	1 of 3 top heavy iron stain 0-4 cm
651					middle 10-15 cm black layer
652					deeper layer 20-30 cm grey/black
653	49-35.514	124-52.842	364078	5494738	upper inter tidal zone iron cemented surface layer hard pan
654	49-35.516	124-52.836	364085	5494741	top of coal pile 15-20cm mdst
655					surface top 4 cm coaly mdst
Estuary					
660	49-35.661	124-53.078	363800	5495017	by creek black sand layer surface sample top 10-20 cm coaly
661					15-20 cm deep iron stained coaly
662	49-35.597	124-53.215	363632	5494903	waste coal/rock pile 30 cm down from top mdst
663					waste coal/rock pile 1.5 m down from top mdst
Top of waste Pile					
664	49-35.564	124-53.000	363894	5495002	top of coal hills 30 cm deepmdst
665	49-35.564	124-53.1	363769	5494838	Surface sample top 4 cm mdst
Cedar Cove/Canary Cove					
666	49-05.566	123-48.152	441408	5437859	coal waste pile adjacent to beach surface top 4 cm coaly
667					depth 30-35 cm taken coal waste pile adjacent to beach coaly
668	49-05.577	123-48.192	441360	5437880	surface top 4 cm coaly
669					65 cm deep coaly
Intertidal Zone					
670	49-05.614	123-48.188	441365	5437949	surface sample top 4 cm
671					depth to sample 20 cm coaly
Clam Bay					
672	49-05.498	123-48.184	441368	5437734	surface top 4 cm coaly
673					deep sample 30-40 cm hole 80 cm deep coaly
674	49-05.497	123-48.188	441363	5437732	surface top 4 cm mdst
675					sample 20 cm deep mdst
Ladysmith Slag Point					
676	48-59.706	123-48.537	440824	5427007	beach surface sample top 5 cm coaly
677					beach asmples 20-30 cm deep coaly
678	48-59.740	123-48.494	440877	5427070	surface top 5 cm coaly
679					30 cm deep sample coaly
Intertidal SE side of pile beach on ocean side					
680	48-59.669	123-48.418	440968	5426937	surface sample top 5 cm coaly
681					sample 20 cm deep coaly
Coaly Bluff					
682	48-59.612	123-48.457	440920	5426832	surface to 30 cm mdst
683					1.5 m down from top mdst
Beach Above tide					
684	48-59.698	123-48.522	440842	5426992	surface top 5 cm sandy
685					50 cm deep Lots of iron/cable debris
Top of Waste pile					
686	48-59.728	123-48.496	440874	5427047	surface top 5 cm coaly
687					sample 40 cm deep coaly

**TABLE 2: COAL-SPECIFIC ANALYSES OF SOME SAMPLES.**

sample	Moist adb	Ash adb	Moist res	VM adb	FC adb	CV db	CV	S%	Forms Of Sulfur		
									Pyritic S%	sulphate S%	Organic S%
<b>Union Bay</b>											
641	2.14	48.15	1.33	21.18	29.34			0.54			
642	2.12	28.34	1.26	26.27	44.13			0.66	0.235	0.001	0.420
643	1.86	53.13	1.08	20.34	25.45			0.50			
644	1.29	87.49	0.79	9.69	2.03	3506	3478	0.31			
645	1.77	66.37	0.81	16.55	16.27	4431	4395	0.50			
646	1.08	85.80	0.69	8.95	4.56	3401	3378	0.54			
647	1.94	76.27	1.16	13.08	9.49						
648	1.38	67.37	1.07	16.15	15.41						
649	1.17	91.88	0.63	7.72	-0.23						
660	3.40	39.46	1.67	23.95	34.92	4477	4402	0.87			
661	1.50	74.81	1.05	13.67	10.47	979	969	1.22			
<b>Cedar Cove</b>											
666	2.75	24.57	1.82	32.10	41.51	5463	5364	0.55			
667	2.51	27.66	1.64	31.06	39.64	5440	5351	0.59			
668	31.17	61.31	1.11	20.16	17.42	2509	2481	0.47			
669	2.42	37.98	1.30	26.44	34.28	4657	4596	0.55			
670	1.92	55.53	1.12	21.07	22.28						
671	1.27	60.00	0.86	21.04	18.10						
672	1.57	69.75	1.03	16.59	12.63						
673	1.60	67.93	0.93	18.19	12.95						
<b>Ladysmith Slag Point</b>											
676	2.06	60.36	1.07	19.57	19.00						
677	2.02	49.50	1.04	23.82	25.64						
678	1.46	83.89	0.92	11.49	3.70	600	594	0.14			
679	1.67	75.36	1.00	14.48	9.16	981	971	0.31			
680	1.54	75.65	0.94	15.74	7.67						
681	1.52	71.33	1.10	16.61	10.96						
684	1.75	77.94	0.83	12.89	8.34	786	779	0.23			
685	2.14	60.23	1.24	18.93	19.60	2349	2320	0.28			
686	1.61	82.82	0.90	11.87	4.41						
687	1.74	76.44	1.04	14.59	7.93						

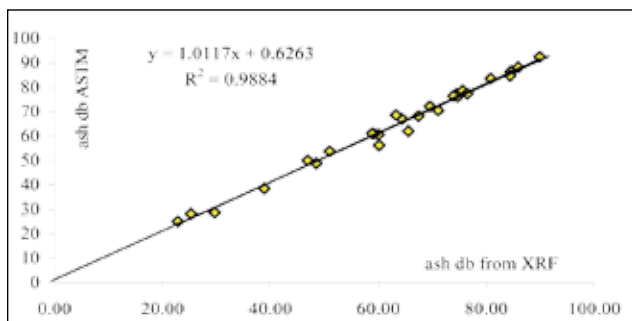


**Figure 5: Correlation of ash determined by ASTM standard method and by XRF.**

## ECONOMIC CONSIDERATIONS

There are a number of coal refuse piles on Vancouver Island, especially in the Nanaimo area, and the total tonnage may be as high as 2.5 million tonnes (Gardner 1997). Portable wash plants exist that can upgrade the material by removing some of the ash until the remaining product has a useable heat value. Generally this means reducing the ash content to less than 15%. A number of companies have investigated the possibility of upgrading material to a marketable thermal coal product, but at present there are no active proposals. Coking coal properties such as fluidity (a measure of coal rheology) or free-swelling index (FSI) are lost as the coal weathers or ages at surface, so that there is no possibility of processing refuse piles to produce a coking coal product.

Most of the samples collected for this study have high ash contents (Table 3) with the exception of samples collected at Cedar Cove. It should be remembered that when

**TABLE 3: XRF MAJOR OXIDE ANALYSES.**

sample	Ash	SiO <sub>2</sub>	TiO <sub>2</sub>	Al <sub>2</sub> O <sub>3</sub>	Fe <sub>2</sub> O <sub>3</sub>	MnO	MgO	CaO	Na <sub>2</sub> O	K <sub>2</sub> O	P <sub>2</sub> O <sub>5</sub>	Ba(F)
641	48.5	57.34	1.26	30.63	5.39	0.04	0.49	1.27	0.38	1.43	0.19	0.03
642	29.7	51.54	1.35	29.47	4.57	0.04	0.39	6.16	0.38	1.27	0.26	0.04
643	51.0	57.53	1.30	30.59	4.28	0.02	0.59	1.91	0.34	1.47	0.10	0.03
644	85.9	57.00	0.99	19.71	10.65	0.05	1.81	4.46	2.11	1.08	0.13	0.03
645	64.4	55.80	1.20	24.96	7.02	0.05	1.39	3.74	1.55	1.25	0.12	0.03
646	84.6	57.50	1.03	16.97	8.85	0.07	2.64	6.63	2.62	0.90	0.13	0.03
647	74.5	56.16	1.03	23.26	7.97	0.03	1.32	3.88	1.81	1.33	0.18	0.03
648	67.4	52.38	1.21	23.65	7.59	0.05	1.93	6.40	1.79	1.13	0.16	0.03
649	89.9	53.03	1.06	13.55	8.17	0.10	3.52	12.56	3.08	0.63	0.13	0.02
650	71.5	39.05	0.84	13.89	34.56	0.04	1.80	4.06	2.45	0.67	0.22	0.02
651	74.3	54.30	1.42	23.32	7.19	0.10	2.15	6.17	1.62	0.91	0.15	0.02
652	93.5	51.27	1.19	14.15	9.61	0.13	4.84	12.04	3.16	0.53	0.14	0.01
654	78.0	55.52	1.07	23.61	11.40	0.03	1.57	2.51	1.28	1.35	0.16	0.03
655	85.3	45.75	1.11	17.43	22.68	0.08	2.80	5.15	1.72	0.78	0.21	0.02
662	58.7	56.77	1.18	28.12	3.05	0.01	0.43	2.84	0.56	1.67	0.07	0.06
663	69.0	52.75	1.14	23.92	2.74	0.01	0.34	6.65	0.55	1.57	0.05	0.05
664	54.8	52.28	2.22	26.25	9.84	0.05	2.10	3.42	1.12	0.93	0.13	0.05
665	49.1	57.47	1.67	29.40	6.73	0.01	0.40	0.19	0.52	1.50	0.12	0.05
666	22.9	55.25	1.26	24.55	6.68	0.06	2.60	2.49	0.78	1.72	0.99	0.20
667	25.3	51.71	1.16	22.67	5.51	0.04	2.76	6.61	0.73	1.56	0.82	0.17
668 S	65.6	56.60	0.91	21.70	7.23	0.07	3.66	3.66	1.12	1.76	0.18	0.05
668 T	59.7	55.59	0.92	21.12	6.97	0.06	3.50	4.81	1.17	1.71	0.21	0.05
669 T	38.9	57.67	1.27	23.49	5.88	0.05	2.86	2.27	1.54	1.65	0.31	0.08
669 S	31.5	55.06	1.15	23.71	6.54	0.07	3.52	2.10	1.91	1.76	0.53	0.09
670	60.2	58.89	0.79	18.70	5.27	0.05	2.72	5.02	2.28	1.70	0.24	0.06
671	60.1	54.27	0.81	17.45	5.20	0.06	2.89	9.40	2.24	1.46	0.31	0.08
672 T	71.1	59.98	0.76	17.41	8.12	0.13	2.85	3.94	1.40	1.36	0.22	0.04
672 S	63.3	57.66	0.88	19.84	7.64	0.10	3.45	3.29	1.76	1.65	0.26	0.05
673 T	70.0	57.88	0.83	18.04	8.31	0.14	3.07	3.98	1.69	1.46	0.21	0.04
673 S	58.5	56.14	0.94	21.10	7.72	0.09	3.63	3.25	1.91	1.71	0.29	0.06
674	67.1	56.12	0.82	18.34	7.50	0.08	3.06	5.99	1.55	1.44	0.29	0.05
675	68.1	53.44	0.79	17.61	9.47	0.07	2.92	6.19	1.45	1.38	0.25	0.05
676 T	56.6	59.51	1.14	24.04	4.11	0.03	2.05	2.45	1.93	1.85	0.13	0.06
676 S	59.2	60.07	1.14	23.66	4.31	0.03	2.10	1.67	1.90	1.85	0.12	0.06
677 T	46.9	59.12	1.19	25.10	4.06	0.03	2.00	1.26	1.88	1.88	0.13	0.07
677 S	49.6	59.25	1.19	24.71	4.06	0.02	2.02	1.69	1.85	1.88	0.13	0.07
678 t	84.4	58.46	1.08	21.86	6.38	0.06	2.58	3.58	1.42	1.72	0.16	0.05
678 S	81.3	58.60	1.09	23.40	5.57	0.05	2.17	3.11	1.09	1.87	0.09	0.05
679 T	74.7	58.56	1.10	23.29	5.05	0.05	2.05	3.26	1.69	1.87	0.08	0.05
679 S	74.0	58.55	1.10	24.06	5.03	0.05	2.10	2.72	1.32	1.90	0.10	0.06
680 T	73.9	56.49	1.08	24.81	4.30	0.05	1.94	4.24	1.08	1.86	0.08	0.05
680 S	74.1	56.49	1.06	24.40	3.89	0.04	1.90	4.97	1.19	1.87	0.09	0.05
681 T	69.6	57.47	1.11	25.31	4.08	0.02	1.92	3.54	1.09	1.92	0.08	0.06
681 S	68.6	57.45	1.12	25.09	3.94	0.03	1.90	4.00	1.05	1.93	0.09	0.05
682	77.4	58.90	1.13	25.26	4.11	0.04	1.77	3.50	0.57	1.80	0.12	0.07
683	73.6	57.49	1.10	24.40	4.69	0.05	1.95	4.25	0.53	1.82	0.07	0.06
684 T	74.2	61.32	1.03	22.24	5.05	0.04	2.10	2.63	1.72	1.72	0.10	0.05
684 S	76.6	62.19	0.99	21.80	4.81	0.04	2.11	2.17	1.92	1.74	0.09	0.05
685 T	58.9	60.13	1.24	25.85	4.53	0.03	1.99	0.81	1.27	1.90	0.18	0.06
685 S	58.2	60.04	1.22	25.80	4.59	0.04	2.03	0.88	1.27	1.91	0.12	0.07
686 t	80.8	58.23	1.07	22.67	5.77	0.05	2.50	3.66	1.44	1.78	0.09	0.05
686 S	80.4	58.84	1.08	24.03	5.05	0.04	2.25	2.99	1.10	1.92	0.08	0.05
678 T	76.5	58.25	1.07	23.65	4.89	0.04	2.18	3.67	1.11	1.89	0.11	0.06
678 S	76.3	58.37	1.10	24.47	4.90	0.03	2.17	2.88	1.09	1.92	0.10	0.06

**TABLE 4: ICP-MS MAJOR AND MINOR ELEMENT ANALYSES.**

sample	Ca %	Fe %	Mg %	Na %	K %	P ppm	S %	Ba ppm	As ppm	Bi ppm	Cd ppm	Co ppm	Cr ppm	Cu ppm	Ga ppm	La ppm	Mn ppm	Mo ppm	Ni ppm	Pb ppm	Sb ppm	Se ppm	Sr ppm	Th ppm	Tl ppm	U ppm	V ppm	Zn ppm
Union Bay																												
641	0.81	3.21	0.22	0.05	0.46	514	0.12	118	13	0.3	0.3	11	59	74	16.7	20	395	1.8	217	10.7	0.4	21.1	147	3.8	0.6	1.0	136	70
642	4.08	2.45	0.15	0.04	0.41	1294	1.01	202	17	0.2	0.2	17	69	89	16.4	20	372	2.4	167	12.8	0.4	25.1	332	3.4	0.6	1.2	238	70
643	1.21	2.37	0.25	0.04	0.50	418	0.32	137	9	0.2	0.2	16	60	72	15.9	21	255	2.1	32	12.7	0.3	22.9	150	3.5	0.4	1.2	187	85
644	1.80	6.78	0.62	0.24	0.40	579	0.53	70	15	0.1	0.1	9	59	43	11.1	10	261	2.8	25	6.1	0.1	11.8	116	1.9	0.2	0.9	90	46
645	2.05	4.32	0.57	0.37	0.56	550	0.67	154	10	0.2	0.4	17	88	76	16.5	16	363	1.7	38	10.9	0.2	19.1	164	2.9	0.4	0.9	125	62
646	2.66	5.09	0.77	0.34	0.34	606	0.51	76	12	0.1	0.1	15	100	44	10.6	5	355	1.4	32	5.8	0.1	11	160	1.5	0.2	0.6	112	49
647	2.18	5.15	0.58	0.42	0.59	885	0.60	108	23	0.2	0.1	6	90	49	14.7	15	276	1.8	27	9.8	0.2	16.3	185	2.6	0.3	1.1	117	52
648	3.50	4.83	0.65	0.39	0.56	809	0.84	127	24	0.1	0.1	10	101	66	16.5	10	301	1.7	37	9.1	0.2	17.5	298	2.6	0.4	1.3	133	60
649	6.19	3.97	1.06	0.37	0.20	527	0.17	38	11	<1	<1	11	91	47	9.2	<2	458	0.8	29	3.1	<1	9.8	394	0.7	<1	0.3	120	49
650	1.48	19.70	0.55	0.64	0.31	1015	0.57	87	22	0.1	0.1	3	78	55	9.7	8	256	13.2	21	6.9	0.3	9.5	162	1.3	0.1	3.1	90	22
651	2.70	3.45	0.52	0.17	0.34	687	0.44	59	11	0.1	0.1	14	89	58	13.8	10	566	0.9	31	6.6	0.1	15	105	1.9	0.2	0.6	118	48
652	4.80	3.99	1.24	0.26	0.15	584	0.14	29	13	<1	<1	16	83	54	9.7	<2	538	0.6	33	2.0	<1	9	284	0.6	<1	0.2	115	47
654	0.64	6.55	0.50	0.22	0.44	597	0.20	83	20	0.1	<1	7	56	48	11.1	13	207	5.4	373	7.6	0.3	11.8	72	2.3	0.1	2.0	96	48
655	1.34	13.39	0.69	0.32	0.31	698	0.46	59	20	0.1	0.1	7	46	65	9.9	10	291	12.7	447	5.8	0.4	9.7	85	1.5	0.2	3.5	93	37
662	2.09	1.90	0.21	0.13	0.63	210	1.50	89	27	0.2	<1	<1	49	18	12.6	19	28	2.6	10	11.3	0.2	15	243	3.0	0.5	1.5	104	23
663	4.89	1.70	0.15	0.07	0.58	185	3.60	45	25	0.2	<1	<1	45	15	11.0	14	28	2.3	10	6.0	0.9	11.8	224	2.3	0.6	1.1	77	18
664	1.12	5.37	0.42	0.27	0.39	535	0.10	389	149	0.1	<1	6	127	55	18.6	16	101	1.8	34	9.7	1.1	15.7	200	2.8	0.7	0.8	204	27
665	0.13	5.00	0.20	0.07	0.69	542	0.08	325	79	0.2	<1	3	131	38	20.3	17	39	2.6	28	12.5	0.7	21.5	222	3.7	0.6	1.9	196	31
Hg all values less than 20 ppb														Se only 1 value greater than 1 ppm														
sample	Ca %	Fe %	Mg %	Na %	K %	P ppm	S %	Ba ppm	As ppm	Bi ppm	Cd ppm	Co ppm	Cr ppm	Cu ppm	Ga ppm	La ppm	Mn ppm	Mo ppm	Ni ppm	Pb ppm	Sb ppm	Se ppm	Sr ppm	Th ppm	Tl ppm	U ppm	V ppm	Zn ppm
Cedar Cove																												
666	1.70	4.08	1.24	0.19	0.80	4914	0.58	394	14	0.3	0.3	13	219	111	17.6	15	487	2.1	140	32.6	0.2	27.7	2317	3.1	0.4	1.3	195	85
667	4.75	3.71	1.55	0.16	0.71	4067	1.23	150	24	0.2	0.2	16	208	113	18.5	7	432	2.4	147	12.5	0.1	28.7	2409	2.9	0.4	1.3	187	75
668 S	2.74	4.79	1.96	0.35	0.88	961	0.58	254	11	0.1	0.1	11	180	56	16.1	12	614	0.8	144	15.8	0.1	21.3	376	2.1	0.2	0.8	145	104
668 T	3.33	3.89	1.65	0.33	0.75	946	0.57	270	9	0.1	0.1	9	146	55	15.2	10	503	1.0	116	11.1	0.1	20.8	479	2.1	0.2	0.9	135	79
669 T	1.25	3.25	1.35	0.62	0.90	1499	0.51	421	10	0.2	0.1	11	182	99	18.0	14	402	1.7	109	18.4	0.2	24.3	673	2.9	0.2	1.7	175	77
669 S	1.59	4.35	1.89	0.93	1.04	2413	0.88	274	14	0.1	0.1	15	254	118	19.3	12	615	2.2	166	11.9	0.2	26.5	1013	2.4	0.2	1.8	217	77
670	2.72	2.77	1.20	0.56	0.63	1000	0.53	245	5	0.1	0.1	6	148	44	13.3	9	319	0.7	87	12.0	<1	17.3	461	1.9	0.2	0.8	107	59
671	6.22	3.15	1.42	0.67	0.67	1522	0.83	303	10	0.1	0.1	8	169	61	12.9	2	397	1.3	95	13.9	0.1	17.9	1073	1.8	0.2	1.1	127	61
672 T	2.69	5.26	1.58	0.36	0.72	1008	0.71	206	12	0.1	0.1	12	125	45	12.5	15	1018	1.3	112	10.1	0.1	17.5	301	1.9	0.2	0.8	112	92
672 S	2.44	5.88	2.11	0.61	0.99	1390	0.64	309	15	0.1	0.1	16	192	99	16.4	14	878	1.2	158	14.1	0.1	22.3	458	2.4	0.3	1.0	152	131
673 T	2.99	6.27	1.85	0.41	0.91	1100	0.89	210	26	0.1	0.1	18	170	57	13.7	17	1248	1.3	153	9.2	0.1	20.5	284	2.1	0.4	1.2	134	120
673 S	2.24	4.80	1.91	0.58	0.90	1348	0.63	328	21	0.2	0.1	13	167	79	16.9	14	731	1.7	142	12.5	0.1	23.6	567	2.2	0.3	1.0	152	94
674	4.35	5.39	1.68	0.54	0.83	1569	1.10	235	23	0.1	0.1	13	155	55	14.1	10	720	1.2	127	11.2	0.1	19.3	692	1.9	0.2	0.9	131	95
675	5.00	8.29	1.83	0.54	0.90	1531	1.93	157	41	0.1	0.1	15	167	59	13.7	10	722	1.2	145	13.2	0.1	18.3	640	1.8	0.8	0.7	135	114
Hg all values less than 20 ppb														Se only 1 value greater than 1 ppm														
sample	Ca %	Fe %	Mg %	Na %	K %	P ppm	S %	Ba ppm	As ppm	Bi ppm	Cd ppm	Co ppm	Cr ppm	Cu ppm	Ga ppm	La ppm	Mn ppm	Mo ppm	Ni ppm	Pb ppm	Sb ppm	Se ppm	Sr ppm	Th ppm	Tl ppm	U ppm	V ppm	Zn ppm
Ladysmith																												
676 T	1.33	2.16	0.97	0.74	0.95	542	0.38	339	11	0.2	0.2	6	116	87	16.2	19	226	1.4	55	27.3	0.2	20	205	3.0	0.3	1.2	139	114
676 S	0.79	2.69	1.12	0.74	1.12	658	0.35	366	7	0.2	0.2	8	170	94	17.3	21	276	1.5	67	29.7	0.2	20.9	178	3.1	0.3	1.2	158	134
677 T	0.72	2.57	1.10	0.86	1.17	707	0.41	470	7	0.3	0.3	10	207	102	19.3	21	240	5.0	76	24.7	0.2	24.8	284	3.7	0.4	1.5	182	141
677 S	0.92	2.48	1.08	0.75	1.08	652	0.41	451	4	0.3	0.3	9	168	94	18.1	20	243	5.6	70	25.7	0.3	23.1	247	3.5	0.4	1.3	164	122
678 T	2.11	4.26	1.30	0.33	1.04	511	0.20	274	10	0.2	<1	10	114	55	16.2	21	500	1.5	73	17.4	0.1	19	142	2.7	0.3	0.6	122	166
678 S	2.03	3.63	1.10	0.33	1.06	431	0.19	275	10	0.2	0.1	7	102	56	15.9	22	444	0.6	67	20.5	0.1	18.6	118	2.6	0.3	0.7	113	178
679 T	2.25	3.31	1.08	0.47	1.08	410	0.33	313	8	0.2	0.1	8	115	70	16.8	22	441	0.6	64	20.1	0.2	20.9	150	2.9	0.3	0.8	128	130
679 S	1.90	3.37	1.14	0.50	1.09	484	0.27	311	10	0.2	0.1	8	117	72	17.2	22	449	0.6	67	18.8	0.1	21.7	143	3.1	0.3	0.7	131	147
680 T	3.30	3.10	1.11	0.48	1.11	423	0.51	300	12	0.2	0.1	8	111	66	17.6	20	391	0.3	74	15.9	0.1	21.6	172	3.1	0.5	0.7	127	119
680 S	3.59	2.32	1.02	0.51	1.05	371	0.31	259	11	0.2	0.1	5	93	63	16.5	21	367	0.3	55	15.8	0.1	20.2	163	3.1	0.4	0.7	118	96
681 T	2.73	2.73	1.11	0.50	1.09																							

a sample is ashed, there is a loss of weight from the mineral matter, so that a concentration of approximately 85% ash corresponds to a mineral matter concentration of 100% (i.e., no organic carbon content).

## RESULTS AND DISCUSSION

### Major Elements in Coal Waste

Sulphur occurs in coal as sulphides, as sulphates, or as organic sulphur. Trace metals may be associated with sulphur if the sulphur is present as sulphides. These sulphides may be dispersed in coal or associated with ash. Sulphur has a negative correlation with ash and no correlation with Fe (Figure 6), indicating that a lot of the sulphur is occurring as organic or sulphate sulphur associated with the coal. This is probably because sulphides originally present in the coal waste have oxidized and released  $\text{SO}_3$ . Trace metals would also be released and mobilized by the acidic water.

One of the advantages of pairing XRF and ICP-MS analyses is that it provides information on what proportion of major elements may be in a soluble form. XRF measures the total amount present, whereas ICP-MS measures the amount that is soluble in a hot acid leach. The amount of Fe detected by ICP-MS is similar to that detected by XRF, indicating that most of the iron is probably soluble and probably occurs in sulphides, carbonates, or hydroxides. A similar comparison for Ca, K, and Na indicates that lower percentages of these elements are potentially soluble and mobile (Figure 7).

### Trace Elements in Coal Waste

As a starting point, it is important to understand how trace elements are distributed in coal. Coal is not 100% organic carbon—even when washed it contains an amount of included mineral matter analysed as ash. Consequently concentrations of trace elements in coal can have either an ash or an organic carbon affinity. To complicate the picture further, a lot of trace elements are associated with sulphide minerals in coal, and these sulphide minerals (mainly pyrite) may be associated with ash in the seam or with coal in the seam. In coals with varying ash contents, one should try to assign an affinity of the trace elements to either the organic material, the ash, or the sulphides (if present in reasonable amounts). Average trace element concentrations in shales and continental crust are shown in Figure 8. There are some data for coals from Vancouver Island (Van De Flier-Keller and Dumais 1988) and for coals from northeastern and southeastern British Columbia (Grieve 1991) (Figure 9). It is obvious from Figures 8 and 9 that the distribution of trace elements in crustal rocks,

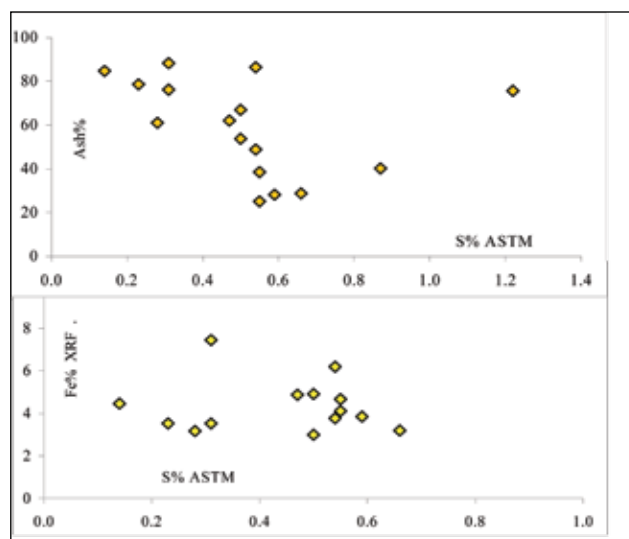


Figure 6: Association of sulphur with ash and iron; data from Union Bay, Cedar Cove, and Slag Point.

shales, and coals is similar. It appears that average element concentrations for coal waste are generally similar to world coal values (Figure 9) and a bit higher than Vancouver Island fresh coal values. The waste coal material has much higher ash concentrations than these suites of coal samples and probably should be compared to the average shale data (Figure 8).

There is no evidence of major enrichment or depletion of elements in the waste coal material, except for possibly enrichment in copper and chromium, which are both higher than the average values for Vancouver Island and world coals (Figure 9).

### Trace Element Associations

The association of trace elements for the various areas is demonstrated using linear correlation matrixes. This works well in most cases but can be misleading when the data contain a few very high or low values that overly influence linear correlations. Correlation matrixes are constructed for the 3 study areas—Union Bay, Cedar Cove, and Ladysmith (Tables 5, 6, and 7). These tables help identify elements that have an ash association or a sulphur (possibly pyrite) association. Most of the elements have a negative association with ash, indicating a coal or sulphide association. Plots for copper (Figure 10) indicate that copper has a weak negative correlation with ash and a correlation with sulphur that is possibly positive at low concentrations but negative at high concentrations (secondary sulphate sulphur). Copper also has no correlation with iron (Figure 10), which does not support a sulphide association. The association of copper in samples is therefore not clear, but it may have been released from sulphides and since bound to the organic material. The association of chromium is not

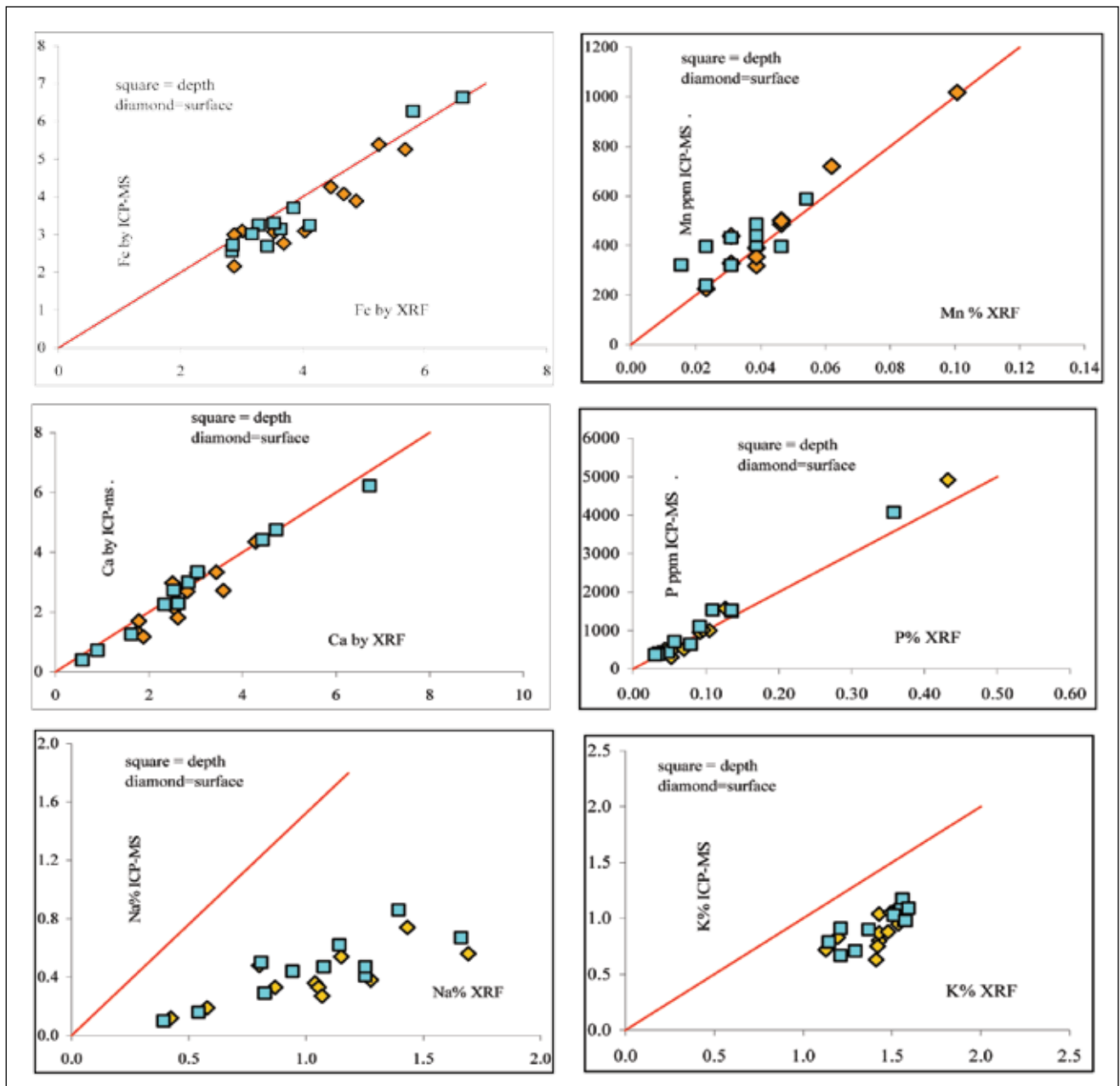


Figure 7: Comparison of Fe, Ca, Na, and K analyses by XRF and ICP-MS.

clear; it has a negative correlation with ash and no correlation with sulphur (Tables 5 and 6), though it does correlate with other trace metals. Copper may have been bound to the organic material after being released from sulphides.

Mercury is a trace element of general concern; however, in this study only 2 analyses were above the detection limit of 10 ppb, and they were both less than 20 ppb.

Arsenic is often associated with pyrite, and in this study there is no correlation with ash and, except for the 2 high values for samples 664 and 665 (Table 4), only a weak correlation with sulphur (Figure 11). There is no explanation for the 2 high arsenic values.

Only 2 elements (chromium and copper) are above both world averages (Clarke and Sloss 1992) and values from the Nanaimo and Comox Basins (Van Der Flier-Keller and Dumais 1988) (Figure 9). These elements do not correlate with sulphur or ash but appear to correlate with other trace metals (Tables 5, 6, and 7). It appears that they are not present in sulphides but may be bound to the organic material.

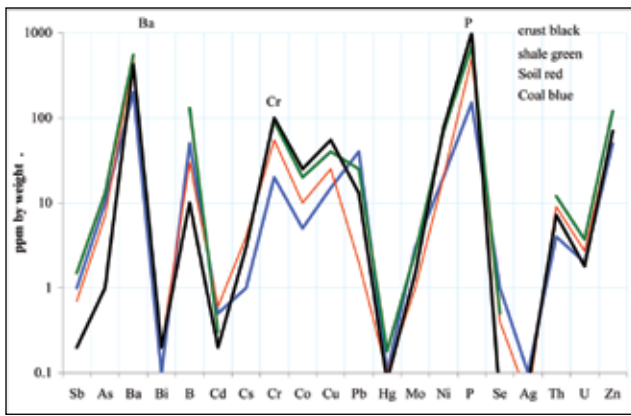


Figure 8: Average trace element data from Clark and Sloss (1992).

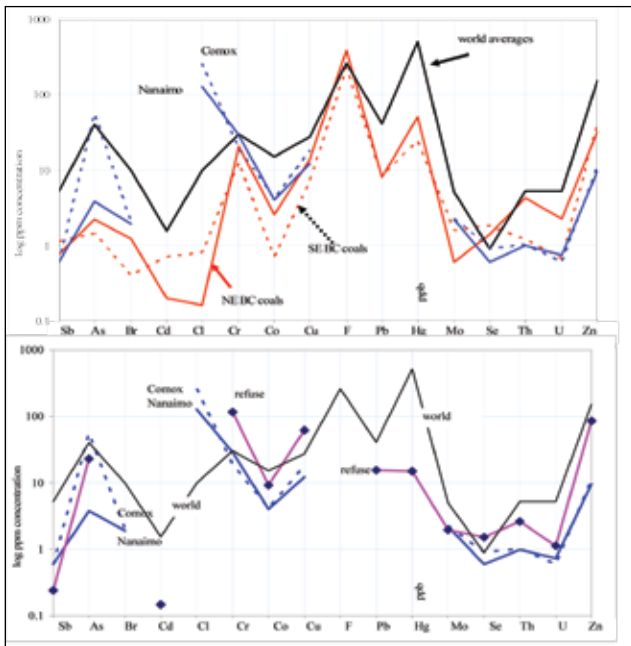


Figure 9: Trace elements concentrations in coals and waste material (BC and world data).

### Depth Profile Data

A number of small trench samples were collected at Union Bay, Cedar Cove, and Ladysmith. At each location a sample was collected at surface, a second at about 20 cm, and sometimes a third at about 50 cm depth. Data available for the sets of samples include total ash, major oxide, and trace metal concentrations. The data from Union Bay are displayed in a number of plots (Figure 12 a, b, c, d, and e). Major elements are plotted for some of the profiles—these are concentrations determined by ICP-MS and therefore represent the soluble component of the total concentration. Comparing the total concentration of iron and calcium (by XRF) to the ICP-MS concentration does not indicate a change in concentrations with depth or a change in the proportions extracted by acid leach and ICP-MS analysis

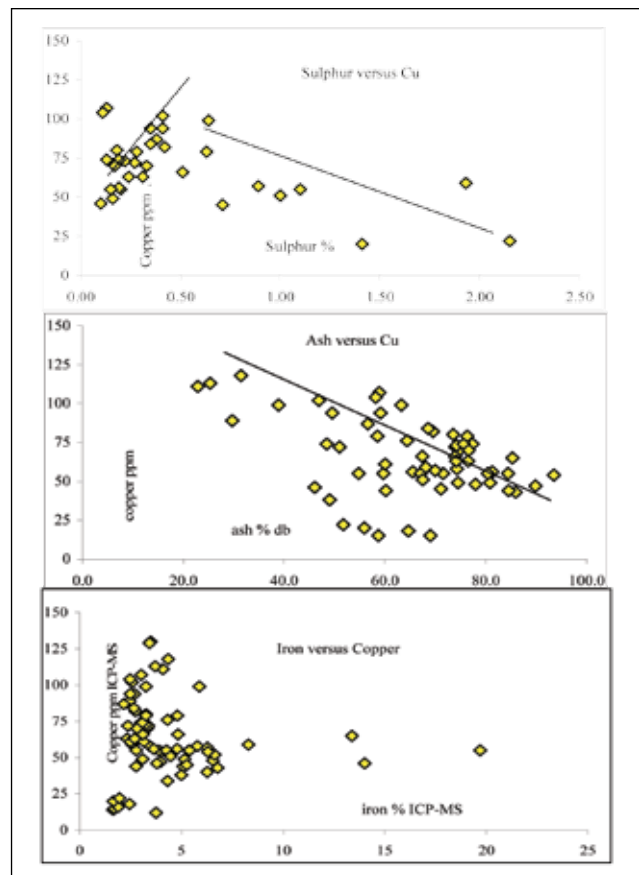


Figure 10: Copper versus sulphur, ash, and iron.

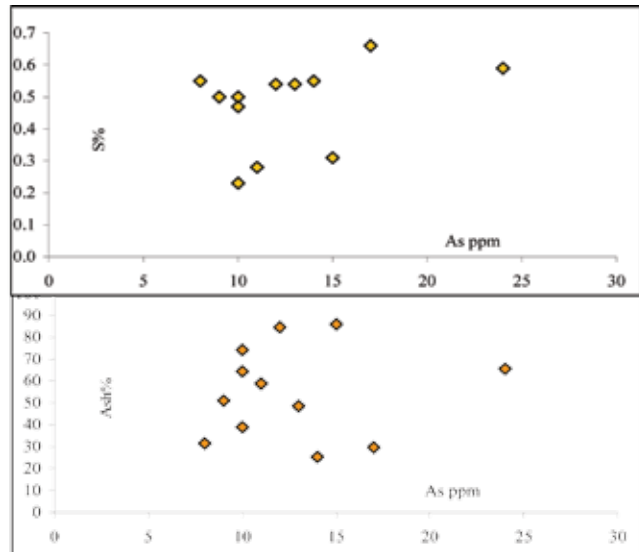


Figure 11: Relationship of arsenic with ash and sulphur.

(Figure 7). For both elements, most of the iron and calcium is acid-leachable. Trace element concentrations do not vary much with depth, indicating a lack of mobility or that any mobile component has already moved on. Ash contents of all samples are high, with little variation with depth.

**TABLE 5: CORRELATION MATRIX FOR TRACE ELEMENTS, UNION BAY AREA.**

x	ash	As	Ba	Bi	Cd	Co	Cr	Cu	Ga	Mo	Ni	P	Pb	Sb	Sc	Sr	Th	U	S	Zn
ash	1.00																			
As	-0.65	1.00																		
Ba	<b>-0.79</b>	<b>0.92</b>	1.00																	
Bi	-0.42	-0.20	-0.07	1.00																
Cd	0.11	-0.50	-0.24	0.29	1.00															
Co	<b>0.48</b>	-0.35	-0.20	-0.41	0.68	1.00														
Cr	-0.33	0.61	<b>0.73</b>	-0.27	-0.12	0.28	1.00													
Cu	0.06	0.05	0.23	-0.34	0.56	<b>0.78</b>	0.56	1.00												
Ga	<b>-0.80</b>	0.66	<b>0.87</b>	0.09	0.03	-0.08	<b>0.72</b>	0.44	1.00											
Mo	-0.39	0.19	0.24	0.18	-0.27	-0.51	-0.21	-0.35	0.29	1.00										
Ni	0.07	0.17	0.33	-0.47	0.37	<b>0.78</b>	<b>0.75</b>	<b>0.95</b>	0.47	-0.37	1.00									
P	0.22	-0.04	0.08	-0.35	0.11	0.49	0.54	<b>0.72</b>	0.33	-0.22	<b>0.74</b>	1.00								
Pb	<b>-0.86</b>	0.43	<b>0.70</b>	0.46	0.22	-0.20	0.40	0.23	<b>0.87</b>	0.41	0.18	0.18	1.00							
Sb	-0.61	<b>0.80</b>	0.64	0.09	-0.48	-0.52	0.30	-0.23	0.43	0.20	-0.15	-0.40	0.17	1.00						
Sc	<b>-0.75</b>	0.36	0.66	0.35	0.30	-0.03	0.56	0.44	<b>0.93</b>	0.32	0.41	0.34	<b>0.92</b>	0.16	1.00					
Sr	0.12	-0.06	-0.15	0.10	-0.28	-0.07	0.13	0.00	-0.15	-0.61	0.03	-0.02	-0.34	0.27	-0.16	1.00				
Th	<b>-0.91</b>	0.47	0.69	0.54	0.06	-0.38	0.29	0.05	<b>0.84</b>	0.59	0.01	0.01	<b>0.96</b>	0.41	<b>0.88</b>	-0.37	1.00			
U	<b>-0.73</b>	0.23	0.43	0.48	-0.21	-0.54	0.16	-0.19	0.64	0.69	-0.18	<b>0.00</b>	<b>0.77</b>	0.19	<b>0.74</b>	-0.18	<b>0.86</b>	1.00		
S	-0.05	-0.28	-0.43	0.39	-0.09	-0.49	-0.72	-0.61	-0.37	0.25	-0.72	-0.64	-0.20	0.23	-0.29	-0.03	0.01	0.12	1.00	
Zn	0.46	-0.46	-0.27	-0.28	0.62	<b>0.85</b>	0.26	<b>0.83</b>	0.04	-0.41	<b>0.77</b>	<b>0.78</b>	-0.05	-0.66	0.17	0.04	-0.24	-0.28	-0.49	1.00

**TABLE 6: CORRELATION MATRIX FOR TRACE ELEMENTS, CEDAR COVE AREA.**

x	ash	As	Ba	Bi	Cd	Co	Cr	Cu	Ga	Mo	Ni	P	Pb	Sb	Sc	Sr	Th	U	S	Zn
ash	1.00																			
As	0.16	1.00																		
Ba	-0.36	-0.53	1.00																	
Bi	<b>-0.74</b>	-0.02	0.53	1.00																
Cd	-0.72	0.01	0.22	<b>0.82</b>	1.00															
Co	-0.13	0.66	-0.28	0.11	0.17	1.00														
Cr	<b>-0.78</b>	0.04	0.25	0.40	0.46	0.44	1.00													
Cu	<b>-0.86</b>	0.00	0.39	0.62	0.54	0.45	<b>0.88</b>	1.00												
Ga	<b>-0.82</b>	-0.09	0.40	0.57	0.41	0.34	<b>0.82</b>	<b>0.90</b>	1.00											
Mo	<b>-0.84</b>	0.16	0.17	0.67	0.59	0.49	0.73	<b>0.86</b>	<b>0.74</b>	1.00										
Ni	-0.21	0.51	-0.17	0.10	0.18	<b>0.88</b>	0.64	0.53	0.54	0.44	1.00									
P	<b>-0.85</b>	0.12	0.15	<b>0.77</b>	<b>0.93</b>	0.31	0.67	<b>0.73</b>	0.58	<b>0.80</b>	0.32	1.00								
Pb	-0.59	-0.16	0.64	<b>0.79</b>	<b>0.81</b>	-0.06	0.43	0.48	0.40	0.35	0.05	0.68	1.00							
Sb	<b>-0.74</b>	-0.31	0.65	0.54	0.41	-0.02	0.66	0.68	0.64	0.59	0.09	0.50	0.63	1.00						
Sc	<b>-0.89</b>	0.00	0.32	<b>0.72</b>	0.64	0.44	<b>0.82</b>	<b>0.92</b>	<b>0.94</b>	<b>0.86</b>	0.56	<b>0.78</b>	0.49	0.60	1.00					
Sr	<b>-0.84</b>	0.08	0.08	<b>0.72</b>	<b>0.88</b>	0.18	0.60	0.67	0.52	<b>0.77</b>	0.18	<b>0.97</b>	0.59	0.38	<b>0.73</b>	1.00				
Th	<b>-0.87</b>	-0.14	0.49	<b>0.82</b>	<b>0.72</b>	0.30	0.66	<b>0.86</b>	<b>0.82</b>	<b>0.74</b>	0.31	<b>0.76</b>	0.67	0.68	<b>0.90</b>	<b>0.70</b>	1.00			
U	<b>-0.76</b>	-0.19	0.47	0.41	0.25	0.27	<b>0.75</b>	<b>0.79</b>	<b>0.73</b>	<b>0.75</b>	0.26	0.45	0.27	<b>0.82</b>	<b>0.71</b>	0.41	0.69	1.00		
S	<b>0.11</b>	<b>0.90</b>	-0.67	-0.19	-0.03	0.45	0.05	-0.04	-0.17	0.13	0.31	0.13	-0.24	-0.29	-0.11	0.16	-0.25	-0.19	1.00	
Zn	0.45	0.54	-0.19	-0.20	-0.16	0.70	-0.03	-0.05	-0.08	-0.20	0.66	-0.21	-0.10	-0.37	-0.08	-0.36	-0.11	-0.28	0.26	1.00

**TABLE 7: CORRELATION MATRIX FOR TRACE ELEMENTS, LADYSMITH AREA.**

x	ash	As	Ba	Bi	Cd	Co	Cr	Cu	Ga	Mo	Ni	P	Pb	Sb	Sc	Sr	Th	U	S	Zn
ash	1.00																			
As	0.05	1.00																		
Ba	-0.11	-0.04	1.00																	
Bi	0.17	0.19	<b>0.82</b>	1.00																
Cd	0.20	0.00	<b>0.88</b>	0.62	1.00															
Co	0.41	-0.29	0.35	0.04	0.64	1.00														
Cr	-0.32	-0.43	0.37	-0.15	0.32	0.66	1.00													
Cu	<b>-0.86</b>	-0.13	0.49	0.12	0.31	-0.06	0.59	1.00												
Ga	-0.19	0.35	<b>0.84</b>	<b>0.81</b>	0.68	0.13	0.10	0.44	1.00											
Mo	<b>0.70</b>	-0.17	-0.30	-0.14	-0.28	0.48	0.09	-0.52	-0.38	1.00										
Ni	0.06	-0.16	0.28	-0.18	0.52	<b>0.82</b>	<b>0.75</b>	0.20	0.07	0.12	1.00									
P	0.32	-0.14	-0.68	-0.54	<b>-0.72</b>	0.17	0.02	-0.42	-0.53	0.69	0.00	1.00								
Pb	0.27	-0.14	-0.46	-0.20	-0.58	-0.21	-0.30	-0.36	-0.33	0.34	-0.43	0.62	1.00							
Sb	0.10	-0.14	0.57	0.67	0.31	0.06	-0.06	0.08	0.54	-0.07	-0.30	-0.38	0.20	1.00						
Sc	-0.63	0.06	<b>0.76</b>	0.42	0.71	0.18	0.52	<b>0.85</b>	<b>0.78</b>	-0.56	0.35	-0.58	-0.54	0.24	1.00					
Sr	-0.67	-0.27	0.26	-0.15	0.27	0.12	0.56	0.66	0.11	-0.43	0.43	-0.42	-0.76	-0.23	0.60	1.00				
Th	-0.68	0.25	0.37	0.31	0.24	-0.24	0.06	0.69	0.69	-0.52	-0.11	-0.28	-0.25	0.13	0.77	0.37	1.00			
U	-0.68	-0.24	-0.32	-0.38	-0.57	-0.47	0.10	0.52	-0.19	-0.27	-0.26	0.19	0.41	-0.05	0.11	0.18	0.38	1.00		
S	-0.57	0.28	-0.46	-0.44	-0.69	-0.43	-0.04	0.19	-0.12	-0.32	-0.18	0.19	0.07	-0.23	<b>0.01</b>	0.26	0.29	0.57	1.00	
Zn	0.69	-0.18	0.03	0.05	0.22	0.56	0.14	-0.40	-0.14	0.60	0.37	0.45	0.46	-0.02	-0.32	-0.58	-0.49	-0.28	-0.60	1.00

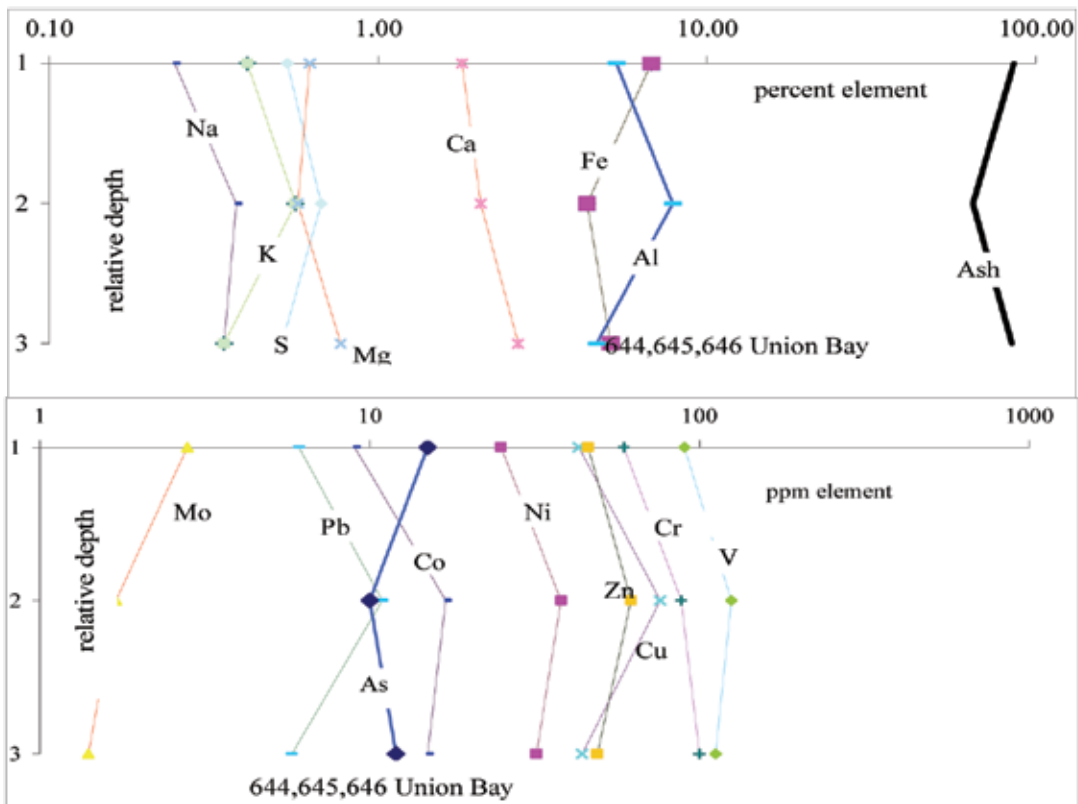
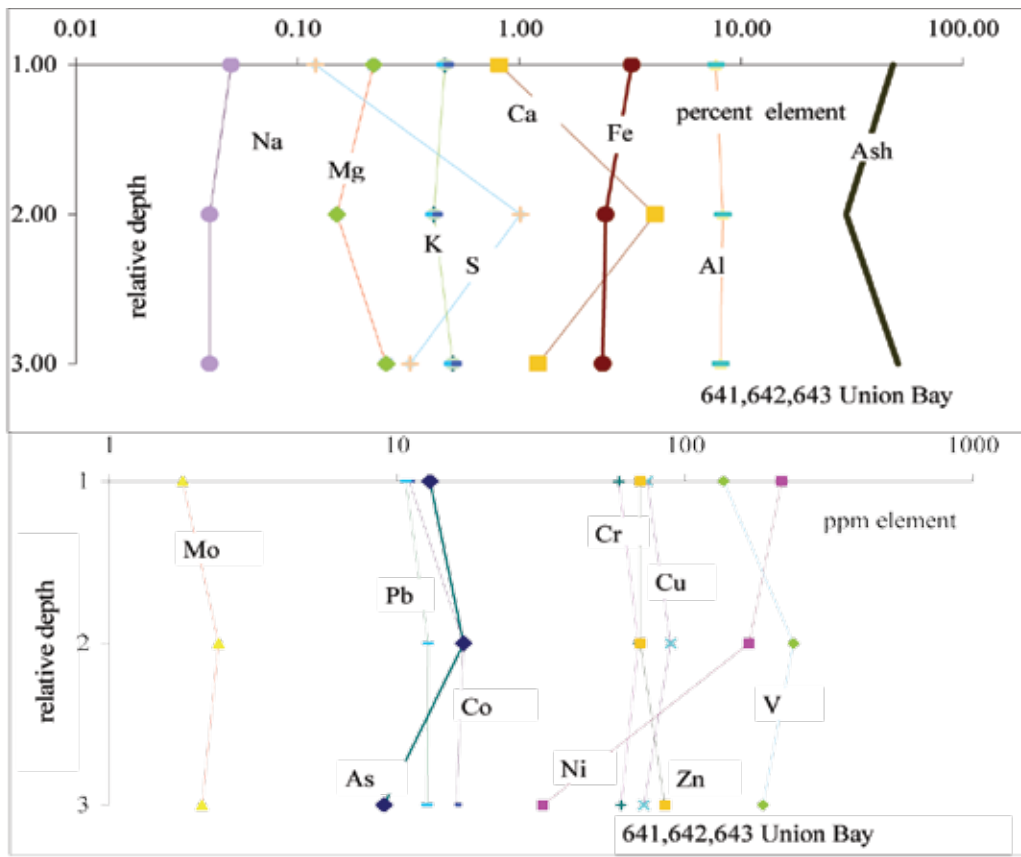


Figure 12a: Depth profile data for major and trace elements for locations Union Bay. Relative depths are surface and approximately 20 cm and 50 cm.

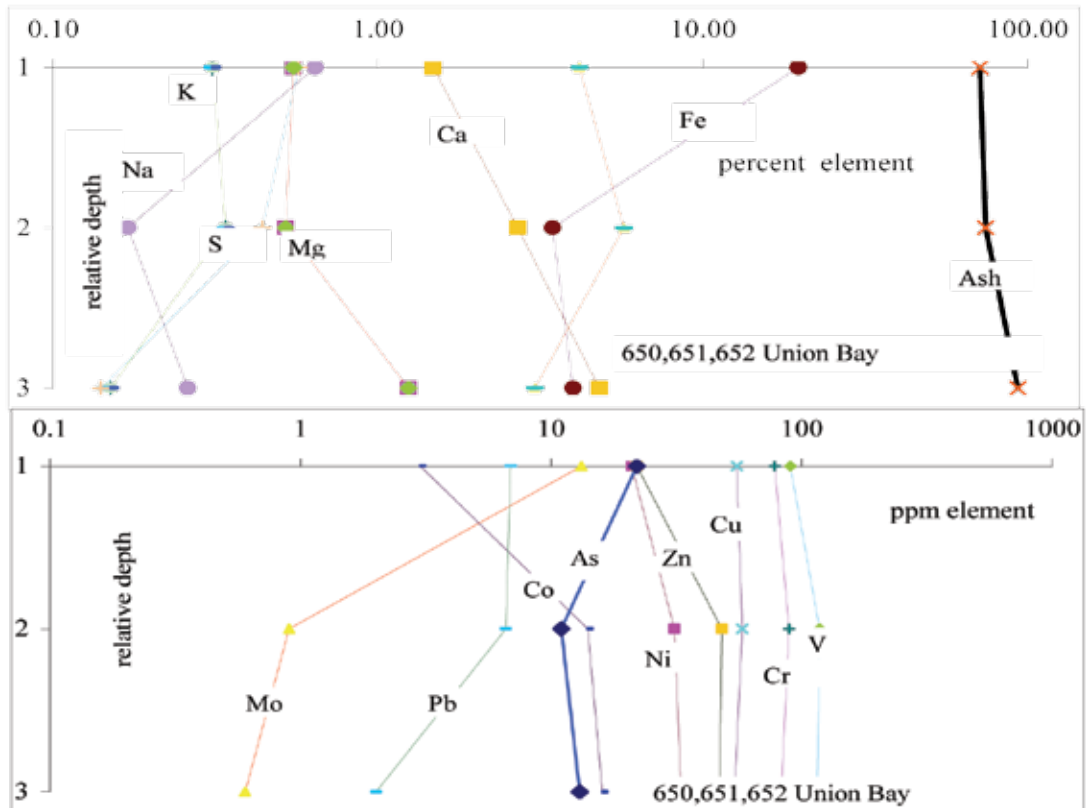
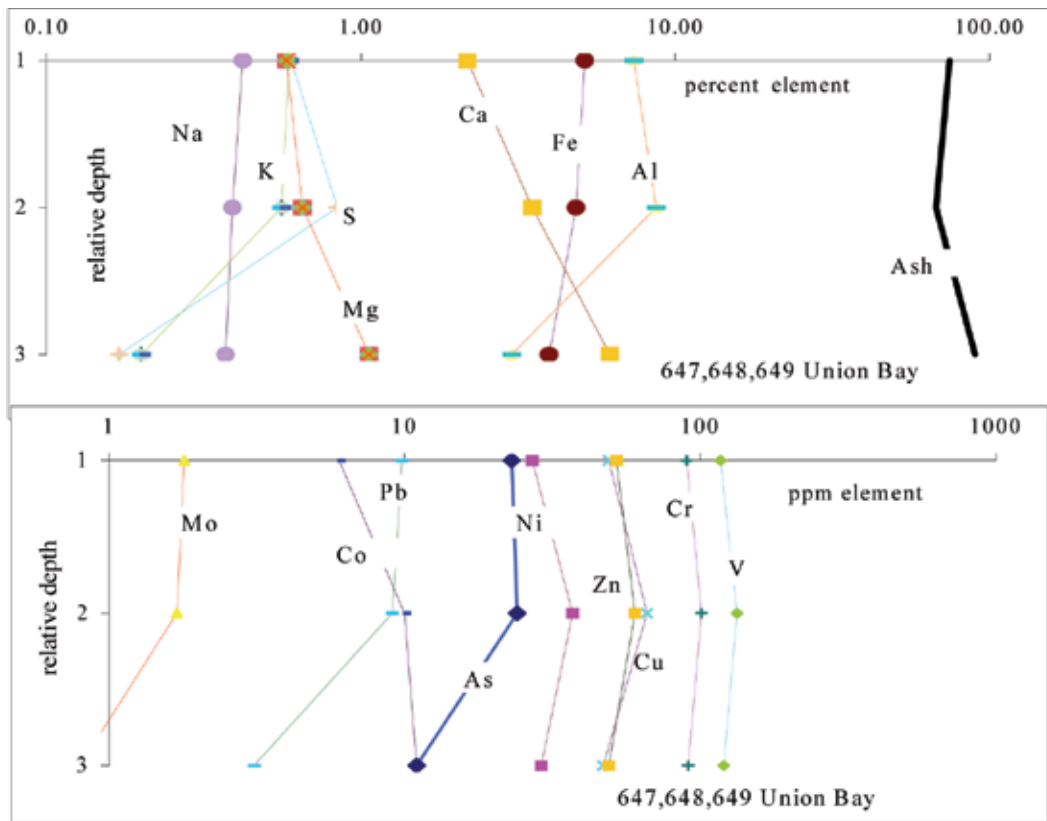


Figure 12b: Depth profile data for major and trace elements for locations Union Bay. Relative depths are surface and approximately 20 cm and 50 cm.

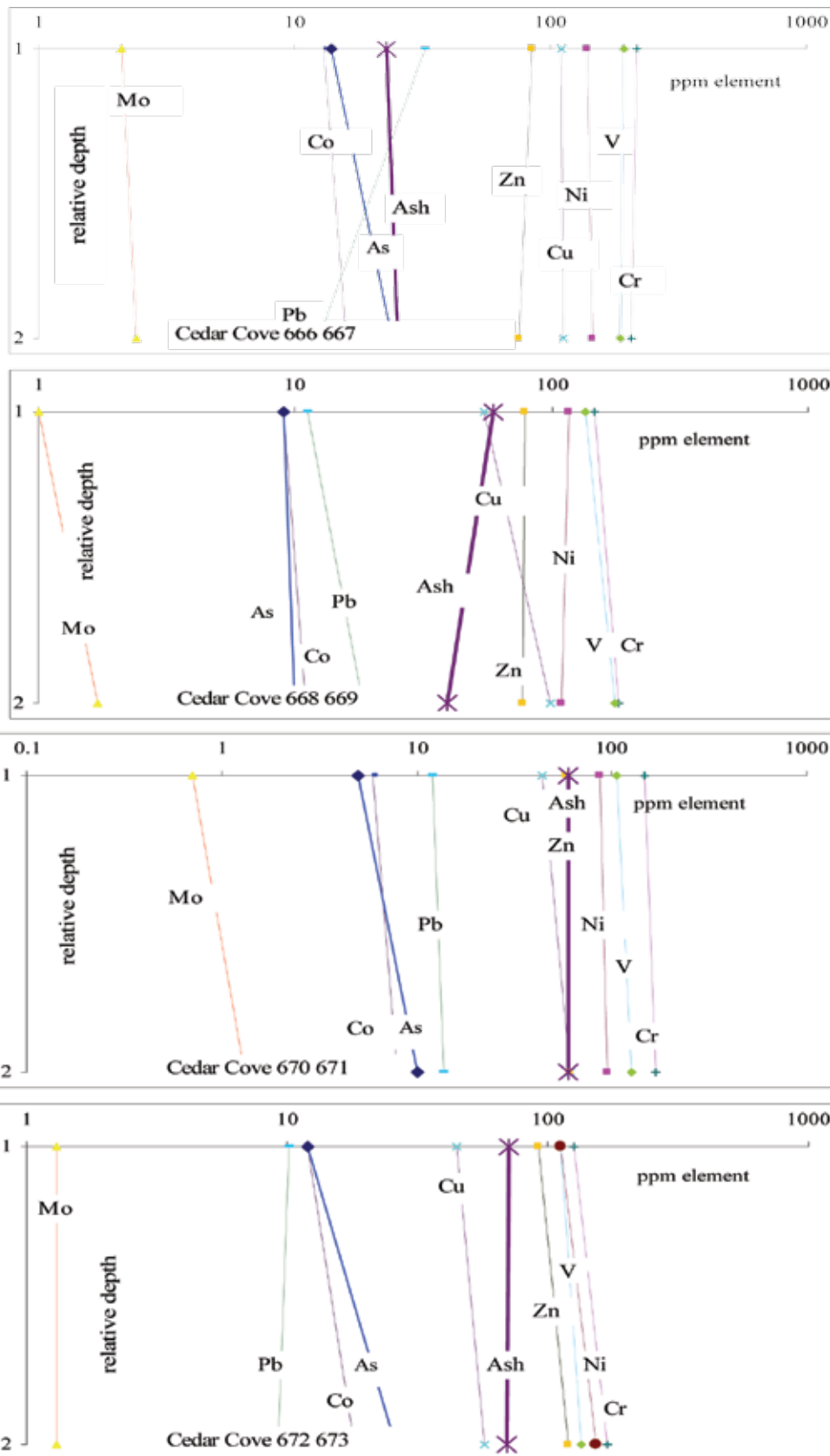


Figure 12c: Depth profile data for major and trace elements for locations Cedar Cove. Relative depths are surface and approximately 20 cm and 50 cm.

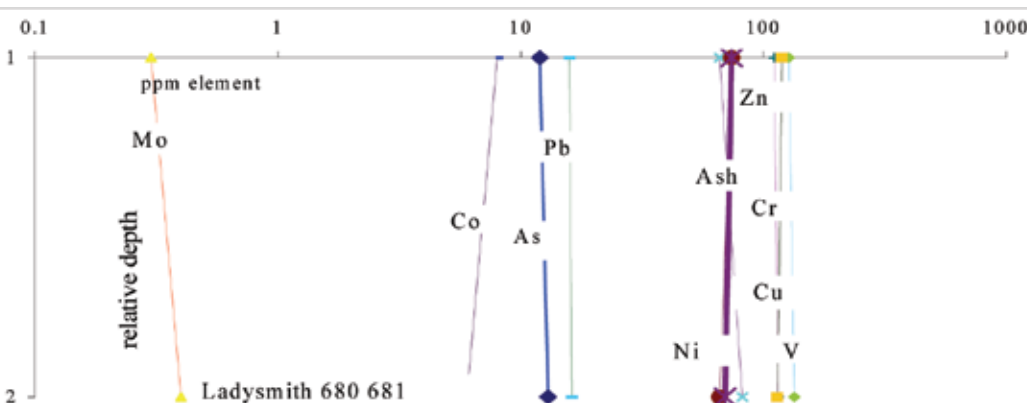
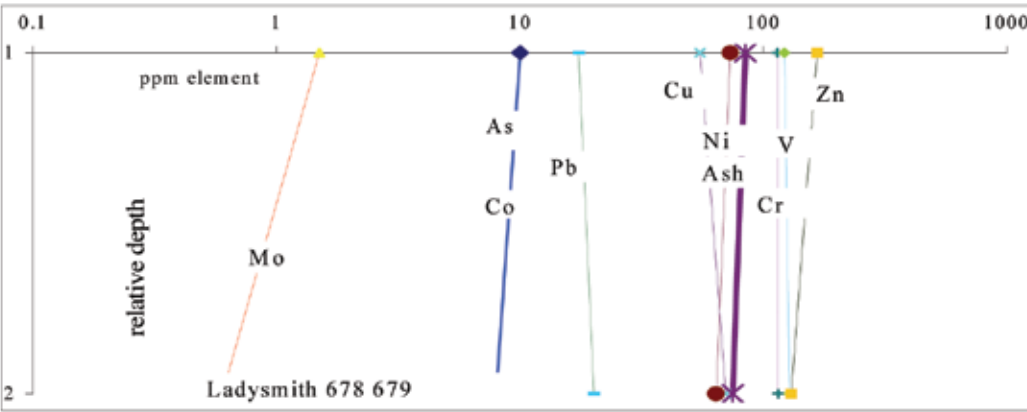
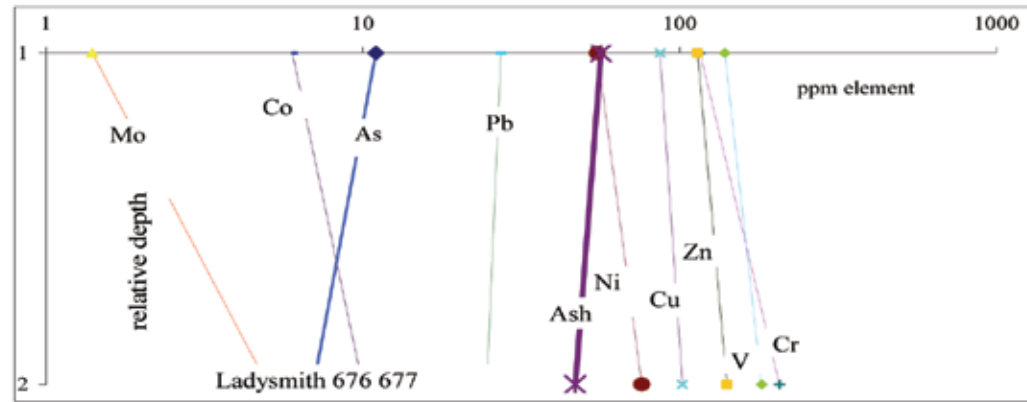
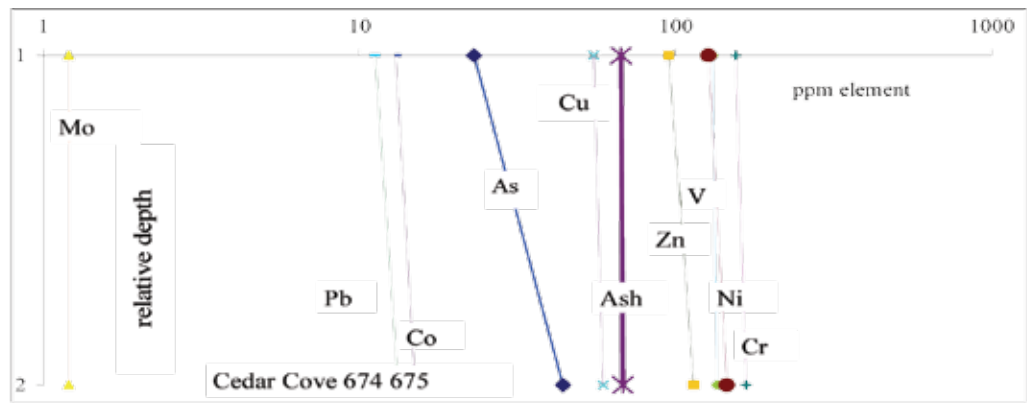


Figure 12d: Depth profile data for major and trace elements for locations Ladysmith. Relative depths are surface and approximately 20 cm and 50 cm.

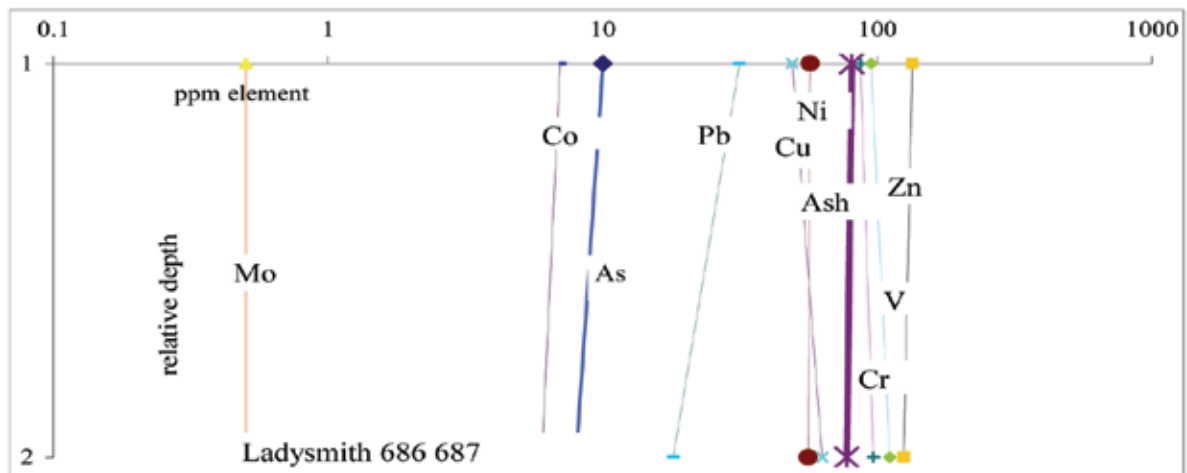
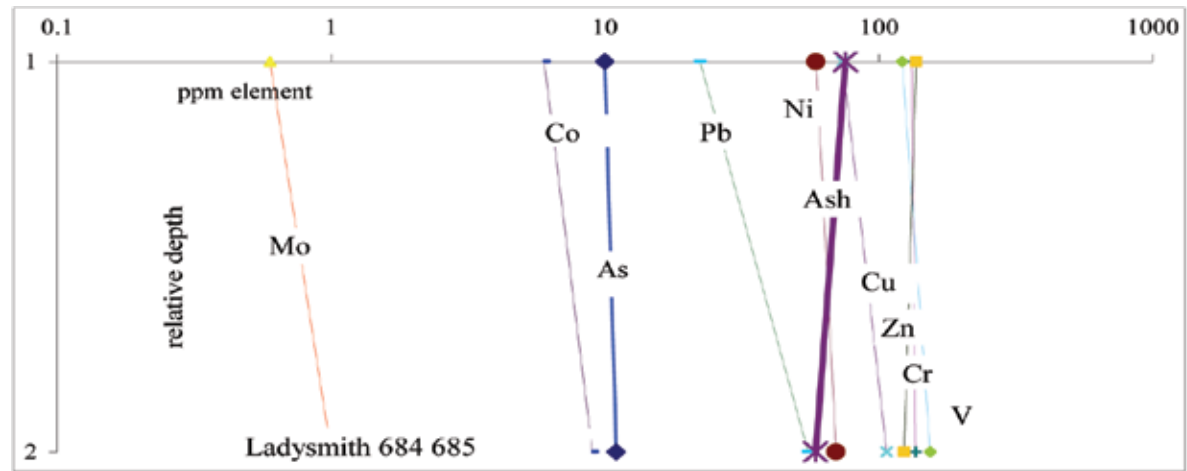
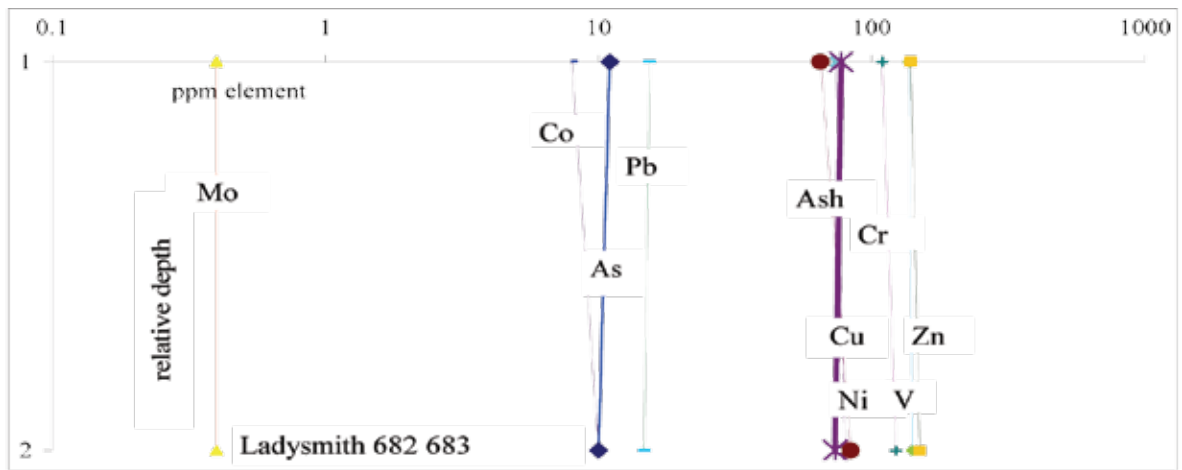
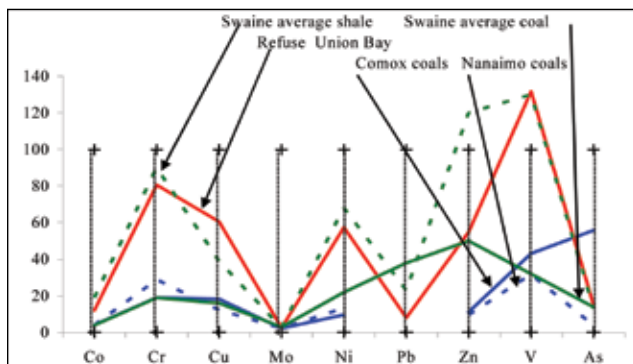


Figure 12e: Depth profile data for major and trace elements for locations Ladysmith. Relative depths are surface and approximately 20 cm and 50 cm.

Union Bay beach is characterized by heavy iron staining and samples (644, 645, 646) (647, 648, 649), and (650, 651, 652) were collected at different depths in 3 test holes dug on this beach. There are no major changes in trace or major element chemistry with depth down to about 0.7 m at the bottom of the holes. Samples of the heavily rust-stained section at the surface have higher concentrations of iron and molybdenum, and in all 3 profiles sulphur decreases with depth. The material is weathered refuse from which most of the pyrite probably has been oxidized to yield sulphates and iron oxides. Samples generally have high ash contents, and this influences major oxide and trace metal concentrations in terms of comparisons to coal with less ash. Swaine (1990) provides a table of average trace element concentration in coal, soils, and shale, and Van Der Flier-Keller and Goodarzi (1992) provide average trace element and major oxide contents for coals from the Comox and Nanaimo coalfields. Data from these sources are plotted with average data from Union Bay (Figure 13). It is apparent that the Union Bay data plot in between average coal and average shale and have higher contents of most elements than do the Nanaimo and Comox coals. This is probably because the Union Bay samples have higher ash contents, which range from 30% to 94% and are generally higher than the coal samples analysed by Van Der Flier-Keller and Goodarzi (1992).



**Figure 13: Comparison of trace metal data for Union Bay and Comox and Nanaimo coals.**

### Sized Data

A number of samples were split, and one split from each sample was screened into coarse and fine fractions (8-mesh). Both the original split and the fine-fraction split were analysed by XRF and ICP-MS. Comparing analyses for the original and fine-fraction splits should provide indications of fractionation of elements by particle size and

possible mobility of trace elements out of fine fractions. Data (Figure 14 a and b) do not indicate any consistent pattern of element distribution. Major element concentrations change little from the original split (numbered 1 on the x axis in the figures) to the fine-fraction split (numbered 2 on the x axis in the figures). Trace element concentrations are more variable but still do not provide a consistent pattern.

### Heat Value

The heat value of coal is dependent on organic carbon and volatile matter contents of samples. It decreases with oxidation of coal and destruction of volatile matter, but generally the decrease is not large. In this study, the heat value of the samples has not been degraded, based on a plot of calorific value (dry basis) versus ash (dry basis) (Figure 15), which compares heat values for fresh coals from the Comox and Nanaimo Basins (Coal Quality Catalogue 1992) to the samples in this study. The zero-ash heat value for all samples averages about 7929 kcal/kg, compared to 7993 kcal/kg for fresh coal samples from Nanaimo and Comox coal basins. The main influences on heat value of coal are ash and moisture contents. A sample with 20% ash (dry basis) and 10% water would have a gross calorific value of 5555 kcal/kg (Figure 15). This is a useable heat value, though the ash chemistry becomes important, because boilers must handle and remove large quantities of fly ash or slag.

As an aside, it is important to understand the difference between measured heat values (gross as-received, or GAR) and useable heat (net as-received, or NAR). In a power plant, the moisture associated with the coal is heated and then converted to steam when the coal is burnt. This heat is generally lost, and this is part of the reason that NAR heating value is less than GAR heating value. A gram of water at 20 °C will require 620 calories if it is heated and turned into steam. Consequently, coal with 10% moisture will lose, when burnt, about 62 calories because of water. This means that a 40% ash sample with about 5000 kcal/kg air-dried basis (adb) will actually have about 6% less useable heat, in part because there is 10% less material and in part because of the lost 62 calories.

Tidal samples from Union Bay appear to have higher heat values than other samples at comparable ash contents (Figure 15). These samples (644, 645, and 646) were collected from a flat area of beach covered by a prominent iron-oxide staining. The heat value may be influenced by recent organic matter.

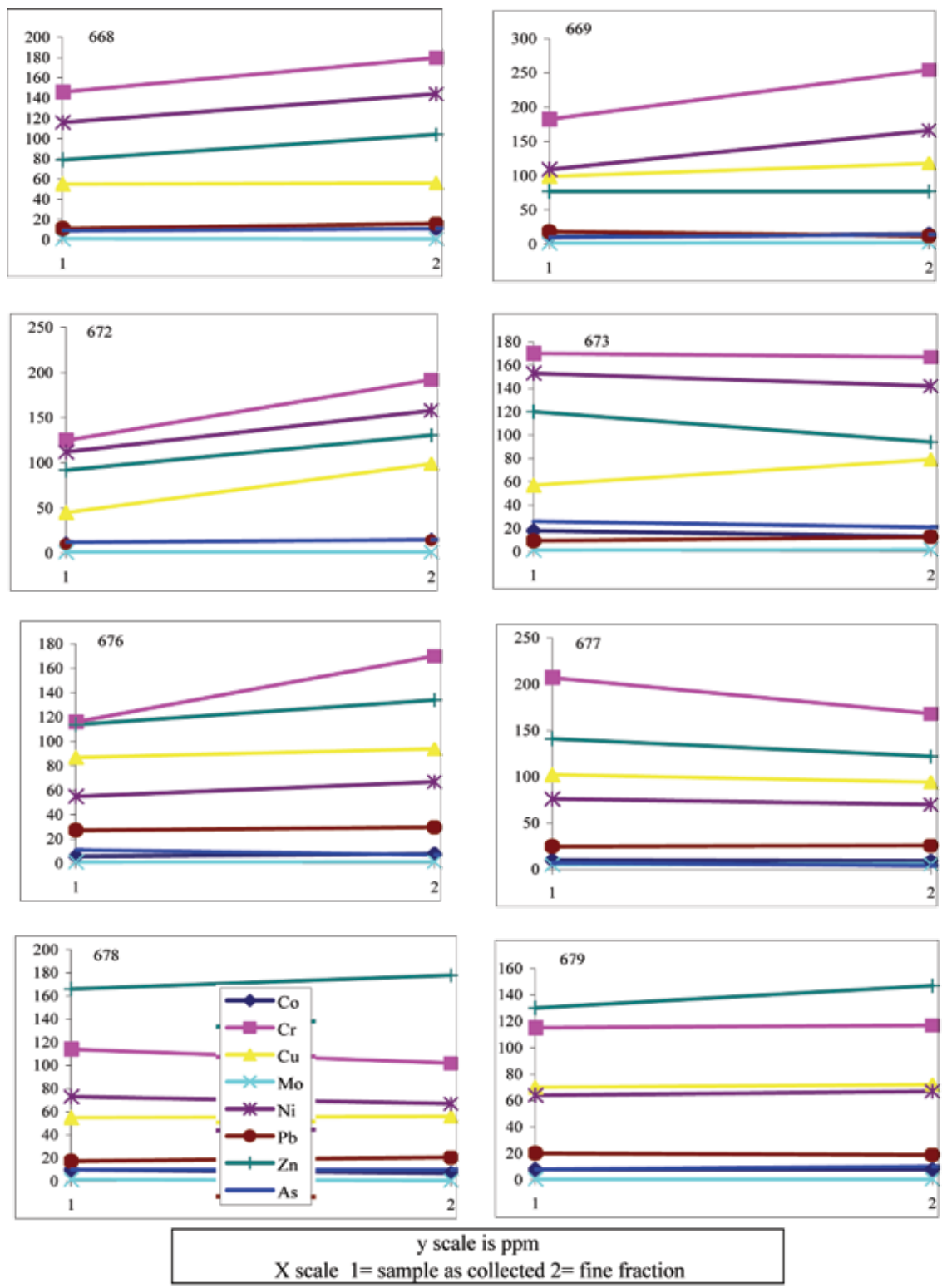


Figure 14a: Comparison trace metal data from original samples and fine fraction of samples.

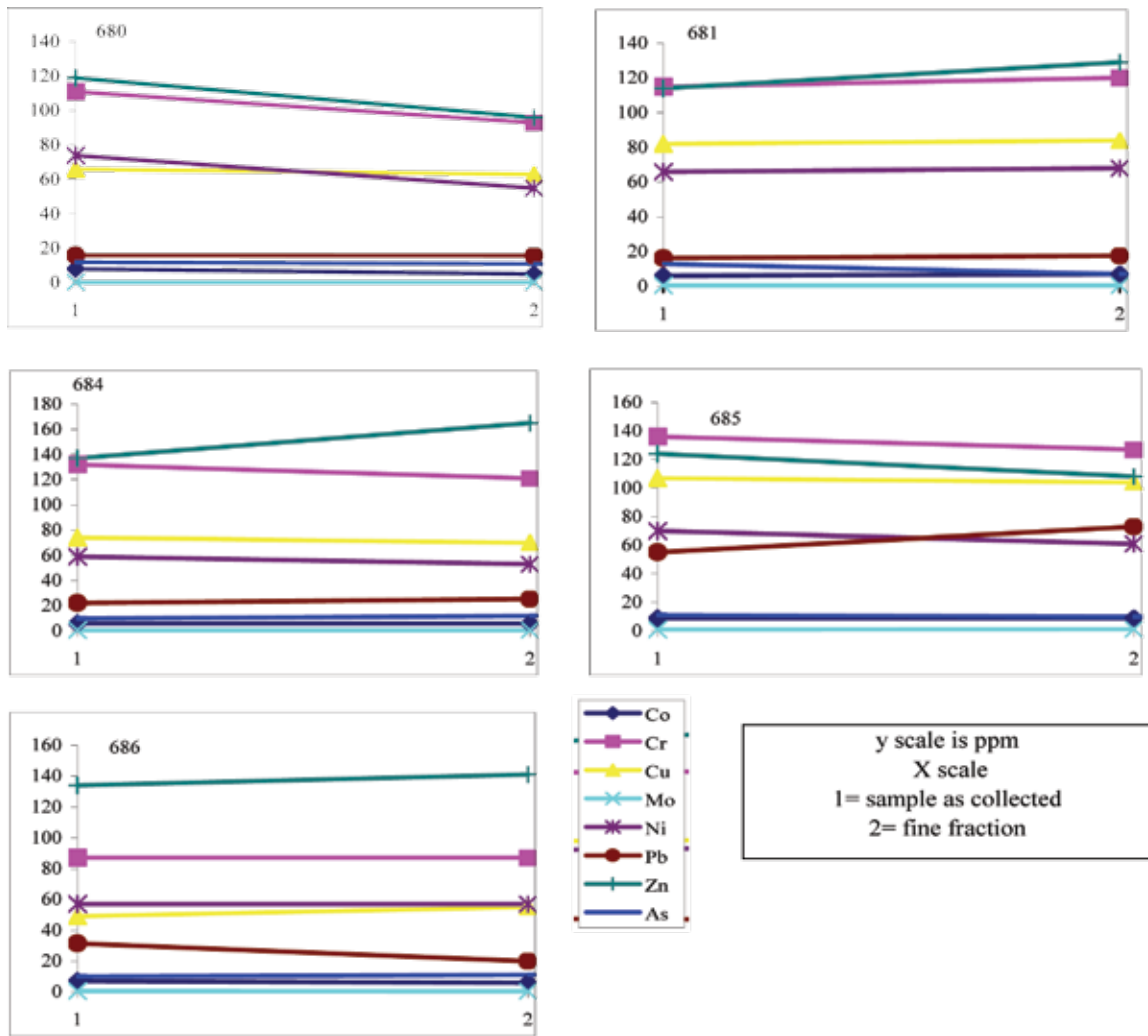


Figure 14b: Comparison trace metal data from original samples and fine fraction of samples.

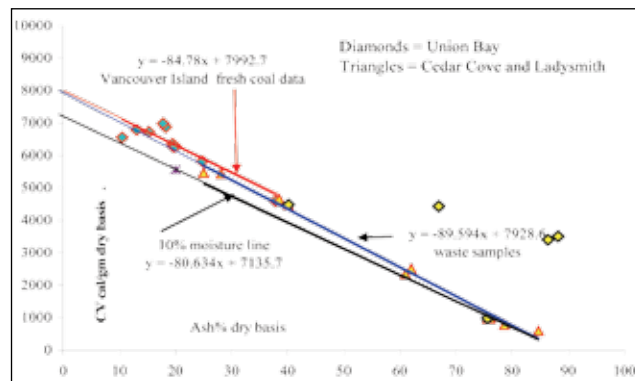


Figure 15: Heat value of fresh Vancouver Island coals and weathered samples from Union Bay, Cedar Cove, and Ladysmith Slag Point.

## CONCLUSIONS

The data provide some background information on the major and trace element chemistry of the coal refuse material on and near beaches along the east coast of Vancouver Island. Generally, coal waste is fairly benign, unless it contains high concentrations of pyrite that can release trace metals and generate acid-rock drainage. Samples collected in this study generally do not have abnormally high concentrations of trace metals or high concentrations of pyrite. There is no indication that they are releasing metals into the environment. It is possible that all or most of the pyrite is already oxidized and trace metals released and migrated out of the samples.

## ACKNOWLEDGEMENTS

Samples were collected in conjunction with a study by Remi Odense, Risk Assessment and Remediation, Ministry of the Environment, BC Government. Warren Walsh assisted with sampling in the field, and Jessica Verhagen helped with sample preparation.

## REFERENCES

- Clarke, L.B. and Sloss, L.L. (1992): Trace elements emissions from coal combustion and gasification; International Energy Agency (IEA) Coal Research Publication 49.
- Coal Quality Catalogue (1992): *British Columbia Ministry of Energy, Mines and Petroleum Resources*, Information Circular 1992-20.
- Gardner, S.L. (1997): Coal Resources and Coal Mining on Vancouver Island; *British Columbia Ministry of Employment and Investment*, BC Geological Survey, Open file 1997-19.
- Grieve, D.A. and Goodarzi, F. (1994): Trace elements in coals of the East Kootenay and Peace River coalfields, *British Columbia; British Columbia Ministry of Energy, Mines and Petroleum Resources*, Open file 1994-15.
- Swaine, D.J. (1990): Trace Elements in Coal; *Butterworths*, London. 1-273.
- Van Der Flier-Keller, E. and Dumais, S. (1988): Inorganic matter content and specialized element potential of the Nanaimo and Comox coalfields, Vancouver Island (92G,F,K) *British Columbia Ministry of Energy, Mines and Petroleum Resources*, Geological Fieldwork 1987, pages 435–439.
- Van Der Flier-Keller, E. and Goodarzi, F. (1992): Regional variations in coal quality in the Canadian Cordillera; *Geological Society of America*; Special Paper 267, pages 165–175.

# A FIRST LOOK AT THE ELECTRICAL RESISTIVITY STRUCTURE IN THE NECHAKO BASIN FROM MAGNETOTELLURIC STUDIES WEST OF NAZKO, B.C. (NTS 092 N, O; 093 B, C, F, G)

Authors: J. Spratt<sup>1,2</sup> and J. Craven<sup>2</sup>

---

## ABSTRACT

*The Mesozoic Nechako sedimentary basin, located within the Intermontane belt of the Canadian Cordillera in central British Columbia, is a forearc basin deposited in response to terrane amalgamation along the western edge of ancestral North America. Limited exploration of the basin to date has indicated the potential for significant oil and gas reservoirs. An important impediment to hydrocarbon exploration, however, is the inability of traditional geophysical methods to see through the thick Neogene volcanic sequence burying the basin. As the magnetotelluric method is not hampered by these volcanics, 734 combined AMT and MT sites were recorded throughout the southern Nechako Basin in the fall of 2007. The survey was designed to evaluate the technique as a tool in both hydrocarbon exploration as well as geological characterization of the basin. Preliminary analyses of these data suggest that they are sensitive to variations in the depth extent of the sedimentary basin and that there are lateral changes in the conductivity structure within the sediments. These lateral variations could be attributed to compositional differences, the presence of fluids, or changes in porosity.*

Spratt J. and Craven J., (2008): A first look at the electrical resistivity structure in the Nechako Basin from magnetotelluric studies west of Nazko, B.C. (NTS 092 N, O; 093 B, C, F, G); Geoscience Reports 2008, B.C. Ministry of Energy, Mines and Petroleum Resources, pages 119-127.

<sup>1</sup>Geoscience BC, Vancouver, BC

<sup>2</sup>Geological Survey of Canada, Ottawa, ON

**Key Words:** Electromagnetics, magnetotellurics, Nechako Basin.

---

## INTRODUCTION

In response to the rapid spread and destructive effects of the mountain pine beetle, a number of projects designed to assess mineral and petroleum potential have been undertaken to develop economic diversification opportunities for forestry-based communities in the affected areas of British Columbia. The potential for hydrocarbons has been noted within several interior basins of British Columbia, including the Nechako Basin. A 1994 estimate by the Geological Survey of Canada, based on very limited information, suggested that the Nechako Basin may contain as much as a trillion cubic meters of gas and a billion cubic meters of oil, although these estimates are qualified as being highly speculative (Hannigan et al. 1994).

It has been shown that the magnetotelluric (MT) method can be useful in resolving geological structures less suitable for seismic methods, such as areas that are covered by volcanic or basaltic sequences, and that it may prove to be a useful tool in the exploration of hydrocarbons (Unsworth 2005; Spratt et al. 2006; Xiao and Unsworth 2006). In the fall of 2007, 734 combined broadband and high frequency MT sites were deployed throughout the Nechako Basin

(Figure 1). The primary objectives of the survey are to evaluate the technique as a tool both for oil and gas exploration and geological characterization of the Nechako Basin and to contribute to a better understanding of the potential for hydrocarbon resources in the region.

## GEOLOGICAL AND GEOPHYSICAL BACKGROUND

### *Geology of the Nechako Basin*

The Mesozoic Nechako Basin, located in the Intermontane Belt of the Canadian Cordillera, includes overlapping sedimentary sequences deposited in response to terrane amalgamation to the western edge of ancestral North America (Monger et al. 1972; Monger and Price 1979; Monger et al. 1982; Gabrielse and Yorath 1991). Regional transcurrent faulting and associated east-west extension, beginning in the Late Cretaceous, were accompanied by the extrusion of basaltic lava in Eocene and Miocene times to form a sheet that covers much of the basin at thicknesses varying

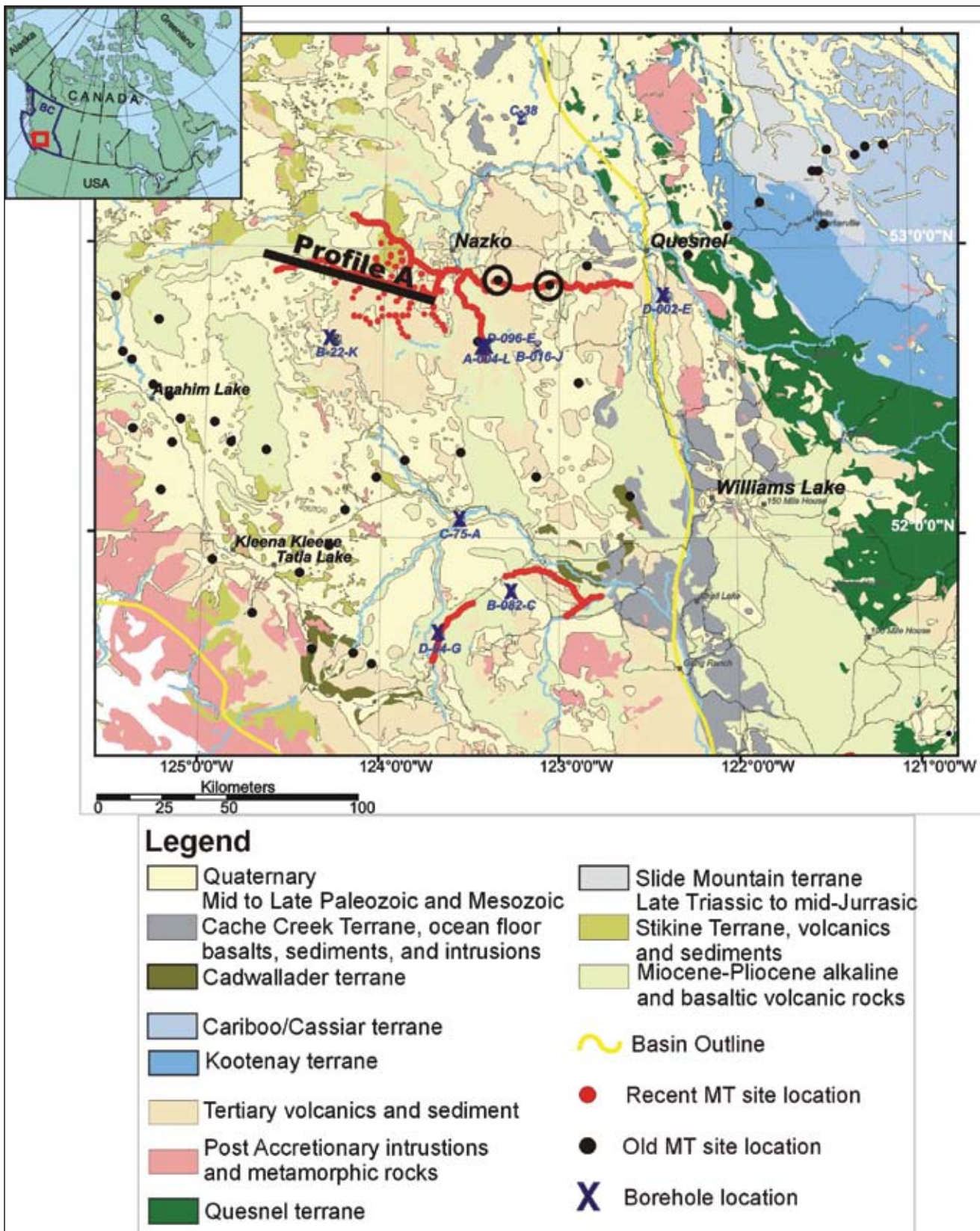


Figure 1: Map showing the location and geology of the Nechako Basin along with the locations of the boreholes, old MT sites, and the newly acquired MT sites. The black line shows the trace of profile A, and the black circles indicate the locations of sites ten 24, eo61, ten 21, and eo5 shown in Figure 3.

between 3 and 200 m (Mathews 1989; Andrews and Russell 2007). The main geological elements in the southern Nechako area include Miocene basalt, Tertiary volcanic and sedimentary rocks, and Cretaceous and Jurassic sedimentary rocks (Figure 1).

### ***Geophysical Studies***

The MT survey parameters, such as site locations, data ranges, and site spacing, were strongly influenced by early geophysical studies, such as gravity, magnetic, and resistivity measurements in borehole logs. In the early 1980s, a regional gravity survey was carried out by Canadian Hunter Exploration Limited that identified a gravity low in southern Nechako Basin. In the early 2000s, Bemex Consulting International confirmed this anomaly with ground gravity and magnetic data collected in the southern tip of the basin. In addition to these regional surveys, several boreholes were drilled throughout the southern portion of the basin between 1960 and 1986 (Figure 1), providing detailed geological information as well as a variety of borehole logs that included natural gamma-ray spectroscopy, neutron porosity, and resistivity.

Due to absorption and reflection effects, the presence of the surface basaltic flows and Tertiary volcanic rocks covering most of the region has, to date, prevented uniform and consistent seismic-energy penetration and complicated the magnetic interpretations. However, re-analysis with modern processing techniques of these data from the southernmost part of the Nechako Basin is yielding a better resolution of local structures (Hayward and Calvert 2007). New seismic information will soon be available from 7 long-term teleseismic stations deployed in the Nechako Basin as part of a joint project between the Geological Survey of Canada (Pacific), the BC Ministry of Mines, Energy and Petroleum Resources, and the University of Manitoba. Additionally, Geoscience BC is planning a Vibroseis® survey, and Natural Resources Canada an explosive-source seismic reflection investigation, which will both coincide closely with the MT survey locations. Information from these geophysical data will both complement and constrain the results and interpretations of the magnetotelluric survey.

More than 100 rock samples have been sent to John Katsube's Geological Survey of Canada petrophysical laboratory in Ottawa for measurement of the resistivities and porosities of key lithological units in the Nechako Basin. The intent of this analysis is to provide information on the primary electrical conduction mechanisms and level of electrical anisotropy of the different units. These, along with the resistivities from existing well logs, will place constraints on the conductivity models generated and make it possible to account for distortion due to anisotropy and static shift effects.

### ***MT method and previous studies***

The magnetotelluric (MT) method provides information on the electrical conductivity of the subsurface of the Earth by measuring the natural time-varying electric and magnetic fields at its surface (Cagniard 1953; Wait 1962; Jones 1992). At low frequencies, the signal is generated by interaction of solar winds with the ionosphere. At high frequencies, the signal is produced from distant lightning storms. The phase lags and apparent resistivities (MT response curves) can be calculated from the measured fields at various frequencies for each site recorded. The depth of penetration of these fields is dependent on frequency (lower frequencies penetrate more deeply) and the conductivity of the material (deeper penetration with lower conductivity), and therefore depth estimates can be made from the response curves beneath each site (Kearey and Brooks 1991). The frequency range recorded is therefore dependent on the target depth of interest. AMT (audio magnetotellurics) sensors measure data in the highest frequencies (10 000 to 5 Hz), where MT sensors measure lower frequencies (380 to 0.001 Hz).

As MT data are sensitive to changes in the resistivity of materials, the method can distinguish between some lithological units. For example, basalt and igneous basement rocks typically have electrical resistivity values of more than 1000 ohm-m, whereas sedimentary rocks are more conductive, with values of 1 to 1000 ohm-m. Aside from lithology, other factors are known to affect the overall conductivity of a specific unit in the crust. The presence of saline fluids, changes in porosity, and the presence of graphite films and interconnected metallic ores are all factors that can substantially increase the conductivities of rocks (Haak and Hutton 1986; Jones 1992). Because the method is sensitive to, but not impeded by, the surface volcanic rocks and can detect variations within the different units, it should prove useful in locating the boundaries of the Nechako Basin and defining the structure within. In addition to lithology, the MT method may be able to provide some estimate of bulk properties, such as porosity (Unsworth 2005; Xiao and Unsworth 2006). Measured resistivity and salinity can be used to estimate porosity through Archie's law.

Early magnetotelluric data, in the frequency ranges of 0.016 to 130 Hz, were collected by the University of Alberta in the 1980s (Majorwicz and Gough 1991). These data showed that the data were successful in penetrating the surficial basalts and revealed a conductive upper crust that was interpreted as saline water in pore spaces and fractures (Jones and Gough 1995). Since then, instrumentation improvements, as well as the development of signal processing algorithms and advancements in 2- and 3-dimensional modelling inversion programs, have significantly improved the ability of the MT method to image subsurface structures.

## DATA ANALYSIS

### Acquisition and Processing

The data were recorded during the fall of 2007 using MTU-5A systems manufactured by Geosystems Canada of Toronto. In general, 3 teams each deployed 6 sites per day, where 2 of the sites were telluric only, 2 of the sites were 5-channel AMT sites, and the remaining 2 sites were 5-channel MT sites. The tight station spacing of 500 m and the generally layered subsurface conditions mean that the magnetic field recordings (AMT or MT) at the different sites could be used with the telluric channels at all sites (Figure 2). The end result was that a total of 734 combined AMT and MT sites were recorded throughout the region (Figure 1).

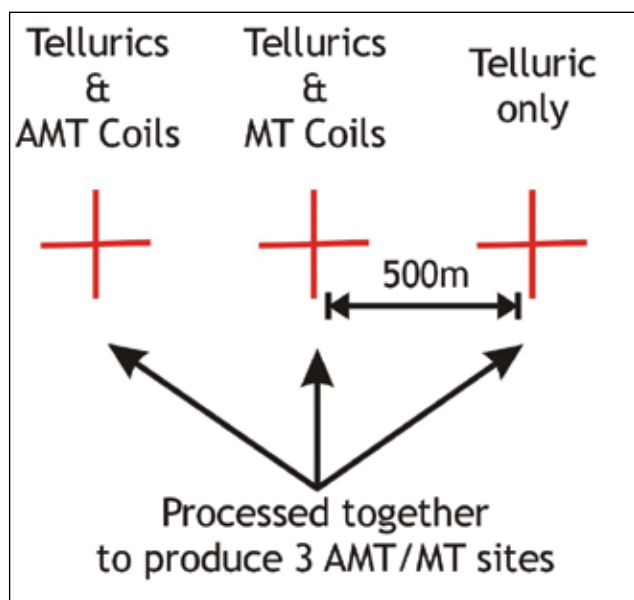


**Figure 2: Illustration of the site deployment and processing scheme developed to maximize the data quality and frequency range at each site.**

The data were processed by Geosystems Canada using robust remote reference techniques as implemented by the Phoenix Geophysics software package Mt2000. Figure 3 shows examples of response curves generated both for sites collected nearly 20 years ago as part of the Lithoprobe project (Figures 3a and 3c) and for sites collected in the fall of 2007 (Figures 3b and 3d). The response curves for the new sites show significant improvement in data quality over a much larger period range extending from 0.00001 to 1000 s. This, along with tighter station spacing, will provide better resolution at shallow depths and will allow deeper structures to be modeled.

### Decomposition Analysis

Single site and multi-site Groom-Bailey decompositions were applied to each of the MT sites along profile A in Figure 1 in order to determine the most accurate geoelectric strike direction and analyze the data for distortion effects (Groom and Bailey 1989). Figure 4 illustrates the results of single site strike analysis for each decade period band recorded at each site along the profile. The direction of the arrows shows the preferred geoelectric strike direction with a 90° ambiguity, and the colour scale represents the maximum phase difference between the 2 modes.

Nearly all the sites along the profile show a maximum phase difference that is less than 10°, at periods below 0.1 s, indicating that the data are independent of the strike angle. The maximum phase splits, where the data are most dependent on the 2-dimensional strike direction, are observed between 0.1 and 10 s. The westernmost sites along the profile consistently indicate a preferred geoelectric strike angle of approximately 5° between 0.1 and 10 s, whereas the eastern half of the profile prefers an angle of 30° to 35°. Special analysis and model appraisals will need to be undertaken to account for this change in strike angle when generating 2-dimensional models of the profile.

## DATA MODELING AND PRELIMINARY RESULTS

### Validity of 1-D models

Pseudosections of the observed phase values with increasing periods in both the XY and YX modes were generated along profile A (Figure 5). Where the phases of the 2 modes are the same, the data are independent of the geoelectric strike angle and are considered 1-dimensional. The red line in Figure 5 illustrates the maximum period to which the phases are similar, below which the data are either 2- or 3-dimensional. The 1-dimensional models generated are therefore only accurate to periods of 0.1 to 1 s at most of the sites along profile A. Schmucker's c-function analysis was applied to each site, providing a depth estimate at these periods by calculating the depth to maximum eddy current flow (Schmucker 1973). These indicate that the 1-dimensional models should accurately represent the conductivity structure of the subsurface to depths of 1000 to 2500 m.

### 1-D Models

One-dimensional layered earth resistivity Occam models were generated for each site along profile A using the WinGLink MT interpretation software package. These

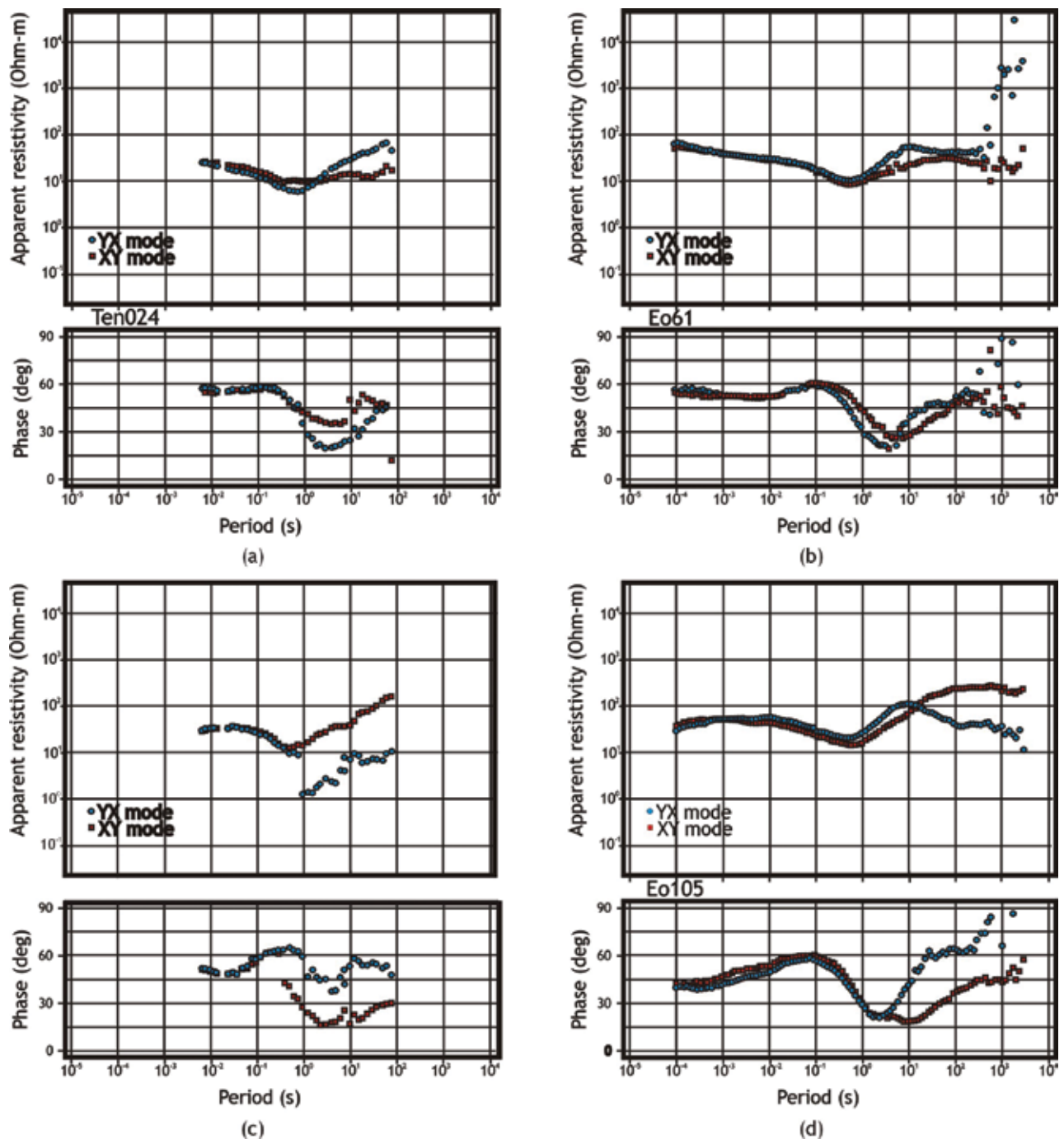


Figure 3: Examples of the improved data quality between the old Lithoprobe sites and the recent data acquisition in the Nechako Basin. The locations of the sites are shown in Figure 1, where (a) lithoprobe site ten24 and (b) Nechako site eo61 have the same position and (c) lithoprobe site ten21 and (d) Nechako site eo5 have the same position.

models are shown in Figure 6, where the warm colours illustrate conductive regions and the cold colours reveal more resistive material. For some sites, there appears to be a very thin (approximately 100 to 200 m) resistive layer (greater than 1000 ohm-m) near the surface that thickens towards the east. This most likely represents the surficial volcanic rocks, as the geology strip at the top of Figure 6 shows more volcanic cover in the eastern half of the profile. The data are not sensitive to the extremely shallow structures

and may not reveal a volcanic cover that is less than 50 m thick. Nearly all of the sites reveal a significant decrease in resistivity (from 10 to 100 ohm-m to more than 1000 ohm-m) at depths ranging between 1000 and 3000 m, shown by the black line in Figure 6. These depths are consistent with those of the Nechako Basin, suggesting that the data are imaging the base of the sediments and penetrating into the deeper basement units.

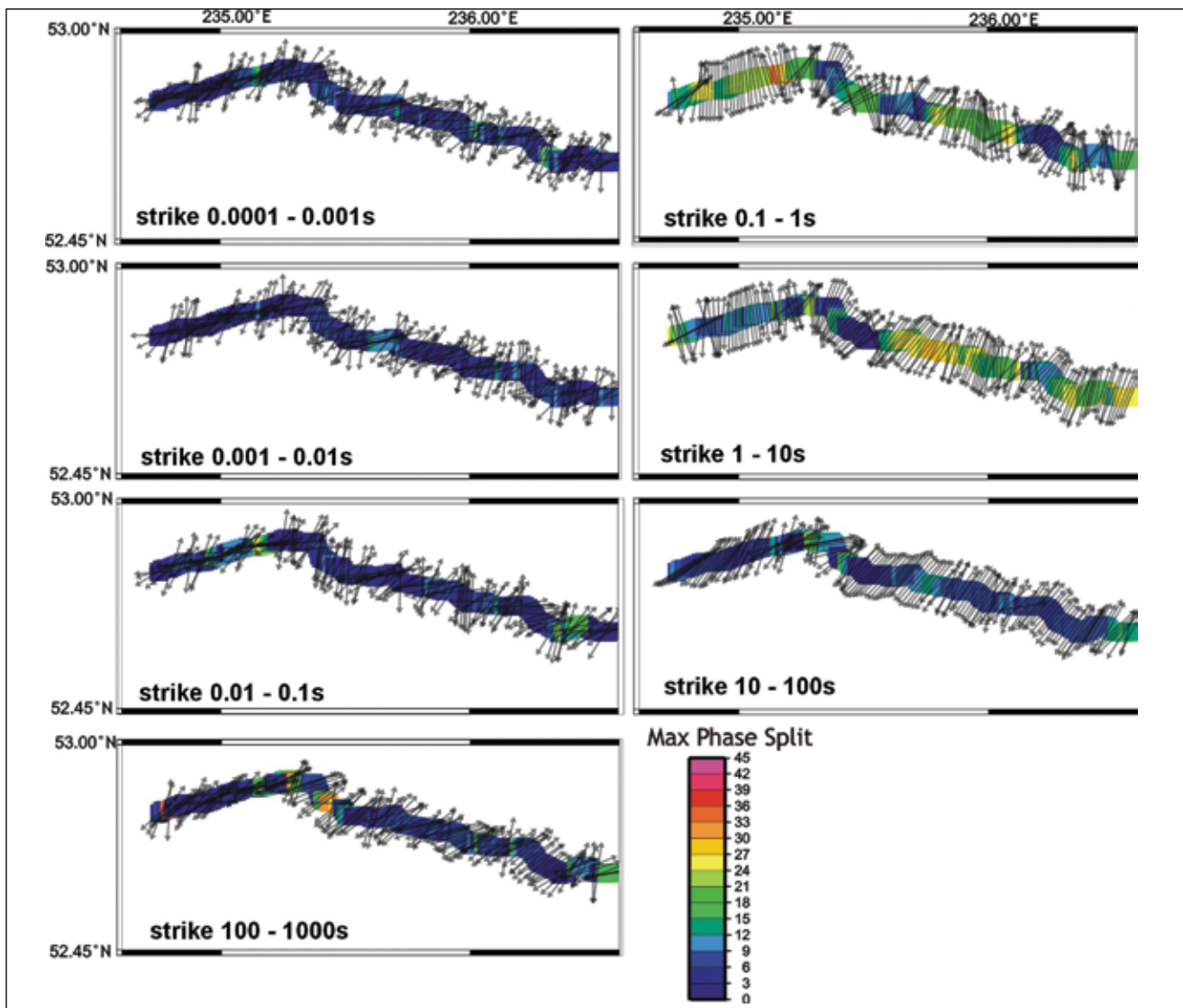


Figure 4: Map illustrating the preferred geoelectric strike angle for each site along Profile A for each decade period band. The colour shows the maximum phase split between the 2 modes.

The 1-dimensional models were stitched together with a smoothing parameter applied, resulting in Figure 7. The colour scale is the same as that used in Figure 6. The black line illustrates the variations in the depth of the boundary between the upper sediments and the lower basement rocks along the profile. Additionally there are lateral variations in the conductivity structures within the sediments that could be attributed to compositional changes, the presence of fluids, or changes in the effective porosity of the material. These variations appear to correlate with results from a regional gravity survey, seen at the top of Figure 7, that was collected by Canadian Hunter in the 1980s.

Although a limited number of samples have been analyzed for percent effective porosity and electrical conductivity in the horizontal direction only, preliminary results show a direct correlation between the resistivity and porosity of certain rock units (Figure 8). This indicates that the

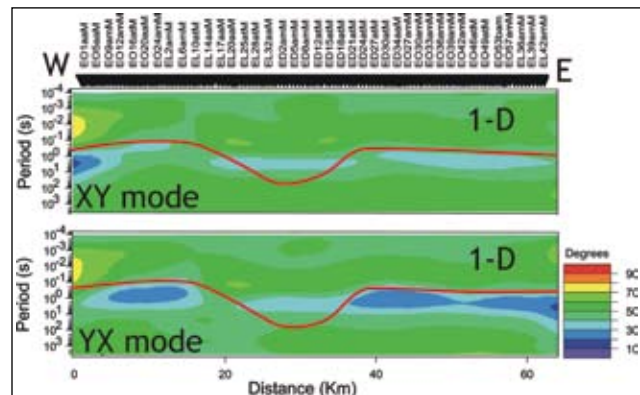


Figure 5: Pseudosections of the phase values in the XY and YX directions along Profile A. The red line marks the maximum period to which the data can be considered 1-dimensional.

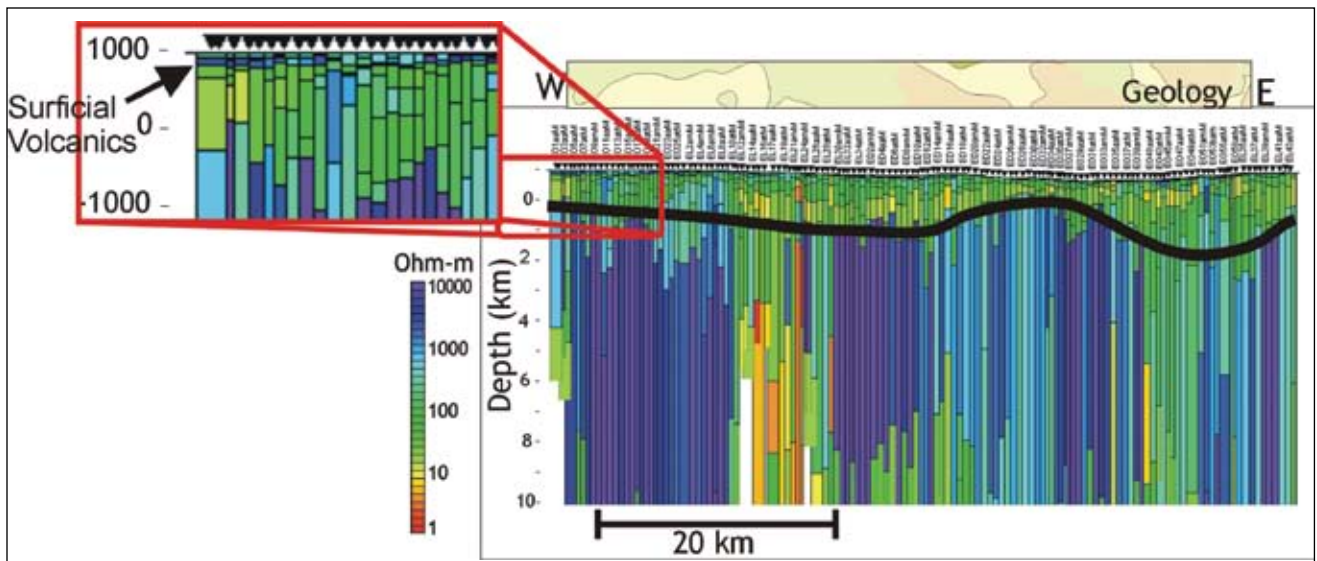


Figure 6: One-dimensional models generated for each site along profile A. The warm colours illustrate regions of high conductivity, and the cool colours indicate resistive regions. The thick black line marks the boundary between the sedimentary sequences and the underlying crystalline rocks. The local geology along the profile is shown in a strip above the cross-section.

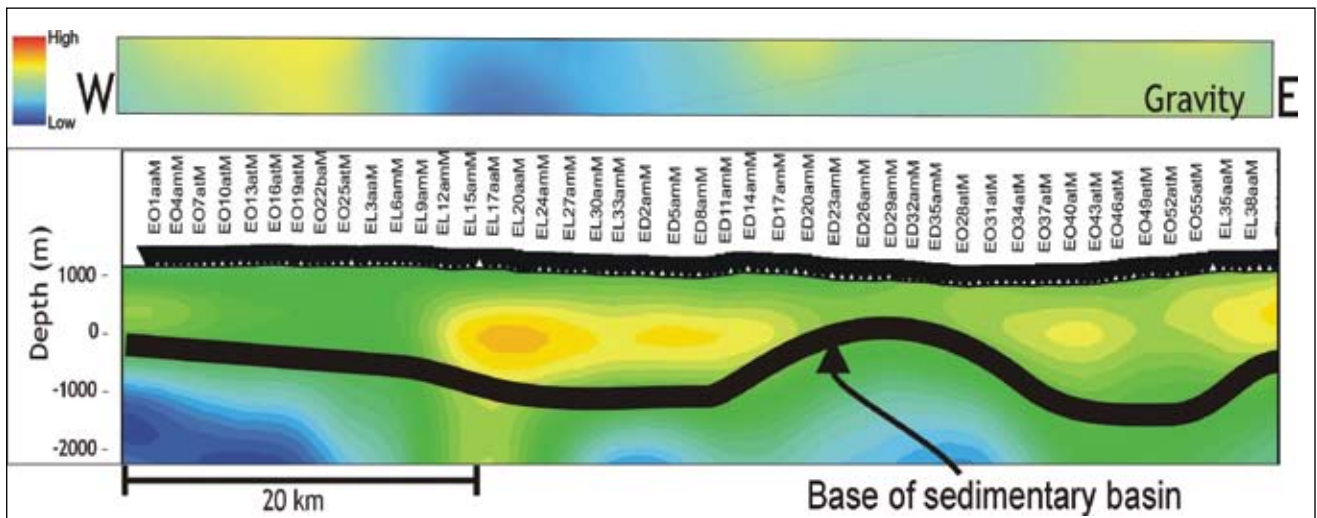


Figure 7: Smoothed, stitched one-dimensional models along profile A. Gravity results along the profile are shown in a strip above the cross-section; the blues show gravity lows, and the reds, high anomalies.

MT method is sensitive to porosity changes in the sedimentary units and suggests a cause for the link between areas of low density observed in the gravity data and areas of low resistivity in the MT data.

## DISCUSSION AND CONCLUSIONS

Magnetotelluric data, in the AMT and MT frequency ranges, were collected at 734 sites within the Nechako Basin. Strike analyses of 134 sites show changes in the preferred geoelectric strike angle along the 70-km-long profile. These changes suggest that localized structure is influencing the strike direction at periods between 0.1 and

10 s. The different strike angles may represent different tectonic pulses, resulting in compressional faulting that causes a juxtaposition of conductive sediments and resistive basement rocks.

Initial results of 1-dimensional modelling of the data reveal in some areas a shallow resistive layer that is interpreted as the surficial volcanic rocks. The data also show a significant decrease in the apparent resistivity values at depths, which corresponds to the approximate boundary between the sedimentary basin and the underlying basement rocks. These results indicate that the MT method is sensitive to thicker regions of volcanic cover and that it is able to penetrate these volcanics and image the deeper structure. A cross-section of the stitched 1-dimensional MT models

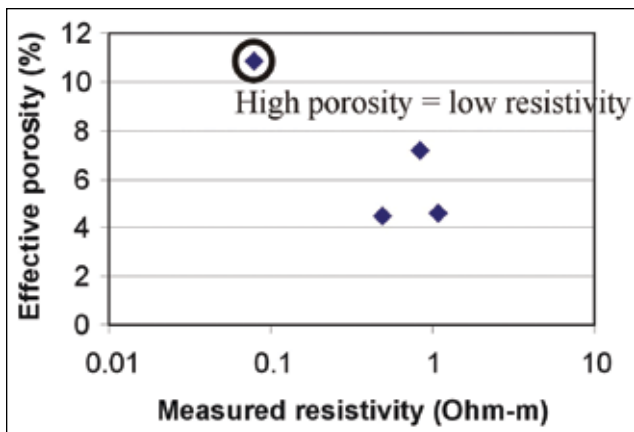


**Figure 8: Results of petrophysical analysis of several rock samples, showing the relationship between porosity and resistivity.**

indicates variations in the depth of this boundary from east to west. Additionally, at shallow depths within the sedimentary basin, changes in the conductivity values of up to 1 order of magnitude are observed. This suggests lateral changes in the physical properties of the basin that could be attributed to compositional difference or the presence of fluids. However, preliminary results of laboratory tests on rock samples, along with a correlation between high conductivity and low gravity, suggest that these changes may be related to changes in the effective porosity of the material.

Future work on this data will include 2-dimensional modeling and model appraisals of the presented profile, 3-dimensional modeling of the northernmost sites, and integrated modeling and interpretations of various geophysical data sets, including new seismic and gravity information.

## ACKNOWLEDGMENTS

Financial support for this work comes from the Geological Survey of Canada, Geoscience BC, and the BC Ministry of Energy, Mines and Petroleum Resources. Additional instrumentation was provided by the Polaris consortium, and special thanks are given to the Geosystems Canada crew for collecting the data.

## REFERENCES

- Andrews, G.D.M. and Russell, J.K. (2007): Mineral exploration potential beneath the Chilcotin Group (NTS 0920, P; 093A, B, C, F, G, J, K), south-central British Columbia: preliminary insights from volcanic facies analysis; in *Geological Fieldwork 2006, BC Ministry of Energy, Mines and Petroleum Resources, Paper 2007-1 and Geoscience BC, Report 2007-1*, pages 229–238.
- Cagniard, L. (1953): Basic theory of the magnetotelluric method of geophysical prospecting; *Geophysics*, Volume 18, pages 605–635.
- Gabrielse, J. and Yorath, C.J., Editors (1991): Geology of the Cordilleran Orogen in Canada; in *Geology of Canada*, number 4, *Geological Survey of Canada* and in *Geology of North America*, volume G-2, *Geological Society of America*.
- Groom, R. W., and R.C. Bailey (1989): Decomposition of magnetotelluric impedance tensors in the presence of local three-dimensional galvanic distortion, *Journal of Geophysical Res.*, Volume 94, pages 1913–1925.
- Haak, V. and Hutton, V.R.S. (1986): Electrical resistivity in continental lower crust; *Geological Society of London, Special Publication*, Volume 24, pages 35–49.
- Hannigan, P., Lee, P.J., Osadetz, K.G., Dietrich, J.R. and Olsen-Heise, K. (1994): Oil and gas resource potential of the Nechako-Chilcotin area of British Columbia, *Geological Survey of Canada, Geofile 2001-6*, 38 pages.
- Hayward, N. and Calvert, A.J. (2008): Structure of the southeastern Nechako Basin, south-central British Columbia: preliminary results of seismic interpretation and first-arrival tomographic modeling. Geoscience BC Summary of Activities 2007, *Geoscience BC Report 2008-1*.
- Jones, A.G. (1992): Electrical conductivity of the continental lower crust; in *Continental Lower Crust*, D.M. Fountain, R.J. Arculus and R.W. Kay (ed), *Elsevier*, pages 81–143.
- Jones, A.G. and Gough, D.I. (1995): Electromagnetic images of crustal structures in southern and central Canadian Cordillera; *Canadian Journal of Earth Sciences*, Volume 32, pages 1541–1563.
- Kearey, P. and Brooks, M. (1991): An Introduction to Geophysical Exploration (Second Edition); *Blackwell Scientific Publications*.
- Majorowicz, J.A. and Gough, D.I. (1991): Crustal structures from MT soundings in the Canadian Cordillera; *Earth and Planetary Science Letters*, Volume 102, pages 444–454.
- Mathews, W.H. (1989): Neogene Chilcotin basalts in south-central British Columbia; *Canadian Journal of Earth Sciences*, v. 23, p. 1796–1803.
- Monger, J.W.H. and Price, R.A. (1979): Geodynamic evolution of the Canadian Cordillera — progress and problems; *Canadian Journal of Earth Sciences*, Volume 16, pages 770–791.
- Monger, J.W.H., Price, R.A. and Tempelman-Kluit, D. (1982): Tectonic accretion of two major metamorphic and plutonic belts in the Canadian Cordillera; *Geology*, Volume 10, pages 70–75.

- Monger, J.W.H., Souther, J.G., and Gabrielse, H. (1972): Evolution of the Canadian Cordillera — a plate tectonic model; *American Journal of Science*, Volume 272, pages 557–602.
- Schmucker, U. (1973): Regional induction studies: a review of the methods and results. *Physics of the Earth and Planetary Interiors*, Volume 7, pages 365–378.
- Spratt, J.E., Craven, J., Jones, A.G., Ferri, F., and Riddell, J. (2006): Utility of magnetotelluric data in unravelling the stratigraphic-structural framework of the Nechako Basin, British Columbia from a re-analysis of 20 year old data, in Geological Fieldwork 2006, *BC Ministry of Energy, Mines and Petroleum Resources*, Paper 2007-1, *Geoscience BC Report 2007-1*, pages 395-404.
- Unsworth, M.J. (2005): New Developments in conventional hydrocarbon exploration with EM methods, *CSEG recorder*.
- Wait, J.R. (1962): Theory of magnetotelluric fields; *Journal of Research of the National Bureau of Standards*, Volume 66D, pages 509–541.
- Xiao, W. and Unsworth, M.J. (2006): Structural imaging in the Rocky Mountain Foothills (Alberta) using magnetotelluric exploration, *American Association of Petroleum Geologists Bulletin* Volume 90, pages 321-333.





